



NEUTRONS
FOR SCIENCE

INSTITUT LAUE-LANGEVIN

THE EUROPEAN NEUTRON SOURCE



Annual Report 20**18**

FIND US ON:   

Contents

| | |
|--------------------------------------------------------|-----|
| FOREWORD | 4 |
| WHAT IS THE ILL | |
| About the ILL | 6 |
| Why neutron scattering is useful | 7 |
| THE ILL IN THE PRESS | 8 |
| SCIENTIFIC HIGHLIGHTS | 10 |
| College introductions | 12 |
| Biology and health | 14 |
| Soft matter | 24 |
| Magnetism | 34 |
| Materials science | 48 |
| Chemistry and crystallography | 58 |
| Nuclear and particle physics | 64 |
| Theory | 68 |
| MODERNISATION PROGRAMMES AND TECHNICAL DEVELOPMENTS | 72 |
| Modernisation programme and instrument upgrades | 74 |
| Technical developments | 80 |
| Projects and Techniques Division activities | 84 |
| INDUSTRIAL ACTIVITIES | 90 |
| EXPERIMENTAL AND USER PROGRAMME | |
| User programme | 93 |
| User and beamtime statistics | 94 |
| Instrument list | 98 |
| REACTOR OPERATION | 100 |
| MORE THAN SIMPLY NEUTRONS | 104 |
| Scientific support laboratories | 106 |
| Training and outreach | 108 |
| European programmes | 110 |
| WORKSHOPS AND EVENTS | 112 |
| Chronicle | 113 |
| Scientific events | 114 |
| FACTS AND FIGURES | 118 |
| Facts and figures | 119 |
| Publications | 121 |
| Organisation chart | 122 |

Publishing information

Editors:

Giovanna Cicognani and Mark Johnson

Scientific advisors:

Sandra Cabeza, Elisa Rebolini,
Skyler Degenkolb, Lucile Mangin-Thro,
Oscar R. Fabelo Rosa, Navid Qureshi,
Dirk Honecker, Michael M. Koza, Tobias
Weber, Nicolas Coquelle,
Ingo Hoffmann, Philipp Gutfreund

Production team:

Giovanna Cicognani, Virginie Guerard

Design:

Morton Ward Limited

Photography:

ILL (unless otherwise specified), and
C. Tresca for ILL's Directors' portraits)

Further copies can be obtained from:

Institut Laue-Langevin
Communication Unit
CS 20156, F-38042 Grenoble Cedex 9
communication@ill.eu
www.ill.eu

FIND US ON:   



THE ILL and its staff are second to none in neutron scattering around the world!

It was my pleasure to chair the Steering Committee of this outstanding facility for the fourth time, against the backdrop of a changing scientific landscape. Society is our main financial partner and has every reason to expect a positive impact from the solutions, resulting from our basic research, to the grand challenges facing it. I know, 'grand challenges' is a big buzz word. But honestly, we all know that energy resources are limited, that we have to find alternatives to fossil-based products, that nothing is changing our lives more than the rapid evolution of information technology and last, but not least, that we are fortunate to have a life expectancy twice as long as that of 100 years ago—albeit accompanied by health problems not known before. Many breakthroughs in science and technology are due to a deeper understanding of the structure, dynamics and function of biological or artificial materials, all of which require advanced characterisation methods. Naturally, our favourite probe is the neutron, with all its unique features. In 2018, the ILL and its users produced an impressive number of high-level publications, many of them presenting novel findings addressing the above-mentioned societal challenges and often related to applications.

The landscape of neutron scattering is, however, changing. Some successful sources will soon be switched off: the BERII reactor in Berlin and the Orphée reactor in Saclay. The ILL Associates discussed this new situation in a workshop in Unkel, Germany, in the spring of 2018. Regarding the ILL, we are pleased to report that their intention is to sign a sixth protocol, securing its operation for another ten-year period: 2024–2033.

In 2018, the last instrument of the Millennium upgrade—WASP—was put into operation while the Endurance2 upgrade programme received funding for 2019. The Scientific Members have expressed their willingness to keep using the ILL instruments and share the costs accordingly—95 % of the funding has been renewed and new membership possibilities are being explored in the context of the FILL2030 European project. Indeed, one highlight of 2018 was the celebration of 31 years of Spanish membership, by way of a perfectly organised event in Madrid in December—thank you, dear Spanish colleagues!

A prerequisite for our continued success is the safe and secure operation of the research reactor itself. This year the ILL ran three successful cycles and a contract for the supply of 30 fuel elements until ~2028 was signed. My compliments to everybody involved in this demanding but essential aspect of our work.

The ILL is leading in shaping the new neutron landscape, as a founding member of the League of European Neutron Sources (LENS). I believe that this European initiative is of the utmost importance if we are to unleash the full potential of the community and its sources across national borders and to the advantage of the entire European network of neutron scattering institutions. This potential was visible in the first ILL/ESS user meeting held in Grenoble in October 2018, which was attended by an impressive 650+ participants.

On behalf of the ILL Associates, I express my thanks and my appreciation to the directorate and the entire staff of the ILL, the scientific members and users across Europe.

Sebastian M. Schmidt
Chair of the ILL Steering Committee



DIRECTOR'S FOREWORD

THROUGHOUT 2018, the ILL Associates devoted themselves to the task of securing

a bright future for the Institute, in particular through their formal engagement to seek an extension of the ILL's Intergovernmental Convention for the period 2024 to 2033. In parallel, negotiations with the ILL's Scientific Members saw significant progress towards renewing the membership agreements for the next five years. All this, combined with the Associates' firm commitment to our latest upgrade programme, Endurance, is excellent news for ILL users, who can continue to count on the Institute's outstanding service for many years to come.

The continued trust shown by our Associates and Scientific Members is a clear sign of their recognition of the quality of the scientific work performed at the ILL. A convincing display of the ILL's scientific excellence was apparent at the hugely successful user meeting co-organised with the ESS in October, and throughout the pages of this report you will find details of a host of outstanding results confirming the ILL's position as the flagship centre for neutron science.

While 2017 was dominated by efforts to maintain and upgrade our neutron source, 2018 saw the successful delivery of three reactor cycles, allowing our users to perform over 800 experiments. The results of previous experiments also found their way into an impressive number of high-quality publications in 2018.

Given the importance of safe and reliable reactor operation for the scientific programme, the ILL never ceases to invest heavily in its infrastructure. This year saw the official close of the post-Fukushima reinforcement programme, which has allowed us to strengthen still further the ILL's defences in the event of extreme situations, thus paving the way for safe reactor operation throughout and beyond the next decade. In parallel, we were also able to successfully conclude negotiations on the manufacture of fuel elements and have secured the supply of this key component for many years to come.

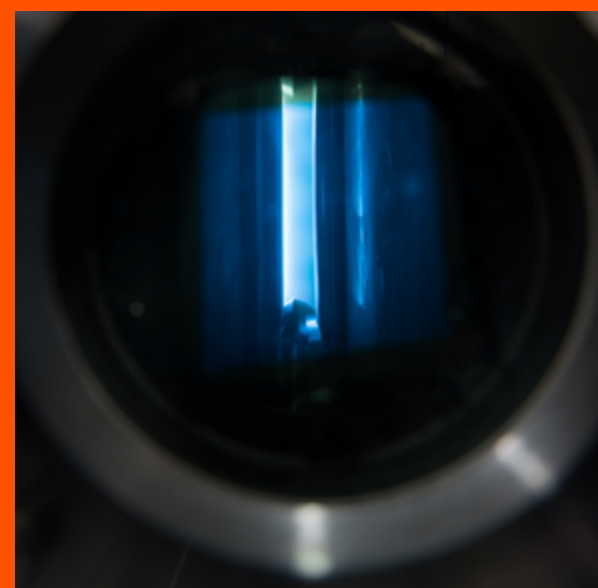
Of course, even the best neutron source in the world is only as good as the instruments it feeds, which is why the ILL instrument suite is constantly being upgraded. With the commissioning of the new, wide-angle spin-echo spectrometer WASP in 2018, the Millennium upgrade programme has been brought to a successful conclusion. Representing a total investment of close to 100 ME, Millennium has contributed enormously to maintaining the world-leading performance levels of ILL instruments. Its successor programme, Endurance, is now in full swing. Its first phase is due to be completed by 2020, while the roll-out of the second phase has already begun.

We all know that modern societies are placing ever-increasing emphasis on the strict regulation of industrial processes in order to minimise the inherent risks these processes present to society and the environment. As a responsible nuclear operator, the ILL is determined to respond to these regulatory developments by pursuing an ambitious compliance programme. This programme encompasses all aspects of safety and security, including physical protection. Every possible measure is being taken to achieve maximum levels of compliance while at the same time preserving the quality of service our users deserve.



I hope that, with these few lines, I have been able to convince you not only that the ILL can be proud of its distinguished past but that it is facing an equally bright future. The ILL's success has been and always will be a joint achievement. I therefore wish to express my gratitude to all those who have helped, either 'on stage' or behind the scenes, to prepare this future, whether as members of the ILL's highly motivated staff or its governing bodies, as valued collaborators or as ILL users. I am convinced that your efforts will be rewarded by many more exciting scientific discoveries on a par with those that you can read about in this year's annual report.

Helmut Schober
ILL Director



WHAT IS THE ILL



© R. Cubitt

FIND US ON:   

About the ILL

The Institut Laue-Langevin (ILL) is an international research centre providing world-leading facilities in neutron science and technology. Neutrons are used at the ILL to probe the microscopic structure and dynamics of a broad range of materials at molecular, atomic and nuclear level.

The ILL operates the most intense neutron source in the world: a 58.3 MW nuclear reactor designed for high brightness. The reactor normally functions round-the-clock for four 50-day cycles per year, supplying neutrons to a suite of 40 high-performance instruments constantly maintained at the highest state of the art.

The ILL is owned by the three founding countries—France, Germany and the United Kingdom. These three Associate countries contributed some 65 M€ to the Institute in 2018, a sum enhanced by significant contributions from the ILL's Scientific Member countries—Austria, Belgium, the Czech Republic, Denmark, Italy, Poland, Slovakia, Spain, Sweden and Switzerland. The ILL's overall budget in 2018 amounted to around 103 M€.

As a service institute, the ILL makes its facilities and expertise available to visiting scientists. It has a global user community, with roughly 2 000 researchers from almost 40 countries coming to work at the ILL every year. The 850 experiments they perform annually are pre-selected by a scientific review committee. In 2018, 570 publications were published, following the treatment and interpretation of data obtained by using our facilities. Of these articles, 158 were published in high-impact journals. This is a factor of two higher than the next most productive neutron source in the world.

NEUTRONS AND SOCIETY

The scope of the research carried out at the ILL is very broad, embracing condensed matter physics, chemistry, biology, materials and earth sciences, engineering, and nuclear and particle physics. Much of it impacts on many of the challenges facing society today, from sustainable sources of energy, better healthcare and a cleaner environment, to new materials for information and computer technology.

PREPARING FOR THE FUTURE

To maintain its status as leader in neutron science, the Institute has constantly upgraded its instruments, infrastructure and scientific equipment over the last 50 years. The latest modernisation exercise—the Endurance programme—will continue to develop instrumentation and support services with a view to maintaining the Institute's world-leading position for another decade at least. Endurance phase I is currently underway (2016–2019), with a second phase anticipated to run between 2020 and 2023.

Why neutron scattering is useful

When used to probe small samples of materials, neutron beams have the power to reveal what is invisible using other forms of radiation. Neutrons can appear to behave as particles, waves or microscopic magnetic dipoles; with these very specific properties they can provide information that is often impossible to obtain using other techniques. Below are a few of their special characteristics.

WAVELENGTHS OF TENTHS OF NANOMETRES

Neutrons have wavelengths varying from 0.01 to 100 nanometres. This makes them ideal for probing atomic and molecular structures, whether composed of single atomic species or complex biopolymers.

ENERGIES OF MILLI-ELECTRONVOLTS

The milli-electronvolt energies associated with neutrons are of the same magnitude as the diffusive motions of atoms and molecules in solids and liquids, the coherent waves in single crystals (phonons and magnons) and the vibrational modes in molecules. Any energy exchange, therefore, of between 1 μ eV (or even 1 neV with neutron spin-echo techniques) and 1 eV between the incoming neutron and the sample is easy to detect.

MICROSCOPICALLY MAGNETIC

Neutrons possess a magnetic dipole moment that makes them sensitive to the magnetic fields generated by unpaired electrons in materials. They therefore play an important role in investigating the magnetic behaviour of materials at the atomic level. In addition, as the neutron scattering effect of the atomic nuclei in a sample depends on the orientation of the spin of both the neutron and the atomic nuclei, neutron scattering techniques are ideal for detecting nuclear spin order.

ELECTRICALLY NEUTRAL

As neutrons are electrically neutral they can penetrate far into matter without doing damage. They are therefore precious allies for research into biological samples or engineering components under extreme conditions of pressure, temperature or magnetic field, or within chemical-reaction vessels.

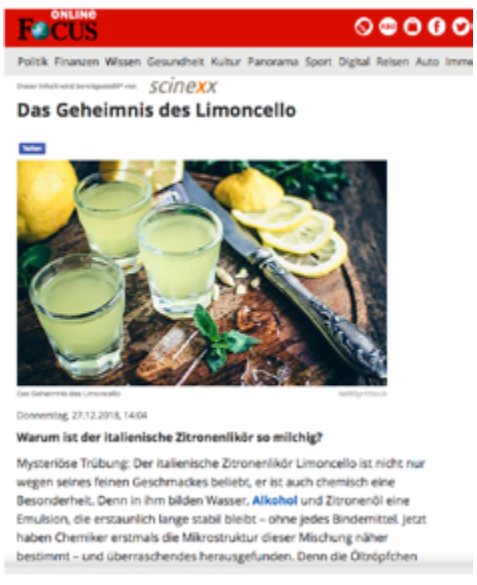
HIGH SENSITIVITY AND SELECTIVITY

The scattering from nucleus to nucleus in a sample varies in a quasi-random manner, even for different isotopes of the same atom. This means that light atoms remain visible in the presence of heavy atoms, and atoms close to each other in the periodic table can be clearly distinguished. This makes it possible to use isotopic substitution in order to vary the contrast in certain samples and thus highlight specific structural features.

Neutrons are also particularly sensitive to hydrogen atoms and are therefore essential for research into hydrogen storage materials, organic molecular materials, and biomolecular samples or polymers.

1. Published in *Online Focus* on 27 December 2018
2. Published in *News Medical* on 14 November 2018
3. Published in *SCITECH Europa* on 12 November 2018
4. Published in *WIRED* on 20 October 2018

More articles at <https://www.ill.eu/news-press-events/press-corner/ill-in-the-media/>

1. 

Das Geheimnis des Limoncello

Warum ist der italienische Zitronenlikör so milchig?

Mysteriöse Trübung: Der italienische Zitronenlikör Limoncello ist nicht nur wegen seines feinen Geschmacks beliebt, er ist auch chemisch eine Besonderheit. Denn in ihm bilden Wasser, Alkohol und Zitronenöl eine Emulsion, die erstaunlich lange stabil bleibt – ohne jedes Bindemittel. Jetzt haben Chemiker erstmals die Mikrostruktur dieser Mischung näher bestimmt – und überraschendes herausgefunden. Denn die Öltröpfchen

2. 

Galectins – An Ancient Family with a Significant Future

By Keynote Contributor
Dr. Matthew Blakeley
Prof. Derek Logan
Institut Laue-Langevin (ILL)
Lund University

Written by Dr. Matthew Blakeley, ILL-III beamline scientist at Institut Laue-Langevin (ILL) and Prof. Derek Logan, associate professor in structural biology at Lund University.

Galectins are sugar-binding proteins, characterised by their binding to a specific carbohydrate, galactoside, on the surface of other structures, and from which galectins derive their name. Many physiological functions essential to life rely on galectins including the regulation of inflammation, immune response, and cell-to-cell communication. On the other hand, they have been linked through their dysfunction to a number of serious diseases, including heart disease and cancer.

3. 

Why we need a better structural knowledge of E.coli

Giovanna Fragneto, Head of Soft Matter Science and Support at the Institut Laue-Langevin (ILL), explains why a better structural knowledge of E.coli is needed to tackle antimicrobial resistance.

4. 

Neutronenquelle in Grenoble: Ein Atomreaktor für die Wissenschaft

Radioaktivität hat ein mieses Image. Dabei gibt es Atomreaktoren, die nicht zur Stromerzeugung dienen – und von denen nicht die Gefahr der Meiler von Tschernobyl oder Fukushima ausgeht. Die europäische Neutronenquelle in Grenoble etwa ist ein Mekka für Physiker, Biologen, Geologen und andere Forscher. WIRED-Reporter Dominik Bardow konnte sich dort umsehen und berichtet in

5. 

Institut Laue-Langevin (ILL) and ESRF collaborate on space technologies

19th August 2018

Space exploration has led to many useful benefits that have vastly improved quality of life on Earth.

Professor Helmut Schober, director of the Institut Laue-Langevin (ILL) discusses a new partnership between the ILL and the ESRF and leading European space companies to tackle industry challenges.

The Institut Laue-Langevin (ILL) and the European Synchrotron Radiation Facility (ESRF) have

6. 

Looking for symmetrons and dark matter

16th July 2018

A high-precision experiment led by Vienna's Technical University has set its sights on pinpointing the so-far hypothetical 'symmetron fields' using the PF2 ultra-cold neutron source at the Institut Laue-Langevin (ILL), France. The existence of symmetrons could provide an explanation for dark matter.

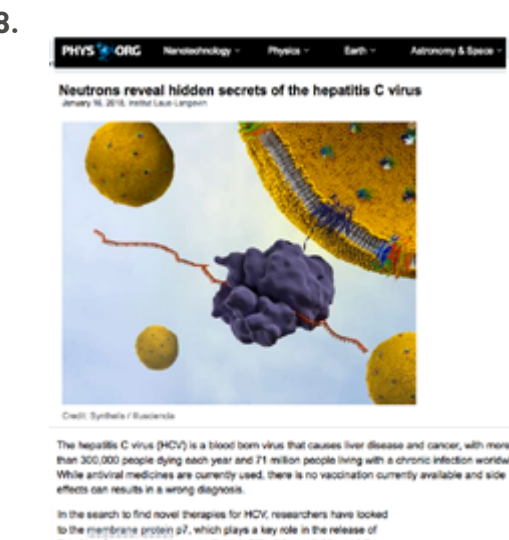
7. 

biomedical devices

Targeted infection control

27 Jun 2018

Medical devices that incorporate hydrogels into silicone rubber could release antibiotics into areas where they are needed most. Erik Brek, Caroline Boudou, Martis Alm and Peter Thomsen describe how neutron scattering is helping researchers to understand and optimize the structure of these silicone-hydrogel networks.

8. 

Neutrons reveal hidden secrets of the hepatitis C virus

January 16, 2018, Institut Laue-Langevin

The hepatitis C virus (HCV) is a blood born virus that causes liver disease and cancer, with more than 300,000 people dying each year and 71 million people living with a chronic infection worldwide. While antiviral medicines are currently used, there is no vaccination currently available and side effects can result in a wrong diagnosis.

In the search to find novel therapies for HCV, researchers have looked to the membrane protein p7, which plays a key role in the release of the virus, for answers. However, there is little data available, and the crystallographic structure of the protein has not yet been resolved.

5. Published in *SCITECH Europa* on 13 August 2018
6. Published in *SCITECH Europa* on 24 July 2018
7. Published in *Physics World* on 27 June 2018
8. Published in *PhysOrg* on 16 January 2018
9. Published in *Scientific American* on 29 January 2018

9. 

Missing Neutrons May Lead a Secret Life as Dark Matter

be the reason experiments can't agree on the neutron lifetime, according to a new idea

By Cora Morozoff on January 29, 2018

Neutrons, the enigmatic building blocks of atoms, could be hiding a secret connection to dark matter, according to a new proposal. Credit: Edoardo Sestini/Getty Images

SCIENTIFIC HIGHLIGHTS

The scientific highlights presented in this annual report demonstrate how research with neutrons continues to push back the frontiers of science.

- 12** COLLEGE INTRODUCTIONS
- 14** BIOLOGY AND HEALTH
- 24** SOFT MATTER
- 34** MAGNETISM
- 48** MATERIALS SCIENCE
- 58** CHEMISTRY AND CRYSTALLOGRAPHY
- 64** NUCLEAR AND PARTICLE PHYSICS
- 68** THEORY

570



ILL PUBLICATIONS RECORDED IN 2018
OF WHICH **158** PUBLISHED IN HIGH-IMPACT JOURNALS



9 PRESS RELEASES
WERE PRODUCED IN
2018, LEADING TO
31 ARTICLES IN
THE GENERAL PRESS



KEEP UP-TO-DATE:

-  facebook.com/ILLGrenoble
-  twitter.com/ILLGrenoble
-  linkedin.com/company/institut-laue-langevin

THE VIBRANT scientific life at the ILL is centred on our interaction with the user community. Over time, this has evolved into a subtle balance between experiments, publications, studentships, PhD projects, seminars, workshops and so on.

This year was a good one for experiments, with three cycles of reactor operation allowing the backlog from 2017 to be absorbed. It was also a good year for scientific output, which typically reflects experiments performed two years earlier. In particular, the trend towards a higher proportion of high-impact publications observed in 2017, together with an increasing number of publications using data from more than one instrument, has continued in 2018. The scientific highlights in the following pages illustrate this high-quality output from ILL experiments and, in many cases, complementary measurements at other facilities and with other techniques.

In 2018, the ILL hosted more than 50 seminars and colloquia and was involved in organising more than 25 scientific events. Five workshops covering interfaces, energy materials, magnetism, spectroscopy and dynamics were grouped together to form the basis of the ILL-ESS User Meeting, which took place last October. More than 500 participants attended the meeting, forcing us to close registration early because of the limited capacity of the venue. In May, the Nuclear and Particle Physics group organised its 'user meeting'—particle physics at neutron sources—which attracted around 150 participants and included a celebration of 50 years since the discovery of ultra-cold neutrons. Bringing together more than 650 scientists, these two events testify to the vitality of neutron science in Europe.

The physical foundation of the vibrant user community at the ILL is its state-of-the-art infrastructure. As described elsewhere in this report, the Endurance programme is now in full swing, with PANTHER, the new time-of-flight spectrometer, and SuperSUN, a new UCN source, to be commissioned in the first cycle of 2019. There are, however, other ingredients for success, such as the external reviews of instruments—IN16b and D33 in 2018—and the internal monitoring of instrument groups—Large Scale Structures and Nuclear and Particle Physics groups in 2018—which help to ensure that our hardware and services are optimally aligned with current and future user needs. In addition, there are many smaller projects and support services that make important contributions



to the overall user experience. For example, a single crystal, X-ray diffractometer has been ordered which will make corresponding neutron diffraction experiments more efficient, while the Partnership for Soft Condensed Matter received 15 applications for around six new scientific partners. Instruments and services are what we provide, but how we provide them is also evolving: flexible use of beamtime is increasing through Director's Discretionary Time, which actually involves evaluation by the subcommittees; and Easy Access for short measurements on mail-in samples is now available on all the condensed matter science instruments.

Looking ahead, the future depends on young scientists and new users. The ILL's PhD programme is flourishing, with a cohort of about 40 students of which one-third are renewed each year. In 2018 we, along with the ESRF, submitted a COFUND-ITN application to the European Horizon-2020 programme, focusing on innovation with neutrons and X-rays. We were delighted to learn recently that this InnoVaXN project will be funded, providing 40 PhD studentships at the ILL and the ESRF. There will be open calls in 2020 and 2021 for projects, which must involve an industry partner, so watch our website for more information! New users are equally essential in developing the use of neutrons, and we have initiated a study to carefully map our user base both geographically and scientifically. The results will form the basis of an outreach campaign in 2020–2021, during a long shutdown in which more new guides and instruments will be installed. We are preparing for the future provision of beamtime, when there will be fewer time-consuming reactor developments (e.g. post-Fukushima work) and maintenance (e.g. beam-tube renewals), although operating cycles will still have to be balanced with the roll-out of the second phase of Endurance. We look forward, with you, to more great science in 2019 and beyond...

Mark R. Johnson

Associate Director,
Head of Science Division

COLLEGE 1 – APPLIED MATERIALS SCIENCE, INSTRUMENTATION AND TECHNIQUES**S. Cabeza** (College 1 Secretary)

College 1 deals with applied physics and new instrumentation techniques in neutron scattering. The main topics covered are metallurgy, applied neutron scattering, cultural heritage, new neutron scattering techniques, instrumentation and scientific computing. Stress mapping accounts for about half of the proposals submitted, and during the past year metal additive manufacturing was a hot topic for neutron residual stress characterisation. Furthermore, a certain proportion of the proposals represent current industrial collaborations.

SANS is an attractive, yet underused, technique for the whole materials science community—the College still has a few days available (with Highlight proposals not allocated in the last round). Nevertheless, the ILL's efforts to reach out directly to the materials science and engineering community are increasing, as are the number of proposals we are receiving as a result. A growing number of non-member countries are also presenting highly ranked experiments. *In situ* and *operando* work is needed in all fields and on all instruments, and users are collaboratively engaged in proposing and developing new sample environments at the ILL. These include, for example, the set-up for *in situ* metal printing on SALSA (with the Fraunhofer-IWS team), the development of a confined shear cell (with Malmo University) on FIGARO and the development of a method proposed recently on D33 (with PSI teams) to deal with ToF Bragg imaging.

COLLEGE 2 – THEORY**E. Rebolini** (College 2 Secretary)

College 2 focuses on research fields covering hard condensed matter, electronic structure and soft matter. It pursues independent research in synergy with researchers from the other Colleges and ILL users, and hosts many long-term and occasional visitors as part of successful collaborations. In 2018, a new postdoc and a new PhD student joined the ILL Theory group, working respectively on magnetism in high-Tc superconductors and finite-temperature spin dynamics. A long-term visiting PhD student also joined us for a year to conduct simulations of iron-sulphur metalloproteins and their redox potentials. In 2018, College 2 also reached out to experimentalists by organising the Theory day 'Theoreticians at the ILL—at your service' as well as a series of lectures within the framework of the ILL's PhD seminars.

COLLEGE 3 – NUCLEAR AND PARTICLE PHYSICS**S. Degenkolb** (College 3 Secretary)

College 3 uses the ILL reactor to address questions in nuclear and particle physics, including experiments concentrating on particles other than the neutron and studies of the neutron itself. In 2018, the STEREO experiment published its first constraints on sterile neutrinos in the eV mass range, proposed to explain observations of unexpectedly low electron antineutrino flux at nuclear reactors. The decennial conference on 'Particle Physics at Neutron Sources' (PPNS-2018) was co-organised with the LPSC, and hosted there in May. A total of 136 participants attended, and celebrated 50 years since the first experimental observations of ultracold neutrons. LOHENGRIN (PN1) saw a series of successful nuclear spectroscopy experiments using conversion electron and fast timing set-ups, respectively complementing spectroscopy of the 2012 EXILL campaign, and FIPPS today, with mass-separated fission products. FIPPS had its first fission experiments during cycle 184, using an active target with ^{235}U diluted in a scintillator. This system, used to study structure in neutron-rich nuclei,

combines for the first time the selectivity of multiple-gamma-ray coincidences with tagging of neutron-induced fission events.

COLLEGE 4 – MAGNETIC EXCITATIONS**L. Mangin-Thro** (College 4 Secretary)

College 4 is dedicated to magnetic excitations in ordered and disordered magnets, superconductors and frustrated systems. Both the subcommittees and the ILL's 2018 Highlights confirm interest in the latter to be particularly strong: two articles deal with geometrically frustrated magnetism in a pyrochlore and a kagome antiferromagnet respectively; another concerns a low-dimensional material, an Ising-like antiferromagnetic spin chain. In addition, a hyperfine interaction study has been performed on double perovskites. From an experimental point of view, significant demand for IN4 was observed during the last proposal round. This could not be satisfied, however, due to the absence of this thermal time-of-flight spectrometer following its decommissioning. To take its place, the new instrument PANTHER is being built as part of the Endurance suite of upgrades. Another development in terms of instruments concerns IN5, which should soon benefit from a new beam guide, increasing flux by a factor of three. Moreover, considerable effort is being made to achieve higher fields (10T), a sample environment also in high demand in the last proposal round.

COLLEGE 5A – CRYSTALLOGRAPHY**O. Fabelo** (College 5A Secretary)

During 2018, College 5A accepted 87 proposals carried out on ten different ILL and CRG instruments. The samples studied were mainly single crystals or powder samples, although some amorphous or poor crystalline materials were also treated during the three reactor cycles. This number of proposals, with its slight increase with respect to previous years, continues an increasing trend. The scientific topics covered include hydrogen storage materials, ionic conductors (cationic and anionic), superconductors, catalysts, memory shape materials, high-voltage battery materials and the anharmonicity of light atoms, among others. It should be noted that Materials for Energy is an area that, as in previous years, has received significant support from the College 5A community, highlighting the importance of neutron scattering techniques for shedding light on the physics behind these prominent materials. College 5A's user community is formed largely of experienced and well-established groups within the chemistry, solid-state and condensed-matter physics communities, and spans 14 different countries. Moreover, our user database has expanded with the inclusion of several new research groups, thereby ensuring the health of the community over the coming years.

COLLEGE 5B – MAGNETIC STRUCTURES**N. Qureshi** (College 5B Secretary) and **D. Honecker** (focus group Secretary)

College 5B deals with static magnetic properties of crystalline materials, investigated by means of powder or single-crystal diffraction—including more sophisticated techniques such as spherical neutron polarimetry, as can be seen from two of this year's Magnetism Highlights—as well as small-angle neutron scattering (SANS) and reflectometry techniques.

Strong interest in frustrated compounds with exotic ground states, some of them in form of thin films and nanomaterials, persists. Multiferroic materials remain 'trendy', but an upturn in the trend for low-dimensional systems can also be observed.

The search for new classes of skyrmion-hosting materials and studies of the phase stability of chiral magnets are at the focus of the SANS community.

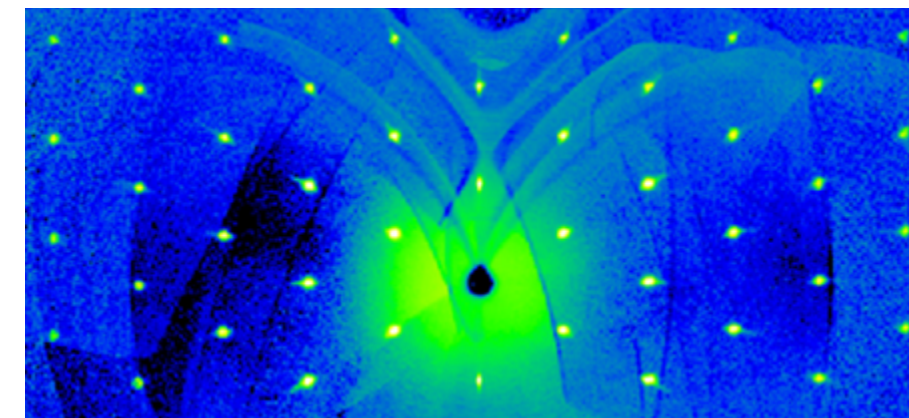
Electric field effects on the spin structure of multiferroics are addressed using a newly available electric-field set-up for SANS. Two Highlight articles demonstrate the continued interest in superconductivity and magnetic nanoparticles. Polarised neutron reflectometry explores the structural and magnetic integrity of thin layers, while science cases range from proximity effects of superconductivity on ferromagnetism to magnetic nanoparticles assemblies under alternating fields.

COLLEGE 6 – STRUCTURE AND DYNAMICS OF DISORDERED SYSTEMS**M.M. Koza** (College 6 Secretary)

Over the past few years, experiments on water and ionic liquids have become the two supporting columns of College 6's activities. The broadening of the College's sphere of action to confined and porous systems consolidated this trend in 2018. With this consolidation, the complexity of materials has increased and the experimental protocols have become more refined. Pressure experiments, polarisation analysis and multiple instruments are requested for the majority of projects, for complementary studies of structure and dynamics and extensive coverage of structure and dynamic ranges. Two Highlights reflect the wide spread of College 6 interests. In the first, inelastic polarisation analysis is exploited to quantitatively determine the magnitude of quantum effects in the dynamics of H_2O and D_2O — essential information for confronting inconsistent data in the literature and improving widely employed water potentials. In the second, layered structures of halogen-free ionic liquids and propylene carbonate are examined for their practicality as actively friction-controlled lubricants, highlighting the potential of ionic liquids beyond their application in batteries, solar cells, super-capacitors and electrochemical devices.

COLLEGE 7 – SPECTROSCOPY IN SOLID STATE PHYSICS AND CHEMISTRY**T. Weber** (College 7 Secretary)

College 7 deals with non-magnetic spectroscopy in solid-state systems, encompassing a broad range of topics that include the determination of phonon dispersion relations and densities of states, phonon softening effects due to anharmonic interactions, and structural and orbital-ordering phase transitions. Additional topics include ionic relaxation and diffusion, as well as the dynamics of molecular and physio-/chemisorbed systems. While College 7 has a wide variety of cold- and thermal-neutron spectrometers and diffractometers at its disposal, in the recent proposal round most days of beamtime were awarded to experiments on the high-flux, thermal-neutron, three-axis spectrometer IN8, the IN1-LAGRANGE spectrometer, the high-resolution spin-echo instrument IN11 and the time-of-flight spectrometers IN6-SHARP and IN5. The complexity of both the investigated systems and the instrumental resolution functions typically require sophisticated theoretical models and data analysis tools. Assistance in these fields is provided by the ILL's Theory and Software groups.

**COLLEGE 8 – STRUCTURE AND DYNAMICS OF BIOLOGICAL SYSTEMS****N. Coquelle** (College 8 Secretary)

College 8 focuses on biological samples, using a large palette of techniques and instruments to unravel molecular structure and link it to their function and/or dynamics. Neutron crystallography (D19, LADI and soon DALI) provides a unique technique for visualising hydrogen/deuterium atoms of proteins and finely understanding their catalytic mechanism or binding of small molecules. Studies in solutions are performed using the SANS machines (D11, D22 and D33); taking advantage of the deuteration, signals from a molecular type (DNA vs protein, for example) can be masked out. Reflectometers (Figaro, D17) as well as the diffractometer D16 are excellent instruments for studying the properties of bio-mimicking surfaces (model lipidic bilayers) and how some macromolecules can interact with and/or modify these surfaces. Finally, the set of neutron spectrometers (IN15, IN13, IN11) is used to gain insight into the dynamics of these biological system over a large range of time and q .

Multiple laboratories are available on the EPN campus to help with sample preparation, e.g. the D-lab for the perdeuteration of biological molecules as well as the EMBL biology laboratories for specific sample preparation. Also, the PSB platform and the PSCM offer a large variety of complementary techniques to further characterise samples.

COLLEGE 9 – SOFT CONDENSED MATTER**I. Hoffmann** (College 9 Secretary) and **Ph. Guiffré** (focus group Secretary)

More than 200 proposals in the last two proposal rounds underline both the high level of overall activity in the field of soft condensed matter and the great demand for neutrons. In 2018 we saw a sustained trend in the use of custom-made sample environments, allowing the study of ever more complex systems. For example, a new confinement sample cell for the reflectometer FIGARO and the small-angle scattering instrument D22 has been commissioned. Additionally, a project to combine neutron reflectometry with infrared spectroscopy and ellipsometry was approved by the College. Recently, microfluidic-SANS measurements have been performed on D22. This opens up the possibility of using SANS as a fast and efficient tool for screening large areas of the phase diagram in complex multicomponent systems. This will be very useful for industrial applications, where a quick overview of many different sample compositions is often required. Soft matter experiments continue to benefit from the facilities provided by the Partnership for Soft Condensed Matter (PSCM) which allow users to obtain a preliminary characterisation of their samples, thereby ensuring optimal use of their neutron beamtime.

More information on the support facilities cited here can be found on p.106.



Derek Logan. British and Swedish Department of Biochemistry and Structural Biology, Lund University, Sweden
‘We’ve been using neutrons at the ILL and other sources for six years now, after two-and-a-half decades of purely X-ray crystallography. This has opened up a whole new world for me.’

First study of galectin proteins with neutrons, guiding future drug development

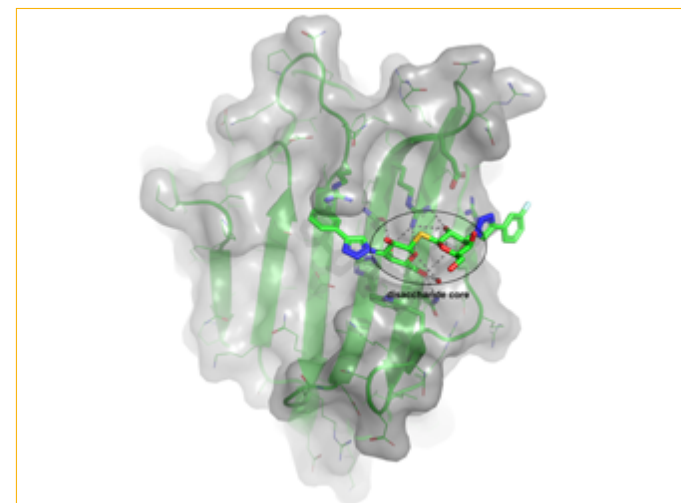
Quasi-Laue diffractometer LADI-III

MaNDi instrument at Oak Ridge

National Laboratory

BIODIFF instrument at MLZ in Garching

Galectins are a large protein family found in all higher organisms. Galectin dysfunction is involved in a variety of diseases, including cancer, inflammation and diabetes. Galectins are thus highly attractive drug targets. One common feature of all successful inhibitors to date is that they are based around a disaccharide core, *i.e.* two sugar units joined together. In an attempt to understand why, we probed the hydrogen-bonding patterns in the substrate binding site of galectin-3 using neutrons.



AUTHORS

D.T. Logan (Lund University, Sweden)
M. Blakeley (ILL)
E. Oksanen (ESS-ERIC, Lund University, Sweden)

ARTICLE FROM

J. Med. Chem. (2018)—doi: 10.1021/acs.jmedchem.8b00081

REFERENCES

- [1] L. Johannes, R. Jacob and H. Leffler, *J. Cell. Sci.* 9 (2018) 10.1242/jcs.208884
- [2] G.A. Rabinovich *et al.*, *J. Scand. Immunol.* 66 (2007) 143
- [3] G. Pugliese *et al.*, *Clin. Chem. Lab. Med.* 52 (2014) 1413
- [4] D. Laaf, P. Bojarová, L. Elling and V. Křen, *Trends Biotechnol.* (2018) Nov 6. pii: S0167-7799(18)30264-6—doi:10.1016/j.tibtech.2018.10.00

The ubiquitous protein family known as galectins has 15 members in mammals, and is defined by the affinity that all its members have for glycans containing β -D-galactoside groups [1]. One of the most studied members is human galectin-3, found in both the nucleus and the cytoplasm of cells, and also secreted to the outside of cells where it interacts with β -galactoside-containing glycoproteins and glycolipids, *e.g.* in glycosylated proteins. Galectin-3 consists of two domains. The N-terminal one is involved in higher order oligomerisation, a characteristic unique among galectins [1], through an as yet unknown mechanism. This is followed by a C-terminal carbohydrate-recognition domain.

Human galectin-3 is a current pharmaceutical target as it is involved in various major diseases, such as inflammation, cancer proliferation and metastasis, and diabetes [2, 3]. The galectin-3 inhibitor Td139 is about to enter phase II/III clinical trials for the treatment of idiopathic pulmonary fibrosis. We and others have determined many high-resolution X-ray crystal structures of the C-terminal domain of galectin-3 (galectin-3C) in complex with synthetic ligands, as part of the structure-based design of new inhibitors [4]. The most successful of these are invariably based on the natural substrate lactose, or the very similar dithiogalactoside. Instead of modifications to the disaccharide core, affinity has been enhanced through the exploration of additional adjacent binding pockets. We wanted to understand why the disaccharide core is so important in terms of hydrogen-bond directionality.

Figure 1

Binding of the drug candidate Td139 to the carbohydrate recognition surface of galectin-3 (from PDB entry 5H9P). The Td139 molecule is shown in stick representation, as are important residues in the shallow binding groove involved in interactions with the ligand. The disaccharide core on which all the most potent galectin-3 inhibitors to date are based is indicated by an oval.

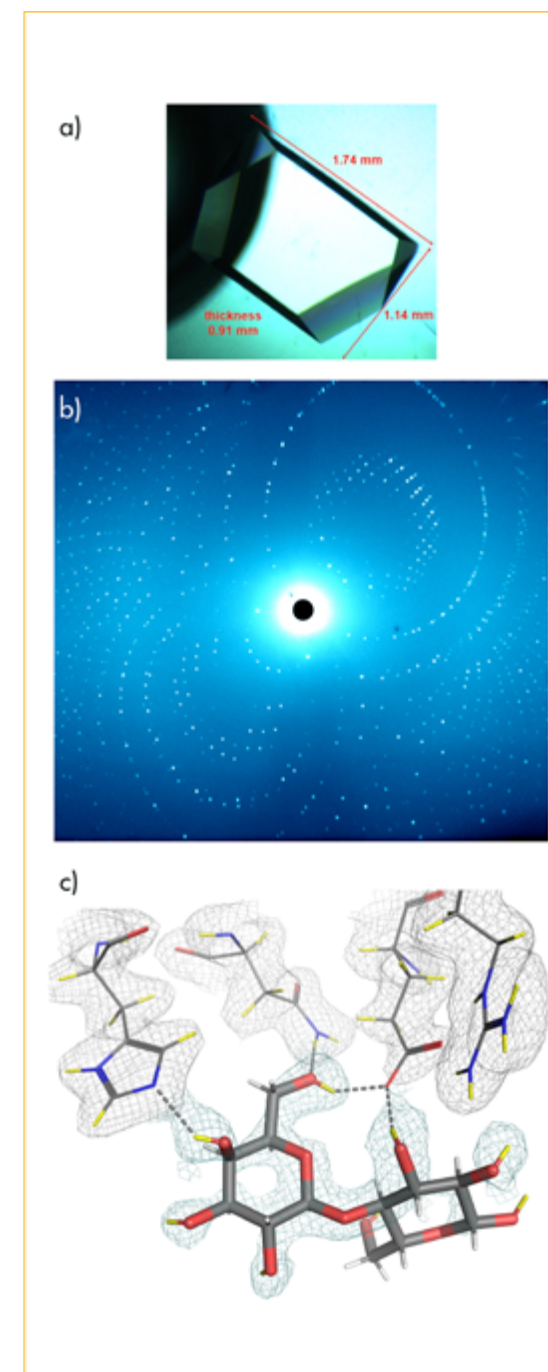


Figure 2

- a) The galectin-3C crystal used to collect data for the complex with lactose at LADI. The volume of this crystal was 1.8 mm³.
- b) Part of the diffraction pattern from this crystal, which extended to 1.7 Å resolution. The increase in the crystal size from 0.4 mm³ to 1.8 mm³ reduced data collection time by a factor of 3.5 and increased the resolution.
- c) The nuclear density map for the complex of galectin-3C with lactose. The protonation states of all amino acid side chains in the binding site are clearly defined, as are three critical hydrogen bonds from hydroxyl groups on the upper face of lactose to the protein. The high degree of tailoring of the protein surface to the exact hydrogen-bonding pattern of the natural disaccharide confirms that drug design strategies have been wise to include this core in all developed inhibitors.

The relatively polar, surface-exposed ligand binding site of galectin-3 contains several residues that interact with the ligands through hydrogen bonds (figure 1), as well as a number of water molecules. Despite it being possible to consistently obtain very high-resolution X-ray data (up to 0.86 Å), the geometries of key hydrogen bonds in the binding site remained ambiguous. Experimentally determined hydrogen atom positions could also provide an unambiguous foundation for molecular dynamics simulations, free-energy perturbation calculations and quantum chemical calculations in future drug design efforts. To find the hydrogen atoms, we thus turned to neutron crystallography. In order to obtain good data from our initial, modestly-sized crystals, we worked with perdeuterated galectin-3C from the outset. Our first diffraction patterns from crystals of galectin-3C in complex with the natural ligand lactose were obtained at LADI-III in 2012, from crystals measuring about 0.35 mm³ that diffracted to 1.9 Å resolution. However, the data collection times were prohibitively long: 16 days for a complete dataset. By optimising crystal growth over the following couple of years we were able to obtain crystals of up to 1.8 mm³, which reduced the data collection time at LADI to six days and increased the resolution to 1.7 Å. These data were combined with data from the MaNDi instrument at Oak Ridge National Laboratory in order to obtain data of exceptional completeness. We also obtained data for ligand-free galectin-3C at LADI-III in 2016, and a complex with the non-natural ligand glycerol from the BIODIFF instrument at MLZ in Garching in 2015. Thus, the final analysis built on data from a number of neutron sources, although the data from LADI-III were of key importance.

The neutron crystal structures of galectin-3C in complex with lactose and glycerol, as well as without ligand, highlighted the exquisite fine-tuning of hydrogen bonding from protein atoms to match the exact geometry of the natural disaccharide ligand. All the polar oxygen atoms on the ‘inside’ of the ligand are involved in highly directional hydrogen bonds. A common method for discovering new protein inhibitors is ‘fragment screening’, in which libraries of small molecular fragments (typically under 300 Da) are screened for weakly-binding hits that are then developed into larger, more potent inhibitors. It is likely that such libraries, which are often dominated by aromatic moieties, would be especially effective in finding new drugs against the shallow, hydrophilic binding sites of galectins, which are exquisitely tailored to recognise the hydrogen-bonding patterns on their carbohydrate ligands. It thus appears wise to continue the current trend of developing inhibitors based on disaccharide cores.



Timothy C. Mueser. American Department of Chemistry and Biochemistry, University of Toledo, Toledo, Ohio USA
‘We use biophysical methods to analyse enzyme mechanisms and transient complexes. A recent emphasis on neutron crystallography has led us to use the microgravity environment on the International Space Station to obtain large uniform crystals necessary for neutron diffraction.’

Re-writing biochemistry textbooks: neutrons observe protons critical for a vitamin B₆-dependent enzyme function

Quasi-Laue diffractometer LADI-III
IMAGINE diffractometer at Oak Ridge
National Laboratory

Vitamin B₆, or pyridoxine, and its derivatives are involved in neurotransmitter synthesis, amino acid metabolism and a plethora of other physiological pathways in all known living organisms. When vitamin B₆ is derivatised inside cells, a very powerful co-factor, pyridoxal 5'-phosphate or PLP, is produced, which is used by many enzymes to catalyse various biochemical transformations (**figure 1**). In fact, enzymes that are dependent on PLP for their function are responsible for ~4 % of all classified enzymatic activity in nature. The PLP-dependent enzymes catalyse over 150 different chemical reactions, some of which do not even have analogues in organic chemistry. Moreover, the considerable dependence of micro-organisms on the action of these enzymes makes them good targets for novel antimicrobial drugs. The diverse chemistry performed by these enzymes is not well understood. Additionally, to understand PLP-dependent enzymes' specificity, *i.e.* how they facilitate so many disparate chemical reactions using a single co-factor, locations and movement of hydrogen atoms need to be mapped experimentally along the reaction pathways. Our recent published study [1] demonstrated the power of macromolecular neutron crystallography to accurately pinpoint hydrogen atoms and to overturn long-held views on the catalytic mechanism of a PLP-dependent enzyme aspartate aminotransferase—a classic biochemistry textbook example.

AUTHORS

S. Dajnowicz and T.C. Mueser (University of Toledo, USA)
R.C. Johnston, J.M. Parks, K.L. Weiss and A. Kovalevsky (Oak Ridge National Laboratory, Tennessee, USA)
M.P. Blakeley (ILL)
D.A. Keen (ISIS, UK)
O. Gerlits (University of Tennessee, Tennessee, USA)

ARTICLE FROM

Nat. Commun. [2017]—doi: 10.1038/s41467-017-01060

REFERENCES

- [1] S. Dajnowicz, R.C. Johnston, J.M. Parks, M.P. Blakeley, D.A. Keen, K.L. Weiss, O. Gerlits, A. Kovalevsky and T.C. Mueser, Nat. Commun. 8 [2017] 955
- [2] S. Dajnowicz, J.M. Parks, X. Hu, R.C. Johnston, A.Y. Kovalevsky and T.C. Mueser, ACS Catal. 8 [2018] 6733
- [3] Lehninger Principles of Biochemistry, Eds. D.L. Nelson and M.M. Cox, by W. H. Freeman & Co. New York, 7th Edition, 2017, pp. 679–682.

Aspartate aminotransferase is crucial for amino acid metabolism, reversibly converting L-aspartic and L-glutamic amino acids. The study aimed to locate and reveal movement of hydrogen atoms within the enzyme's active site in two states: before and after substrate binding, called internal aldimine and external aldimine, respectively. Internal aldimine is a Schiff base generated when the PLP co-factor reacts with the enzyme's catalytic lysine residue. External aldimine is similar, but the Schiff base connection is with the nitrogen of a substrate amino acid (**figure 1**). For this study, room-temperature neutron crystallographic experiments were carried out on the LADI-III diffractometer at the ILL and the IMAGINE diffractometer at the High Flux Isotope reactor at Oak Ridge National Laboratory. Neutron crystallography is uniquely able to provide accurate locations of hydrogen atoms in a biological macromolecule. To trap the enzyme in the substrate-bound, external aldimine state and directly visualise hydrogen atoms, a pseudo-substrate, α -methylaspartic acid, was used.

The conventional catalytic mechanism for aspartate aminotransferase is depicted in **figure 2**. It shows protonation of the Schiff base, the phenolic oxygen and the pyridine nitrogen in both the internal and external aldimine states, while the approaching substrate amino acid is depicted protonated at the N-terminal amino group. How the substrate is deprotonated to obtain a reactive amine and where hydrogens move when the latter attacks the carbon of the internal aldimine Schiff base to generate the external aldimine, was not known. Now, the two neutron structures of aspartate aminotransferase provide the answers, requiring biochemists to re-think this enzyme's catalytic mechanism.

The neutron structure of aspartate aminotransferase in the internal aldimine state showed the presence of a hydrogen atom attached to the pyridine nitrogen of the PLP co-factor, whereas neither the phenolic oxygen nor the Schiff base nitrogen was protonated (**figure 3**). When the pseudo-substrate was soaked into the crystal, the external aldimine formed in which the Schiff base nitrogen

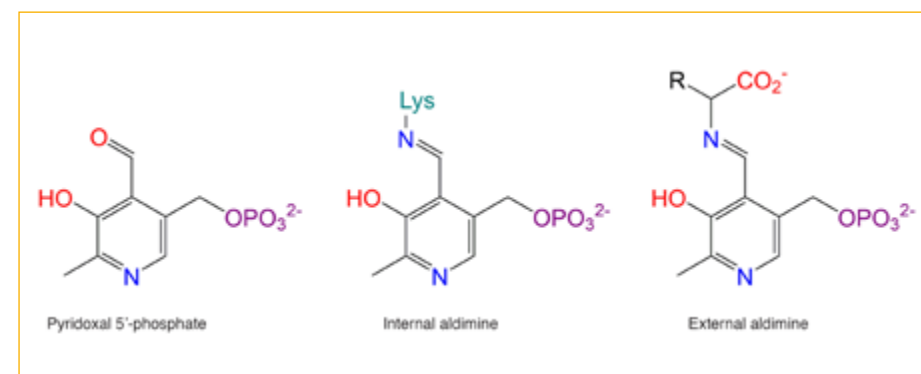


Figure 1

Chemical structures of pyridoxal 5'-phosphate (PLP) co-factor and its covalent adducts with the catalytic lysine (Lys) residue and a substrate (R is $-\text{CH}_2\text{COO}^-$ for L-aspartic acid).

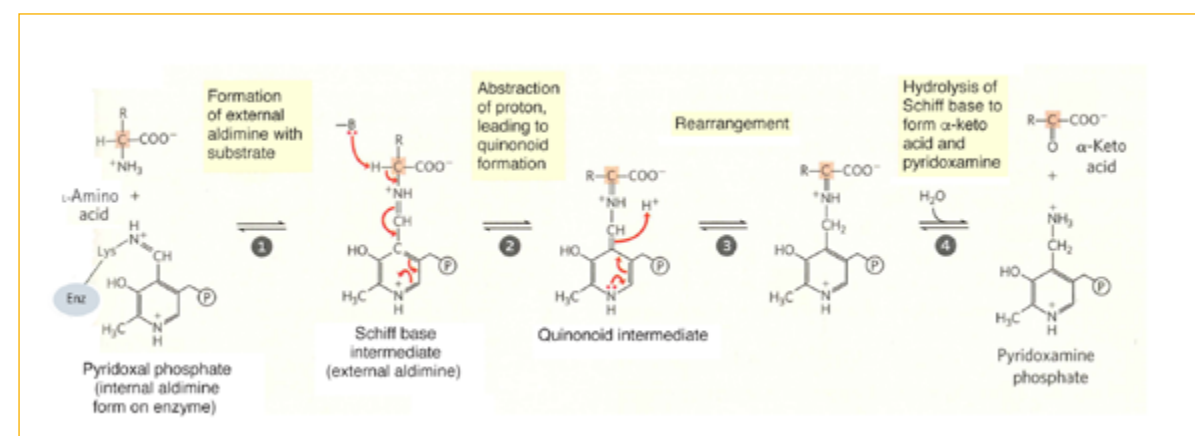


Figure 2

Conventional mechanism of aspartate aminotransferase [3]. The neutron structures revealed that protonation states of the phenolic oxygen and the Schiff bases are incorrect in the internal and external aldimine states.

was now protonated, while keeping the protonation states of the pyridine nitrogen and the phenolic oxygen unchanged. This could only happen if the substrate came in as a zwitter-ion, with the N-terminal nitrogen protonated and the C-terminal carboxylic group deprotonated. Quite unexpectedly, the Schiff base hydrogen of the external aldimine was observed located halfway, and thus shared, between the nitrogen and an oxygen of the carboxylate in an apparent low-barrier hydrogen bond.

Quantum chemistry calculations [1, 2] using the neutron structures to construct accurate theoretical models have

demonstrated no involvement of the ground state strain or destabilisation to explain the power of aspartate aminotransferase, overturning previous mechanistic proposals. Instead, favourable stereo-electronic effects in the internal and external aldimine states contribute significantly to the enzyme's ability to lower the transition state energy, increasing the rate of catalysis by as much as 10^{12} times.

These results demonstrate that neutrons are indispensable for biochemical investigations to identify the molecular determinants of the catalytic power of enzymes.

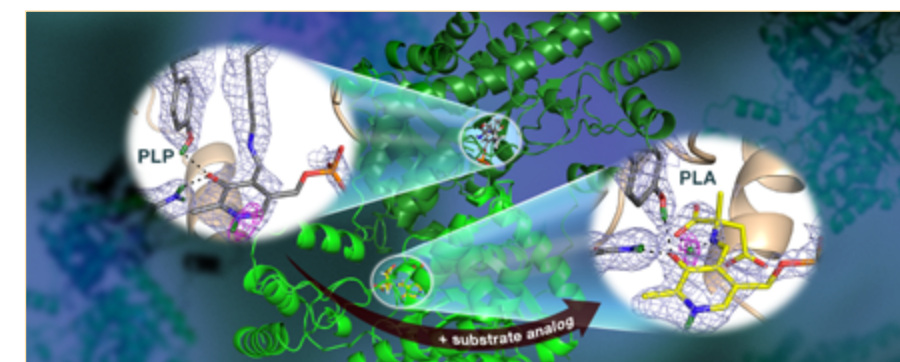


Figure 3

The neutron structures of aspartate aminotransferase in the internal (**left**) and external (**right**) aldimine states. The nuclear density map for the PLP co-factor and surrounding residues is shown as a grey mesh. The omit nuclear density map (magenta mesh) shows exact locations of hydrogen atoms observed as deuteriums.



Lourdes Marcano, Spanish Universidad del País Vasco (UPV/EHU), Spain 'Small-angle neutron scattering is a useful method for understanding the underlying mechanisms of complex natural structures such as magnetosome chains.'

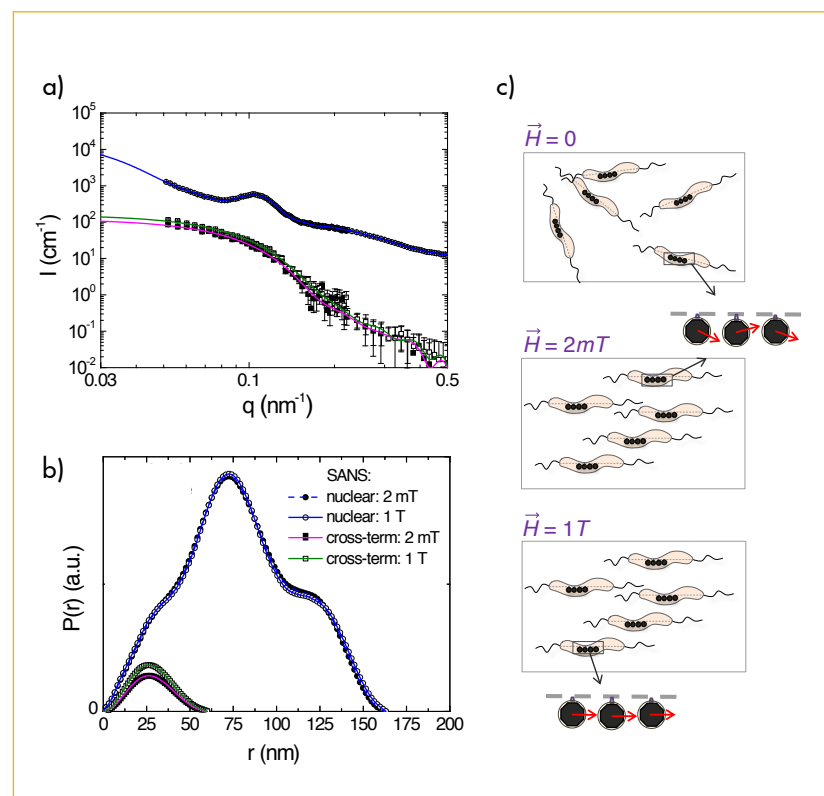
On the magnetosome chain configuration: a natural magnetic nanostructure

Small-angle neutron scattering diffractometer D33

The potential use of magnetotactic bacteria as biorobots makes comprehension of the magnetosome chain configuration an issue of paramount importance. Rather than the *a priori* expected straight lines, magnetosome chains present a helical-shaped structure. This configuration has been investigated by polarised small-angle neutron scattering. Our experimental and theoretical results suggest a mechanism of chain formation arising from competition between the dipolar interaction of magnetosomes within the chain and the forces exerted on each particle by the cytoskeleton.

Figure 1

- a)** Field-dependence of the nuclear scattering intensities $I_{nuc}(q)$ and cross-terms $I_{cross}(q)$ at 2 mT and 1 T, respectively.
b) Pair-distance distribution function $P(r)$ obtained by indirect Fourier transform of the 1D scattering intensities in (a).
c) Schematic representation of the two-step magnetisation process.



AUTHORS

I. Orue, L. Marcano, A. García-Prieto, A. García Arribas, A. Muela and M.L. Fdez-Gubieda (University of País Vasco, Leioa, Spain)
 P. Bender (University of Luxembourg, Luxembourg)
 S. Valencia and M.A. Mawass (Helmholtz-Zentrum Berlin, Germany)
 L. Fernández Barquín (CITIMAC, University of Cantabria, Santander, Spain)
 D. Gil-Cartón (CIC bioGUNE, CIBERehd, Derio, Spain)
 D. Alba Venero (ISIS, Didcot, UK)
 D. Honecker (ILL)

ARTICLE FROM

Nanoscale (2018)—doi: 10.1039/c7nr08493e

REFERENCES

- [1] R. Blakemore, *Science* 190 (1975) 377
 [2] A. Muela *et al.*, *J. Phys. Chem. C* 120 (2016) 24437
 [3] S.R. Mishra *et al.*, *Nanoscale* 8 (2016) 1309
 [4] D. Honecker *et al.*, *Eur. Phys. J. B* 76 (2010) 209

Magnetospirillum gryphiswaldense is an aquatic micro-organism able to biomineralise high-quality magnetite nanoparticles called magnetosomes. The bacteria contain a variable number of 45 nm-sized cuboctahedral magnetite magnetosomes arranged in a chain [1]. Since magnetosomes are single magnetic domains, the chain behaves like a large, permanent magnetic dipole able to orient all the bacteria along Earth's magnetic field in order to swim towards the riverbeds they inhabit.

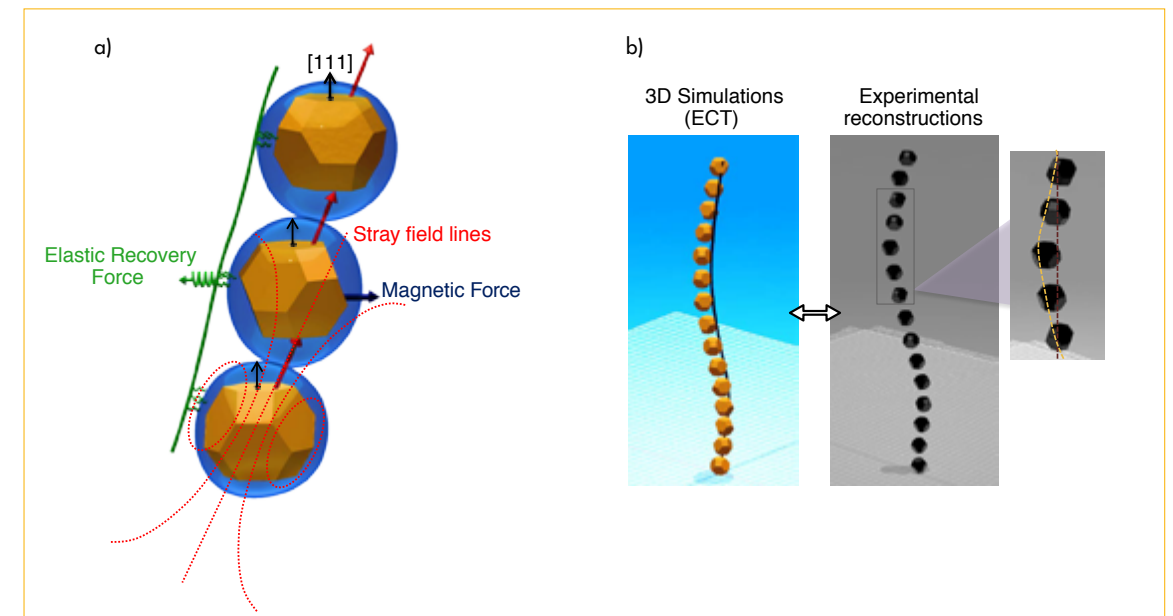


Figure 2

- a)** Schematic representation of the forces involved in the construction of the chain.
b) Experimental reconstruction from ECT images and 3D simulation of the chain.

The magnetosome chain is a natural paradigm of 1D magnetic nanostructure. Due to the large magnetic anisotropy, such arrangements show potential for biomedical applications [2] and actuation devices such as nanorobots [3]. Rather than displaying straight lines, magnetosome chains are slightly bent, as demonstrated by electron cryotomography (ECT). This complex structure must have an effect on the magnetic behaviour of the chain. The present study was devoted to shedding light on the underlying mechanisms that determine the arrangement of the magnetosomes and, consequently, the geometry of the chain. With this aim we explored, on a bacterial colloid, the orientation of the magnetic moments using the small-angle neutron scattering instrument D33 with longitudinal neutron-spin analysis (POLARIS). The major advantage of using POLARIS lies in the proper separation of coherent nuclear and magnetic scattering by measuring the two non-spin-flipped (nsf) intensities and two spin-flipped (sf) cross-sections.

Figure 1a presents the purely nuclear scattering intensities $I_{nuc}(q)$ determined by integration of the nsf channels in 10° sectors along the applied field direction for two different field strengths of $\mu_0 H = 2 \text{ mT}$ and 1 T , respectively. The indirect Fourier transform of $I_{nuc}(q)$ results in the pair-distance distribution function $P(r)$ displayed in figure 1b. The nuclear intensities $I_{nuc}(q)$ and $P(r)$ for the two fields are identical, showing that at 2 mT the bacteria are already

fully aligned in the field direction (see figure 1c). On the other hand, the cross-term $I_{cross}(q)$ obtained by integration of $I^-(q)-I^+(q)$ in 10° sectors around $\Theta = 90^\circ$ ($q \perp H$) yields information on the polarisation-dependent nuclear-magnetic interference scattering [4]. The cross-terms $I_{cross}(q)$ detected at 2 mT and 1 T (figure 1a) and the extracted distribution functions (figure 1b) display the same functional form. However, the absolute values of $P(r)$ at 2 mT over the whole r -range are reduced by a factor of 0.83 compared with a saturating field of 1 T. In combination with isothermal magnetisation measurement, these results suggest two individual steps in the magnetisation process: chain alignment, followed by coherent rotation of the magnetic moments within a magnetosome into the field direction. At 2 mT, the nanoparticle magnetisation deviates by 20° from the chain axis, which coincides with the crystallographic easy axis of magnetite along [111].

The direction of the net magnetic moment, which remains along the chain axis, is not affected. However, the tilt turns out to be the key to understanding the arrangement of magnetosomes in helical-shaped chains. The chain shape can be reproduced by considering an interplay between magnetic dipole-dipole interactions, ruled by the orientation of the magnetosome magnetic moment, and a lipid-/protein-based elastic recovery force caused by the connection of the magnetosome with cytoskeletal filaments that traverse the cell (see figure 2).



Martine Moulin. French Life Sciences group at the ILL
 'I work in support of the user programme of the Deuteration Laboratory. I have just received my PhD from Keele University in the UK. My thesis work, carried out in collaboration with Uppsala University (Sweden) and the Universities of Namibia and Botswana, focused on the biophysical and structural characterisation of seed proteins from the *Moringa oleifera* plant, in the context of potential applications for water purification in developing areas of southern Africa.'

Deuterated cholesterol for the study of lipids and lipid cargoes in health and disease

Deuteration facility D-Lab, fluid interfaces grazing angles reflectometer FIGARO, Diffractometer D16 and Small-angle scattering diffractometer D22

Cholesterol is well known for its significance in health and disease, and in particular for its implication in the formation of atherosclerotic plaques in heart disease and stroke—major first-world killers. The risk factors underlying these pathologies are well known to us, through routine measurements of low-density lipoprotein (LDL—'bad cholesterol') and high-density lipoprotein (HDL—'good cholesterol') in blood tests. There is considerable scientific interest in characterising the exchange kinetics between LDL and HDL particles, which is believed to be important for an understanding of the development of plaques in blood vessels.

AUTHORS

M. Moulin (ILL)

ARTICLE FROM

Chem. Phys. Lip. (2018)—doi: 10.1016/j.chemphyslip.2018.01.006

REFERENCES

- [1] M. Moulin, G.A. Strohmeier, M. Hirz, K.C. Thompson, A.R. Rennie, R.A. Campbell, H. Pichler, S. Maric, V.T. Forsyth and M. Haertlein, Chem. Phys. Lip. 212 (2018) 80
- [2] S. Waldie, T.K. Lind, K. Browning, M. Moulin, M. Haertlein, V.T. Forsyth, A. Luchini, G.A. Strohmeier, H. Pichler, S. Maric and M. Cárdenas, Langmuir 34 (2018) 472
- [3] A. Luchini, R. Delhom, B. Demé, V. Laux, M. Moulin, M. Haertlein, H. Pichler, G.A. Strohmeier, H. Wacklin and G. Fragneto, Colloids Surf. B. Biointerfaces 168 (2018) 126
- [4] S. Waldie, M. Moulin, L. Porcar, H. Pichler, G.A. Strohmeier, M. Skoda, V.T. Forsyth, M. Haertlein, S. Maric and M. Cárdenas, Sci. Rep. (submitted)

What is less well known is the fact that cholesterol is a vital constituent of mammalian membranes, and whose presence in lipid bilayers has important structural consequences of direct relevance to diffusional properties and ordering within lipid bilayers. These factors, along with the nature of the lipid systems involved (and in particular the degree of lipid tail saturation), are thought to influence the location of cholesterol, which may be toward the head of the lipid molecule (in the case of saturated lipid membranes) or toward the inner interface between the two bilayer leaflets (polyunsaturated lipids). Cholesterol is also centrally involved in the structure and behaviour of lipid rafts, which are believed to be of importance in physiological events such as signal transduction.

Neutron diffraction and neutron reflection are in many ways ideal probes for investigating lipid interactions with molecules such as cholesterol. However, the scope of these methods is limited by the fact that the contrast (the difference in scattering length density of one component with respect to another) between protiated lipid and protiated cholesterol is very low; it is therefore extremely difficult to view either component independently of the other.

Cholesterol is a challenging molecule to produce by chemical synthesis, and the availability of perdeuterated cholesterol has been a serious limitation for neutron scattering work in this area. In collaboration with colleagues at the University of Graz (Austria) and Malmö University (Sweden), staff from the ILL's Life Sciences Group have developed a biosynthetic method for producing perdeuterated cholesterol using the yeast *Pichia pastoris* (Moulin *et al.* [1]). Natural ('wild type') yeast of this type does not produce cholesterol, but instead produces a related molecule called ergosterol.

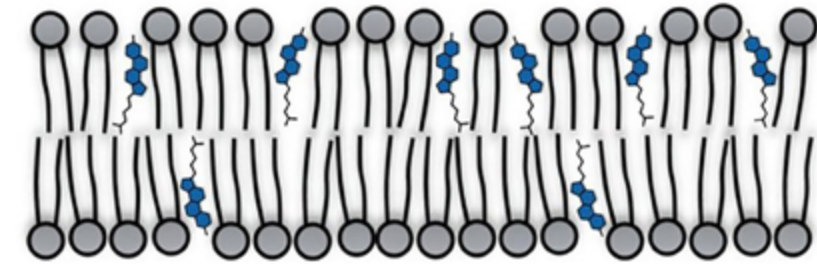


Figure 1

The location of deuterated cholesterol in a membrane bilayer, as visualised by neutron reflectometry.

The approach used here was to use a metabolically engineered strain of *Pichia* to alter the biosynthesis pathway such that cholesterol is produced as the final product in place of ergosterol. The yeast system is grown in high cell density cultures using heavy water and a deuterated carbon source. The perdeuterated cholesterol is purified using chromatography, and characterised by gas chromatography and mass spectrometry—yielding a final product that is deuterium-labelled to a level greater than 98 %.

There has been a great deal of interest from ILL users in exploiting the availability of fully deuterated cholesterol for a wide variety of applications. The initial synthesis and characterisation work described by Moulin *et al.* demonstrated the effectiveness of the labelling and the type of structural information that could be yielded in neutron studies. Waldie *et al.* [2] have since used this labelling regime to analyse the location of cholesterol within lipid bilayers composed

of a natural mixture of phosphatidylcholine (PC), demonstrating that cholesterol is located closer to the lipid head–tail interface rather than in the centre of the core of the bilayer (**Figure 1**). Luchini *et al.* [3] have also used perdeuterated cholesterol to carry out the structural characterisation of lipid extract. Other ongoing research includes investigations into lung surfactants at the air–water interface, and Raman microscopic work on the migration and distribution of cholesterol in mammalian cells.

This biosynthetic approach for producing cholesterol has since been developed by Waldie *et al.* [4] to allow the routine production of 'matchout-deuterated' cholesterol, whose scattering length density is matched to that of 100 % D₂O; this will be invaluable in SANS and reflectometry studies of membrane proteins studied in nanodiscs, allowing molecular models to be built of protein systems in a native habit and free of detergents.

Cholesterol plaques blocking a blood vessel in atherosclerosis.





Emanuel Schneck. German Biomaterials Department, Max Planck Institute of Colloids and Interfaces, Potsdam
‘Neutron reflectometry is the ideal tool for the structural characterisation of complex biomolecular layers with high depth resolution.’

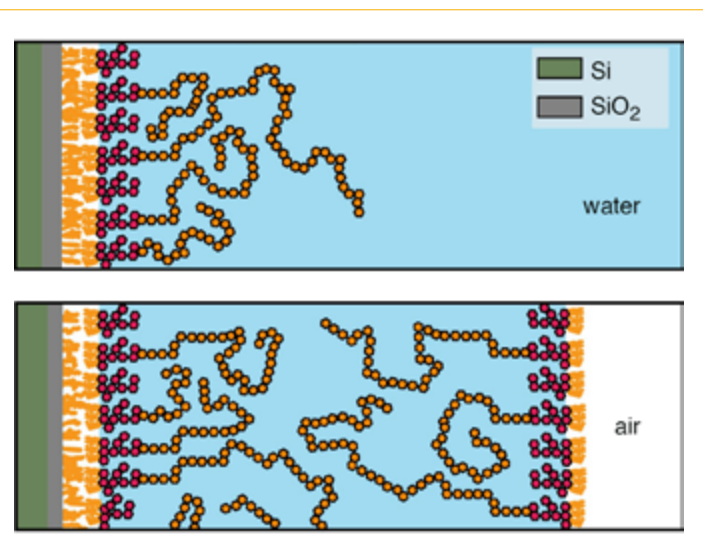
Sugar polymers at the outermost surface of bacteria

Vertical reflectometer D17

Lipopolysaccharide (LPS) molecules form the outer surfaces of Gram-negative bacteria, where they expose oligo- and polysaccharides to the aqueous environment. This structurally complex molecular layer is of great scientific interest as it mediates the interaction of bacteria with antimicrobial agents as well as neighbouring bacteria in colonies. Structural studies on LPS surfaces, however, have to date used chemically simple LPS molecules, so-called rough mutant LPS. Here, by using neutron reflectometry (NR), we have structurally characterised monolayers of wild-type LPS form featuring strain-specific O-side chains in contact with aqueous solutions and under controlled interaction conditions. The model used for the reflectivity analysis gave access to the volume fraction profiles of all the chemical components. The saccharide profiles were found to be bimodal, with dense inner oligosaccharides and more dilute, extended O-side chains. For interacting LPS monolayers, NR revealed the distance-dependent saccharide conformation.

Figure 1

top) Schematic illustration of a single, solid-supported LPS monolayer in aqueous buffer. The solid surface is hydrophobically functionalised with octadecyltrichlorosilane. All LPS molecules comprise the inner oligosaccharide, while only a certain fraction display O-side chains.
bottom) Schematic illustration of two interacting LPS monolayers in a double-monolayer configuration.



AUTHORS

E. Schneck, I. Rodriguez Loureiro and V.M. Latza
(Max Planck Institute of Colloids and Interfaces, Potsdam, Germany)
G. Fragneto (ILL)

ARTICLE FROM

Biophys. J. (2018)—doi: 10.1016/j.bpj.2018.02.014

REFERENCES

- [1] C. Erridge, E. Bennett-Guerrero and I.R. Poxton, *Microbes Infect.* 4 (2002) 837
- [2] E. Schneck, T. Schubert, O.V. Konovalov, B. Quinn, T. Gutsmann, K. Brandenburg, R.G. Oliveira, D. Pink and M. Tanaka, *Proc. Natl. Acad. Sci. USA* 107 (2010) 9147
- [3] L.A. Clifton, S.A. Holt, A.V. Hughes, E.L. Daulton, W. Arunmanee, F. Heinrich, S. Khalid, D. Jefferies, T.R. Charlton, J.R.P. Webster, C.J. Kinane and J.H. Lakey, *Angew. Chem. Int. Ed.* 54 (2015) 11952
- [4] I. Rodriguez Loureiro, V.M. Latza, G. Fragneto and E. Schneck, *Biophys. J.* 114 (2018) 1264

Lipopolysaccharides (LPSs) are the main constituents of the outer monolayer of the Gram-negative bacterial outer membrane [1]. They govern the mutual interaction between neighbouring bacteria in colonies and (undesired) biofilms, and act as protection against harmful molecules. This protection is weakened, however, when divalent cations such as calcium or magnesium are absent from the aqueous environment.

LPS molecules consist of an extremely invariant part that is itself constituted of four to seven hydrocarbon chains and a headgroup composed of the inner oligosaccharide (8-12 sugar rings) that carries a negative net charge. A certain fraction of LPS molecules possess strain-specific O-side chains (OSC) in the form of repetitive oligosaccharide motifs.

The considerable biomedical relevance of Gram-negative bacterial outer-surfaces has motivated numerous structural investigations of LPS layers by X-ray and neutron scattering techniques [2, 3]. These studies have, to date dealt almost exclusively with rough mutant LPSs, neglecting the OSC as an important feature of most bacterial surfaces.

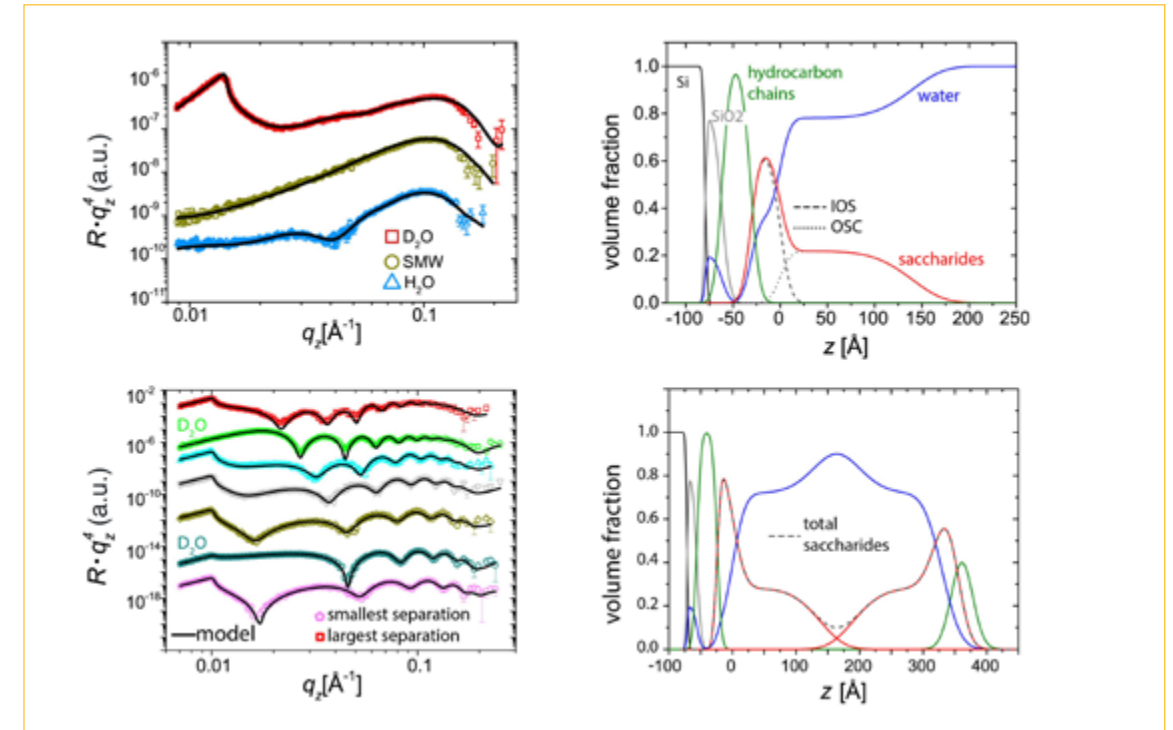


Figure 2

top left) Neutron reflectivity curves (symbols) of a single, solid-supported LPS monolayer obtained with three water contrasts: D₂O, SMW (silicon-matched water) and H₂O. Solid lines indicate the simulated reflectivity curves according to the best-matching parameters in the common model.

top right) The corresponding volume fraction profiles of Si, SiO₂, hydrocarbon chains, inner oligosaccharides (IOS), O-side chains (OSC) and water.

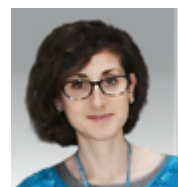
bottom left) Neutron reflectivity curves and simulated reflectivity curves of interacting LPS monolayers for various relative humidities corresponding to different surface separations at r H₂O and D₂O contrasts.

bottom right) Corresponding volume fraction profiles.

In a recent study [4] we prepared single and interacting planar monolayers of wild-type LPS from *E. coli* O55:B5, featuring not only the inner oligosaccharides (IOS) but also the strain-specific OSC. These surfaces realistically mimic the outer surface of Gram-negative bacteria both individually (**figure 1, top**) and when mutually interacting in a colony or biofilm (**figure 1, bottom**). The samples were investigated by NR with contrast variation. The reflectivity curves (**figure 2, left**) were analysed with a parameterised model based on the volume fraction profiles of all chemical components of interest (**figure 2, right**), namely silicon (Si), silicon oxide (SiO₂), hydrocarbon chains, IOS, OSC and water. The saccharide volume fraction profiles exhibit a clearly bimodal distribution consistent with a picture of a dense and compact saccharide layer accommodating the negatively charged IOSs, and a more dilute, extended region accommodating the OSC (**figure 2, right**). The structure of single, solid-supported LPS monolayer (**figure 1, top**) was found to be significantly affected by a depletion of calcium (data not shown). Specifically, the lateral packing is reduced, and water appears to overlap with the hydrocarbon chain region. At the same time, the IOSs become more extended in the perpendicular direction. Both effects can be attributed

to enhanced electrostatic repulsion in the absence of divalent cations. For two opposing LPS surfaces (**figure 1, bottom**), we were able to interpret the corresponding NR curves obtained at various surface separations (**figure 2, bottom left**) with a single model involving global and separation-dependent parameters describing the volume fraction profiles. The analysis revealed that the OSC conformation is nearly unperturbed at the largest separation. The corresponding central water fraction reaches over 90 %. The heterogeneous water release upon surface approach reflects differences in connectivity and chemical nature between the IOSs and the OSC.

The low saccharide fraction at the midplane (**figure 2, bottom right**) demonstrates the existence of a liquid-like aqueous layer between neighbouring bacteria when they are situated side by side, both in the absence of dehydrating pressures and when subject to physiological osmotic pressures. Hydrodynamic pathways for the intercellular transport of small enough molecules can therefore be sustained in colonies and biofilms. At the same time, the observed significant mutual interpenetration of adjacent OSC ‘brushes’ suggests that shear friction between adjacent bacteria is considerable and affects the viscoelastic properties of bacterial biofilms.

**Samantha Micciulla**, Italian ILL

'Scientists have the unique privilege of looking at the most intimate side of nature to learn from its excellence. In my research, understanding the behaviour of supramolecular assemblies at interfaces, as governed by the interactions

between their fundamental constituents, is not only driven by genuine curiosity; it is also motivated by the belief that each small, individual contribution to scientific knowledge is a resounding achievement for a better life on our planet.'

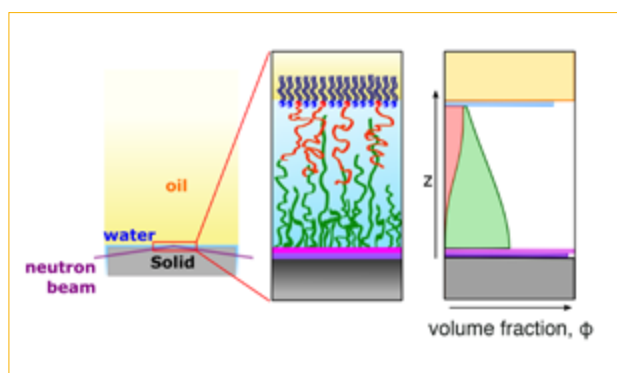
3PhaseNR: a new approach for structural studies of soft interacting interfaces

Fluid interfaces grazing angles reflectometer FIGARO

Interactions between soft interfaces have a major influence on the function of biological entities and the properties of colloidal systems. The nature of such forces can be revealed from the interfaces' structural response to variations in the surface separation, for which surface-sensitive scattering techniques are best suited. We have developed a novel approach for probing distance-dependent structures of soft buried, interacting soft thin films by neutron reflectometry, starting from independent molecular layers at a solid/water and water/oil interface at tuneable interaction distances. A variety of conditions can rapidly be realised by tuning the mutual interaction pressure and, in turn, the distance and molecular structure.

Figure 1

From left to right: schematic representation of the experimental set-up of a solid/liquid/liquid interface, a molecular picture of the interacting interfaces and the volume fraction distribution of components across the interface.

**AUTHORS**

S. Micciulla and Y. Gerelli (ILL)
R.A. Campbell (Manchester University, UK)
E. Schneck (Max Planck Institute of Colloids and Interfaces, Potsdam, Germany)

ARTICLE FROM

Langmuir (2018)—doi: 10.1021/acs.langmuir.7b02971

REFERENCES

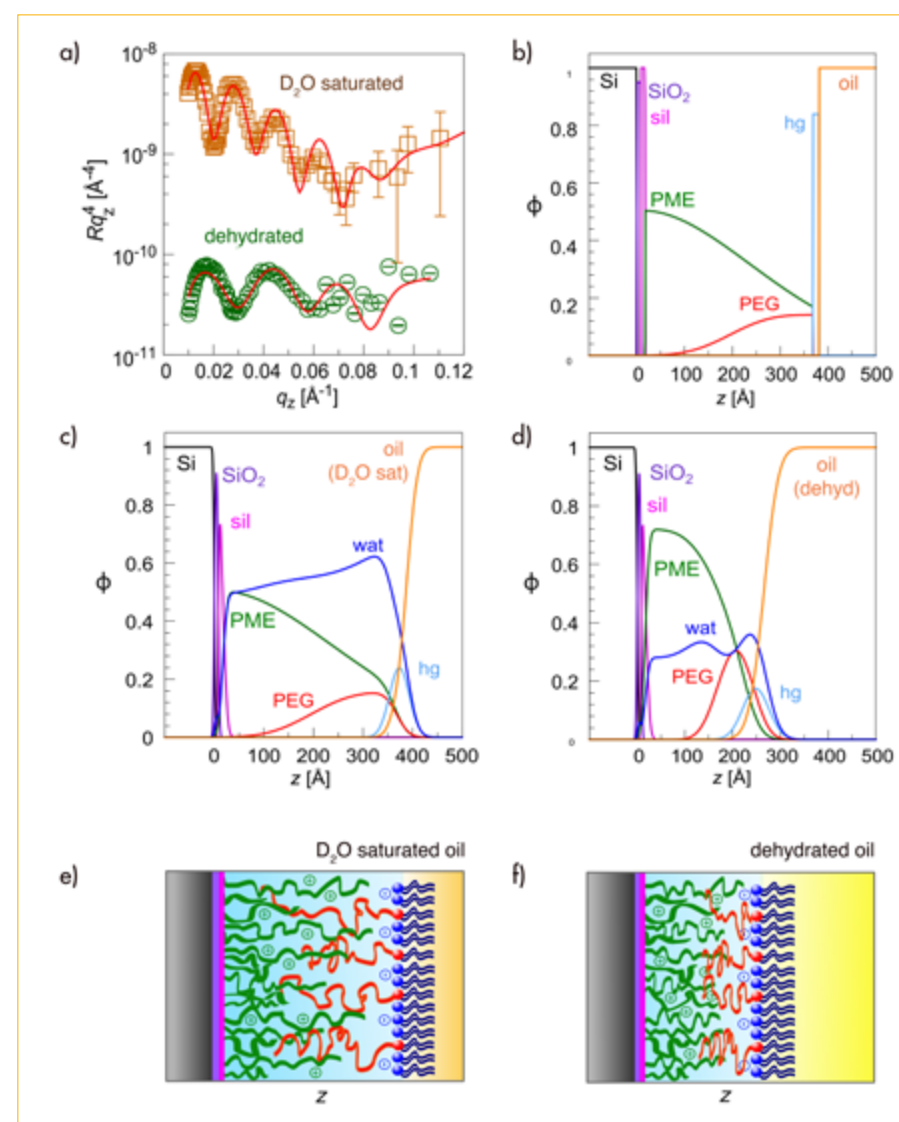
- [1] P.C. Lau, T. Lindhout, T.J. Beveridge, J.R. Dutcher and J.S. Lam, J. Bacteriol. 191 (2009) 6618
- [2] T. Nylander, R.A. Campbell, P. Vandoolaeghe, M. Cardenas, P. Linse and A.R. Rennie, Biointerphases 3 (2008) 3 FB64
- [3] W.M. De Vos, L.L.E. Mears, R.M. Richardson, T. Cosgrove, R.M. Dalgliesh and S.V. Prescott, Rev. Sci. Instr. 83 (2012) 113903
- [4] I. Rodríguez-Loureiro, V.M. Latza, G. Fragneto and E. Schneck, Biophys. J. 114 (2018) 1624

Interactions involving biological membranes govern complex phenomena such as cell adhesion and the formation of bacterial biofilms [1]. Such soft interfaces exhibit a close relation between their interaction properties, in terms of range and strength, and the spatial organisation of the molecules residing at the interface. Molecular conformations and ion distributions show a considerable response when interfaces approach and mass exchange across them occurs [2]. Knowledge of such structural details is thus valuable, and sometimes a prerequisite, to understanding and controlling these interfacial interactions.

Approaches developed so far, using rigid or flexible substrates under compression [3] or surfaces separated by swelling in humid air [4], present certain limitations, such as intolerance to impurities, a restricted range of surface separation and the impossibility of independent layer characterisation prior to their interaction.

Within the framework of a Röntgen-Ångström Cluster grant (3phaseNR), we have developed a new experimental set-up that allows us to bring two arbitrary soft interfaces from non-interacting conditions, *i.e.* macroscopic separation, to controlled interactions at nanometric separation distances (**figure 1**).

As schematically illustrated in **figure 1**, one of the interfaces is created by modifying a solid substrate (solid/liquid interface), the other by functionalisation of a fluid interface between two immiscible liquids (liquid/liquid interface). Planar geometry and the macroscopic size of the contact

**Figure 2**

a) Experimental reflectivity data for the two soft interfaces, the lipid-anchored polymer brush and the solid-grafted polyelectrolyte brush, in contact at full hydration (**top**) and under dehydrated conditions (**bottom**). Solid lines are the best-matching reflectivities from the data analysis.

b) Theoretical model of the volume fraction profiles of all chemical components.

c & d) Best-matching components' volume fraction profiles at full hydration (**c**) and under dehydrated conditions (**d**), according to the solid lines in Panel A. Labels: silicon substrate (Si), silicon oxide (SiO₂), silane (sil), polyelectrolyte brush (PME), lipid-anchored polymer brush (PEG), water (wat), lipid head groups (hg) and oil.

e & f) Schematic illustration of the samples at full hydration (**e**) and under dehydrated conditions (**f**). Reproduced with permission from Micciulla *et al.*, Langmuir 34 (2018), 789.

region enable the use of reflectivity techniques to resolve the molecular-scale structure at different separation (or interaction) distances, which is crucial to highlight the interaction-associated structural properties.

Proof of concept: a lipid-anchored brush at the oil/water interface interacting with a polyelectrolyte brush located at the water/silicon interface was investigated by neutron reflectometry. The chemical nature of the surface components is one of the fundamental parameters for achieving a wide spectrum of interaction scenarios, from no adhesion to strong, nearly dry, adhesion.

A weak adhesion with partial brush interpenetration was observed when the two interfaces achieved contact (**figure 2e**). The highly hydrated brushes kept a stretched conformation, resulting from the balance between the weak, long-range electrostatic attraction of opposite surface charges and the polymer-induced repulsion preventing the collapse of the brush. The application of osmotic stress (**figure 2f**) from water-saturated to

dehydrated oil resulted in significant layer compression and dehydration as a result of a new equilibrium between dehydrating pressure and osmotic pressure from permanent charges in the polyelectrolyte brush.

As demonstrated here, water saturation of the oil can be used as a simple parameter for varying surface separation on long time scales, with the advantage of monitoring the structural response to interfacial forces by reflectometry *in situ*.

Of more general scientific interest, the impact of the proposed approach is its wide applicability to investigating the structure and interactions of soft interfaces in general, including non-specific and specific adhesion of biological membranes as well as molecular exchange. This method may also help to elucidate the lateral distributions of solutes under confinement and the physical mechanisms of foam stability.



Patrick Guenoun, French Laboratoire Interdisciplinaire sur l'Organisation Nanométrique et Supramoléculaire (LIONS) at Université Paris-Saclay (CEA Saclay) 'My research belongs to the experimental soft condensed matter area, focusing on polymers at interfaces for controlling emulsion stabilisation, the orientation of nanocomposites made of plasmonic nanoparticles and copolymer blocks, and omniphobic wetting properties.'

Neutron reflectivity measurements at the oil-water interface for studying stimuli-responsive emulsions

Fluid interfaces grazing angles reflectometer FIGARO

Emulsions are metastable dispersed phases of either oil drops in water (direct emulsions O/W), water drops in oil (inverse emulsion W/O) or even water drops nested in oil drops in water (multiple emulsions, W/O/W). We developed a system based on an emulsion superior stabilisation by a single amphiphilic copolymer PS-*b*-(PS-*stat*-PDMAEMA made of polystyrene (PS) and poly(dimethylaminoethyl methacrylate) (PDMAEMA) moieties. It is capable of stabilising the three kinds of emulsions depending on certain strength conditions [1]. Our system is therefore unique in elucidating how amphiphile conformation is related to emulsion type. This is important for providing molecular guidelines aimed at designing future polymeric emulsions, since these phases are currently used in many applications of encapsulation in pharmacy, food and the cosmetic industry.

AUTHORS

P. Guenoun (University Paris-Saclay, CEA Saclay, France)
M. Protat, N. Bodin-Thomazo and F. Malloggi (CEA, CNRS, University Paris-Saclay, France)
J. Daillant (Synchrotron Soleil, Saint-Aubin, France)
R.A. Campbell (Division of Pharmacy and Optometry, University of Manchester, UK)
G. Fragneto and E.B. Watkins (ILL)
P. Perrin and N. Pantoustier (ESPCI Paris, PSL University, Sorbonne-University, CNRS, France)

ARTICLE FROM

Eur. Phys. J. E (2018)—doi: 10.1140/epje/i2018-11693-8

REFERENCES

- [1] L. Besnard, F. Marchal, J.F. Paredes, J. Daillant, N. Pantoustier, P. Perrin and P. Guenoun, *Adv. Mater.* 25 (2013) 2844
- [2] R.A. Campbell, H.P. Wacklin, I. Sutton, R. Cubitt and G. Fragneto, *Eur. Phys. J. Plus* 126 (2011) 107
- [3] L.T. Lee, D. Langevin and B. Farnoux, *Phys. Rev. Lett.* 67 (1991) 2678
- [4] M. Protat, N. Bodin-Thomazo, F. Malloggi, J. Daillant, R.A. Campbell, F. Fragneto, E.B. Watkins, P. Perrin, N. Pantoustier and P. Guenoun, *Eur. Phys. J. E* 41 (2018) 85

A tool of choice for providing insight into this conformation is neutron reflectometry [2]. However, neutron reflectivity measurements at liquid/liquid interface are rarely performed and have been limited to date to a few particular examples [3]. A dedicated cell was designed and optimised for such a study, with systems in which the oil phase scatters a large number of neutrons because of the dissolved polymer. A sapphire crystal is used in support of a water phase, through which the neutron beam reaches the interface, yet the need to match the water phase's isotopic contrast with that of the sapphire means that it is still partly hydrogenous (10 % v/v H₂O in D₂O) and must be reduced to minimal thickness (**figure 1**). This is possible thanks to the high flux FIGARO (Fluid Interfaces Grazing Angles ReflectOmeter) reflectometer, which has the ability to reflect a collimated beam of neutrons down at a horizontal interface. A particularly high flux configuration can be selected thanks to the use of dephased choppers and the instrument being on a continuous reactor source.

Figure 1

Scheme of the liquid/liquid cell and incident neutron beam. The black part to the left is used for sucking water and modifying the level, while the white Teflon parts are also indicated. Adsorbed polymer chains are indicated on the sapphire (made hydrophilic by plasma cleaning beforehand) and their contribution is taken into account in the data treatment. The main signal comes from the chains adsorbed at the oil-water interface.

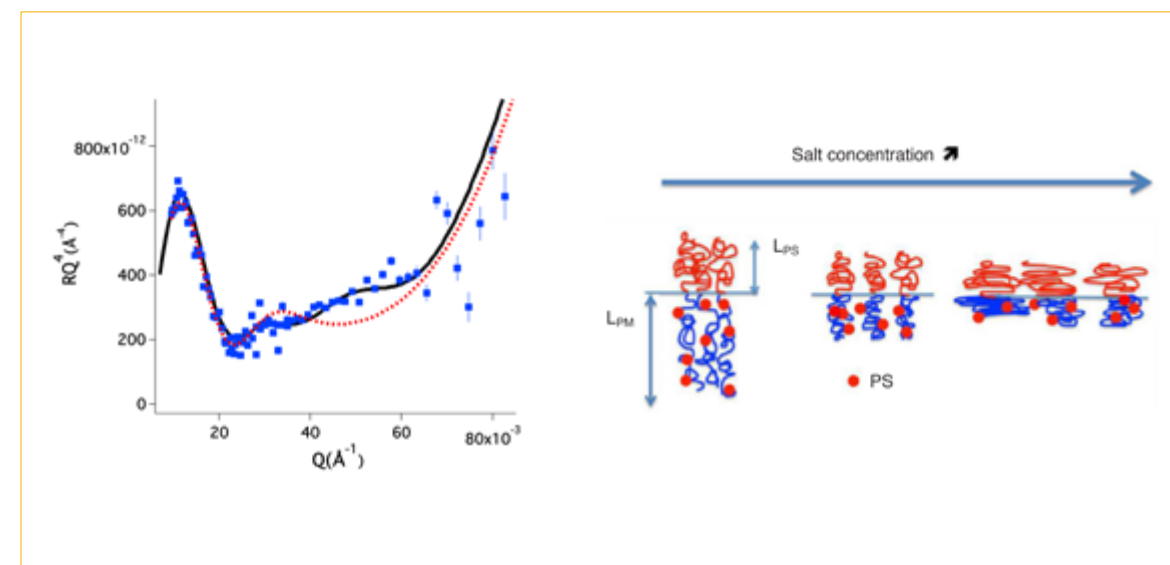
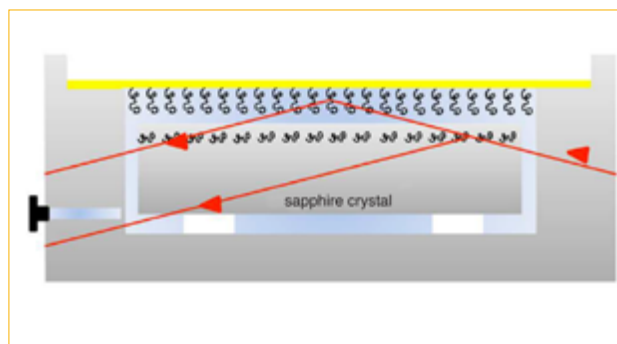


Figure 2

a) Reflectivity (R) data as a function of wavevector Q for the direct emulsion case. Satisfactory fit involving two layers of different polymer densities (full curve) contrary to the dotted curve (one polymer layer). Extensions of layers are on the water side $LWS=183 \text{ \AA}$ and on the oil side $LOS=74 \text{ \AA}$.

b) Sketch of the models with different polymer conformations in agreement with values obtained from the fits. From left to right are presented the direct emulsion case with two extended, charged and neutral brushes on the lower (upper) water (oil) side, the multiple emulsion case where both extensions of chains are roughly similar on each side maintaining a low molecular area, and the inverse emulsion case where the water side is more contracted than the oil side in a larger molecular area. Red balls are used to represent some of the PS monomers included in the hydrophilic (PS-*stat*-PDMAEMA) block: in the direct emulsion case, these PS monomers are assumed to have little interaction between themselves; in the multiple and inverse emulsion cases they act as stickers to make intra- or inter-molecular bridges.

Three cases, corresponding to conditions in which direct, multiple and inverse emulsions are formed, were investigated by varying salt concentration. The reflectivities found corresponding to the conditions described were markedly different, indicating—before any quantitative interpretation of the data—that different chain conformations occur in each case [4]. Data analysis revealed that the observed differences were related to changes in the extensions of the polymer on the water side (LWS) and the oil side (LOS). These results can be understood in terms of changes in conformation, as salt addition screens the charged moieties more and more to the benefit of hydrophobic interactions induced by the PS monomers (**figure 2**).

The exceptional stability and very high reproducibility of formation—a rare feature for multiple emulsions—are consistent with a specific polymer conformation corresponding to a well-defined kind of emulsion. The kinetics and pathway of formation leading to multiple architectures in a single step has still to be explored. The absence of observed multiple emulsions of the O/W/O kind is probably more indicative of a slight asymmetry between bulk phases than a noticeable asymmetry in the polymer interfacial conformation.

Neutron reflectivity measurement at the liquid/liquid interface is an invaluable tool, despite requiring careful calibration procedures, for exploring complex polymer conformations at the oil-water interface. Such an advance was possible thanks to the optimisation of a sample cell involving a macroscopic oil phase suited to measurements at the water-oil interface in a 'reflection down' configuration, and exploiting the high flux FIGARO reflectometer at the ILL. Interpretation of the data is another complex procedure that requires careful consistency checks. Such a procedure was possible here because a model was constructed for refining the parameters. The next experimental challenges will involve better mastering of the wetting of the substrates in order to reach a controlled water thickness.



Yuuya Nagata, Japanese
Kyoto University, Japan
'I am an assistant professor working in Kyoto University, Japan. My research interests are in the development of new chiral materials based on the helical polymers. In order to reveal the intriguing nature of the helical polymers, I am so interested in the use of the neutron beam scattering techniques, including SANS and GENS.'

Elucidating the solvent effect on the switch of the helical chirality of poly(quinoxaline-2,3-diyl)s

Small-angle diffractometer D22

Reversible control of macromolecular helical chirality has attracted increasing attention because of its potential application for new functional materials. In this report, the mechanism of determining helical chirality by chiral side chains was successfully revealed through small-angle neutron scattering (SANS) experiments in conjunction with theoretical calculations.

AUTHORS

Y. Nagata, T. Nishikawa and M. Sugimoto (Graduate School of Engineering, Kyoto University, Japan)
S. Sato (University of Tokyo, Japan)
M. Sugiyama, R. Inoue and N. Sato (Kyoto University Institute for Integrated Radiation and Nuclear Science, Japan)
L. Porcar and A. Martel (ILL)

ARTICLE FROM

JACS (2018)—doi: 10.1021/jacs.7b11626

REFERENCES

- [1] E. Yashima, K. Maeda, H. Iida, Y. Furusho and K. Nagai, *Chem. Rev.* 109 (2009) 6102
- [2] E. Yashima, N. Ousaka, D. Taura, K. Shimomura, T. Ikai and K. Maeda, *Chem. Rev.* 116 (2016) 13752
- [3] Y. Nagata, T. Yamada, T. Adachi, Y. Akai, T. Yamamoto and M. Sugimoto, *J. Am. Chem. Soc.* 135 (2013) 10104

The helix is the most essential and fundamental structural motif of the macromolecule [1, 2]. For over half a century, control of the screw sense of helical macromolecules has attracted considerable attention, owing to the development of unprecedented functional materials. Here, a side-chain-based induction of helicity is advantageous not only because it allows the independent design of the main-chain and side-chain structures, but also because it enables the reversible formation of *P*- (right-handed) and *M*- (left-handed) helical main-chain structures upon varying external conditions. However, although the side-chain-based induction of helicity has been reported, to date no attempts have been made to elucidate the underlying mechanism.

In our recent paper, we revealed the mechanism of the reversible formation of single-handed *P*- and *M*- helical main chains of a poly(quinoxaline-2,3-diyl) that bear (*R*)-2-octyloxymethyl chiral side chains (**2oct**) in two different solvents, *i.e.* tetrahydrofuran (THF) and a mixed solvent of 1,1,2-trichloroethane (1,1,2-TCE) and THF (8/2) (**figure 1**) [3]. The proposed mechanism was supported by a detailed analysis of the high-scattering vector (*q*) region from small-angle neutron scattering (SANS) experiments, in conjunction with theoretical calculations for the structural models obtained thus.

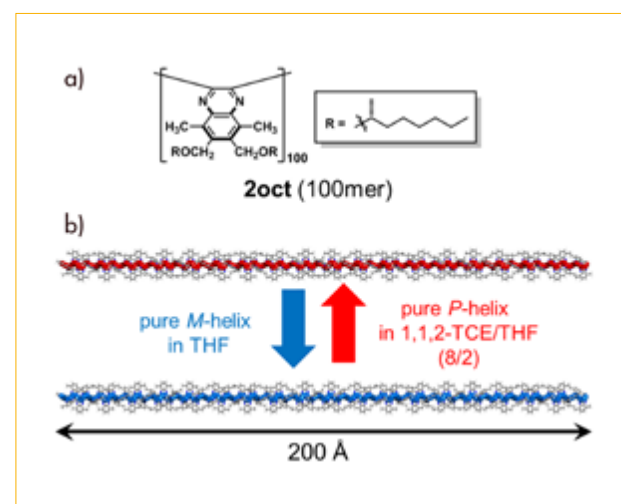


Figure 1

a) Chemical structure of **2oct**, which is a poly(quinoxaline-2,3-diyl) with 100 repeating units, bearing (*R*)-2-octyloxymethyl side chains.
b) Structure of the backbone of **2oct** together with the absolute helix inversion, which depends on the solvents THF and the mixed solvent 1,1,2-TCE/THF (8/2).

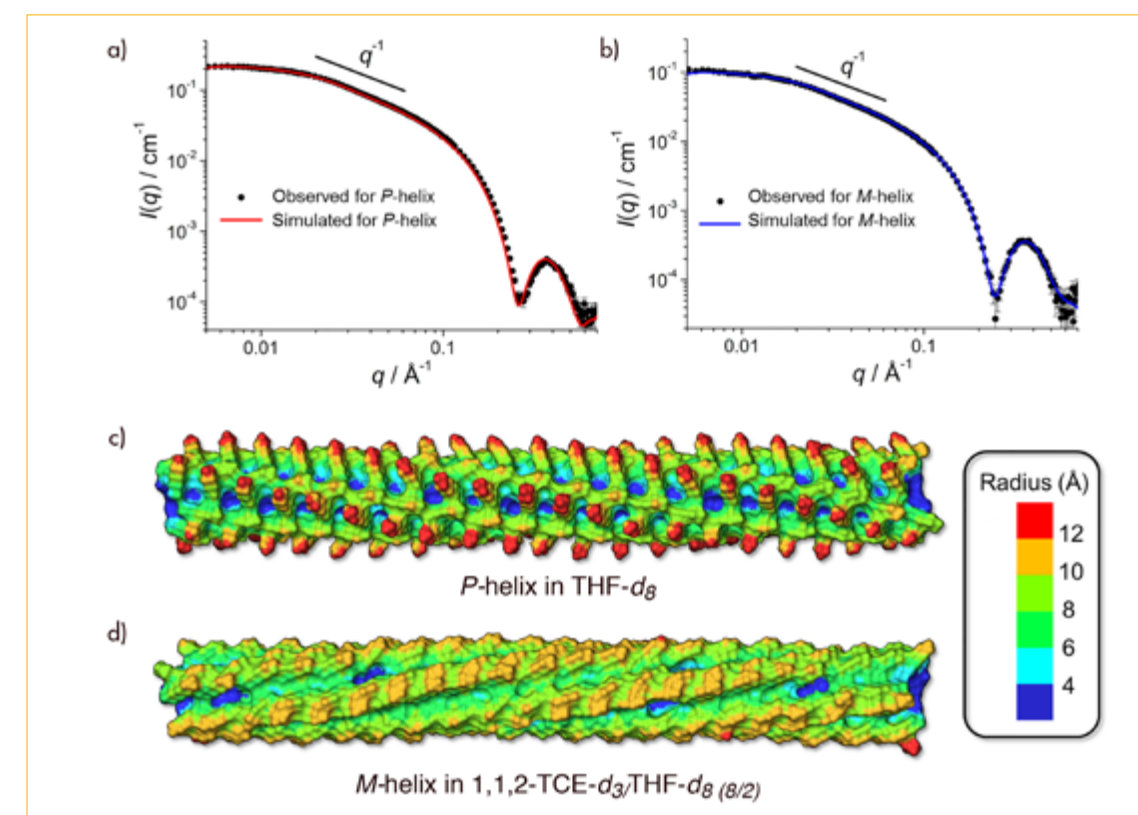


Figure 2

Observed and simulated SANS patterns for **a)** *P*-helical **2oct** in THF-*d*₈, and **b)** *M*-helical **2oct** in 1,1,2-TCE-*d*₃/THF-*d*₈ (8/2), with fitted lines in the Guinier region. Solvent-excluded surfaces (SESs) of **c)** *P*-helical **2oct** in THF-*d*₈, and **d)** *M*-helical **2oct** in 1,1,2-TCE-*d*₃/THF-*d*₈ (8/2). The calculated surfaces were coloured using a colour gradient (blue → red) that illustrates increasing distance from the axis of the main chain.

In order to determine the fine structures of *P*- or *M*-helical **2oct**, dilute solutions of **2oct** in THF-*d*₈ or a 1,1,2-TCE-*d*₃/THF-*d*₈ mixture (8/2) in quartz cells were studied using SANS measurements at 313 K. Remarkably, clear scattering peaks were observed in the high-*q* region ($0.2 \text{ \AA}^{-1} < q < 0.7 \text{ \AA}^{-1}$), allowing the elucidation of the fine structure of the polymer including the conformation of the side chains through simulation of the SANS patterns. It should be emphasised that neutron scattering was crucial to revealing the detailed structures of **2oct** because the peaks in the high-*q* region originate from the difference in neutron scattering length densities between the side chains and the backbone, which cannot be distinguished by small-angle X-ray scattering.

For the simulation of the SANS patterns, we carried out a conformational analysis of **2oct**. Initially, conformers of a model for the repeating unit of **2oct** were generated and optimised by molecular mechanics calculations. After connecting the conformers of the model for the repeating unit, the theoretical models of *P*- or *M*-helices of **2oct** were further optimised for the simulation of the SANS patterns. SANS patterns corresponding to the 20 macromolecular models were calculated by assuming a random orientation of the molecules in consideration of the solvents, and compared with the experimentally obtained SANS pattern in THF-*d*₈ or the 1,1,2-TCE-*d*₃/THF-*d*₈ mixture (8/2).

Finally, we obtained *P*- and *M*-helical models showing good agreement with the observed SANS patterns of **2oct** in THF-*d*₈ and the 1,1,2-TCE-*d*₃/THF-*d*₈ mixture (8/2) (**figures 2a** and **2b**). In order to visualise the solvated structures of *P*- and *M*-helical **2oct**, solvent-excluded

surfaces (SESs) of the two macromolecular models were calculated with a probe sphere radius of 2.0 Å (**figures 2c** and **2d**). The *P*-helical structure showed an undulating SES due to the extended side-chain orientation, whereas the SES of the *M*-helical structure exhibited a smooth surface. These results clearly demonstrate that the *P*-helical structure is well solvated while the *M*-helical structure is less solvated, *i.e.* solvation plays a crucial role in determining the conformation of the side chains and, consequently, the macromolecular helical chirality.

These results reveal that the accumulation of small energy differences in the solvation of the chiral side chains altered the conformation of the two chiral side chains per repeating unit, resulting in absolute control over the macromolecular helical chirality. This is the first demonstration of the effect of solvation of chiral side chains on the helicity of the main-chain conformation of helical macromolecules. Given that the side-chain-based strategy is widely applicable not only to macromolecular systems but also to supramolecular architectures, this study should accelerate the design of a wide range of new chirality-switchable helical molecular systems.



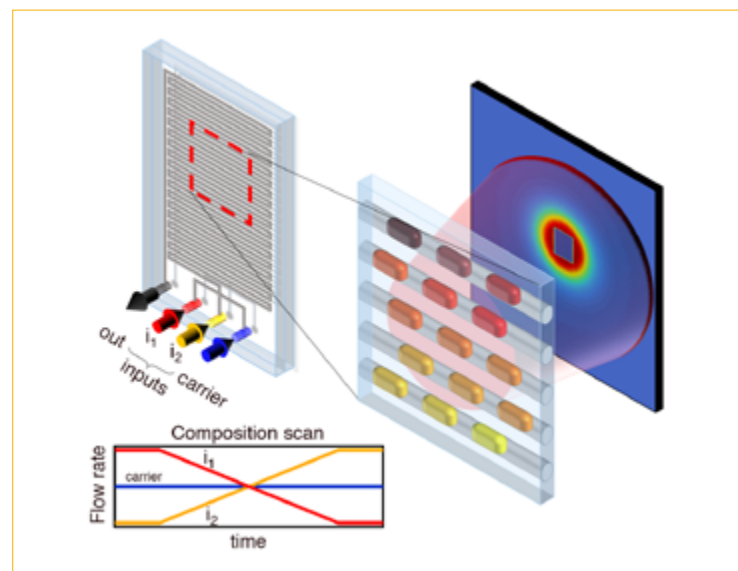
Marco Adamo, Italian Imperial College, London
 'While SANS is a unique probe for studying soft matter and complex fluids, microfluidics is a powerful tool for sequentially preparing formulations. My work focuses on the coupling of microfluidics and SANS for the study of soft matter.'

Droplet microfluidic SANS

Small-angle scattering diffractometer D22

The coupling of microfluidics and small-angle neutron scattering (SANS), made possible by judicious choice of microfabrication techniques and materials, enables a range of new experiments on soft matter. Microfluidic chips can be used as formulators to precisely scan an unprecedented parameter space of a phase diagram by tuning the relative flow rates of the inputs. By adding an immiscible fluid, it is possible to generate segmented flows that minimise axial dispersion and 'cross-talk' between fluid compositions. Using D22, we investigated an aqueous suspension of silica nanoparticles by contrast variation and serial dilution, paving the way for phase mapping in microfluidic-SANS and global, constrained, data-fitting.

Figure 1
Schematic of the microfluidic-SANS set-up.



AUTHORS

M. Adamo, A.S. Poulos, C.G. Lopez and J.T. Cabral (Imperial College, London, UK)
 A. Martel and L. Porcar (ILL)

ARTICLE FROM

Soft Matter 14 (2018) 1759—doi: 10.1039/C7SM02433A

REFERENCES

- [1] C.G. Lopez *et al.*, *Sci. Rep.* 5 (2015) 7727
- [2] M. Adamo *et al.*, *Lab. Chip.* 17 (2017) 1559
- [3] C.G. Lopez *et al.*, *J. Appl. Crystallogr.* 51.3 (2018) 570

Microfluidics has been demonstrated to be compatible with SANS, in particular in the processing of complex fluids [1]. Furthermore, new approaches for data correction and calibration have been proposed to take into account beam over-illumination [2, 3]. This study employs microfluidics to prepare liquid samples, in order to resolve a SANS bottleneck without resorting to automated, liquid-handling robots, and enabling adaptive, responsive protocols for composition scanning. Typically, experimental approaches require the user to prepare five to ten solutions, pipette them into quartz cells, perform the experiment and then start again. While robotics requires a large capital investment (and is arguably less flexible), microfluidics enables liquid samples to be rapidly prepared from stock solutions at a relatively low cost compared with other techniques. Furthermore, it is possible to adjust the resolution of the scan in order to adapt the experiment to the properties of the scatterer: for highly scattering systems (concentrated surfactant solutions, nanoparticle suspensions), data acquisition times can be reduced to a few seconds, enabling the scanning of 100s–1000s compositions; whilst for weakly scattering systems (e.g. dilute polymer or protein solutions) the resolution can be reduced

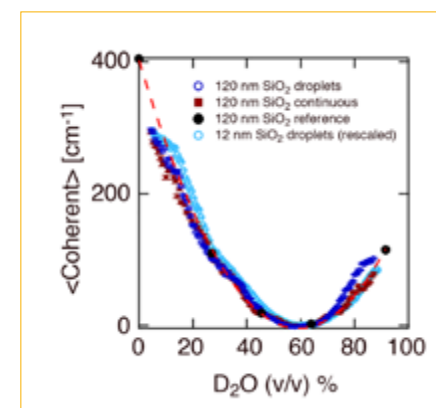
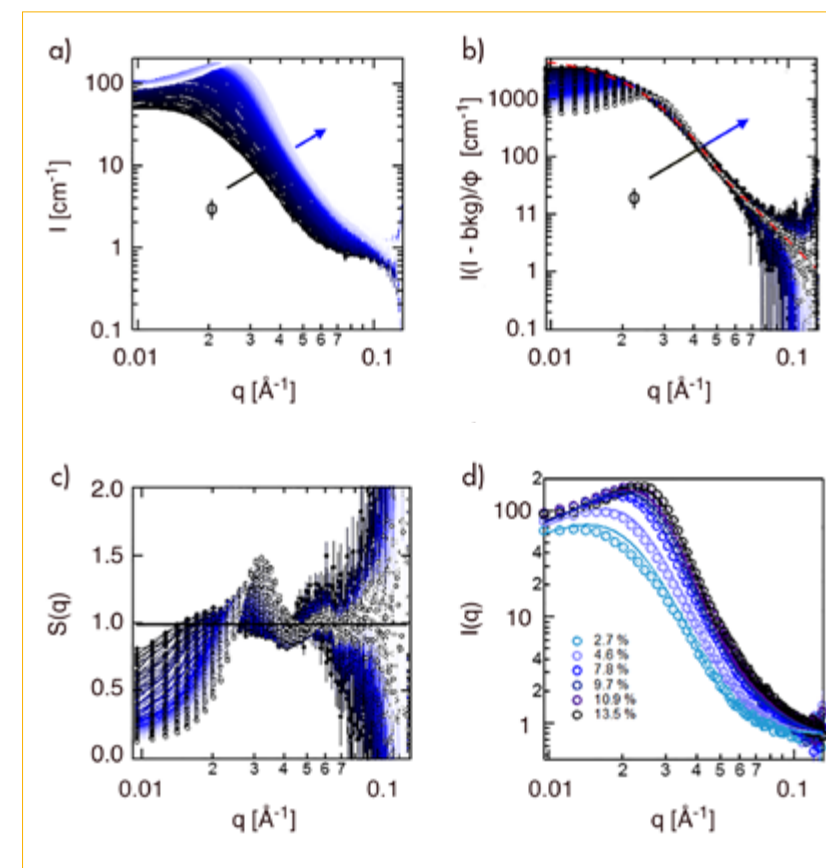


Figure 2

Comparison between contrast variation of 120 and 12 nm silica nanoparticles in segmented flow, continuous flow and discrete approach.

Figure 3

- Raw data from the dilution of Ludox HS-40 from 13.05 to 1.4 %.
- Normalisation of the dilution set by the concentration of nanoparticles, after having removed the high- q background.
- Structure factor, calculated as [b] divided by the form factor, measured from the dilute system.
- Constrained fit of the dilution series.



appropriately to increase the counting time within a finite experimental timeframe. Significantly, operating this system with feedback enables rapid decision-making, e.g. to seek phase boundaries or refine a parameter of interest (such as a match point). The set-up is composed of a crown glass microfluidic chip, in which typically two aqueous solutions are injected at controlled flow rates (see **figure 1**). By changing the relative flow rates, different samples are formulated. By injecting a third stream, of a water-immiscible oil, it is possible to create a segmented flow and thus eliminate the effect of axial dispersion, *i.e.* the 'smearing' of fluid composition over time. The adaptive liquid formulator then becomes a conveyor belt of distinct mixture compositions. As the plugs reach the neutron beam footprint, typically over-illuminating several channels, the scattered intensity is recorded and a composition assigned to that spectrum. By using a semi-transparent beamstop, the data can be (simultaneously) calibrated in absolute units and, by triangulating the input composition, incoherent background and transmission, data self-consistency is ensured.

Following an optimisation procedure, we selected fluorinated oils as the immiscible phase, due to the immiscibility with water and low neutron signal and

cost. The paper reports on a comparison between the continuous approach (single-phase flow), the segmented flow and the standard, discrete approach in **figure 2**, and establishes the conditions to which each method is best suited in terms of system of interest, availability of the material and required experimental time.

Furthermore, we applied droplet microfluidic-SANS to study the dilution of a suspension of 12 nm silica nanoparticles (Ludox HS-40) in water. We produced solutions ranging from 13.05 to 1.4 (v/v) % nanoparticles in water and recorded 120 scattering patterns in 120 steps (**figure 3a**), for a total experiment time of 10 mins. Two analysis approaches are proposed: on the one hand, it is possible to remove the background and normalise the scattering pattern by the concentration of the nanoparticles (**figure 3b**) and then divide each curve by the form factor (measured for the dilute system), thus obtaining the structure factor (**figure 3c**); on the other, one can perform a constrained fit on the entire set of curves (**figure 3d**), thus achieving unprecedented precision in determining the unknowns of the system. The availability of large datasets in microfluidic-SANS enables simultaneous, constrained, data fits which significantly improve accuracy by effectively providing many 'more equations for the same number of variables'.



Christine M. Papadakis, German Technical University of Munich, Germany 'My group uses scattering methods to investigate, among other things, self-assembling and (multi-)responsive polymer systems. A recent emphasis is on time-resolved neutron scattering experiments after a temperature or pressure jump.'

Fast and furious: pressure jumps combined with time-resolved small-angle neutron scattering reveal aggregate growth in a stimuli-responsive polymer

Small-angle scattering diffractometer D11

Aggregation processes are ubiquitous in soft matter, e.g. in polymers, colloids and proteins, and frequently evolve through transient states. While small-angle neutron scattering (SANS) provides structural information on length scales of ~ 1 –100 nm and a time-resolution of milliseconds, pressure jumps allow a rapid change of state. In the present study, we apply a pressure jump to a semidilute solution of the thermoresponsive polymer poly(N-isopropylacrylamide) (PNIPAM) in D_2O [1], inducing phase separation, and employ kinetic SANS to study the aggregation process with a focus on the early stages of mesostructure formation.

Figure 1

a) Coexistence line in the temperature-pressure frame (black line). The red arrow indicates the pressure jump carried out. **Inset)** Chemical structure of PNIPAM.
b) SANS data before (black) and after (coloured) the pressure jump. The growth regimes I (blue), II (red) and III (orange) are indicated.

AUTHORS

B.-J. Niebuur, X. Zhang, F. Jung, Ch.M. Papadakis (Technical University of Munich, Germany)
L. Chiappisi (ILL and Technical University of Berlin, Germany)
A. Schulte (University of Central Florida, Orlando, USA)

ARTICLE FROM

ACS Macro Lett. 7 (2018) 1155—doi: 10.1021/acsmacrolett.8b00605

REFERENCES

- [1] V. Aseyev, S. Hietala, A. Laukkanen, M. Nuopponen, O. Confortini, F.E. Du Prez and H. Tenhu, *Polymer* 46 (2005) 7118
- [2] R. Stepanyan, J.G.J.L. Lebouille, J.J.M. Slot, R. Tuinier and M.A. Cohen-Stuart, *Phys. Rev. Lett.* 109 (2012) 138301
- [3] K. Kyriakos, M. Philipp, J. Adelsberger, S. Jaksch, A.V. Berezkin, D.M. Lugo, W. Richtering, I. Grillo, A. Miasnikova, A. Laschewsky, P. Müller-Buschbaum and C.M. Papadakis, *Macromolecules* 47 (2014) 6867
- [4] T. Tanaka, *J. Phys. Condens. Matter* 12 (2000) R207

Pressure jumps present a well-controlled way to trigger the phase transition of PNIPAM, because they allow a fast change of state even for large sample volumes—as they are necessary for SANS—without thermal effects. In our experiment, a temperature-controlled copper beryllium pressure cell was used, in which the sample is separated from the pressurising medium by a movable piston. The pressure jump was accomplished within less than 0.1 s by a pneumatically driven valve. Starting in the one-phase regime at 31 MPa and 35.1 °C, a sudden pressure reduction by $\Delta p = -15$ MPa triggered the phase transition (**figure 1a**). Kinetic SANS measurements were carried out on instrument D11 with a time resolution of 0.05 s.

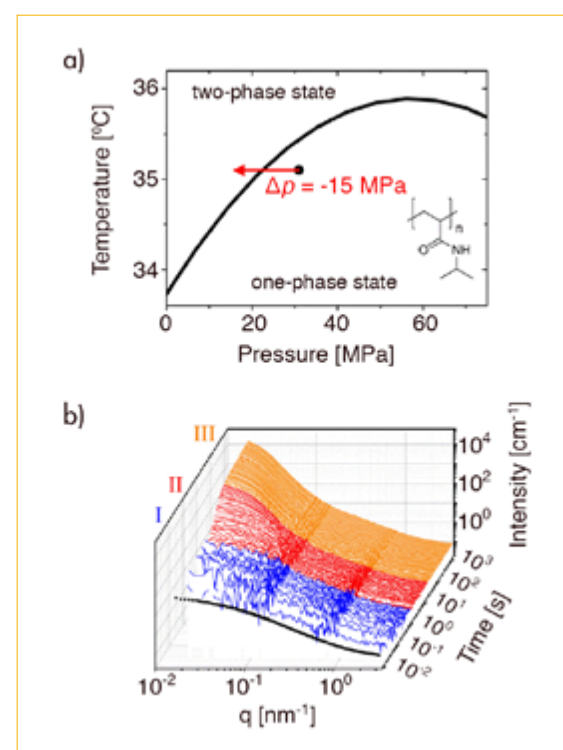
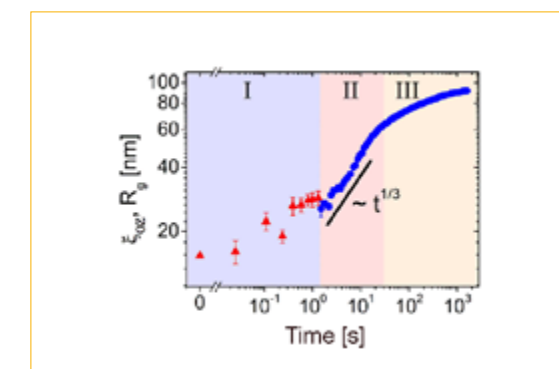


Figure 2

Time dependence of correlation length (red triangles) and radius of gyration of the mesoglobules (blue circles) obtained from fits to the SANS data.



The pre-release SANS curve, as well as the initial kinetics (regime I), are characteristic of semidilute solutions undergoing concentration fluctuations (**figure 1b**). After 1.4 s, an additional contribution with rapidly increasing intensity appears at low momentum transfers ($q < 0.1 \text{ nm}^{-1}$), reflecting the formation and growth of aggregates from collapsed chains called mesoglobules (regime II). After ~ 30 s, their growth slows down significantly (regime III).

Fitting of structural models yields characteristic lengths (**figure 2**). In regime I, the correlation length of the concentration increases, but the intensity only increases weakly. These findings indicate that small clusters form by a nucleation and growth mechanism (**figure 3**). In regime II, mesoglobules are formed, and their radius of gyration increases with time according to a power law $R_g(t) \propto t^{1/3}$, i.e., they grow by diffusion-limited coalescence [2]. Moreover, a dense shell emerges that traps water inside the mesoglobules. In regime III, the growth follows $R_g(t) \propto \log(t)$, suggesting the appearance of an energy barrier that hinders coalescence. A large energy barrier (several $k_B T$) implies that aggregation is greatly slowed down in regime III [3]. This may be

attributed to the viscoelastic effect (entanglement force) hindering the coalescence of two mesoglobules because of the low mobility of the polymers [4].

Thus, *in situ*, real-time SANS in combination with a fast pressure jump initiating a phase transition captures a comprehensive view of the structure-forming processes over time scales ranging from tens of milliseconds to thousands of seconds. Detailed structural information could be gained on length scales of ~ 1 –100 nm. In particular, our study reveals that, in a semidilute PNIPAM solution, the growth of the mesoglobules features several regimes. First, loose clusters form from the homogeneous solution by a nucleation process. Second, the clusters evolve into compact aggregates having a dense shell and grow rapidly by diffusion-limited coalescence. Finally, their growth slows down substantially because the low polymer mobility in the aggregates hinders their coalescence. These findings could only be made possible by combining a milli-second pressure jump and fast SANS. The method opens up new opportunities for investigating the pathways of structural changes in complex systems with unprecedented time resolution.

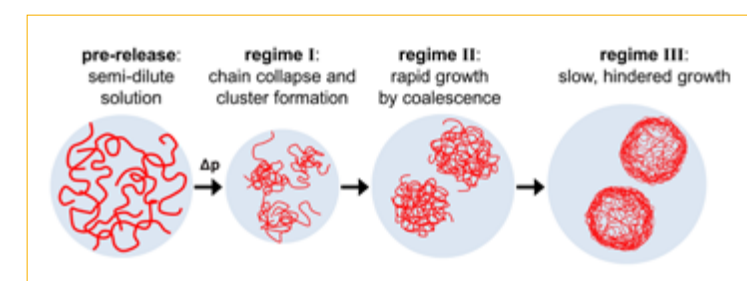


Figure 3

Schematic representation of the formation and structural evolution of the mesoglobules during the pressure jump.



Mark Laver, British University of Birmingham, UK www.birmingham.ac.uk/laver
'I did my PhD at the ILL many years ago. I am now a lecturer at the University of Birmingham. My research interests include superconductors and functional materials, e.g. for nuclear applications.'

Vortex disordering and the peak effect in

superconductors

Small-angle diffractometer D22

SANS-II instrument at PSI

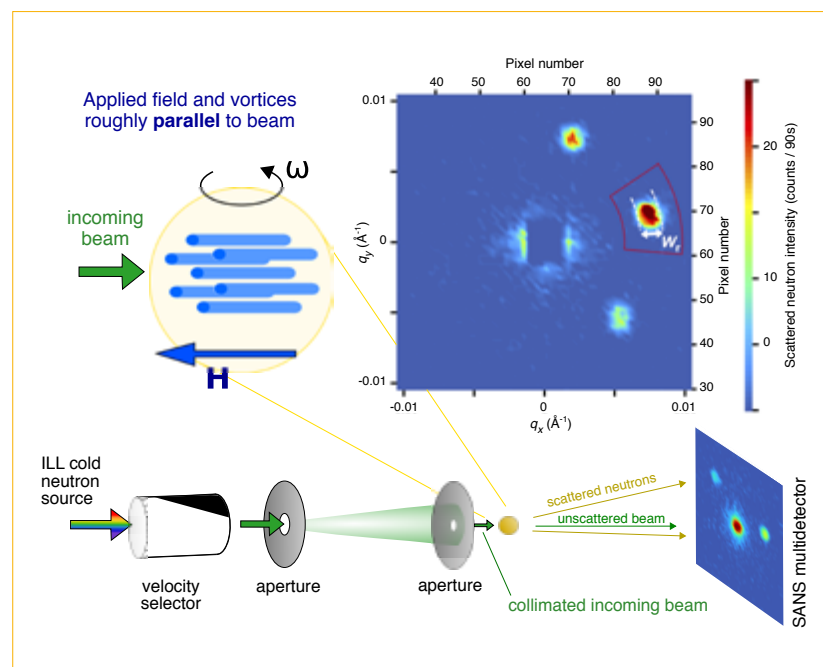
NG7 instrument at NCNR

Underlying disorder pins vortices in type-II superconductors, giving zero resistivity below a critical current j_c . Peaks are often observed in the temperature and field dependences of j_c .

This 'peak effect' is commonly believed to stem from an order-disorder transition of the vortex ensemble [1]. Using SANS, we find an order-disorder transition from a quasi-long-range-ordered phase (the 'Bragg glass') to a vortex glass in a vanadium crystal. The peak effect, however, lies at higher fields and temperatures, challenging the common dogma of its origin.

Figure 1

Experimental geometry used on the D22 SANS instrument. The magnetic field profile presented by superconducting vortices diffracts neutrons. Rocking curves are collected by rotating the sample, field and vortices together through the Bragg condition. A typical image of the 2D SANS multidetector at the peak of the rocking curve of the right Bragg spot is shown.



AUTHORS

R. Toft-Petersen and A.B. Abrahamsen (Technical University of Denmark, Denmark)
 S. Balog (University of Fribourg, Switzerland)
 L. Porcar (ILL)
 M. Laver (University of Birmingham, UK)

ARTICLE FROM

Nat. Commun. 9 (2018) 901—All figures adapted from article

REFERENCES

- [1] See, e.g. T. Matsushita, Flux Pinning in Superconductors (Springer, 2007)
- [2] A.I. Larkin, Sov. Phys. JETP. 31 (1970) 784
- [3] T. Giamarchi and P. Le Doussal, Phys. Rev. B 52 (1995) 1242
- [4] G.P. Mikitik and E.H. Brandt, Phys. Rev. B 64 (2001) 184514
- [5] M. Laver et al., Phys. Rev. Lett. 100 (2008) 107001

It has taken many decades to unravel the effects of weak disorder on the ensemble of vortices that form in type-II superconductors. In the 1970s it was initially thought that any random disorder, no matter how weak, would destroy long-range order in the vortex ensemble [2].

However, it turns out that lattice periodicity becomes crucial at large scales, where vortex displacements grow to be of the order of inter-vortex spacing—a distance set by flux quantisation. At these asymptotic scales the growth of displacements slows, giving rise to quasi-long-range order with algebraically diverging Bragg peaks. The resulting phase is accordingly known as the 'Bragg glass' [3].

The Bragg glass picture, which holds when underlying disorder is weak, breaks down when dislocations become important. Upon increasing field or disorder strength, a transition to a short-range ordered vortex glass phase is expected. Then, at temperatures close to the upper critical field $B_{c2}(T)$ where bulk superconductivity disappears, thermal fluctuations subsequently drive a proliferation of dislocations and a thermodynamic melting of the vortex lattice.

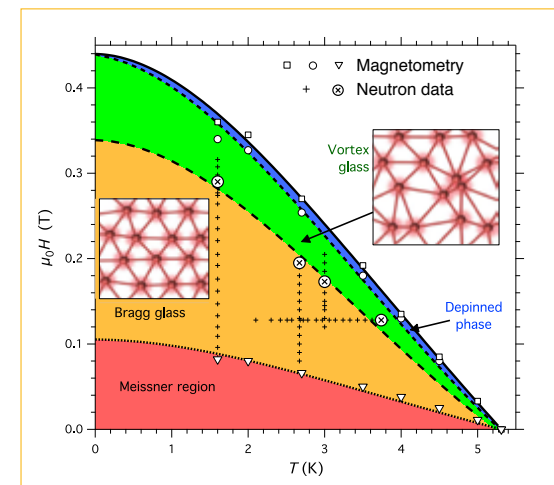


Figure 2

Phase diagram for our vanadium crystal. Plus signs mark where SANS data were measured. The vortex order-disorder transition is marked by crosses in circles. The dashed lines are fits based on Lindemann criteria. The peak effect is observed close to the depinning line rather than at the order-disorder line.

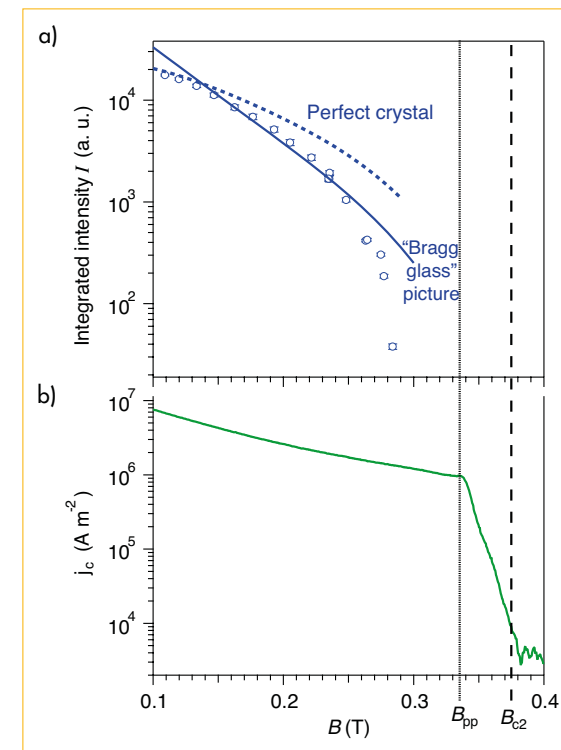


Figure 3

Results at $T = 1.6$ K.

a) Diffracted SANS intensity integrated over the rocking curve. The lines show the form of $I(B)$ expected if the vortex ensemble has either perfect order or the quasi-long-range order of the Bragg glass.

b) Critical current density j_c calculated from magnetisation. j_c decreases monotonically except for a small peak, labelled B_{pp} , just before the sharp downturn where thermal depinning takes over. The SANS intensity vanishes much before the peak effect B_{pp} .

The field and temperature dependences of the order-disorder transition $B_{dis}(T)$ and the melting transition can be estimated using phenomenological Lindemann criteria, which state that the respective transition occurs when vortex displacements become a certain fraction of the lattice spacing [4].

Here we use small-angle neutron scattering (SANS) to probe the long-range correlations of vortex ensembles in a superconducting vanadium crystal. We find a Bragg glass at intermediate fields in the phase diagram (figure 2). This phase is characterised by:

1. The field dependence of the integrated SANS intensity $I(B)$, measured on the D22 instrument (figure 3a) using the experimental geometry illustrated in figure 1.
2. The shape of the Bragg peaks, measured on the SANS-II instrument at PSI using an experimental geometry with high resolution in the plane of the vortex ensemble. Reverse Monte Carlo refinement [5], with up to 220 000 computer-simulated vortices, is used to analyse the peak shape and extract spatial correlation functions [see original article for details].

At $T = 1.6$ K, $I(B)$ is well described by the Bragg glass picture up to $B = 0.26$ T (figure 3a). Above this field the SANS intensity plummets, becoming indiscernible from the background at $B = 0.29$ T. This vanishing of the neutron intensity as a function of field or temperature is used to locate the order-disorder line $B_{dis}(T)$ (crosses in circles in figure 2). $B_{dis}(T)$ lies well below $B_{c2}(T)$; it is mediated only by the weak underlying disorder in our crystal.

Looking at the critical current density j_c determined from magnetometry (figure 3b), we find no features around $B_{dis}(T)$ that might be expected from the common paradigm [1]. Instead, a nascent peak effect is observed at fields and temperatures close to $B_{c2}(T)$ (figure 3b) in a region where thermal fluctuations start to become significant.

In conclusion, our combined SANS and magnetometry study shows that the peak effect may not *a priori* be due to a vortex order-disorder transition. We suggest that the peak effect may instead arise from a sudden accommodation of weak pinning by a rapid but local change in the vortex core structure. This instability, localised to the vortex cores, is not necessarily significant at larger length scales, such that vortex order does not necessarily need to be disturbed through the peak effect.



Noriki Terada, Japanese National Institute for Materials Science, Japan
'I am a senior scientist working at NIMS, Tsukuba, Japan. I am mainly studying pressure effects on strongly correlated electron systems including multiferroic materials. Recently, I developed a non-magnetic Hybrid Anvil Cell for Spherical Neutron Polarimetry experiments, based on collaborations with the ILL and JAEA, Tokai.'

Spherical neutron polarimetry under high pressure for a multiferroic delafossite ferrite

Spin-polarised hot-neutron diffractometer D3

The analysis of three-dimensional neutron spin rotation at the interaction with a sample, using a technique referred to as spherical neutron polarimetry (SNP), is a very powerful means of determining complex magnetic structures in magnetic materials. In the present study, we successfully carried out the first SNP experiment under high pressure up to 4.0 GPa on the D3 instrument, studying the magnetoelectric multiferroic delafossite CuFeO_2 . The results presented here demonstrate that SNP measurements are feasible under high-pressure conditions, and that this method is a useful approach to studying pressure-induced physical phenomena.

AUTHORS

N. Terada (National Institute for Materials Science, Japan)
 N. Qureshi (ILL)
 L.C. Chapon (Diamond Light Source, UK)
 T. Osakabe (Japan Atomic Energy Agency, Japan)

ARTICLE FROM

Nat. Commun. (2018)—doi: 10.1038/s41467-018-06737-6

REFERENCES

- [1] F. Tasset, *Physica B* 156–57 (1989) 627
- [2] N. Terada, D.D. Khalyavin, P. Manuel, T. Osakabe, P.G. Radaelli and H. Kitazawa, *Phys. Rev. B* 89 (2014) 220403(R)
- [3] N. Terada, *J. Phys. Condens. Matter* 26 (2014) 453202
- [4] N. Terada, N. Qureshi, L.C. Chapon and T. Osakabe, *Nat. Commun.* 9 (2018) 4368

Since Tasset developed the ILL's CRYogenic Polarisation Analysis Device (CRYOPAD), which enables three-dimensional neutron polarisation analysis [1], the SNP technique has been used to determine precise spin orientations in complex magnetic structures. In unpolarised neutron diffraction experiments, one needs to collect many magnetic Bragg peaks from different sample positions to perform the standard refinement procedure. In contrast, with the SNP method the so-called polarisation matrix of one Bragg reflection contains an enormous amount of information concerning the magnetic structure; therefore, generally the measurement of just a few reflections yields very precise results. However, since the CRYOPAD requires zero-magnetic field conditions in conjunction with superconducting Meissner screening to avoid neutron depolarisation [1], inside the magnetic vacuum it is necessary to use equipment, such as high-pressure cells, that are made of non-magnetic materials. To date, SNP experiments under high pressures have not been carried out because of this difficulty.

In the present study, we used a newly developed, non-magnetic Hybrid Anvil high-pressure Cell (HAC) (figure 1, left) to overcome this challenge. We employed a combination of a single sapphire crystal and a non-magnetic diamond composite (with an SiC binder) or WC with a non-magnetic Ni binder as the

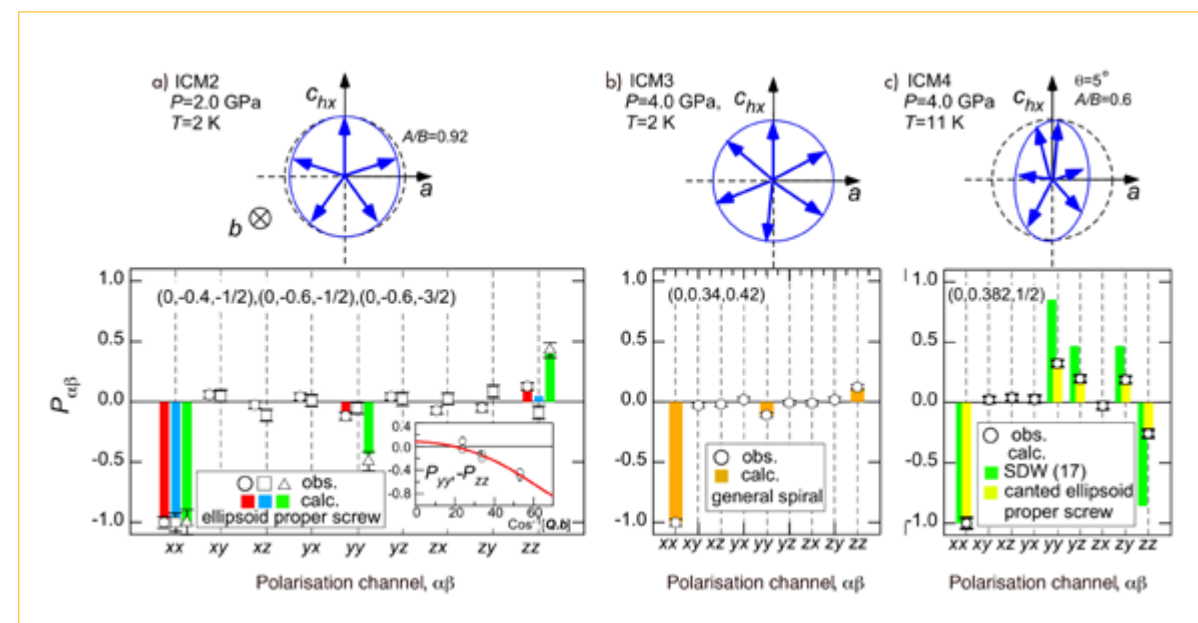


Figure 2

Summary of schematic illustrations of magnetic structure and comparison between observed and calculated values of neutron polarisation matrix elements for the pressure-induced ferroelectric phases in multiferroic CuFeO_2 [4].

anvil materials. We selected the magnetoelectric (ME) multiferroic compound delafossite CuFeO_2 for the first SNP experiment under high pressure. Since the multiferroic ferrite is expected to have various types of magnetic orderings under high pressure, such as collinear spin-density-wave (SDW) and non-collinear spiral structures [2,3], we felt that it was the best candidate for studying the feasibility of SNP analysis under pressure.

First, we confirmed the collinear magnetic structure in the ICM1 and CM1 phases, and found precise spin-canting angles of $17 \pm 2^\circ$ and $5 \pm 2^\circ$ for the ICM1 and CM1 phases, respectively [4]. The magnetic structure parameters are consistent with previously reported values determined by unpolarised neutron diffraction studies. These results therefore demonstrate that SNP measurements are feasible under high-pressure conditions using a non-magnetic HAC.

Secondly, we succeeded in determining the magnetic structures of the pressure-induced ferroelectric phases in CuFeO_2 [4]. The magnetic structures and comparison between experimental and calculated values for the polarisation matrix elements are summarised in figure 2. In the case of the ICM2 phase, an ellipsoidal proper screw

structure with magnetic point group $21'$ was determined with an ellipsoidicity ratio of 0.92 ± 0.05 . This magnetic symmetry is consistent with observed electric polarisation. We also ascertained the magnetic structure in the ICM3 phase, and found a spiral structure with spins confined to the ac -plane. Since the k -vector is of triclinic symmetry [$k = (0, 0.34, 0.42)$], this magnetic structure (termed the general spiral) possesses both a cycloidal modulation along the c -axis and a proper screw modulation along the b -axis in the ICM3 phase, which has point group $11'$, allowing electric polarisation along a general direction. This study also identified the existence of a phase transition between the ICM1 and ICM4 phases in the intermediate temperature region by measuring the temperature dependence of the polarisation matrix elements at several pressures. One possible magnetic structure in the ICM4 phase is presented as a canted ellipsoidal proper screw with point group $21'$.

In conclusion, the present study provides evidence that SNP measurements are viable even in high-pressure conditions [4]. It is our hope that the present technique will allow researchers to elucidate pressure-induced physical phenomena associated with complex magnetic ordering.

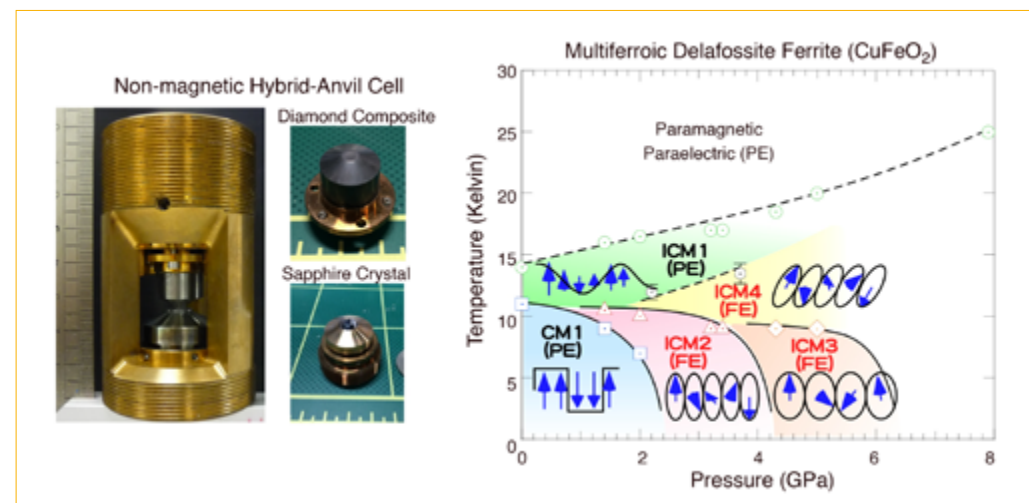


Figure 1

left) Non-magnetic Hybrid Anvil Cell with diamond composite and sapphire anvils.

right) Magnetolectric phase diagram of multiferroic delafossite ferrite CuFeO_2 [4].

**José Alberto Rodríguez Velamazán.**

Spanish. ILL

'I received my PhD from the University of Zaragoza, Spain, in 2007. I then moved to the ILL, where I have been working as a scientist, first for the Spanish CRGs and then as ILL staff. My main research focus is magnetic materials of molecular base.'

Switching of the chiral magnetic domains in the hybrid molecular/inorganic multiferroic $(\text{ND}_4)_2[\text{FeCl}_5(\text{D}_2\text{O})]$

Spin-polarised hot-neutron diffractometer D3

Magneto-electric multiferroics are materials that can host electric and magnetic order simultaneously. A strong coupling between both orders, as achieved in the so-called spin-driven multiferroics, leads to remarkable possibilities for cross-control of the physical properties. Important efforts have in recent years been dedicated to innovative approaches allowing a rational design of such systems. $(\text{ND}_4)_2[\text{FeCl}_5(\text{D}_2\text{O})]$ represents a promising example of the new hybrid molecular/inorganic approach to creating materials with strong magneto-electric coupling.

AUTHORS

J.A. Rodríguez-Velamazán, O. Fabelo, J. Rodríguez-Carvajal and N. Qureshi (ILL)
J. Campo (CSIC-University of Zaragoza, Spain)
L.C. Chapon (Diamond light source, Didcot, UK)

ARTICLE FROM

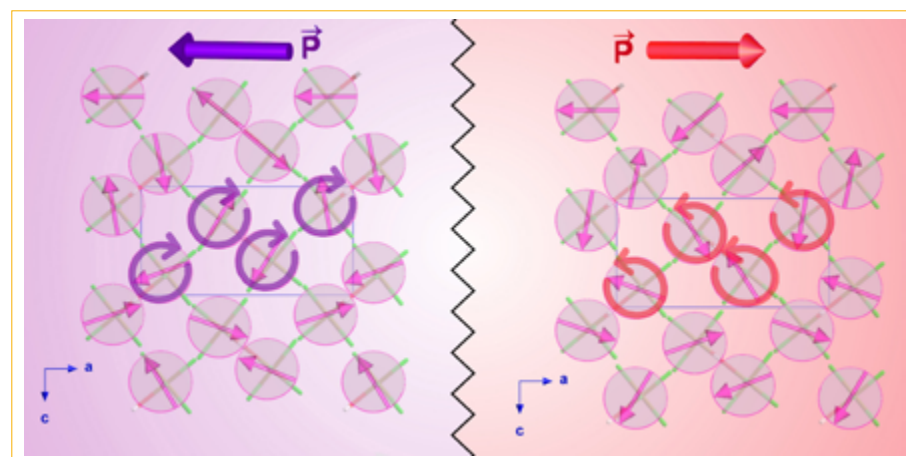
Sci. Rep. (2018)—doi: 10.1038/s41598-018-28883-z
(Publication funded through FILL2030 Open Access programme)

REFERENCES

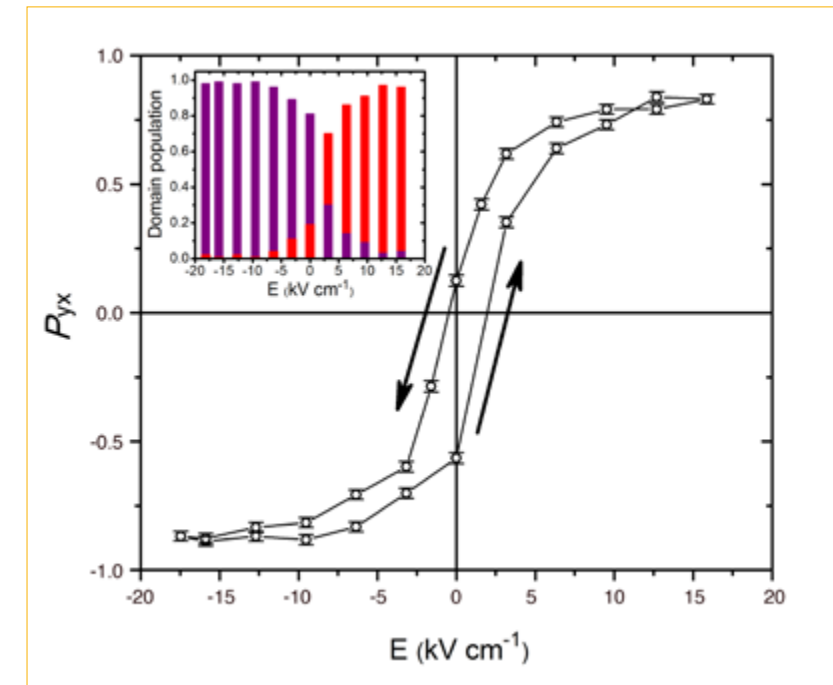
- [1] M. Ackermann, D. Brüning, T. Lorenz, P. Becker and L. Bohatý, *New J. Phys.* 15 (2013) 123001
- [2] J.A. Rodríguez-Velamazán, O. Fabelo, A. Millán, J. Campo, R.D. Johnson and L. Chapon, *Sci. Rep.* 5 (2015) 14475
- [3] Y. Takura, S. Seki and N. Nagaosa, *Rep. Prog. Phys.* 77 (2014) 076501
- [4] N. Qureshi, *Mag2Pol*. arXiv 1801 (2018) 08431

$(\text{ND}_4)_2[\text{FeCl}_5(\text{D}_2\text{O})]$ is a spin-driven multiferroic, with a strong magneto-electric coupling [1] that derives from an incommensurate cycloidal magnetic structure in the ground state (below 6.9 K) [2]. The cycloid propagates along the *c*-axis with magnetic moments mainly contained in the *ac*-plane. A ferroelectric polarisation, primarily directed along the *a*-axis, develops in this phase [1], which is compatible with the spin current mechanism of magneto-electric coupling [3]. The cycloidal spin arrangement implies two 'chiral' domains with opposite rotation of the cycloids (**figure 1**), which directly correspond to electric domains with opposite polarities. Therefore, by applying an E-field, one can manipulate the population of the 'chiral' magnetic domains.

We used spherical neutron polarimetry, which is directly sensitive to the absolute magnetic configuration and domain population, to unambiguously prove the multiferroicity of this material. This technique is ideally suited to studying complex magnetic structures since it allows access to the direction and phase of the magnetic scattering, unreachable by unpolarised methods. For each measured reflection, and in a particular reference frame, we obtain the polarisation matrix *P*, with matrix elements P_{ij} (*i, j* = X, Y, Z), representing the polarisation of the scattered beam in the direction *j*, for

**Figure 1**

Schematic representation of the magnetic structure of the two magnetic domains, with the direction of the resulting electric polarisation.

**Figure 2**

Hysteresis loop measured on the off-diagonal neutron polarisation matrix element P_{yx} of the (0 1 0.23) reflection of a $(\text{ND}_4)_2[\text{FeCl}_5(\text{D}_2\text{O})]$ crystal. The sample was initially cooled down to 4 K under a negative E-field of 17.5 kV cm^{-1} and then warmed to 6.5 K. The temperature was kept constant for the subsequent measurements as a function of a variable E-field. **Inset**) Domain populations corresponding to the increasing E-field branch of the hysteresis loop. Purple and red bars refer to negative and positive chiral magnetic domains, respectively.

an incident beam polarised in the direction *i*. In our experimental configuration, the values of the off-diagonal components, P_{yx} , P_{zx} , of magnetic reflections like the (0 1 0.23) depend not only on the magnetic structure but also on the populations of the possible magnetic domains. In particular, for the same magnetic reflection the off-diagonal terms will give opposite signs for each 'chiral' domain, with the sign indicating the handedness (clockwise or counter-clockwise) of the 'chiral' magnetic domain. If both domains are equally populated, these measured terms average out and $P_{yx} = P_{zx} = 0$; but if the domain populations are unbalanced, which can be achieved by cooling in an applied E-field in the direction of the ferroelectric polarisation, finite values are measured which allow the relative fraction of cycloidal domains to be determined [4].

With these measurements, we have demonstrated that the application of an electric field upon cooling results in the stabilisation of a single-cycloidal magnetic domain below 6.9 K, while poling in the opposite electric field direction produces the full population of the domain with opposite magnetic chirality. Furthermore, we can tune the domain populations by varying the electric field (**figure 2**), reaching a full population reversal by switching the field in a complete hysteresis loop. This provides direct proof at the microscopic level of the multiferroicity of $(\text{ND}_4)_2[\text{FeCl}_5(\text{D}_2\text{O})]$.



Romain Sibille. French Laboratory for Neutron Scattering and Imaging, PSI, Switzerland
 'After getting my PhD in chemistry, I joined PSI in 2012. Since 2016, I have been co-responsible for the thermal neutron diffractometer Zebra. My main research interests are the preparation, crystal chemistry and fundamental properties of magnetic materials with strong fluctuations—especially rare-earth pyrochlores.'

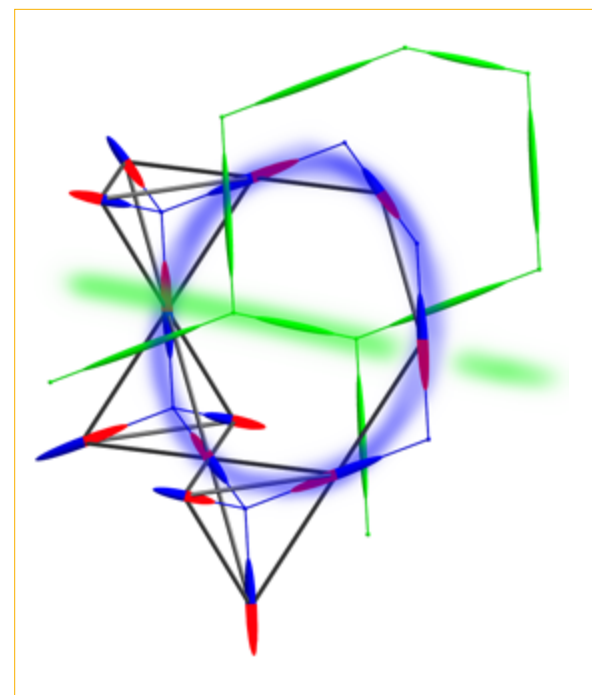
Signatures of a quantum spin ice ground state

Time-of-flight spectrometer IN5
 HYSPEC spectrometer
 at Oak Ridge National Laboratories

Quantum spin ice is an appealing proposition of a quantum spin liquid—systems in which the magnetic moments of the constituent electron spins evade classical long-range order to form an exotic state that is quantum entangled and coherent over macroscopic length scales. Such phases are at the edge of our current knowledge on condensed matter, as they go beyond the established paradigm of symmetry-breaking order and associated excitations. Experiments carried out on the disk chopper time-of-flight spectrometer IN5 reveal signatures of a quantum spin ice that were predicted by theory.

Figure 1

In a classical spin ice, uniaxial magnetic moments decorate a pyrochlore lattice (in black). Magnetic moments (blue/red ellipses) on each tetrahedra are constrained by a local '2-in-2-out' organisation principle. Moments can be viewed as magnetic fluxes forming a diamond lattice (in blue), which can be coarse-grained to define a continuous medium with emergent magnetostatics. Quantum dynamics on a six-member ring creates electric flux variables (in green) that form a second (interpenetrated) diamond lattice. This quantum spin ice ground state can be thought of as a lattice analogue of quantum electrodynamics, making the sample a tiny universe with its own emergent light of gapless magnetic excitations.



AUTHORS

R. Sibille, M. Kenzelmann and T. Fennell (Paul Scherrer Institute, PSI, Villigen, Switzerland)
 N. Gauthier (SLAC National Accelerator Laboratory and Stanford University, California, USA)
 J. Olivier (ILL)

ARTICLE FROM

Nat. Phys. (2018)—doi: 10.1038/s41567-018-0116-x

REFERENCES

- [1] L. Balents, Nature 464 (2010) 199
- [2] M.J.P. Gingras and P.A. McClarty, Rep. Prog. Phys. 77 (2014) 056501
- [3] S. Petit, E. Lhotel *et al.*, Nat. Phys. 12 (2016) 146
- [4] E. Lhotel, S. Petit *et al.*, Nat. Commun. 9 (2018) 3786

Spin ices are crystalline materials with rather peculiar magnetic properties. The magnetic atoms in their lattices are arranged in geometries that resemble that of frozen water, and an analogous local rule for the electronic spins also prevents the formation of a single state of minimal energy—hence the name spin ice. When such systems with degenerate ground states remain dynamic even at zero temperature they are collectively known as quantum spin liquids; and they have long attracted considerable interest from theorists and experimentalists alike, as they harbour a wealth of exotic physics [1].

Discovered in the late '90s in magnetic pyrochlore compounds, classical 'spin ices' are materials that contain magnetic moments distributed on a network of corner-sharing tetrahedra. Because of the structure of the material, each magnetic moment is constrained to align along the direction joining its position and the centres of two tetrahedra. With ferromagnetic interactions, two of the four magnetic moments in each tetrahedron must

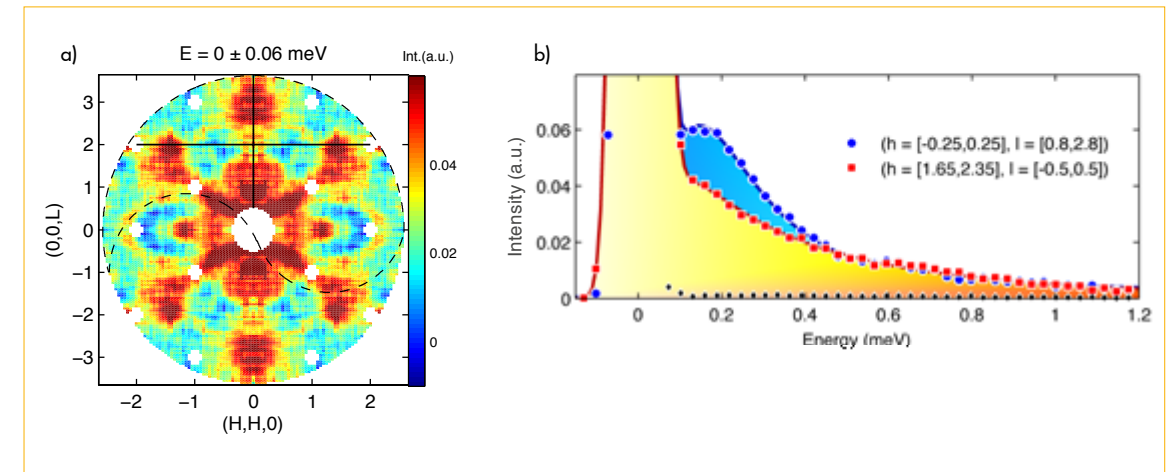


Figure 2

The quasi-elastic structure factor (a) and inelastic spectrum (b) of $\text{Pr}_2\text{Hf}_2\text{O}_7$ measured at 0.05 K on IN5.

be oriented inward and the other two outward. This '2 in 2 out' local constraint can be achieved in a number of ways that grows exponentially with the number of tetrahedra involved, so that no order can occur. A spin ice is therefore better viewed as a fluctuating fluid—a spin liquid—of correlated moments, despite its name being inherited from a form of crystalline water ice.

A famous example of exotic behaviour in spin-ice materials is that of magnetic monopoles. The magnetic moments in the material interact in such a manner that separate magnetic charges can emerge as 'quasi-particles' associated with excitations. But exotic as these phenomena may be, they can nevertheless be fully described within the framework of classical magnetostatics.

An intriguing question, then, is what happens when quantum effects are thrown into the mix [2]? Theoretical work predicts that quantum-mechanical tunnelling between different spin-ice configurations can lead to excitations that are qualitatively different from those in classical spin ice. In quantum spin ice, behaviour emerges that is described by quantum electromagnetism; that is, quantum fluctuations bring an emerging dynamic electromagnetic field into play (figure 1). This leads to a rich set of novel phenomena: not only should variants of magnetic monopoles appear in quantum spin ices, but so should electric monopoles and excitations that behave like photons. The experimental realisation of a quantum spin ice is, however, challenging. Attempts to identify its manifestations in various pyrochlore materials have been made. As a result, spectacular results

of neutron scattering experiments hinting at ground states with quantum origins in rare-earth pyrochlores have been obtained over the past few years (see [3, 4], for example).

In the present study, high-quality single crystals of $\text{Pr}_2\text{Hf}_2\text{O}_7$ were measured on IN5 at the ILL. The results reveal two important signatures of a quantum spin ice state. First, the mapping of the quasi-elastic structure factor at 0.05 K in this material reveals pinch points (figure 2a)—a signature of a classical spin ice—that are partially suppressed as expected in a quantum spin ice. The line shape of the pinch-point scattering was compared with calculations of a lattice field theory of a quantum spin ice, in which low-energy gapless photon excitations explain the broadening of the curve. This result makes it possible to estimate the speed of light associated with magnetic photon excitations. Second, the IN5 data also reveal a continuum of inelastic spin excitations (figure 2b) that resemble predictions of the fractionalised, topological excitations of a quantum spin ice. Complementary polarised-neutron measurements confirming the magnetic origin of these signals were made on the HYSPEC spectrometer at the Spallation Neutron Source (Oak Ridge National Laboratories, USA), using an array of polarisation analysers built at the Paul Scherrer Institute (Villigen, Switzerland). Taken together, these two signatures of a quantum spin ice ground state suggest that the low-energy physics of the magnetic pyrochlore $\text{Pr}_2\text{Hf}_2\text{O}_7$ can be described by emergent quantum electrodynamics. Such observations constitute a concrete example of a three-dimensional quantum spin liquid—a topical state of matter that has so far mostly been observed in lower dimensions.



David Boldrin, British Imperial College London, UK
 'After my PhD in Chemistry I moved to a postdoc in the Physics department of Imperial College London. I'm interested in all things magnetic, from magnets with exotic quantum effects to those for energy efficient refrigeration, and in using neutrons to study them. I love using chemistry to synthesise new things, be it in a lab or in a brewery!'

Exchange anisotropy and multi- \mathbf{k} magnetic order in a spin-1/2 third-neighbour kagome antiferromagnet

Time-of-flight spectrometers IN4 and IN5

When quantum spins form networks of corner-sharing triangles—the so-called kagome lattice—conventional magnetic ordering is suppressed by geometric frustration and quantum fluctuations, leaving room for exotic magnetic states such as quantum spin liquids or unconventionally ordered states. Nature still provides the best examples of these systems and therefore remains the best resource when searching for quantum frustration. Inelastic neutron scattering measurements on IN4 and IN5 on the natural mineral vesignieite, which forms a spin-1/2 kagome lattice, show that the antiferromagnetic exchange interaction between third-nearest neighbour spins dominates all other interactions. The opening of a gap in one of the spin-wave branches reveals a tiny symmetric exchange anisotropy that favours an unconventional coplanar multi- \mathbf{k} magnetic structure. This structure is energetically degenerate with the octahedral state predicted by theory for isotropic Heisenberg exchange.

Figure 1

The kagome lattice of vesignieite showing the ordered arrangement of the Cu^{2+} $S = 1/2$ spins (coloured arrows) of the hexagonal magnetic structure. The black line is the crystallographic unit cell and the green line the magnetic unit cell. The **top right inset** illustrates how the spins point towards the vertices of a hexagon.

AUTHORS

D. Boldrin and A.S. Wills (University College, London, UK)
 H.C. Walker, P. Manuel and D.D. Khalyavin (ISIS, UK)
 B. Fák, E. Canévet and J. Ollivier (ILL)

ARTICLE FROM

Phys. Rev. Lett. (2018)—doi: 10.1103/PhysRevLett.121.107203

REFERENCES

- [1] L. Balents, Nature 464 (2010) 199
- [2] L. Messio, C. Lhuillier and G. Misguich, Phys. Rev. B 83 (2011) 184401
- [3] T.-H. Han, J.S. Helton, S. Chu, D.G. Nocera, J.A. Rodriguez-Rivera, C. Broholm and Y.S. Lee, Nature 492 (2012) 406
- [4] B. Fák, E. Kermarrec, L. Messio, B. Bernu, C. Lhuillier, F. Bert, P. Mendels, B. Koteswararao, F. Bouquet, J. Ollivier, A.D. Hillier, A. Amato, R.H. Colman and A.S. Wills, Phys. Rev. Lett. 109 (2012) 037208

In geometrically frustrated magnets, the topology of the lattice prevents conventional long-range order. Instead, exotic and degenerate ground states are expected, such as quantum spin liquids [1] and unconventional non-collinear multi- \mathbf{k} magnetic structures [2]. In the kagome lattice (**figure 1**), the most frustrated of the simple two-dimensional lattices, theoretical work focused initially on the nearest-neighbour Heisenberg model with isotropic spins, as realised in the emblematic mineral Herbertsmithite, $\gamma\text{-ZnCu}_3(\text{OH})_6\text{Cl}_2$ [3]. More recent work has addressed the case of anisotropic interactions as well as interactions beyond first-neighbours. An example is the mineral kapellasite, $\alpha\text{-ZnCu}_3(\text{OH})_6\text{Cl}_2$, where competition between first- and third-neighbour exchange leads to a chiral quantum spin liquid state with fluctuations born of an unconventional but classic cuboctahedral cuboc2 phase [4].

We studied the natural mineral vesignieite, $\text{BaCu}_3\text{V}_2\text{O}_8(\text{OH})_2$, a rare realisation of a fully stoichiometric kagome lattice of quantum spins $S = 1/2$. The material orders antiferromagnetically at $T_N = 9$ K, ten times below the Weiss temperature, showing the high degree of magnetic frustration. Inelastic neutron scattering measurements were performed on a fully deuterated powder sample using the IN5 and IN4 time-of-flight spectrometers. In addition to the spin excitations shown in **figure 2a**, magnetic Bragg peaks were observed with the unusual propagation vector $\mathbf{k} = (1/2, 0, 0)$,

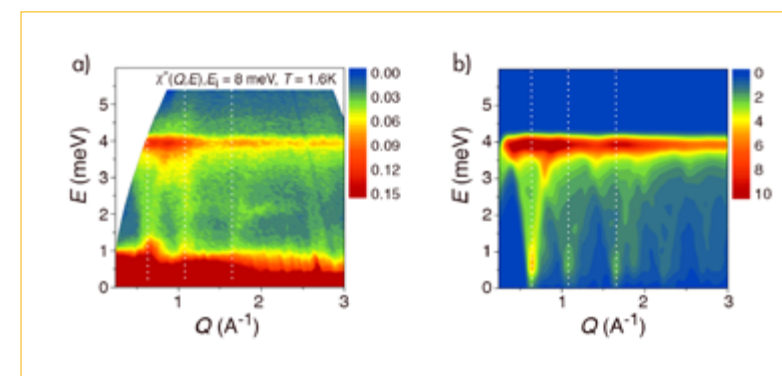
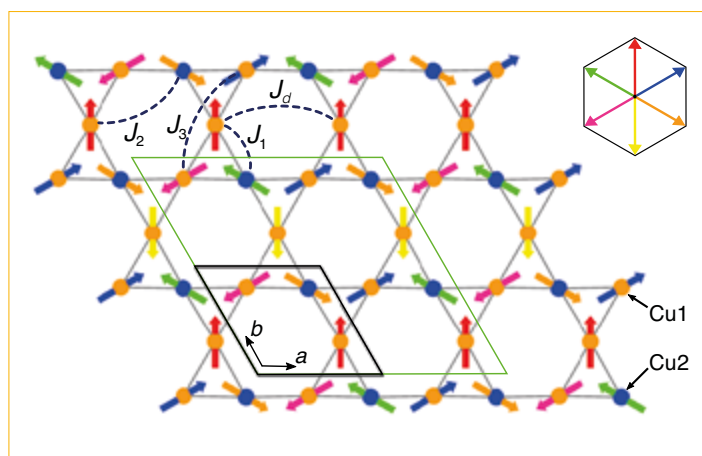


Figure 2

a) Dynamic susceptibility of vesignieite at a temperature of $T = 1.6$ K measured on IN5 with $E_1 = 8.0$ meV.
b) Calculated spin-wave dispersion using a J_3 -only model. Dashed white lines indicate the magnetic Bragg peak positions.

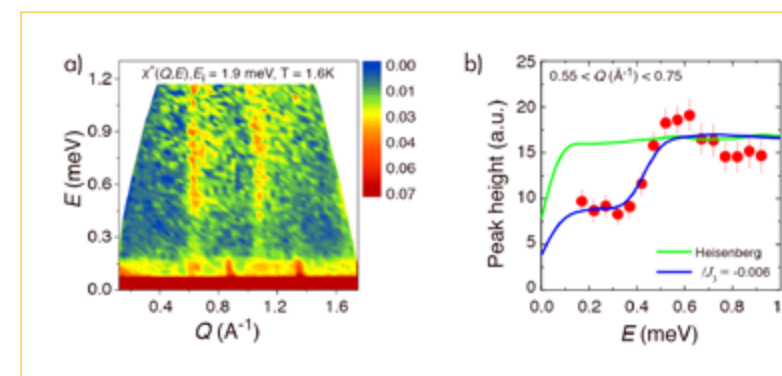


Figure 3

a) Dynamic susceptibility of vesignieite at $T = 1.6$ K measured on IN5 with $E_1 = 1.9$ meV.
b) Energy scan at constant $Q = 0.65 \pm 0.1$ \AA^{-1} (symbols), plotted with spin-wave calculations for the hexagonal magnetic structure using isotropic exchange (green curve) and symmetric exchange anisotropy (blue curve).

corresponding to the M point of the Brillouin zone. This wave vector characterises a number of non-collinear multi- \mathbf{k} magnetic structures predicted theoretically [2], and the observed extinction rule points to the octahedral structure. One particularity of this structure is that it is energetically degenerate with numerous coplanar and collinear magnetic structures. Indeed, subsequent neutron diffraction measurements performed at WISH, ISIS (UK) showed evidence of the coplanar 'hexagonal' magnetic structure illustrated in **figure 1**.

The measured spin-wave spectra shown in **figure 2a** are well reproduced by linear spin wave theory (**figure 2b**) using exchange between third-nearest neighbours only (J_3 in **figure 1**), with all other interactions being at least one order of magnitude smaller. The intensity of these spin-wave excitations shows an unusual energy dependence, see **figure 3**, which can be explained by a small symmetric exchange anisotropy, less than 1% of J_3 . This anisotropy creates a finite energy gap for one of the acoustic spin-wave branches leaving the other modes gapless, resulting in the strong spectral change. The presence of this weak exchange anisotropy also explains the selection of the coplanar hexagonal magnetic structure rather than the non-coplanar octahedral structure predicted for the isotropic Heisenberg case.

A particularity of the multi- \mathbf{k} hexagonal structure we observe in vesignieite is that it consists of three essentially decoupled lattices. In such a 'decoupled' multi- \mathbf{k} structure, disordering one of the sites will have no effect on the magnetic order or magnetic excitations. This is exactly what happens in vesignieite. Orbital disorder on only one of the Cu sites, which occurs because of an inability to arrange the orbitals with threefold rotational symmetry around the kagome triangles, does not destroy the magnetic order. This effect is consistent with the observed multi- \mathbf{k} magnetic structure, since the global trigonal symmetry of the $P3_121$ space group of vesignieite is restored by the 'deselection' of different arms of the star of \mathbf{k} in adjacent kagome layers.

Our results, in addition to being the first experimental observation of symmetric exchange anisotropy in a powder sample using inelastic neutron scattering, have implications well beyond kagome systems since the hexagonal structure of vesignieite can be thought of as three interlocked, skewed, square lattices.

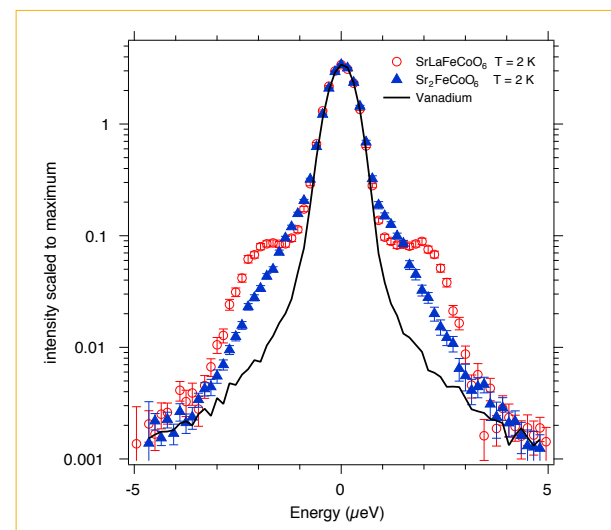


Tapan Chatterji, French ILL, Grenoble
Twitter account: Tapan_Chatterji
'My field of scientific research is magnetism and superconductivity. To study magnetic and superconducting materials, I use neutron scattering along with other laboratory measurements.'

Hyperfine interaction study of $\text{Sr}_{2-x}\text{La}_x\text{FeCoO}_6$ for $x = 0, 1$ and 2 by high-resolution neutron spectroscopy

Backscattering spectrometer IN16B
SPHERES at MLZ, Garching

Double perovskites have been under intense investigation for about a decade or so, by way of *ab initio* electronic structure calculations and many other condensed-matter experimental methods. They show promise as smart, functional materials for electronic industries. Here, we studied the magnetic ground state of these materials by measuring their hyperfine interaction and electronic magnetic fluctuations with inelastic neutron scattering.



AUTHORS

T. Chatterji and M. Appel (ILL)
M. Zamponi (Jülich Centre for Neutron Science at MLZ, Garching, Germany)
H.S. Nair (University of Texas El Paso, USA)
R. Pradheesh, G.R. Haripriya, V. Sankaranarayanan and K. Sethupathi (Indian Institute of Technology Madras, Chennai, India)

ARTICLE FROM

PRB (2018)—doi: 10.1103/PhysRevB.98.094429

REFERENCES

- [1] A. Heidemann, Z. Phys. 238 (1970) 208
- [2] T. Chatterji, B. Frick, M. Zamponi, M. Appel, H.S. Nair, R. Pradheesh, G.R. Haripriya, V. Sankaranarayanan and K. Sethupathi, Phys. Rev. B 98 (2018) 094429
- [3] M. Appel and B. Frick, Rev. Sci. Instrum. 88 (2017) 036105

The study of hyperfine interaction by high-resolution neutron spectroscopy has become a well-established technique [1]. However, among scientific communities it remains considerably less well known than nuclear magnetic resonance (NMR), Mössbauer, perturbed angular correlation, etc. In addition, to date it has mainly been employed for studying long-range magnetically ordered systems and seldom for disordered magnetic systems such as spin glass or the so-called magnetic glasses that are not long-range ordered. Here, we report on detailed, hyperfine interaction studies [2] using high-resolution neutron spectroscopy on three double perovskites, $\text{Sr}_{2-x}\text{La}_x\text{FeCoO}_6$ for $x = 0, 1$ and 2 , with canonical spin-glass, magnetic glass and long-range ordered magnetic ground states, respectively.

These studies were carried out on the backscattering spectrometers IN16B of the Institute Laue-Langevin and the SPHERES of the MLZ in Garching.

Looking at **figure 1**, we can see the inelastic spectra of $\text{Sr}_2\text{FeCoO}_6$ and SrLaFeCoO_6 at $T = 2$ K, along with vanadium resolution spectra obtained on IN16B. These spectra are background corrected, summed in the Q range $0.44 < Q < 1.9 \text{ \AA}^{-1}$ and normalised to the elastic peak maximum. We can see immediately that the spectrum of the canonical spin-glass compound $\text{Sr}_2\text{FeCoO}_6$ (blue triangles), although broader than the vanadium resolution spectra, shows no clear-cut inelastic peaks in the energy loss and energy gain sides, whereas the spectrum for the so-called magnetic glass compound SrLaFeCoO_6 shows clear inelastic peaks on both sides of the central elastic peak.

Presented in **figure 2** is the temperature variation of the inelastic spectra of the magnetic glass compound, SrLaFeCoO_6 . We note that the inelastic peaks on both sides of the elastic peak move towards the central elastic peak as the temperature increases, finally merging with the central elastic peak at about the spin-freezing temperature $T_{\text{sf}} = 90$ K.

Our analysis, provided in reference [2], shows the spin-glass compound $\text{Sr}_2\text{FeCoO}_6$ to exhibit similar softening behaviour.

Figure 1

Inelastic spectra of $\text{Sr}_2\text{FeCoO}_6$ and SrLaFeCoO_6 at $T = 2$ K, along with vanadium resolution spectra obtained on IN16B with high signal-to-noise ratio [HSNR] [3]. These spectra are background corrected, summed in the Q range $0.44 < Q < 1.9 \text{ \AA}^{-1}$ and normalised to the elastic peak maximum.

The quasi-elastic-like spectra also move towards the central elastic peak and finally merge with it at about the spin-freezing temperature $T_{\text{sf}} = 90$ K.

Surprisingly, the third compound, which we know from neutron powder diffraction measurements to undergo a long-range structural and magnetic ordering below about 250 K, shows no inelastic or quasi-elastic scattering in the temperature range 3–300 K investigated [3] (see **figure 3**). The spectra obtained at high and low temperatures are indistinguishable both from one another and from the vanadium resolution spectrum.

It is surprising that this magnetically ordered compound shows no inelastic or quasi-elastic scattering below the transition temperature $T_c = 250$ K. However, the present hyperfine interaction study using inelastic neutron scattering is only sensitive to the magnetic ordering of the Co magnetic sublattice. The absence of inelastic or quasi-elastic scattering implies that the induced local field at the Co site is too weak to detect the splitting of the ground state and that the Co atoms do not order magnetically. We conclude that the magnetic ordering evidenced by the appearance of magnetic Bragg peaks must be from the Fe sublattice only. This is confirmed by the temperature dependence of the Q -integrated elastic intensity ($\Delta E \sim 0$), which provides very useful information about the electronic magnetic ordering and is shown in **figure 4**. We can see clearly that the elastic intensities of the canonical spin glass $\text{Sr}_2\text{FeCoO}_6$ and magnetic glass compound SrLaFeCoO_6 show a step-like increase in elastic intensity, whereas that for the magnetically ordered compound $\text{La}_2\text{FeCoO}_6$ increases continuously with no step-like behaviour.

Our present study revealed a clear inelastic signal for SrLaFeCoO_6 , a possible inelastic signal for $\text{Sr}_2\text{FeCoO}_6$ below the spin-freezing temperatures T_{sf} , but no inelastic signal at all for the magnetically ordered $\text{La}_2\text{FeCoO}_6$ in the neutron scattering spectra. The broadened inelastic signals observed suggest hyperfine field distributions in the two disordered magnetic glassy systems, whereas the absent inelastic signal for the third compound suggests a very small or no hyperfine field at the Co nucleus due to Co electronic moment. The hyperfine splitting on the Co nucleus is induced by the electronic spin state of the magnetic sample atom; our experiments provide additional information on the time scale of electronic spin fluctuations by the appearance of quasi-elastic broadening in the μeV range at low Q due to spin freezing on the nanosecond time scale below T_{sf} . While these features are observed at low Q for $x = 0$ and 1 they are absent for $\text{La}_2\text{FeCoO}_6$, pointing to a gradual increase of the elastic intensity only at large Q near an emerging Bragg peak. Thus, both electronic magnetic-spin freezing and inelastic excitations arising from nuclear hyperfine splitting at the Co site consistently indicate different behaviour for $x = 2$.

In conclusion we have shown that hyperfine interaction studies using inelastic, high-resolution neutron spectroscopy can yield very useful information about the ground state of the spin glass and other disordered magnetic systems. It can also provide information about the slow electronic spin fluctuations on the nanosecond scale.

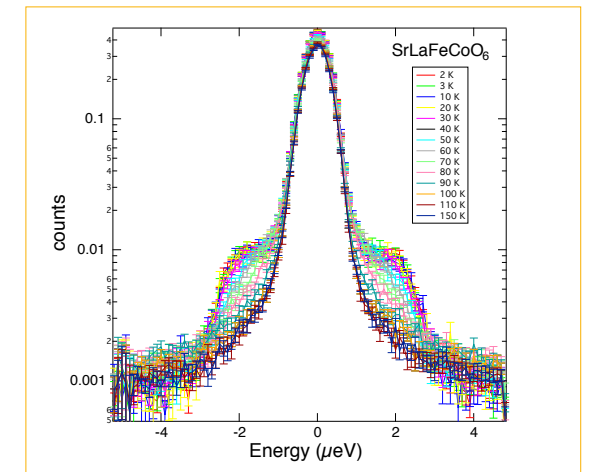


Figure 2

Temperature variation of the inelastic spectra of the magnetic glass compound, SrLaFeCoO_6 . The inelastic peaks on both sides of the elastic peak move towards the central elastic peak as the temperature increases and finally merge with the central elastic peak at about the spin-freezing temperature $T_{\text{sf}} = 90$ K.

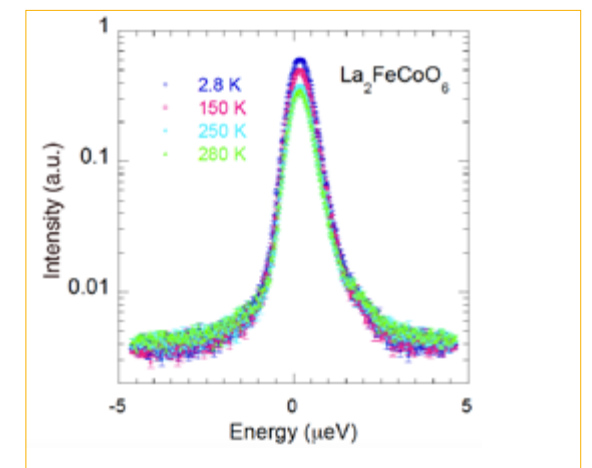


Figure 3

The spectra from $\text{La}_2\text{FeCoO}_6$ at several temperatures. We can observe that the spectra obtained at high and low temperatures are indistinguishable from one another.

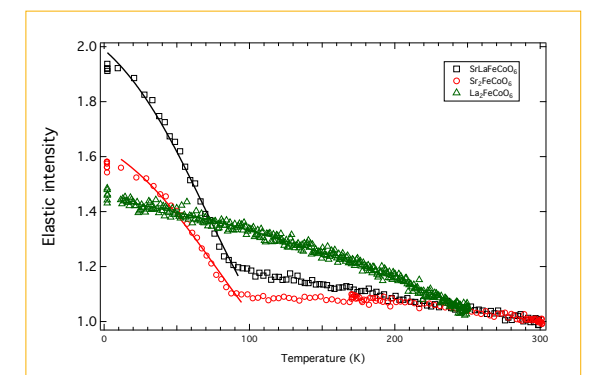
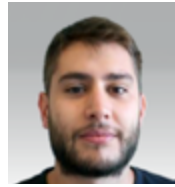


Figure 4

Elastic intensity of $\text{La}_2\text{FeCoO}_6$ (green triangles) measured on IN16B in the high-resolution mode summed over all detectors, compared with the elastic intensities of $\text{Sr}_2\text{FeCoO}_6$ (red circles) and SrLaFeCoO_6 (black squares). The data are normalised to the highest temperature measured above the magnetic ordering temperature.



Quentin Faure. French University Grenoble Alpes, CEA – INAC, Institut Néel, and ILL
'I am finishing my PhD on quantum magnetism, more specifically on antiferromagnetic anisotropic spin chains. This work encompasses neutron scattering, numerical calculations and thermodynamic measurements under pressure. Theoretical input was provided by T. Giamarchi and S. Takayoshi.'

Topological quantum phase transition in the Ising-like antiferromagnetic spin chain $\text{BaCo}_2\text{V}_2\text{O}_8$

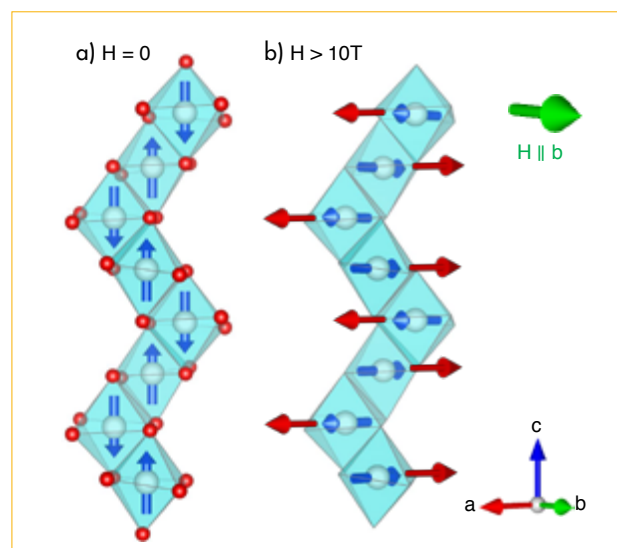
Single-crystal diffractometer D23

Three-axis spectrometers ThALES and IN12

The universal concept of phase transitions, usually characterised by a symmetry breaking, has played a crucial role in the description of many phenomena in condensed matter physics. However, since the seminal ideas of Berezinskii, Kosterlitz and Thouless (Nobel Prize in Physics, 2016), topological excitations are at the heart of our understanding of a novel class of phase transitions. Here, we provide evidence of a quantum phase transition separating two unconventional magnetic phases characterised by different kinds of topological excitations.

Figure 1

a) Zero-field magnetic structure (blue arrows) of a single Co^{2+} screw chain of $\text{BaCo}_2\text{V}_2\text{O}_8$ (blue and red spheres are Co and O respectively).
b) Applying a magnetic field along **b** creates an additional staggered field along **a** (red arrows), which produces a new rotated magnetic arrangement shown by the blue arrows (the O atoms are no longer represented in this figure, for sake of clarity).



AUTHORS

Q. Faure (UGA, CEA-INAC, Institut Néel and ILL)
 S. Petit (ILL, Saclay, France)
 V. Simonet (Institut Néel, Grenoble, France)
 S. Raymond (CEA-INAC, Grenoble, France)
 M. Boehm (ILL)
 B. Grenier (UGA, CEA-INAC, Grenoble, France)

ARTICLE FROM

Nat. Phys. (2018)—doi: 10.1038/s41567-018-0126-8

REFERENCES

- [1] S. Kimura *et al.*, J. Phys. Soc. Jpn. 82 (2013) 033706
- [2] Q. Faure *et al.*, Nat. Phys. 14 (2018) 867
- [3] B. Grenier *et al.*, Phys. Rev. Lett. 114 (2015) 017201

Topology has brought new insight to our understanding of condensed matter physics. For instance, topological phase transitions exhibit no symmetry breaking and are characterised by topological defects / excitations (discontinuities that cannot be removed by continuous deformation unless annihilated by their anti-defects). In most cases, those transitions are controlled by a single type of topological object, for instance solitons (kinks and 360° rotation of a pendulum, for instance) or vortices. However, there are richer and less studied classes of topological phase transitions in which two different sets of topological excitations compete with each other.

This is what we found in the magnetic oxide $\text{BaCo}_2\text{V}_2\text{O}_8$. In this material, which consists of chains of Co^{2+} carrying effective anisotropic spin-1/2, the spins are strongly coupled antiparallel to each other in the 'Ising' **c**-direction (see **figure 1a**). Because of crystallographic peculiarities, applying a transverse uniform magnetic field **H** along **b** produces an additional transverse and staggered magnetic field along **a** [1]. The latter competes with the Ising anisotropy and forces the spins to bend along **a** (see **Figure 1b**), as evidenced by neutron diffraction on D23, driving a phase transition beyond $H_c = 10$ T [2].

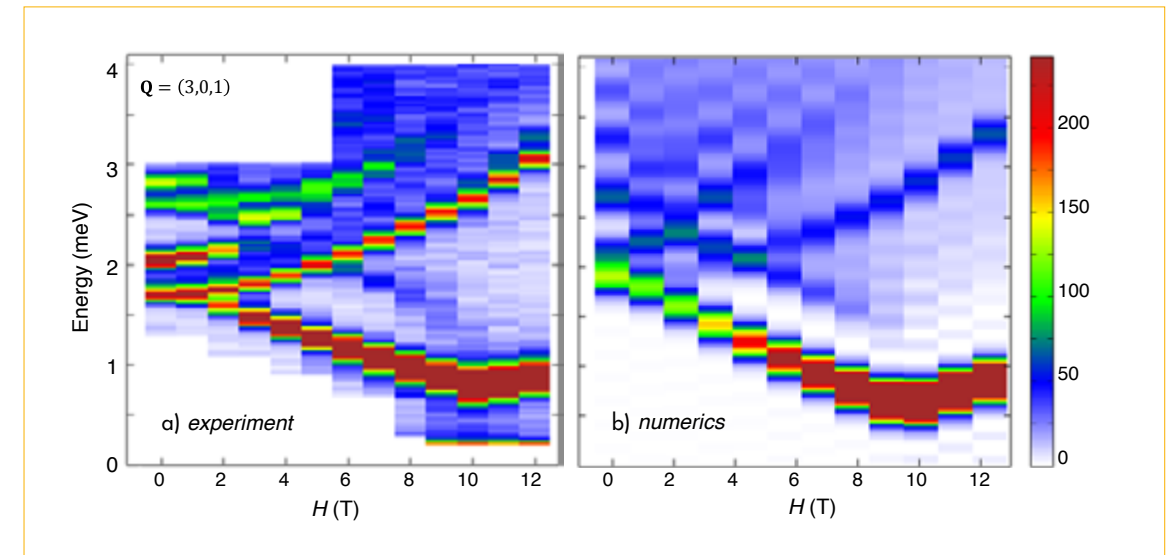


Figure 2

a) Experimental intensity colour map showing the magnetic field dependence of the magnetic excitations in $\text{BaCo}_2\text{V}_2\text{O}_8$ for a transverse field applied along the **b**-axis and for $\mathbf{Q} = (3, 0, 1)$.
b) Theoretical intensity colour map to be compared with the experimental one, obtained from iTEBD calculations of the $S(\mathbf{Q}, \omega)$ neutron scattering dynamical structure factors. The intensity colour scale shown on the right is in arbitrary units.

The nature of this transition was further elucidated by combining inelastic neutron scattering experiments (on ThALES and IN12, using unpolarised and polarised neutrons, respectively) and numerical infinite Time Evolving Block Decimation (iTEBD) calculations [2]. We were able to show that for $H = 0$, the spin dynamics is governed by an assembly of spinons carrying a spin $1/2$. Because of inter-chain couplings, they are tied up in bound states of three flavours (two transverse degenerate, polarised along **a** and **b**, and one longitudinal, polarised along **c**), forming a discrete excitation spectrum [3]. Above H_c , however, the low-energy spectrum essentially consists of two well-defined branches corresponding to spin 1 transverse modes polarised along **b** and **c**. These excitations can be understood as kinetic bound states formed by two adjacent spinons strongly attached by the staggered field and moving together along the chain. **Figure 2** illustrates how the magnetic field operates this change. Importantly, the very good agreement between the experimental and numerical results (see **figures 2a** and **2b**, respectively) fully validates our model.

The magnetic excitations characterising the phases on both sides of the transition are thus two different types of solitonic topological objects in competition. Our experimental results can be further described in field theory by the so-called 'double sine-Gordon model', which is relevant well beyond the field of magnetism.



Dorjan Dauti, Albanian University Grenoble Alpes
Twitter account: twitter.com/DorjanDauti
'I have a PhD in Materials Science and Civil Engineering, my research focus being the behaviour of concrete at high temperature. In my research, I apply my knowledge to heat and mass transfer modelling of porous construction materials, finite element simulations, neutron imaging and digital image analysis.'

Analysing 3D real-time moisture distribution in heated concrete to better understand fire spalling mechanisms

Neutron reflectometer and neutron-imaging instrument D50

The spalling of concrete, a phenomenon frequently encountered in concrete elements exposed to high temperature, can lead to structural failure. The evolution of moisture content in heated concrete is directly linked to spalling. Through this study we contribute to a better understanding of the behaviour of concrete at high temperature, by quantitatively analysing, for the first time in the literature, the moisture migration in heated concrete using *in situ* neutron tomography [1].

AUTHORS

D. Dauti (University Grenoble Alpes, France and Swiss Federal Laboratories for Materials Science and Technology, Switzerland)
A. Tengattini (University Grenoble Alpes and the ILL, France)
S. Dal Pont and **M. Briffaut** (University Grenoble Alpes, France)
N. Toropovs (Swiss Federal Laboratories for Materials Science and Technology, Switzerland)
B. Weber (Swiss Federal Laboratories for Materials Science and Technology, Switzerland and Riga Technical University, Latvia)

ARTICLE FROM

Cement Concrete Res. (2018)—doi: 10.1016/j.cemconres.2018.06.010

REFERENCES

- [1] D. Dauti, A. Tengattini, S. Dal Pont, N. Toropovs, M. Briffaut and B. Weber, *Cement Concrete Res.* 111 (2018) 41
- [2] P. Kalifa, F.-D. Menetau and D. Quenard, *Cement Concrete Res.* 30 (2000) 1915
- [3] N. Toropovs, F. Lo Monte, M. Wyrzykowski, B. Weber, G. Sahmenko, P. Vontobel, R. Felicetti and P. Lura, *Cement Concrete Res.* 68 (2015) 166

When concrete is exposed to high temperature, a number of thermo-hydro-mechanical phenomena, which strongly interact with each other, take place. The most important among these are heat transfer due to temperature gradients, mass flow through the porous structures due to pressure gradients, phase changes (evaporation, condensation and dehydration) and crack opening due to thermally incompatible aggregate-cement paste, etc. While existing experimental techniques provide pointwise measurements [2] or 2D moisture profiles [3], information in 3D is indispensable for taking into account the heterogeneous nature of concrete.

Neutron tomography allows access to the local moisture distribution in concrete. The experiments that we performed consisted of heating test samples to fire-like conditions while simultaneously acquiring rapid neutron tomographies, with the aim of tracking the evolution of moisture content. Cylindrical specimens with a diameter of 3 cm were tested. As one of the objectives was to estimate the influence of aggregate size, two concrete mixes were used: one with a maximum aggregate size of 4 mm

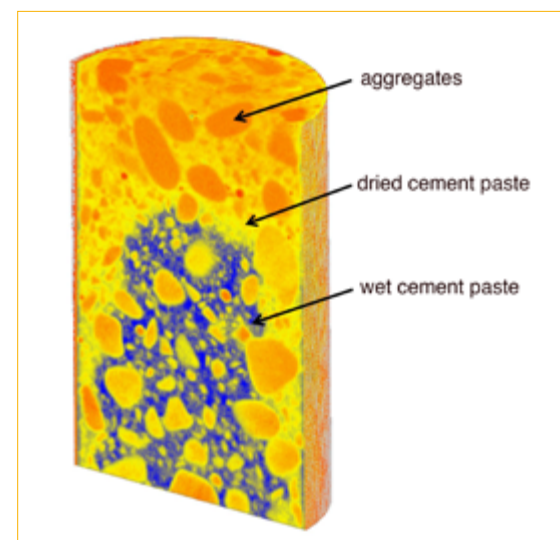


Figure 1

Example of a 3D scan acquired in 1 min with neutron tomography while the concrete is being heated. The 3D volume is cut in half to highlight the drying front around the aggregate.

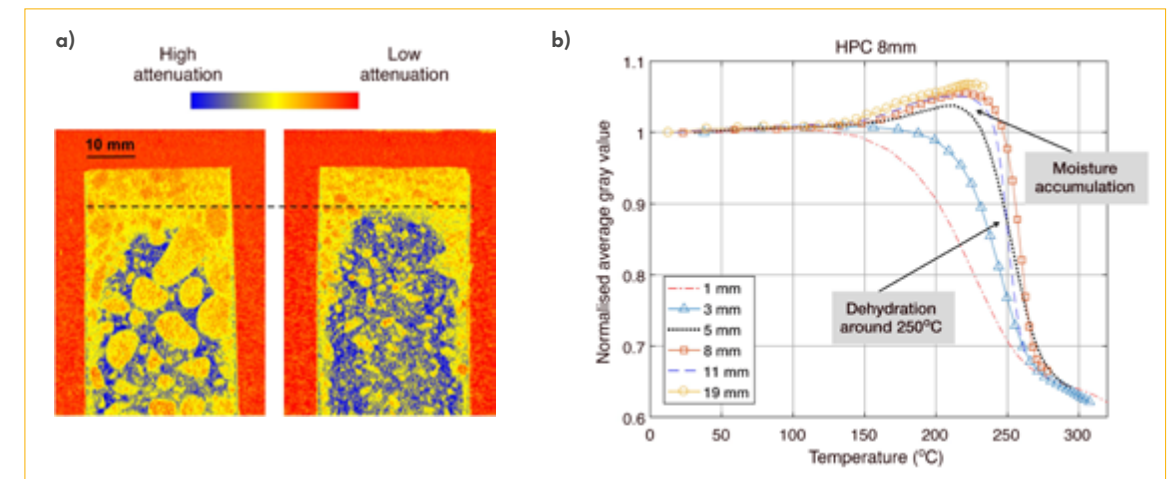


Figure 2

- a)** Vertical slices from reconstructed 3D volumes highlighting the faster drying front in HPC 8 mm (on the left) compared with HPC 4 mm (on the right).
- b)** Image analysis reveals important information about the dehydration of concrete and moisture accumulation.

(HPC 4 mm), the other a maximum aggregate size of 8 mm (HPC 8 mm). Some of the specimens were equipped with thermocouples for temperature measurements at distances 3, 10 and 20 mm from the heated surface.

The specimens were wrapped laterally with self-adhesive aluminum foil and placed inside a heating cell. The radiator heater placed above the sample was heated up to 500 °C. The world-leading flux at the ILL allowed us to take a 3D scan with 500 projections in just one minute (see **figure 1**). This time resolution was sufficient to capture the fast dehydration process occurring inside the concrete.

In **figure 2a**, vertical slices from 3D scans containing the sample's axis of rotation and taken at three different times are shown for two concrete samples of different aggregate size: HPC 8 mm (left) and HPC 4 mm (right). These results show how the drying front moves faster in the HPC 8 mm sample. Another noteworthy finding is that in all the test samples an additional lateral drying occurred despite the use of heat and moisture insulation. In order to understand whether aggregate size has an influence on thermal field, the temperature measurements at three points inside each specimen were compared. The results showed that the temperature was very similar in both samples, indicating that the thermal field was not the reason behind the different drying velocity. One other possible explanation for differences in the drying front is heat-induced cracking and its dependency on aggregate size; the more pervasive fracture network induced in the HPC 8 mm would accelerate the drying process.

The evolution of moisture content is associated with a possible mechanism of spalling, specifically the condensation of vapour in front of the drying front creating an impermeable layer known as moisture clog. For this reason, we performed more in-depth analysis to quantify the variation in water content in space and time by looking at the attenuation coefficient of the cement paste. Using the temperature measurements provided by the thermocouples, we obtained the profiles shown in **figure 2b**, where we observed:

- *water loss at around 250 °C*. This observation reveals important information about the dehydration of concrete and is useful for the community working on numerical modeling of concrete at high temperature.
- *moisture accumulation behind the drying front*. While many studies in the literature have postulated the existence of a moisture clog, its quantification was previously not possible due to the lack of suitable experimental methods. Taking advantage of neutron tomography, we can now quantify this phenomenon. However, special attention should be given to possible imaging artefacts (e.g. beam hardening) that might affect the results.

The results obtained from the neutron tomography tests provide valuable information for understanding and modelling processes relating to the behaviour of concrete at high temperature with respect to spalling. A more comprehensive analysis of the thermo-hydro-mechanical response of heated concrete, as highlighted by these experiments, can be found in [1].



Eleni Stavropoulou, Greek University Grenoble Alpes, 3SR, France
 'My work focuses on the mechanical behaviour of interfaces of geomaterials, these being the weakest points in terms of mechanical resistance in geotechnical structures. The study of interfaces involves understanding not only the materials composing them (rock, concrete, etc.), but also their eventual hydro-thermo-chemo mechanical interaction.'

Liquid water uptake in unconfined Callovo-Oxfordian clay rock studied with neutron and X-ray imaging

Neutron reflectometer and neutron-imaging instrument D50

The Callovo-Oxfordian clay rock (COx) is studied in France for its use in the disposal of radioactive waste, because of its extremely low permeability. This host rock is governed by a hydromechanical coupling of high complexity. This experimental study explores the mechanisms of water uptake in small, unconfined, prismatic specimens of COx. Water uptake is monitored using both X-ray tomography (3SR Lab) and neutron radiography (ILL) for the first time, the combination of these imaging techniques allowing material deformation and water arrival respectively to be quantified.

AUTHORS

E. Stavropoulou (University Grenoble Alpes and Andra Agency, France)
 E. Andò (University Grenoble Alpes, France)
 A. Tengattini (ILL and University Grenoble Alpes, France)
 M. Briffaut, F. Dufour and D. Atkins (ILL)
 G. Armand (Andra Agency, France)

ARTICLE FROM

Acta Geotech. (2018)—doi: 10.1007/s11440-018-0639

REFERENCES

- [1] C. Zhang and T. Rothfuchs, Appl. Clay Sci. 26 (2004) 325
- [2] G. Armand, F. Bumbieler, N. Conil, R. de la Vaissière, J.-M. Bosgiraud and M.N. Vu, J. Rock Mech. Geotech. Eng. 9 (2017) 415
- [3] H.G. Montes, J. Duplay, L. Martinez, S. Escoffier and D. Rousset, Appl. Clay Sci. 25 (2004) 187
- [4] A. Tengattini, D. Atkins, B. Giroud, E. Andò, J. Beaucour and G. Viggiani, ICTMS2017 (2017)

The management of radioactive waste is an important environmental issue. In eastern France, the French National Radioactive Waste Management Agency (Andra) is studying the behaviour of a deep geological repository in Callovo-Oxfordian clay rock (COx). The permeability of the Callovo-Oxfordian stratum is extremely low; it is, however, governed by complex thermo-hydro-mechanical behaviour, which is continuously under investigation in both laboratory and in-field experiments [1].

During the operation phase, tunnels are excavated and then ventilated until they are finally closed. In specific sections, swelling clay such as bentonite is positioned in between two concrete plugs in order to seal the tunnel and apply pressure to the rock wall in sections where the concrete lining is removed [2]. The study of the mechanical behaviour of the concrete/COx interface in the laboratory requires representative and reproducible concrete/COx samples to be created under controlled conditions.

Figure 1

Selected *in situ* images acquired during imbibition for two clay rock samples. X-ray data are presented as a vertical slice in the middle of the specimen, whereas neutron radiographs are averaged together in 5-min intervals in order to match the X-ray tomography times.

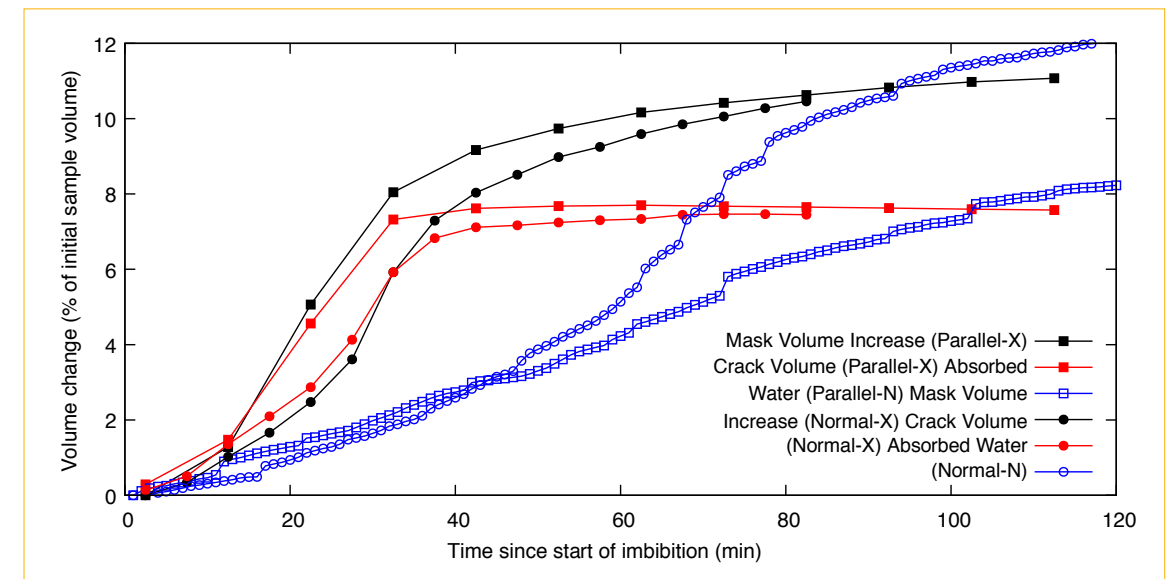
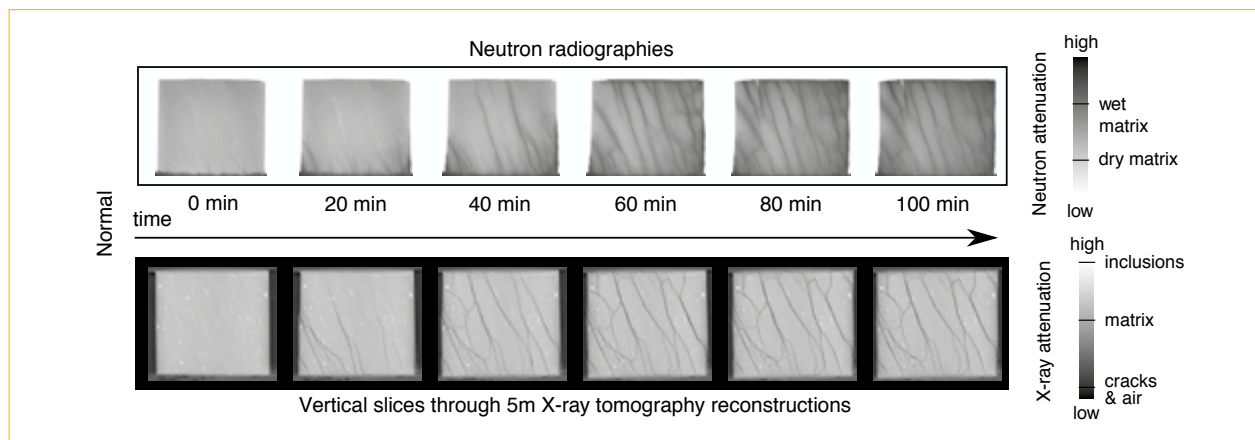


Figure 2

Macroscopic measurements of sample evolution from X-ray tomography (total and crack volumes) and neutron radiography (water volume).

During the preparation of these samples, when fresh concrete is poured directly onto the unconfined COx, macro-cracks in the clay rock have been detected prior to the start of the mechanical experiments. Even though the water sensitivity of COx is known [3], the cause of these macro-cracks in the case of the poured concrete/clay-rock interface must be further investigated in order to understand whether they reflect site conditions. In the lab, the exposed, drying face of the clay rock is rapidly wetted by the free water of the fresh concrete.

To gain some insight into the causes of this phenomenon, a number of *in situ* wetting experiments were carried out using high-speed lab X-ray tomography (in the 3SR laboratory) and neutron radiography (on the ILL instrument D50-tomography or 'NeXT' that has recently come online in Grenoble [4]).

Four prismatic clay rock samples were extracted from a single core: two *normal* and two *parallel* to the bedding plane. For each pair, two practically identical imbibition tests were performed independently under either neutron radiography or X-ray tomography. **Figure 1** shows the images of the two similar samples oriented *normal* to the bedding plane and scanned using both imaging techniques, where one can clearly observe the consistent crack patterns with both imaging techniques for each

orientation. Neutron radiographs allow the detection and measurement of water entry and penetration in the clay rock sample (high attenuation = dark grey values), while X-ray tomographs allow the measurement of changes in density, thus crack opening and propagation (low attenuation = dark grey values).

Analysis of the acquired X-ray tomography and neutron radiography data allow some interesting measurements and observations at the scale of the sample. **Figure 2** shows the evolution of sample-wide quantities that can be obtained: X-ray tomography data is used to measure the change in volume of the external boundary of the specimen and the volume of visible cracks, and neutron radiographs are used to measure water entering the specimen. The upshot of **Figure 2** is that the imbibition process causes a rapid change of volume in the COx samples tested, where most of the sample's increase in volume occurs due to large cracks that appear and develop. In both test samples, after about 50 minutes crack volumes then become relatively constant over the observed time. The water, which causes the cracks, steadily enters the sample at a significantly lower rate than the crack propagation; however, it continues to do so after the cracks have stopped increasing in volume, thus the phase starting from 50 minutes onwards appears to be one of water uptake into the matrix without cracking at the scale observed.



Heiner Meyer. German
Leibniz-Institute for Materials Engineering –
IWT, Bremen Germany
*'I am a physicist working on ex situ and in situ
analysis using diffraction techniques. I conduct
work on the connection between internal
material loading state and the resulting
material modifications in processes with
mechanical influence.'*

Measuring internal material load during metal processing

Strain analyser for engineering applications SALSA

Knowledge about the interdependence between process parameters and the resulting material state in industrial application of the deep rolling process on, e.g. crankshafts, can allow targeted manufacturing and improvements in the service properties of components. *In situ* analyses of the material state during various processes can give valuable insight into the material behaviour due to mechanical, thermal or chemical material load on the workpiece. In the present project, we designed and performed *in situ* neutron diffraction experiments during a mechanical surface finishing process called deep rolling, to determine the internal material load for specific contact parameters.

AUTHORS

H. Meyer, J. Epp and H.-W. Zoch (Leibniz-Institute for Materials Engineering – IWT, Bremen Germany)
T. Pirling (ILL)

ARTICLE FROM

Mater. Perform. Charact. (2018)—doi: 10.1520/MPC20170132

REFERENCES

- [1] B. Scholtesand and E. Macherauch, Z. Metallk. 77 (1986) 322
- [2] E. Brinksmeier, F. Klocke, D.A. Lucca, J. Sölter and D. Meyer, Procedia CIRP 13 (2014) 429
- [3] M. Young, Appl. Opt. 10 (1971) 2763

The deep rolling process is used in industrial production as a finishing step in order to improve the fatigue properties of high-performance components via the introduction of compressive residual stresses, increased surface hardness and reduced roughness [1]. For practical applications however, it is important to understand both the process and how the mechanical load propagates in the sample, leading to a specific material end-state. Using measured internal material loads and residual stresses to solve the inverse problem for process effects is a concept of process signatures, which allow a process-independent approach to final material state depending on internal material load conditions [2].

In the present study, we investigated a deep rolling process using neutron diffraction in order to generate new knowledge about internal material load and resulting residual stress state. Measuring *in situ* poses several challenges to the experimental set-up, both for the measurement and for running the process. To overcome several of these problems, we developed a new strain-imaging approach based on optical methods to determine 2D- and 3D-strain fields in the material under the tool (during the process) and along the plastically deformed path.

In our experiment we used a primary neutron beam defined only by a horizontal collimator, producing a vertical line of 0.6 mm in width (FWHM) and 25 mm

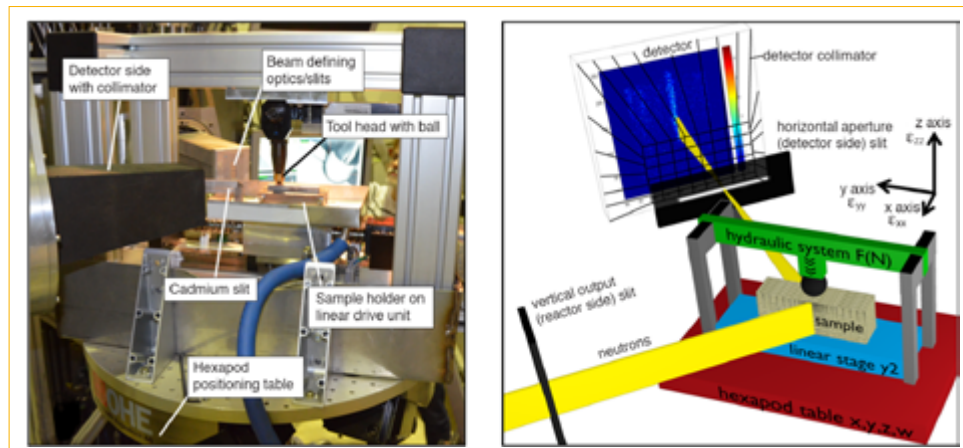


Figure 1

Photo and sketch of the experimental set-up with deep rolling tool and sample in the frame on the hexapod diffractometer table, optical cadmium slit in front of the detector and resulting detector image from the full exposure of the sample under the contact point.

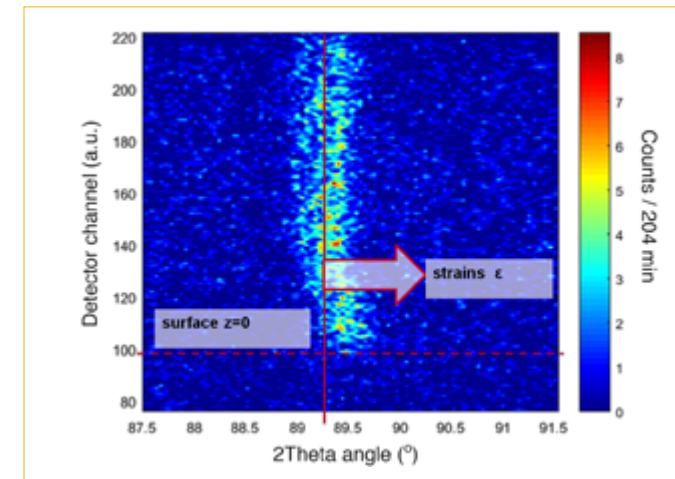


Figure 2

Diffraction image on the detector for single measurement, showing surface cut-off and peak shift due to strains for the measurement position directly under the contact point.

in height. When this beam reaches the workpiece, the diffraction signal is generated over its entire height. The use of a secondary vertical collimator, combined with an optical element in the form of a cadmium slit placed in front of the detector for horizontal resolution, allows the selection of precise gauge volume and a depth-dependent peak position. This new strain-imaging approach generates spatially resolved data about the local strain state along the height of the workpiece with only one single exposition for each x, y-position. The experimental set-up is shown in **figure 1**. For this measurement mode, resolution in depth depends no longer on gauge volume size and distribution but on the size of slit in front of the detector, according to a geometrical pinhole optics formula published by Young [3]. Additionally, the system can reduce influences from process fluctuations, since multiple short measurements are substituted with a single, longer count-time result and the sample surface is always clearly defined, as can be seen in the diffraction image in **figure 2**. Both the strain and the depth below the surface can be recalculated from the detector rows and columns, using Bragg's law and the optical magnification of the system, respectively.

The three-dimensional measurement data confirm the presence of high compressive strain fields in the longitudinal and transversal direction, generated through the elasto-plastic mechanical contact. Overall, the technique allowed an evaluation of both the distribution and amount of strain in each of the different zones that exist during the deep rolling processing, as the reconstructed longitudinal 2D-strain map in **figure 3** shows: the elastic reaction of the material in front of the roller, the elasto-plastically deformed volume followed by the transition region with superposition of residual strains and loading fields, and finally the achieved residual strain state. This study sheds new light on material response to mechanical loads, analysed using a novel neutron diffraction strain-imaging approach for *in situ* process evaluation to enhance our knowledge on the interdependence between process parameters, internal material load fields and the resulting material state for deep rolling.

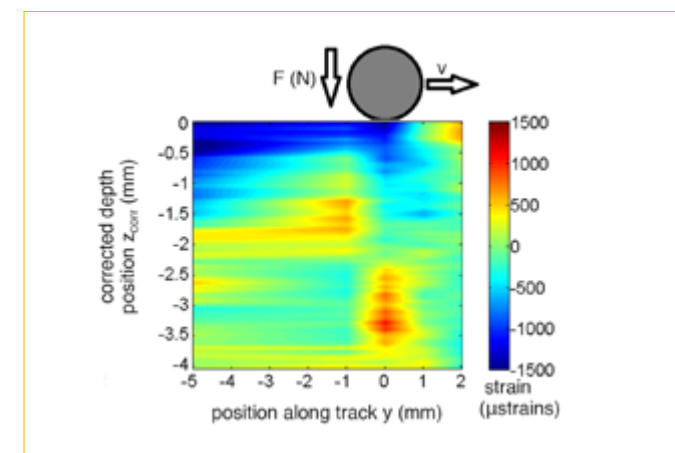
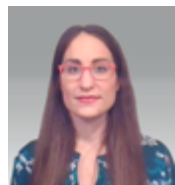


Figure 3

Reconstruction of longitudinal 2D-strain map along the machined track.



Maria Diaz-Lopez. Spanish ISIS and Diamond (UK)
 'I am a postdoctoral researcher working on the structural characterisation of crystallographically challenged materials for energy applications, using a combination of neutron and X-ray total scattering.'

Unravelling the lithium diffusion mechanisms in a highly disordered and nanostructured high-capacity cathode

Disordered materials diffractometer D4

New cathode designs involve more and more disordered/nanosized materials for enhanced Li^+ cation diffusion and larger specific surfaces. This trend poses new challenges for the structural investigation methods employed, which mostly rely on the periodic and long-range ordered nature of the compounds under study. This is especially the case for the recently discovered nanostructured $\text{Li}_4\text{Mn}_2\text{O}_5$ high-capacity cathode material, which shows record reversible capacities and a strongly disordered structure. Here, we demonstrate that a thorough description of such a disordered structure can be achieved by a combination of neutron and synchrotron powder diffraction experiments analysed using the pair distribution function method.

AUTHORS

M. Diaz-Lopez (ISIS and Diamond, Harwell, UK)
 C.V. Colin and P. Bordet (Grenoble Alpes University and Institute Néel, CNRS Grenoble, France)
 V. Pralong (Caen University and CRISMAT, CNRS Caen, France)
 H.E. Fischer (ILL)

ARTICLE FROM

Chem. Mater. 30 (2018) 3060—doi: 10.1021/acs.chemmater.8b00827

REFERENCES

- [1] M. Freire *et al.*, Nat. Mater. 15 (2015) 173
- [2] H. Playford *et al.*, Ann. Rev. Mater. Res. 44 (2014) 429
- [3] M.O. Filsø *et al.*, Chem. Eur. J. 19 (2013) 15535

Although reported to be efficient [1], the migration of Li in the nonstoichiometric $\text{Li}_4\text{Mn}_2\text{O}_5$ (Li4) synthesised by mechanical alloying is not yet understood, due to a lack of detailed knowledge of this disordered structure at the atomic scale. Previous studies based on laboratory X-ray diffraction data revealed Li4 to show on average an MnO-type rock-salt structure, distorted at the local scale as a result of the substitution of $2/3$ manganese for lithium and the presence of $1/6$ oxygen vacancies. Therefore, its full structural description is greatly challenged by its high degree of intrinsic disorder and nanostructuring. In this article, we summarise the complex structural modelling approach that successfully describes, for the first time, the intricate Li-diffusion pathways in this intriguing compound.

First, near-edge X-ray absorption spectroscopy (XANES) at the Mn K-edge was used to probe the co-ordination environment of the manganese, which remained octahedral despite the large number of oxygen vacancies (**figure 1a**). This information was used to build the starting model for the analysis of the total scattering data, where Li atoms are clustered around the O vacancies. Then, a combined neutron and X-ray total scattering refinement was carried out using the Reverse Monte Carlo (RMC) modelling approach performed on a 'large-box' [2] with dimensions similar to the structural coherence length of Li4. Both neutron and X-ray reduced pair distribution function $G(r)$, while total scattering $S(Q)$ functions were simultaneously fitted (**figure 1b**) and soft-chemical bond valence sum (BVS) constraints applied.

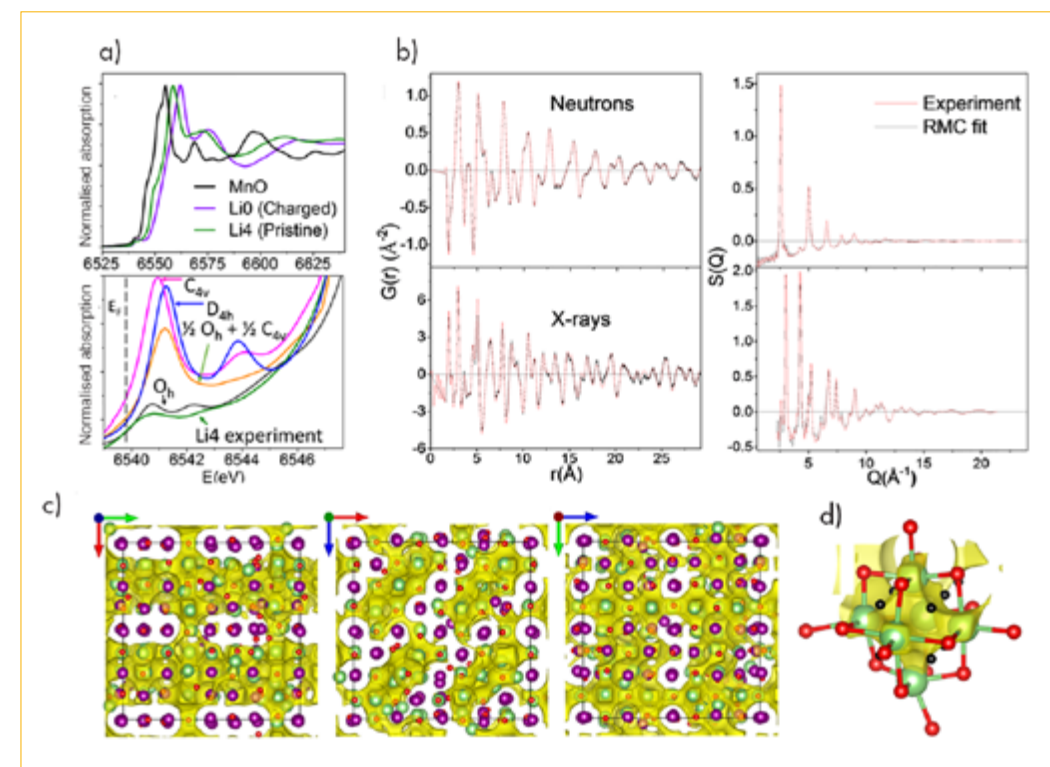


Figure 1

a) Top: Mn K-edge XANES of pristine (Li4) and charged (LiO) cathodes compared with the highly ordered MnO.

Bottom: experimental and simulated pre-edges with Mn in different configurations that might be expected in the presence of oxygen vacancies: square pyramid, square planar, a 1:1 ratio mixture of octahedral and square pyramid, and purely octahedral.

b) RMC fits of Li4 neutron (top) and X-ray (bottom) $G(r)$ (left) and $S(Q)$ (right).

c) Energy landscapes illustrating the 3D Li diffusion in the RMC refined model along a, b and c axes. Green, purple and red spheres denote Li, Mn and O atoms, respectively.

d) Li⁺ diffusion mechanism at the atomic scale. Black spheres denote empty tetrahedral interstices.

Up to ten RMC outputs were evaluated to quantify and ascertain the distribution and local environments of the Mn- framework and the mobile Li ions. Moreover, the accessible Li^+ sites in the RMC refined model were identified by calculating the mismatch of the BVS with respect to Li^+ formal valence, and converted into energy units [3]. The energy landscapes revealed a plausible 3D Li diffusion pathway (**figure 1c**) connecting a large volume of 5-co-ordinated lithium clustered around oxygen vacancies. The diffusion mechanism in Li4 can be better understood when looking at vacancy-lithium octahedral environments (see **figure 1d**), which show that the transport of Li^+ between three lithium sites within the octahedron's faces could occur via the momentary occupation of the neighbouring vacant tetrahedral interstices.

Our results reveal how the combined use of multiple information sources increases the number of constraints for RMC refinements and allows us to reveal fine details in the local structure of advanced functional materials that would otherwise be unattainable.



J.I. Pérez-Landazábal. Spanish Public University of Navarra and Institute for Advanced Materials – INAMAT
‘I received a PhD. degree in solid-state physics from the Basque Country University in 1995. My research interests include ferromagnetic shape memory alloys and magnetic nanoparticles for medical applications. Nowadays, my activity is mainly focused on microstructural and magnetic characterisation, phase transformations and defects in solids. I have authored more than 140 scientific articles SCI.’

Low-temperature, giant magnetocaloric effect in an out-of-equilibrium arrested phase

High-intensity two-axis diffractometer with variable resolution D20

Generally, a magnetic material can be cooled or heated by the application of a magnetic field: the so-called magnetocaloric effect [1]. In particular, in metamagnetic shape memory alloys, the magnetic field can also induce a drastic structural transition—the martensitic transformation (from a high-temperature phase—*austenite*—to a low-temperature phase—*martensite*)—which can lead to a giant magnetocaloric effect [2]. In some of these alloys, the austenite phase can be retained at low temperatures [3], and its ‘anomalous’ transition to martensite on heating promotes a peculiar ‘giant’ and ‘direct’ magnetocaloric effect.

AUTHORS

J.I. Pérez-Landazábal, V. Recarte, V. Sánchez-Alarcos, J.J. Beato-López and C. Gómez-Polo (Public University of Navarra and Institute for Advanced Materials – INAMAT – Pamplona, Spain)
J.A. Rodríguez-Velamazán (ILL)
J. Sánchez-Marcos (Universidad Autónoma de Madrid, Spain)
E. Cesari (University of the Balearic Islands, Palma de Mallorca, Spain)

ARTICLE FROM

Sci. Rep. (2017)—doi: 10.1038/s41598-017-13856-5

REFERENCES

- [1] V.K. Pecharsky, K.A. Gschneidner Jr., A.O. Pecharsky and A.M. Tishin, *Phys. Rev. B* 64 (2001) 144406.
- [2] T. Krenke, E. Duman, M. Acet, E.F. Wassermann, X. Moya, U. Mañosa and A. Planes, *Nat. Mat.* 4 (2005) 450
- [3] V.K. Sharma, M.K. Chattopadhyay and S.B. Roy, *Phys. Rev. B* 76 (2007) 140401.

The magnetocaloric effect is usually evaluated in isothermal conditions through the magnetic field-induced entropy change. In the present case, at low temperature we observe a direct magnetocaloric effect (with positive entropy change after field removing) associated with an ‘anomalous’ forward martensitic transformation, as opposed to the inverse effect (with negative entropy change after field removing) observed in a conventional forward transformation. The magnitude of this magnetocaloric effect is such that large adiabatic temperature changes under moderate applied fields can be induced—almost twice the values obtained in the conventional forward transformation under higher applied fields and among the largest values obtained in magnetic shape memory alloys.

Neutron thermo-diffraction measurements in **figure 1** show direct evidence of both the austenite retention at 10 K after 50 kOe magnetic field cooling and the subsequent phase evolution upon heating in a $\text{Ni}_{45}\text{Mn}_{36.7}\text{In}_{13.3}\text{Co}_5$ alloy. The sample shows a mixture of austenite and martensite at 10 K. The anomalous martensitic transformation from retained austenite to martensite on heating is evidenced by the reduction in intensity of the $(200)_A$ austenitic reflection at $2\theta = 47.5^\circ$ ($\lambda = 2.41 \text{ \AA}$) and the corresponding increase in the martensitic one at around 52° . The austenitic peak intensity does not cancel out due to the concurrence of martensitic and austenitic reflections at the same angle. Conversely, as expected the conventional reverse transformation from martensite to austenite takes place on heating above 200 K, where the austenitic peak intensity starts increasing (and the martensite peak intensity starts decreasing). Therefore, the same forward austenite-to-martensite transformation can be produced by heating and by cooling.

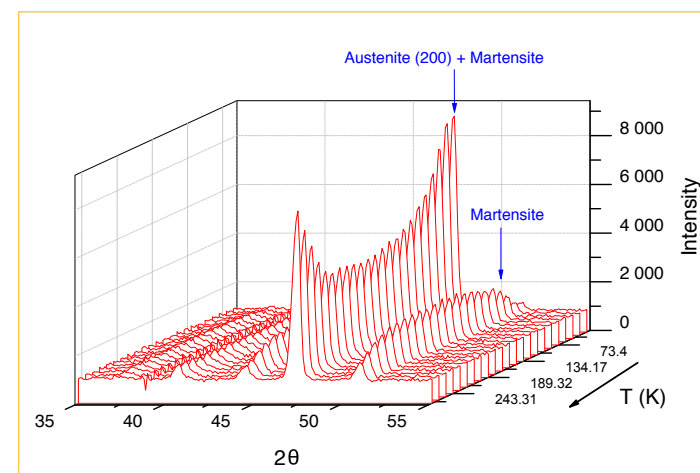


Figure 1

Neutron thermo-diffraction patterns measured on heating (external magnetic field set to zero at 10 K) in a sample cooled from 300 K under a 50 kOe magnetic field.

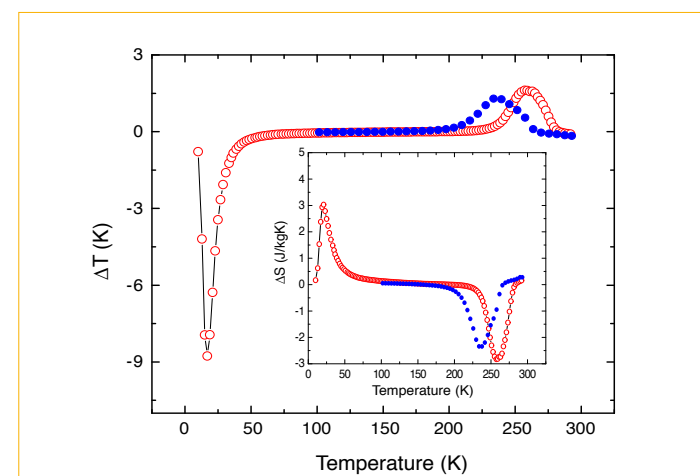


Figure 2

Temperature change $\Delta T(T)$ under a 10 kOe magnetic field reduction estimated through $\Delta T = -(T/C_p) \Delta S$ with C_p the specific heat.

Inset: Entropy change $\Delta S(T) = S(T,0) - S(T,H)$ at 10 kOe on heating after field cooling under 70 kOe (open circles) and during cooling (full circles) with no magnetic field.

The measured entropy change, ΔS , for removing a 10 kOe field and its associated adiabatic temperature change linked to the different possible martensitic transformations (‘anomalous’ forward transformation, reverse transformation on heating and forward transformation on cooling) are shown in **figure 2**. Field reduction implies a transformation from ferromagnetic austenite (high magnetisation) to paramagnetic martensite (low magnetisation). The ‘anomalous’ martensitic transformation produces a positive ΔS while both the reverse and the standard forward transformations show negative values. On the other hand, upon heating negative temperature changes are observed around the forward anomalous transformation while positive values appear around the standard forward and reverse transformations.

In summary, the same austenite-to-martensite transformations on heating (anomalous) and on cooling (standard) show oppositely signed entropy changes. This behaviour can be explained as the total entropy change linked to the transformation having mainly vibrational and magnetic contributions, $\Delta S = \Delta S_{vib} + \Delta S_{mag}$. During the transformation from ferromagnetic austenite to paramagnetic martensite (field removing), $\Delta S_{vib} < 0$ and $\Delta S_{mag} > 0$ typically occur. In the temperature range of the standard transformation the vibrational contribution is

large and then $\Delta S < 0$. In contrast, the vibrational entropy approaches zero at very low temperatures and therefore the vibrational contribution to the MT is expected to be very small. Furthermore, the lower the temperature, the higher the positive magnetic entropy contribution. Thus, in the range where the retained austenite is metastable (below 50 K) the magnetic contribution to the total entropy dominates and $\Delta S > 0$.

Interestingly, a remarkably high value of the adiabatic temperature change ($\sim 9 \text{ K}$) is observed around the ‘anomalous’ forward martensitic transformation under a moderate applied field of 10 kOe (**figure 2**). This is almost twice that obtained in the conventional forward transformation under higher applied fields ($\Delta T \sim 6 \text{ K}$), and one of the largest values obtained in magnetic shape memory alloys. From an application point of view, the magnetocaloric effect at low temperatures could compete with other materials like molecular magnetic compounds for magnetic refrigeration at cryogenic temperatures; while the occurrence of direct and inverse magnetocaloric effects associated with the same forward martensitic transformation could be useful in the design of refrigeration devices based on more complex thermodynamic processes.



Laura Cañadillas Delgado, Spanish ILL & Centro Universitario de la Defensa de Zaragoza, Spain
'Our research is based on the synthesis and characterisation of multifunctional metal-organic materials, aimed at looking for clues for the design of new materials with desired assets.'

The determination of complete structural models including H and other light atoms is needed to determine their properties. Neutron diffraction provides us with unique information about the magnetic structures of these compounds, making it a crucial tool in this field.'

Nuclear and magnetic structure determination of the multiferroic perovskite-like $[\text{CH}_3\text{NH}_3][\text{Co}(\text{COOH})_3]$ compound

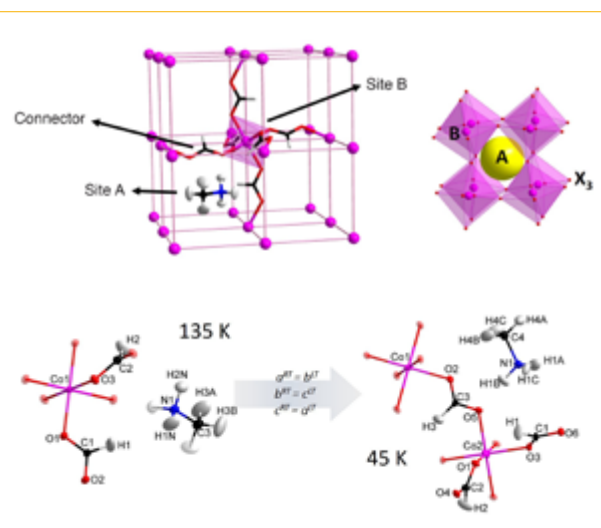
Single-crystal diffractometer D19 and powder diffractometer D1B

BLO4-MSPD beamline at ALBA synchrotron

Co-ordination polymers have attracted intense interest in recent years, not only from a fundamental point of view but also from the possibility of developing new functional materials. We have focused our efforts on finding new multiferroic materials where electric and magnetic order coexist. In order to achieve this objective we have prepared a metal-organic compound, constructed from a 3D-framework, with counterions located in its cavities. This approach has proved an effective method for combining two or more properties in the same compound in order to produce multifunctional materials.

Figure 1

Top) Representation of the perovskite-like structure of compound 1.
Bottom) View of the asymmetric unit at 135 K and at 45 K in ORTEP representation (50 % ellipsoid probability), together with the atom numbering, obtained from the single-crystal neutron refinement at 135 and 45 K, respectively. The cobalt, nitrogen, oxygen, carbon and hydrogen atoms are represented in pink, blue, red, black and light grey, respectively. The transparent mode represents the atoms generated by symmetry operations.



AUTHORS

L. Mazzuca, O. Fabelo and J. Rodríguez-Carvajal (ILL)
L. Cañadillas-Delgado (ILL and Centro Universitario de la Defensa de Zaragoza, Spain)
J. Alberto Rodríguez-Velamazán (ILL and CSIC-Universidad de Zaragoza, Spain)
J. Luzón (Centro Universitario de la Defensa and CSIC-Universidad de Zaragoza, Spain)
O. Vallcorba (Alba Synchrotron, Cerdanyola del Vallès, Spain)
V. Simonet and C.V. Colin (CNRS and UJF, Grenoble, France)

ARTICLE FROM

Chem. Eur. J. (2018)—doi: 10.1002/chem.201703140

REFERENCES

- [1] L. Mazzuca, L. Cañadillas-Delgado, O. Fabelo, J.A. Rodríguez-Velamazán, J. Luzón, O. Vallcorba, V. Simonet, C.V. Colin and J. Rodríguez-Carvajal, Chem. Eur. J. 24 (2018) 388
- [2] M. Azuma, K. Takata, T. Saito, S. Ishiwata, Y. Shimakawa and M. Takano, J. Am. Chem. Soc. 127 (2005) 8889
- [3] Y.-H. Chu, L.W. Martin, M.B. Holcomb, M. Gajek, S.-J. Han, Q. He, N. Balke, C.-H. Yang, D. Lee, W. Hu, Q. Zhan, P.-L. Yang, A. Fraile-Rodríguez, A. Scholl, S.X. Wang and R. Ramesh, Nat. Mater. 7 (2008) 478
- [4] O.M. Yaghi, M. O'Keeffe, N.W. Ockwig, H.K. Chae, M. Eddaoudi and J. Kim, Nature 423 (2003) 705
- [5] (a) R. Ramesh, Nature 46 (2009) 1218; (b) E. Pardo, C. Train, H.B. Liu, L.M. Chamoreau, B. Dkhil, K. Boubekeur, F. Lloret, K. Nakatani, H. Tokoro, S. Ohkoshi and M. Verdaguer, Angew. Chem. 51 (2012) 8356
- [6] D. Ganyushin and F. Neese, J. Chem. Phys. 125 (2006) 024103

In this article, we show how combining molecule-based counterions within a 3D-framework constructed from metal centres connected through organic linkers, gives rise to a final crystal structure that looks like the well-known Perovskite compounds. However, due to the presence of the organic linkers, this compound is transparent and has a relatively low density, making it of interest for various possible applications. Moreover, the synthesised $[\text{CH}_3\text{NH}_3][\text{Co}(\text{COOH})_3]$ compound combines two different ferroic-orders [1] and is a multiferroic of type I [2] material, so electric and magnetic properties are weakly correlated. Multiferroic materials in which electric order coexists in the same phase in which long-range magnetic order occurs, albeit at substantially lower temperatures, are an exciting starting point for the design of new devices based on these new materials [3]. Multiferroic behaviour of this type can be achieved using hybrid inorganic/organic frameworks in which an adequate combination of magnetic transition metal ions

and organic ligands can produce a compound with an order/disorder phase transition involving the hydrogen bond network [4, 5] and resulting in electric order.

The compound studied is both antiferroelectric-like ordered and weak ferromagnetic ordered below 15 K. However, the change in electric behaviour occurs at much higher temperatures. The electric changes are correlated with changes in the crystal structure, and therefore the use of neutron diffraction is an essential tool for exploring these slight changes and relating them to the macroscopic properties of this material.

In the present study we investigate the structural, magnetic and dielectric properties of the $[\text{CH}_3\text{NH}_3][\text{Co}(\text{COOH})_3]$ perovskite-like metal-organic compound, through variable-temperature neutron and X-ray single crystal and powder diffraction, magnetic susceptibility measurements and dielectric constant in the form of relative permittivity and pyroelectric current measurements. These analyses reveal an unreported structural phase transition at around 90 K, correlated with a change in electric behaviour. This phase transition consists of a change from $Pnma$ space group at RT to $P2_1/n$ space group (non-standard space group of $P2_1/c$) at low temperature (see **figure 1**). Full datasets collected on the single-crystal neutron diffractometer D19 at RT, 135 K and 45 K revealed that this phase transition involves slight changes in the orientation of the methylammonium counterions, which are weakly anchored in the cavities, as well as in the Co^{II} octahedral environments. These modifications in the structure are associated with the occurrence of an electric phase transition from paraelectric to antiferroelectric-like state (see **figure 2**).

The powder X-ray studies carried out on BLO4-MSPD beamline at ALBA synchrotron show a notable mixture of orthorhombic and monoclinic phases, even well below the nuclear phase transition. The different ratios between the phases in the different measurements suggest a dependence on the cooling/warming process. Moreover, the broadening of some reflections after the structural transition denotes an important strain contribution (see **figure 3**) in the powder samples.

Together with the occurrence of weak electric transition, the $[\text{CH}_3\text{NH}_3][\text{Co}(\text{COOH})_3]$ compound presents an overall antiferromagnetic coupling with a long-range magnetic order at about 15 K. To investigate the magnetic contribution, neutron powder diffraction experiments were performed on the high-intensity powder diffractometer D1B. This analysis concluded that a weak ferromagnetic component appears due to the occurrence of a non-collinear antiferromagnetic structure where magnetic moments are not strictly compensated. Therefore, below 15 K this material shows the coexistence of an antiferroelectric-like behaviour originating from a structural phase transition, non-significantly coupled with the weak ferromagnetism arising from the non-compensation of the non-collinear antiferromagnetic structure of the metal-organic host framework. Even if weak ferromagnetism is commonly attributed to the Dzyaloshinskii-Moriya interaction, the *ab initio* calculations performed using the CASSCF/NEVPT2 method [6] indicate that the single-ion anisotropy of Co^{II} ions is the dominant term in this case.

The magnetic reflections in the neutron measurements at 2 K are compatible with $Pn'ma'$ and $P2_1/n'$ magnetic models. The best refined models give rise to magnetic structures where the magnetic moments are antiferromagnetically coupled with a small, non-compensated component of the magnetic moment, in agreement with the *ab initio* calculations (see **figure 4**). Moreover, the magnetic structures obtained at zero-field are not compatible with the magneto-electric behaviour previously observed with this compound under applied field. Therefore, further work is needed to understand the origin of the magneto-electric coupling under applied magnetic fields.

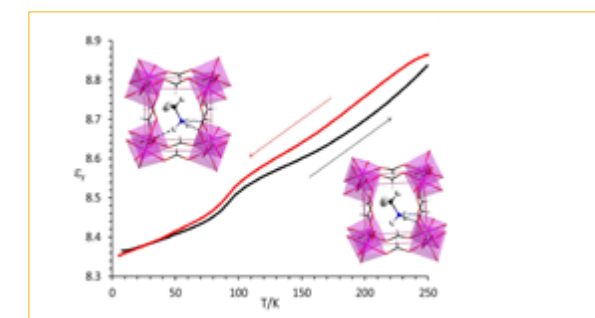


Figure 2

Relative permittivity as a function of temperature (red curve on cooling, black curve on warming) together with a view of the hydrogen bonds between the hydrogens of the methylammonium counterion and the oxygen atoms of the formate ligands at 135 K and 45 K.

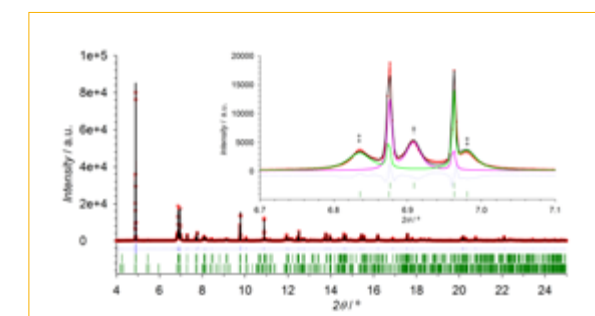


Figure 3

Experimental (open red circles) synchrotron X-ray powder diffraction data and calculated Rietveld refinement (black solid line) pattern. The upper row of vertical green marks represents the position of the Bragg reflections for the orthorhombic phase, while the lower row shows the position corresponding to the monoclinic phase, with refined cell parameters of $a = 8.26226(3)$, $b = 11.6471(2)$ and $c = 8.15991(3)$ Å, $\alpha = \beta = \gamma = 90.0^\circ$ and $a = 8.16148(2)$, $b = 8.26332(1)$ and $c = 11.65342(7)$ Å, $\beta = 91.676(1)^\circ$ for the orthorhombic and monoclinic phases, respectively. The intensity corresponding to the orthorhombic and monoclinic phases (in the inset), is represented by pink and green solid lines, respectively. It should be noted that the orthorhombic (1 2 1) reflection, denoted by the † symbol, is split into (-1 1 2), while (1 1 2) reflections in the monoclinic phase are denoted by the ‡ symbol in the figure.

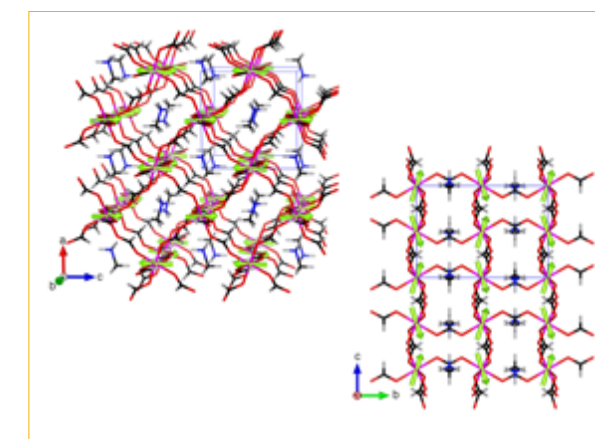


Figure 4

left) Perspective view along the b -axis of the magnetic structure refined in the $Pn'ma'$ Shubnikov space group.

right) Detailed view along the a -axis. The crystal and magnetic unit cell [$k = (0, 0, 0)$] is shown in blue, the magnetic moments in light green. The nuclear structure uses the same colour coding as that in previous figures.

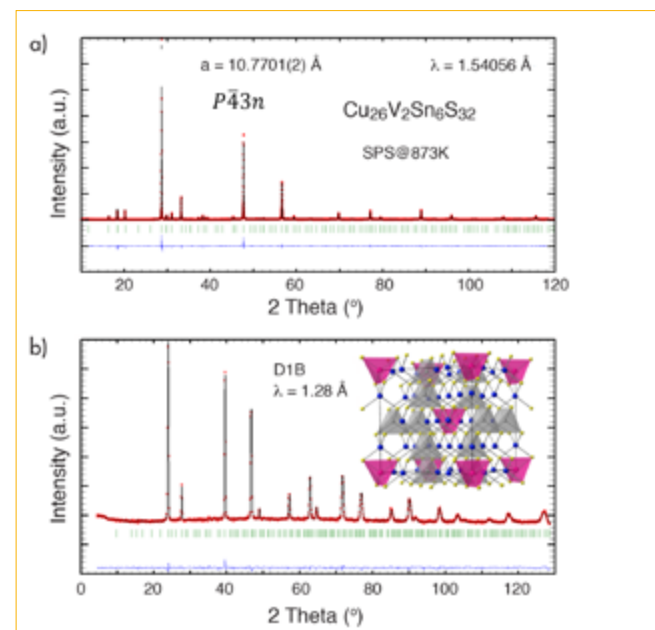


Emmanuel Guilmeau, French Laboratoire CRISMAT, France
‘I received a PhD in materials chemistry in 2003 from the University of Caen. My research interests focus on the discovery/processing of new materials, and especially on the compositional design of thermoelectrics. I use different characterisation techniques to investigate chemical and physical properties.’

Producing high-performance thermoelectric bulk colusite by process-controlled structural disordering

High-intensity two-axis powder diffractometer D1B

The search for optimised thermoelectric materials poses an interesting conundrum because of the delicate balance that must be achieved between charge and thermal transport. In addition, practical factors such as cost and manufacturability play an important role when discussing materials and properties. We have made substantial progress in addressing these issues in synthetic colusite, $\text{Cu}_{26}\text{V}_2\text{Sn}_6\text{S}_{32}$, by controlling the densification process and forming short-to-medium range structural defects [1].



AUTHORS

C. Bourges, O.I. Lebedev, V. Hardy, R. Daou and E. Guilmeau (CRISMAT, Caen, France)
Y. Bouyrie and M. Ohta (National Institute of Advanced Industrial Science and Technology (AIST), Tsukuba, Japan)
P. Lemoine (Institut des Sciences Chimiques de Rennes, Rennes, France)
K. Suekuni (Kyushu University, Fukuoka, Japan)
V. Nassif (Grenoble Alpes University and CNRS-NEEL Institute, Grenoble, France)
Y. Miyazaki (Tohoku University, Sendai, Japan)
A.R. Supka, R. Al Rahal Al Orabi and M. Fornari (Central Michigan University, Mt. Pleasant, USA)

ARTICLE FROM

J. Am. Chem. Soc. (2018)—doi: 10.1021/jacs.7b11224

REFERENCES

- [1] C. Bourges, Y. Bouyrie, A. Supka, R. Al Rahal Al Orabi, P. Lemoine, O.I. Lebedev, M. Ohta, K. Suekuni, V. Nassif, V. Hardy, R. Daou, M. Fornari, Y. Miyazaki and E. Guilmeau, J. Amer. Chem. Soc. 140 (2018) 2186
- [2] K. Suekuni, F.S. Kim, H. Nishiie, M. Ohta, H.I. Tanaka and T. Takabatake, Appl. Phys. Lett. 105 (2014) 132107
- [3] P.G. Spry, S. Merlino, S. Wang, X. Zhang and P.R. Buseck, Am. Mineral. 79 (1994) 750
- [4] O.V. Frank-Kamenetskaya, I.V. Rozhdestvenskaya and L.A. Yanulova, J. Struct. Chem. 43 (2002) 89

The design and optimisation of thermoelectric materials rely on the intricate balance between thermopower (S), electrical resistivity (ρ) and thermal conductivity (κ); perfecting such a balance is key to improving the figure of merit ($ZT = \frac{S^2}{\rho\kappa} T$) and energy recovery systems. Synthetic colusite, $\text{Cu}_{26}\text{V}_2\text{Sn}_6\text{S}_{32}$, represents a prototypical complex sulphide (*i.e.* a large unit cell with 66 atoms and light mass elements) combining p-type metallic behaviour and low lattice thermal conductivity [2]. However, the origin of the low thermal conductivity in colusite is not well understood and the full potential of $\text{Cu}_{26}\text{V}_2\text{Sn}_6\text{S}_{32}$ as an advanced thermoelectric material has not been fully explored. Our goal was to understand and optimise the thermoelectric properties of $\text{Cu}_{26}\text{V}_2\text{Sn}_6\text{S}_{32}$ colusite by controlling the densification temperature and method.

In this context, a reproducible and scalable powder synthesis was performed by mechanical alloying, followed by densification using two different consolidation techniques: spark plasma sintering at 873 K and hot pressing at 1023 K.

Figure 1

Combined Rietveld refinement of **a)** XRPD and **b)** NPD patterns of the colusite sample sintered at 873 K and recorded at room temperature.

The purity and crystallinity of the samples, as well as the crystal structure of colusite— $P\bar{4}3n$, sulphur corner-sharing tetrahedral network (8e, and 24i) centred around Cu (6d, 8e, and 12f) and Sn (6c), with V atoms at interstitial position (2a), (inset of figure 1, [3, 4])—have been confirmed by combined Rietveld refinement of X-ray powder diffraction data and neutron powder diffraction data recorded on D1B with a wavelength of 1.28 Å (figure 1). These latter data were valuable in accurately determining the atomic co-ordinates of the colusite sample sintered at 873 K, which were used as starting values for theoretical calculations. Moreover, a careful analysis of the patterns pointed to some minor differences in the positions and intensities of the superstructure diffraction peaks between the two samples. Despite testing several structural models to refine the diffraction data of the colusite sample sintered at 1023 K, the crystal structure remained ambiguous, suggesting the existence of local structural defects in this sample and requiring further investigations by local probe techniques.

Transmission electron microscopy revealed no defect regions or superstructures for the sample sintered at 873 K. Conversely, analysis of the sample sintered at 1023 K revealed different structural defects/features. The [001] images (figures 2a and 2b) clearly showed the presence of 1D line defects as a result of Sn substitutions with V and/or Cu. Given the sizes of the tetrahedra ($V < Cu < Sn$) and the chemical composition, the Sn–Cu anti-sites are expected to be kinetically more probable; this is supported by total energy calculations indicating that the formation of Cu–Sn anti-sites involving Cu 6d and Cu 8e are energetically favoured. In addition, in some other areas we observed a clear tendency to form larger 3D disordered regions, explaining the ambiguous crystal structure resolution of this colusite sample from powder diffraction data only. These disordered (figure 2c) and ordered (figure 2d) areas are coherently intergrown with equivalent structural frameworks and unit cell parameters, and are in fair agreement with the different domains of ordered and disordered cation distributions observed in natural colusite minerals [3]. These results suggest that sulphur volatilisation occurring at high temperature during hot-pressing at 1023 K favours a balance between an entropy-governed disordered phase and an internal energy-governed ordered phase.

Figure 3

Temperature dependencies of **a)** lattice thermal conductivity (κ_L) and **b)** ZT values of colusite $\text{Cu}_{26}\text{V}_2\text{Sn}_6\text{S}_{32}$ samples sintered at 873 K and 1023 K, respectively.

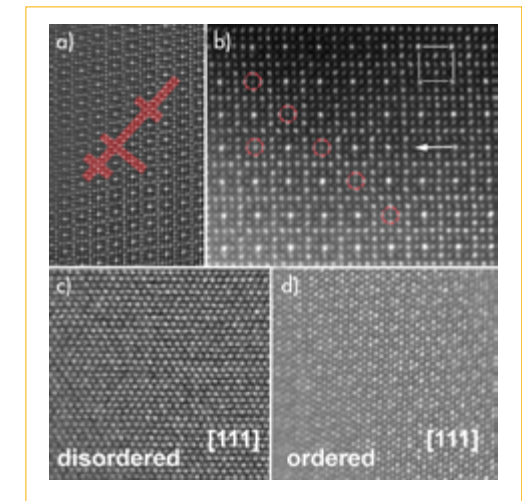
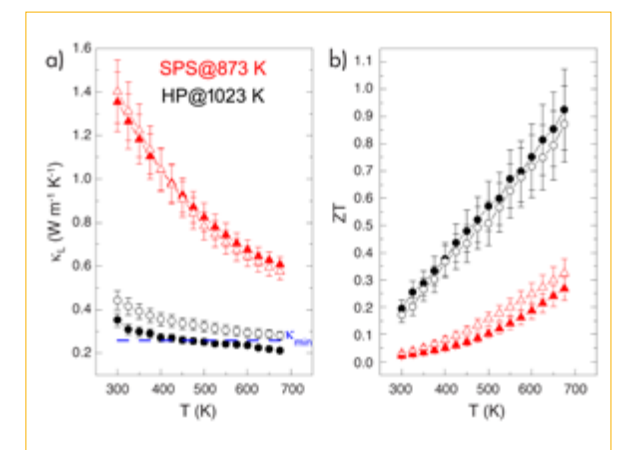


Figure 2

a) [001] HAADF-STEM image of the sample sintered at 1023 K. Red colour indicates 1D line defects distributed in the perfect crystal of $\text{Cu}_{26}\text{V}_2\text{Sn}_6\text{S}_{32}$.
b) Enlargement part of line defect. Red circle depicts Sn-site defects columns. [111] HAADF-STEM images showing the coexistence of
c) disordered and **d)** ordered regions in the same crystallite in the sample sintered at 1023 K.

Finally, by combining experiments and calculations (electronic band structure and vibrational properties), we concluded that the significant decrease in lattice thermal conductivity in the sample sintered at 1023 K (figure 3a) can mainly be attributed to the scattering effects induced by cationic disorder, which scatter short-wavelength phonons. In addition, the ordered and disordered regions being coherently intergrown, their interfaces can also contribute to the scattering of phonons of medium wavelengths, at the same time maintaining good carrier transport without excessive scattering. Recent inelastic neutron scattering experiments on IN6-SHARP have confirmed experimentally the role of structure disordering on phonon scattering in $\text{Cu}_{26}\text{V}_2\text{Sn}_6\text{S}_{32}$ colusites. This leads to a huge enhancement of the figure of merit ZT , up to 0.93 at 675 K in the sample sintered at 1023 K (figure 3b).





Anne A. Y. Guilbert, French
Department of Physics, Imperial College
London, UK

'I am studying the structure-property relationship of organic semiconductors, looking in particular at solar energy applications. Organic semiconductors are soft in nature and thus exhibit

a range of dynamics on various timescales directly relevant to optoelectronic processes. I use various characterisation techniques, including neutron scattering. Synergistically, I also extensively use different numerical simulation approaches to better understand how the different dynamical components in organic semiconductors affect their structure-property relationship.'

Quasi-elastic neutron spectroscopy sheds light on conjugated microporous polymers as potential water-splitting photochemical catalysts

Time-of-flight spectrometer IN6

Most fuels used for transport, for generating electricity and as raw materials for industries are produced from fossil fuels. Technologies harnessing light represent an alternative route to producing liquid and gaseous fuels. Nature offers the concept of making fuels by harnessing light. This is the photosynthesis process. Photosynthesis involves sunlight energy converting water and carbon dioxide into oxygen and sugars and/or other materials.

AUTHORS

A.A.Y. Guilbert (Imperial College London, UK)
R.S. Sprick, Y. Bai, C.M. Aitchison, Y. Yan, D.J. Woods and A.I. Cooper (University of Liverpool, UK)
M. Zbiri (ILL)

ARTICLE FROM

Chem. Mater. (2019)—doi: 10.1021/acs.chemmater.8b02833

REFERENCES

- [1] Royal Society of Chemistry. Solar Fuels and Artificial Photosynthesis—Science and innovation to change our future energy options. January 2012. www.rsc.org/solar-fuels
- [2] G. Crabtree, M. Dresselhaus and M. Buchanan, *Phys. Today* 57 (2004) 29
- [3] R.S. Sprick, J.-X. Jiang, B. Bonillo, S. Ren, T. Ratvijitvech, P. Guiglion, M.A. Zwijnenburg, D.J. Adams and A.I. Cooper, *J. Am. Chem. Soc.* 137 (2015) 3265
- [4] R.S. Sprick, Y. Bai, A.A.Y. Guilbert, M. Zbiri, C.M. Aitchison, L. Wilbraham, Y. Yan, D.J. Woods, M.A. Zwijnenburg and A.I. Cooper, *Chem. Mater.* 31 (2019) 305
- [5] M. Sachs, R.S. Sprick, D. Pearce, S.A.J. Hillman, A. Monti, A.A.Y. Guilbert, N.J. Brownbill, S. Dimitrov, X. Shi, F. Blanc, M.A. Zwijnenburg, J. Nelson, J.R. Durrant and A.I. Cooper, *Nat. Commun.* 9 (2018) 4968

Solar energy can be captured and stored directly in the chemical bonds of a 'solar fuel', to be used when needed. One of the challenges of solar and other intermittent renewable energy sources for generating electricity is precisely how to store the energy. Solar fuels address this challenge. The way that we can use energy from the sun to produce these fuels constitutes a pioneering advance and novel route to designing energy materials.

Among the chemical fuels, hydrogen is of primary interest currently. For instance, hydrogen is used: (i) in the industrial synthesis of ammonia and other chemicals [2]; (ii) to fuel cars and lorries; (iii) to generate electricity using a fuel cell; etc. At the moment, most hydrogen is produced by methane steam reforming from fossil fuels such as natural gas [1]. However, hydrogen can be produced by splitting water using sunlight, with oxygen as the only side product. Producing hydrogen by water-splitting using solar energy has the potential to radically reduce greenhouse gas emissions from fossil fuel combustion.

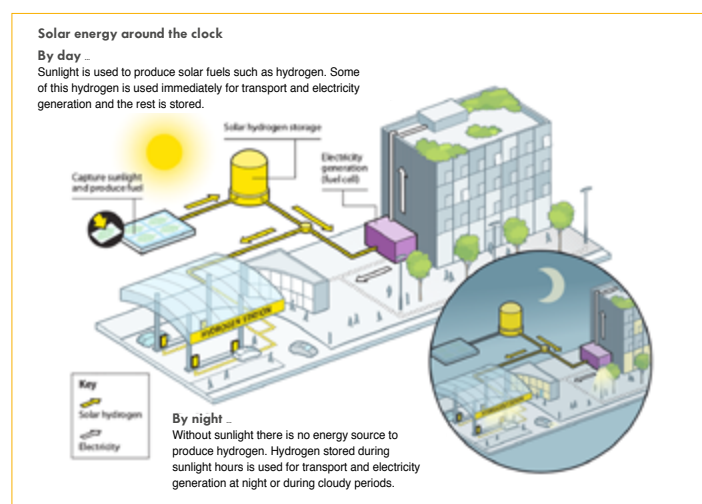


Figure 1
Solar hydrogen cycle [1].

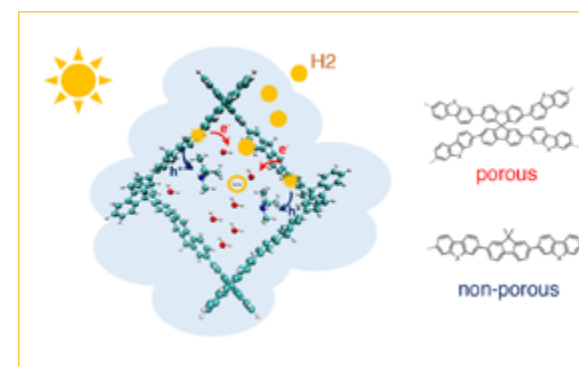


Figure 2

Schematic illustration of the hydrogen evolving half-reaction using conjugated microporous polymers (CMPs). F-CMP and S-CMP are the two porous CMPs examined in this study, corresponding to $X = C(CH_3)_2$ and $X = SO_2$, respectively. Non-porous analogues are also illustrated at the bottom of the right-hand panel.

A photocatalyst is used to harness the sunlight and assist the water-splitting reaction. To be scalable, photocatalysts should be based on earth-abundant and non-toxic elements. Conjugated polymers are promising materials as they have been shown to evolve hydrogen using visible light [3], offering great flexibility too in terms of chemical design. For instance, porosity has the potential to increase the number of catalytic sites if water can travel through the pores.

In this study [4], we focused on two conjugated microporous polymers (CMPs)—labelled F-CMP and S-CMP—showing larger hydrogen evolution than their linear, non-porous analogues (**figure 2**). In F-CMP, $X = C(CH_3)_2$ can be replaced by a sulfone group ($X = SO_2$), in S-CMP, as sulfone groups have been shown to increase hydrophilicity, leading to higher hydrogen evolution [5]. The aim of this study was primarily to understand water transport within the complex pore networks of F-CMP and S-CMP.

Water and CMPs form respectively the 'guest' and 'host' components of the catalytic system, calling for a targeted microscopic probe of its emerging structural dynamics behaviour and evolution. To achieve this, we examined differences between F-CMP and S-CMP in terms of their local dynamics by using the Quasi-Elastic Incoherent Neutron Scattering (QENS) technique. A unique feature offered by this technique is the ability to use D_2O in addition to H_2O for contrast variation purposes, as illustrated in **figure 3**.

Figure 3 shows the Q-averaged dynamical structure factor, $S(E)$, at 300 K, highlighting on the one hand the impact of hydration on the dynamics of S-CMP, and on the other, the impact of pore confinement on the water dynamics. For both CMPs, the QENS signal broadens as the amount of D_2O increases up to a content of 35 wt. % for F-CMP and 55 wt. % for S-CMP. We assign this threshold to the maximum water uptake of each CMP. Although the dry signal of both CMPs is comparable,

S-CMP in D_2O exhibits a broader QENS signal, thus pointing to faster dynamics in S-CMP than in F-CMP when in water, on the probed time scale. For both CMPs, the water signal for partially hydrated samples is narrower than the signal of bulk water, with a clear increase in the elastic contribution. This indicates that the dynamics of the water in the pores is frustrated within the accessible 5–50 ps instrumental time window. This effect is more pronounced in the case of F-CMP. For all the water contents studied, the QENS signal exhibits two contributions: one from the CMP itself and one from the water. Above the maximum water uptake, the QENS signal from the water shows two contributions: one from confined water inside the pores and one from free water. The water contributions to the QENS signal for both CMPs are summarised in **figure 3**; the rest of the signal is attributed to the CMP itself.

The lower water uptake of F-CMP in comparison with S-CMP, combined with more frustrated water dynamics inside the pores, points to reduced mass transport in the F-CMP network that probably contributes to its reduced photocatalytic activity.

Solar hydrogen could help to mitigate the impact of humans on climate change. If CMPs are shown to evolve hydrogen using visible light, understanding mass transport within their complex pore networks has the potential to boost the design of such materials for water-splitting applications. We have shown that QENS is a robust method for probing mass transport, in addition to shedding light on the crucial water uptake process.

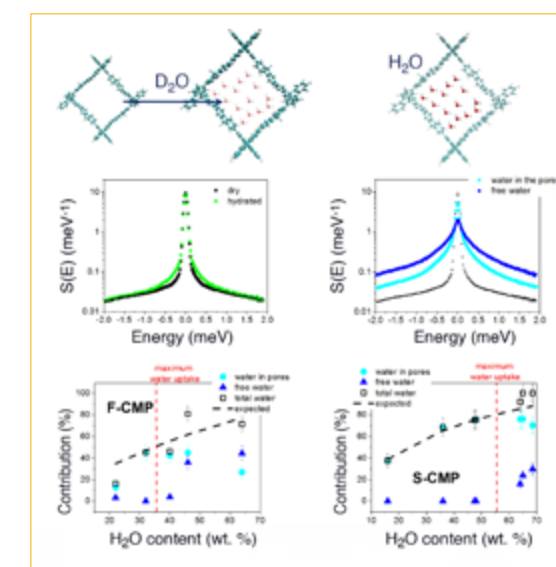


Figure 3

Top: Schematic illustration of the use of D_2O (**left**) and H_2O (**right**) to study hydration of the CMPs. **Middle:** Quasi-elastic neutron scattering (QENS) spectra of dry and hydrated S-CMP (**left**) and confined water in the pore of S-CMP in comparison with free water (**right**). **Bottom:** Summary of the various contributions from water to the QENS signals of F-CMP (**left**) and S-CMP (**right**) as a function of water content. The remaining contribution is assigned to the CMP itself. The maximum water uptake is shown by a red line.

**Hartmut Abele.** German

Atominstytut – TU Wien

‘Our group is working on an analysis of the Standard Model of Particle Physics and Gravitation, where the neutron is the object. We examine gravity at a short distance of one micron. At this level of precision, we are

able to provide constraints on any possible gravity-like interaction. The use of neutrons as test particles bypasses the electromagnetic background induced by van der Waals forces and other polarisability effects, providing the key to a sensitivity of several orders of magnitude below the sensitivity of atoms.’

Dark energy: neutrons rule out symmetrons

Ultra-cold neutron source PF2

A high-precision qBounce-experiment has set its sights on pinpointing the so far hypothetical ‘symmetron fields’ using the ‘PF2’ ultra-cold neutron source at the ILL. For the existence of symmetrons could provide an explanation for the mysterious dark energy. Dark energy is the energy part that is driving the expansion of the universe at an accelerating rate. The form of energy is unknown, hence the term ‘dark’. One possible explanation led to the introduction of additional scalar fields with properties similar to the Higgs field that was discovered six years ago at CERN.

AUTHORS

H. Abele, G. Cronenberg, H. Filter, M. Pitschmann and M. Thalhammer (Atominstytut, Technical University of Vienna, Austria)
P. Brax (University Paris-Saclay, CEA, CNRS, France)
P. Geltenbort and T. Jenke (ILL)
G. Pignol (LPSC, University Grenoble-Alpes, Grenoble, France)

ARTICLE FROM

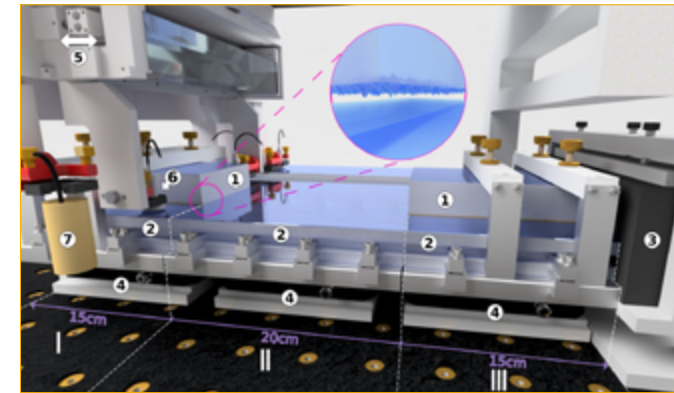
Nat. Phys. (2018) —doi: 10.1038/s41567-018-0205-x

REFERENCES

- [1] G. Cronenberg, Ph. Brax, H. Filter, P. Geltenbort, T. Jenke, G. Pignol, M. Pitschmann, M. Thalhammer and H. Abele, Nat. Phys. 14 (2018) 1022
- [2] K. Hinterbichler and J. Khoury, Phys. Rev. Lett. 104 (2010) 231301
- [3] V. Nesvizhevsky, H. Börner, A. Petukhov, H. Abele, S. Baeßler, F. Rueß, T. Stoeferle, A. Westphal, A. Gagarski, G. Petrov and V. Strelkov, Nature 415 (2002) 299
- [4] T. Jenke *et al.*, Phys. Rev. Lett. 112, 151105 (2014), ‘editors choice’
- [5] T. Jenke, P. Geltenbort, H. Lemmel and H. Abele, Nat. Phys. 7 (2011) 468

One thing is certain: there is something out there that we do not yet know. For years now, scientists have been looking for ‘dark matter’ or ‘dark energy’—with our existing inventory of particles and forces in nature we simply cannot explain major cosmological phenomena, such as why the universe is expanding at an accelerating rate. Several hypothetical theories for ‘dark energy’ have been devised, among them the so-called ‘symmetron fields’ which supposedly fill cosmological space-time similar to the Higgs field. At the TU Vienna and the ILL we have developed an experiment capable of measuring—with the help of neutrons—extremely small forces [1]. The measurements were taken during a 100-day campaign at the ILL, on its PF2 ultra-cold neutron source. They might have provided pointers to the mysterious symmetrons—but no symmetron signal was observed. While we cannot rule out this theory completely, we can exclude the existence of symmetrons across a broad range of parameters, suggesting that ‘dark energy’ must be explained differently.

The symmetron—a little brother of the Higgs boson? The symmetron theory would be a particularly elegant explanation for dark matter [2]. We already have proof of the Higgs field, and the symmetron field ϕ is very closely related. However, as with the Higgs particle, the mass of which was not known until the existence of the particle was confirmed, the physical properties of symmetrons cannot be accurately predicted. The mass of the symmetron quanta and the strength of their interaction with normal matter are free parameters of the theory. That is why it is so difficult to prove their existence experimentally—or their non-existence for that matter. The existence of symmetrons can only be confirmed or refuted within a certain parameter range—symmetrons, in other words, with mass or coupling constants in a specific value range. Experimentalists are therefore proceeding with caution, from one experiment to the other, testing different parameter ranges. It was already clear that a number of ranges could be excluded. For example, symmetrons with high mass and low coupling constants cannot exist because they would have already shown up at the atomic level. Experiments with hydrogen atoms would have given clear signals. Similarly, symmetrons within a certain range with very high coupling constants can also be excluded, as their existence would have been confirmed by other experiments using massive pendula.

**Figure 1**

Schematic views of the experimental setup: ultra-cold neutrons pass through the setup from left to right. In Region (I), they are prepared in the gravitational ground state $|1\rangle$ by passing a slit between a rough surface on the top and a perfectly polished surface on the bottom. Higher states interact with the rough surface and are effectively scattered off the system. In Region (II), transitions between quantum states are induced. The surface for that purpose oscillates with variable frequency and strength. This oscillating boundary condition triggers transitions to higher states, if the resonance condition is met and the oscillation strength is sufficient. Region (III) is identical to Region (I) and only transmits neutrons in the ground state. A highly efficient neutron detector (D) with low background counts the transmitted neutrons.

Practical realisation: the boundary conditions are realised by glass mirrors with rough (1) or perfectly polished (2) surfaces. The rms-roughness of the upper mirror is $(0.38 \pm 0.17) \mu\text{m}$, [see enlargement]. The neutrons are detected using a neutron counter (3). All mirrors are mounted on nano-positioning tables (4). An optical system (parts in 5) controls the induced mirror oscillations. A movable system based on capacitive sensors (6) controls and levels steps between the regions. The experiment is shielded by μ -metal against the magnetic field of Earth. Flux-gate magnetic field sensors (7) log residual magnetic fields.

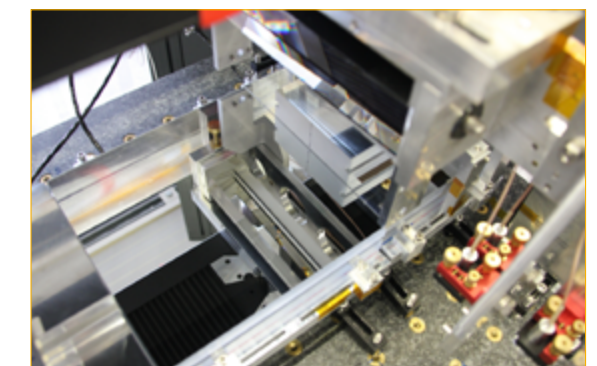
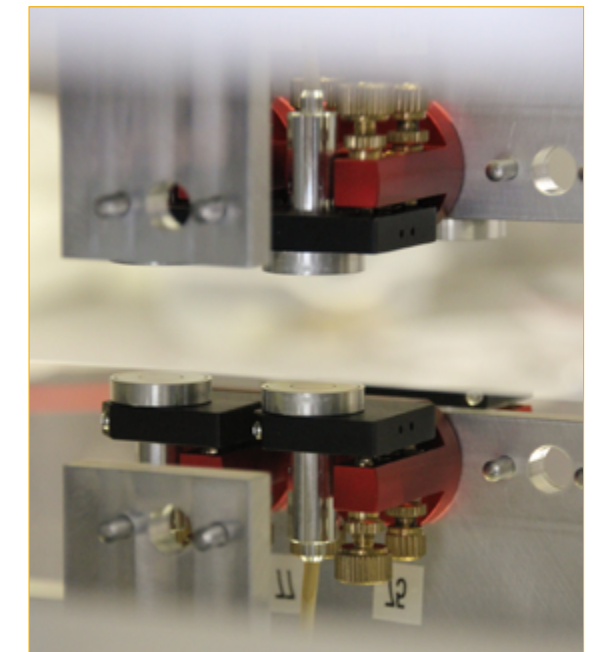
That said, there is still plenty of room left for symmetrons, and this is what we have investigated in our experiments. We propagated a beam of extremely slow neutrons between two mirror surfaces. The neutrons at a certain height z above the mirror can be found in different quantum physical states [3]. The energies of these states depend on the forces exerted on the neutron, and this is what makes the neutron such a sensitive force detector. If close to the surface of the mirror we observed a different force on the neutron from that for higher separations, this would be a strong pointer to the existence of a symmetron field: in our setup, the existence of symmetrons with a coupling M would lead to an additional potential in $V(z)$ in addition to gravity, as seen by neutrons with mass m :

$$V(z) = mgz + \frac{m}{2M^2} \varphi^2(z)$$

This would induce individual shifts in the eigen-energies of the gravitational quantum states, resulting in changes in the transition frequencies. As we could not observe any shifts within our experimental uncertainty, we are consequently able to exclude parts of the parameter space for the existence of symmetron fields. To do so, we use the predicted shifts of the resonance frequencies for the transitions $|1\rangle \rightarrow |3\rangle$ and $|1\rangle \rightarrow |4\rangle$, add the symmetron model parameters as fit parameters, fix Earth’s acceleration χ^2 - to the local value and perform a full-analysis. We found no positive effect. This lack of effect cannot, however, be proven, despite the extreme accuracy of the measurement.

The ultra-cold neutrons required for the experiment were generated by the ILL’s PF2 instrument. With its unrivalled flux of ultra-cold neutrons, PF2 is practically the only instrument out there for this type of high-precision measurement at extremely low count rates [4, 5]. Austria is a Scientific Member of the Institute and thus has access to its suite of instruments. The experiment is an excellent example of scientific collaboration between Austrian and French researchers.

For the moment things are not looking too bright for symmetron theory, although it is too early to completely exclude their existence. We have excluded a broad parameter domain: any symmetrons with properties in this domain would have been revealed by our measurements. To close the remaining loopholes however, science needs even better measurements—or a major discovery providing a completely different solution to the mystery of dark energy.

**Figure 2**

Capacitive sensors control position of and distance between mirrors.

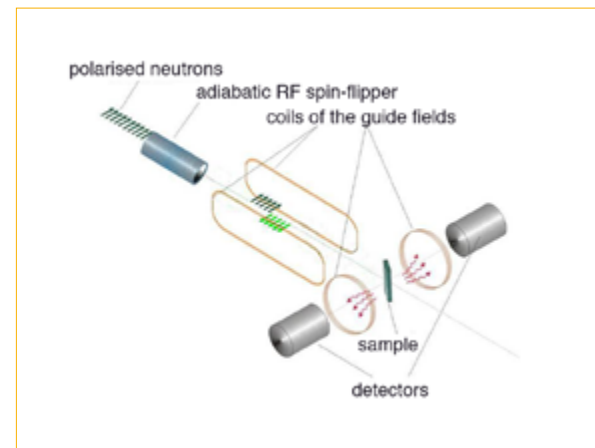


Victor A. Vesna (1938-2017). Russian PNPI, Gatchina, Russia
Viktor Vesna was the initiator, informal permanent leader and 'driving force' of the cycle of experiments on the search for, and measurement of, P-odd asymmetry coefficients in the emission of products of reactions of polarised cold neutrons with light nuclei.

First observation of P-odd asymmetry of the alpha-particle emission in the $^{10}\text{B}(n,\alpha)^7\text{Li}$ nuclear reaction and its consequences

Polarised cold neutron beam facility PF1B

The investigation of spatial parity in the reactions of polarised neutrons with light nuclei is an important topic associated with the fundamental problem of manifestations of weak interaction in nuclear processes and the evaluation of weak nucleon-nucleon (NN) potential.



AUTHORS

V. Nezvizhevsky (ILL)
 V. Vesna (PNPI, Gatchina, Russia)

ARTICLE FROM

Phys. Rev. B (2017)—doi: 10.1016/j.physletb.2017.03.035

REFERENCES

- [1] V.A. Vesna, Yu.M. Gledenov, V.V. Nesvizhevsky *et al.*, Phys. Rev. C 77 (2008) 035501
- [2] V.A. Vesna, Yu.M. Gledenov, V.V. Nesvizhevsky *et al.*, Eur. Phys. J. A 47 (2011) 43
- [3] Yu.M. Gledenov, V.V. Nesvizhevsky, P.V. Sedyshev *et al.*, Phys. Lett. B 769 (2017) 111
- [4] D.R. Phillips, D. Samart and C. Schat, Phys. Rev. Lett. 114 (2015) 062301

In order to describe the contribution of weak interactions in nuclear processes, the problem is often parametrised in terms of single (π , ρ , ω) and multiple meson exchange with one weak and one or more strong vertices. Within this parametrisation, neutral and charged weak currents are described with the coupling constants f_π and h_p^0 , respectively. Neutral weak currents were predicted by the unified theory of electromagnetic and weak interactions, and discovered in the scattering of muon neutrinos by electrons and the rotating polarisation of a laser beam passing through atomic bismuth vapours. The existence of neutral currents in lepton-lepton and lepton-nucleon interactions led to numerous attempts to discover neutral currents in nucleon-nucleon interactions too, the reaction of neutrons with light nuclei being the obvious candidate. The principal difficulty for such experiments lies in the extreme smallness of the contribution of the weak interaction to the strong nuclear interaction ($\sim 10^{-7}$).

Reliable evidence of the existence of the non-zero P-odd asymmetry, $-(8.8 \pm 2.1) \cdot 10^{-8}$, of the triton (^3H) emission in the reaction $^6\text{Li}(n,\alpha)^3\text{H}$ was obtained some years ago in experiments carried out at the ILL [1]. However, the result of an experiment searching for P-odd asymmetry in the γ -quantum channel in the reaction $^{10}\text{B}(n,\alpha)^7\text{Li}^* \rightarrow \nu\text{Li} + \gamma$ ($E_\gamma = 0.480$ MeV) was compatible with zero [2]: $+(0.8 \pm 3.9) \cdot 10^{-8}$ (figure 1 shows a plan of this experiment). The measurement of a non-zero effect in another neutron-induced reaction with light nucleus (^{10}B) would allow us to estimate more accurately the constants of neutral and charged currents.

Figure 1

A plan of the measurement of the asymmetry of the γ -quantum emission in the reaction $^{10}\text{B}(n,\alpha)^7\text{Li}^* \rightarrow \nu\text{Li} + \gamma$, induced by polarised neutrons. Straight green arrows illustrate the direction of neutron spin polarisation, which is periodically flipped (light and dark green shades) by the adiabatic RF (radio frequency) spin flipper. Two γ -detectors are placed on opposite sides of the ^{10}B target; trajectories of γ -quanta are illustrated with wavy arrows.



Figure 2

A photo of the experimental set-up used to measure the asymmetry of the α -particle emission in the reaction $^{10}\text{B}(n,\alpha)^7\text{Li}$, induced by polarised neutrons. The principles of its operation are explained in the text.

Therefore, the observation of the P-odd asymmetry ($\vec{\sigma}_n \vec{p}_p$) of an α -particle emission in the reaction $^{10}\text{B}(n,\alpha)^7\text{Li}$ is of great interest; hence, we performed such an experiment. Here, $\vec{\sigma}_n, \vec{p}_n, \vec{p}_p$ are the spin and momentum of the neutron, and the momentum of the α -particle, respectively. To eliminate the influence of a false effect associated with the so-called left-right asymmetry on the results of measurements of the P-odd asymmetry, we had to ensure that the vectors $\vec{\sigma}_n, \vec{p}_n, \vec{p}_p$ were parallel to each other. To achieve maximum accuracy, we used a method based on two detectors and a special measuring procedure. This method assumes simultaneous measurement of the same process in both detector channels. However, the signs of the P-odd effects are opposite, while those of the effect of synchronous fluctuations are the same. Hence, the P-odd effects were combined and the fluctuation noise cancelled.

A photo of the experimental setup is shown in figure 2. The detector of the α -particles emitted in the reaction $^{10}\text{B}(n,\alpha)^7\text{Li}$ consists of 24 ionising double chambers installed along the beam axis. The targets made of ^{10}B are placed in the centre of each chamber. One side of each double chamber detects α -particles emitted in the neutron beam direction ('forward'), while the other side detects α -particles in the opposite, backward direction. Because of the different orientation of α -particle momenta \vec{p}_p with respect to the neutron spin $\vec{\sigma}_n$, asymmetries measured in forward and backward directions have opposite signs. The electrodes attached to all 'forward' sections of the detector's double chambers are connected to a common, 'forward'

preamplifier; the electrodes attached to 'backward' sections are connected to a separate 'backward' preamplifier. The two preamplifiers convert the electric currents from the 'forward' and 'backward' chambers to electric voltages that are proportional to the α -particle flux. We used gaseous insensitive layers to absorb the heavy component and provide a mean angle of the α -particle emission. The special gaseous detector is an assembly of gaseous ionising chambers placed into an aluminium jacket with a length of 1 800 mm and a diameter of 300 mm. The detector is filled with argon at the pressure of 0.3-0.8 bars. A detector of this type can capture about 80-90 % of the neutrons. A special solenoid, reeled to the jacket, provides the neutron spin guide field inside the detector.

Measurements of the P-odd asymmetry in the reaction $^{10}\text{B}(n,\alpha)^7\text{Li}$ were performed earlier on the polarised cold-neutron beam at the VVWR-M reactor at PNPI (Gatchina, Russia). The integral neutron intensity was about $(1.3) \cdot 10^{10} \text{ s}^{-1}$ and the mean neutron polarisation $P \sim 0.8$. A second experiment was carried out on the horizontal polarised neutron beam PF1B at the ILL [3]. The mean neutron wavelength was $\lambda = 4.7 \text{ \AA}$, the integral flux of polarised neutrons $(4.5) \cdot 10^{10} \text{ s}^{-1}$ and the neutron polarisation $P = 0.92 \pm 0.02$. The results of both experiments, corrected for the corresponding neutron beam polarisation P and the mean cosine of the α -particle emission angle, gave a value of the P-odd asymmetry coefficient of the α -particle emission equal to $-(1.2 \pm 3.4) \cdot 10^{-8}$.

The uncertainty of this result is compatible with uncertainty concerning the P-odd asymmetry in the reaction $^6\text{Li}(n,\alpha)^3\text{H}$. This is the first time in the world that this non-zero result has been obtained. It is only the second light nucleus, in addition to ^6Li , for which a non-zero P-odd effect has been found. This work was awarded 1st prize in two very challenging scientific competitions in 2018 (at PNPI and FLNP JINR).

After decades of development, we have been able to increase the sensitivity of our experiments to the level needed to reliably measure such small asymmetries. Simultaneously, theoretical models such as EFT (Effective Field Theory) have begun to calculate such nuclear reactions reliably. Another new theoretical approach [4] consists of calculating parity-violating NN force in the $1/N_c$ expansion (where N_c is number of colours); this may be of particular interest to the present study as it naturally explains the smallness of the f_π coefficient compared with the h_p^0 observed experimentally. This situation offers exciting opportunities and promises new results.

The microscopic mechanism for the unusual spin-induced electric polarisation in the multiferroic compound GdMn_2O_5

Recently, a large magneto-electric effect (reversing of the polarisation under an applied magnetic field) has been found in two members of the RMn_2O_5 (R = rare earth) manganites, namely TbMn_2O_5 [1] and GdMn_2O_5 [2]. Furthermore, the GdMn_2O_5 compound presents a large electric polarisation of $\sim 3600 \mu\text{C}/\text{m}^2$ [2], a value nearly able to compete with the so-called Bi manganite multiferroics. In this paper we explain the microscopic origin of this spin-induced ferroelectricity, and pinpoint the specificity of the Gd compound among other rare earths.

AUTHORS

M.-B. Lepetit (Institut Néel, CNRS, and ILL, Grenoble, France)
G. Yahia (Laboratoire de Physique des Solides, CNRS, Université Paris-Sud, Université Paris-Saclay, France and Laboratoire de Physique de la Matière Condensée, Université Tunis-El Manar, Tunisia)
F. Damay (Laboratoire Léon Brillouin, CEA-CNRS, France)
S. Chattopadhyay (Indian Institute of Technology, Kharagpur, India)
V. Bal'edent, W. Peng and P. Foury-Leylejian (Laboratoire de Physique des Solides, CNRS, Université Paris-Sud, Université Paris-Saclay, France)
S.W. Kim and M. Greenblatt (Dept. Chemistry and Chemical Biology, Rutgers, State University of New Jersey, USA)

ARTICLE FROM

Phys. Rev. B 97, 085128 (2018)

REFERENCES

- [1] N. Hur, S. Park, P. Sharma, J.S. Ahn, S. Guha and S.-W. Cheong, Nature 429 (2004) 392
- [2] N. Lee, C. Vecchini, Y.J. Choi, L.C. Chapon, A. Bombardi, P.G. Radaelli and S.-W. Cheong, Phys. Rev. Lett. 110 (2013) 137203
- [3] P.G. Radaelli and L.C. Chapon, J. Phys. Condens. Matter 20 (2008) 434213

The RMn_2O_5 compounds crystallise in the Pm space group, but their structure is close to a Pbam symmetry (see **figure 1**). Along c , there are two relevant Mn^{4+} – Mn^{4+} exchange interactions: J_1 (through the R^{3+} layers) and J_2 (through the Mn^{3+} layers) [3]. In the (a, b) plane there are three non-equivalent magnetic exchanges: J_3 and J_4 between Mn^{3+} and Mn^{4+} spins, and J_5 between two Mn^{3+} spins (**figure 1**). The main contribution to these exchanges is the antiferromagnetic (AFM) Mn–Mn super-exchange interaction through a shared oxygen. J_4 and J_5 are expected to be the dominant integrals, while J_3 is frustrated. The influence of the rare earth is generally neglected, owing to the strong spatial localisation of their orbitals. However, at low temperature and in the particular case of Gd^{3+} , the super-exchange interaction between Gd–Mn spins through a common oxygen (labelled J_6 s in the following and in **figure 1**) can become relevant.

Figure 1

Left) RMn_2O_5 structure and magnetic interactions.

Right) Magnetic structure of GdMn_2O_5 at 1.5 K. The blue (orange) ellipses show the $\text{Mn}^{3+}/\text{Mn}^{3+}$ ($\text{Gd}^{3+}/\text{Mn}^{3+}$) AF pairs. Stars identify the Gd/ Mn^{3+} pair proposed by Lee *et al.* in their model [2]. The black dashed lines are guides to visualise the zig-zag chains running according to the dominant magnetic interactions.

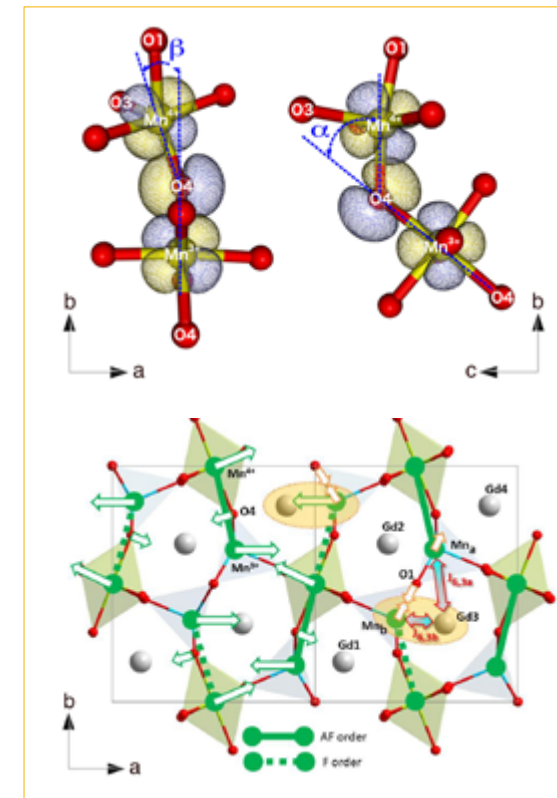
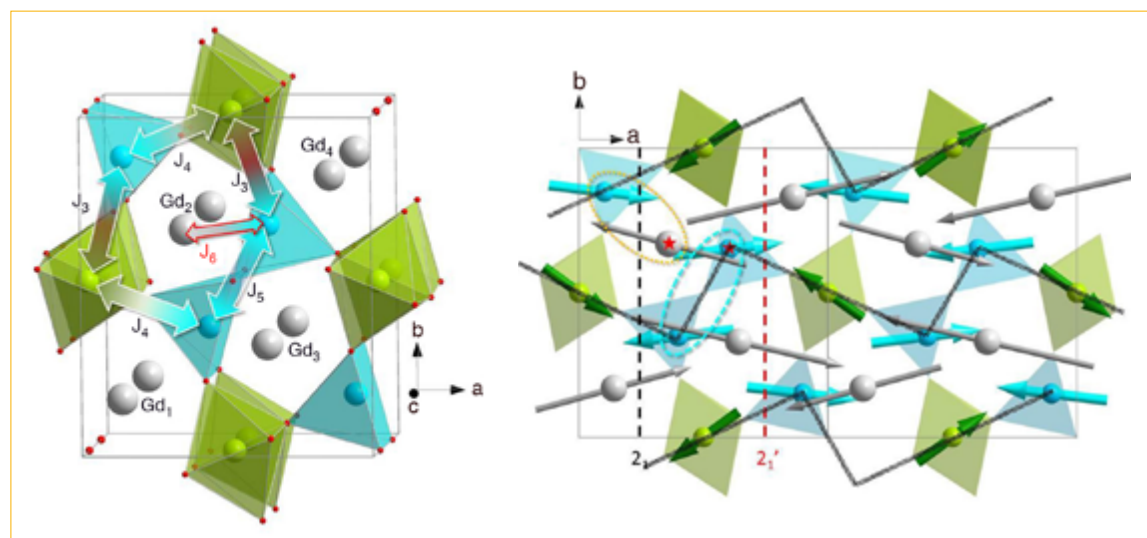


Figure 2

Top) Main super-exchange path for the magnetically frustrated J_3 interaction.

Bottom) Atomic displacements releasing the J_3 (left part) and J_6 (right part) frustrations.

Let us analyse the mechanism at the origin of the electric polarisation.

In the Pbam non-polar group, J_3 does not contribute to the magnetic energy as its two contributions cancel out: in each unit cell one is located between atoms FM-ordered, the other between atoms AFM-ordered (**figure 1**). It is thus the symmetry breaking from Pbam to Pm that allows the two J_3 interactions to be non-equivalent and that is responsible for the observed polarisation. From the picture of the main super-exchange path involved in J_3 (**figure 2**), it is easy to see that the main way to reach this goal is to change the angles α and β so that the increase/decrease of the $\text{Mn}^{3+}(t_{2g})\text{-O}(2p)\text{-Mn}^{4+}(t_{2g})$ orbitals' overlap will increase/decrease the AFM character of J_3 . As a consequence, the Mn^{3+} ions will shift alternatively along the $\pm a$ direction and the Mn^{4+} along the $\pm a + \epsilon b$, while the O4 oxygen bridging the Mn^{3+} and Mn^{4+} ions will move alternatively along the $\pm a - \eta b$ direction (**figure 2**). Within the entire unit cell, these shifts result in a global relative displacement of the negative charges along $-b$, and of the positive ones along the $+b$ direction, *i.e.* in a macroscopic electric polarisation along b and breaking the inversion symmetry.

Let us now analyse the Gd–Mn interactions. One must first remember that the Gd^{3+} ion is in a $4f^7, S = 7/2, L = 0$ configuration. As a result, in a first approximation

(spherical, atomic), the spin-orbit interaction on the Gd^{3+} ground-state and thus the Gd^{3+} magnetic anisotropy is nil. The super-exchange paths depend on the square of the transfer integrals between the set of 4f orbitals of the Gd ion and the 2p orbitals of the bridging oxygen, times the square of the hopping between these oxygen 2p orbitals and the Mn 3d ones. Another consequence of the equal occupation of all 4f orbitals is thus a distance-only dependence of the super-exchange paths involved in the J_6 s. As a result, the strongest J_6 interaction should be the one bridged by the oxygen closest to the Gd. At low temperature this is the O1 oxygen. As O1 mediates the interaction J_5 between the Mn^{3+} dimer and J_6 between the two Mn and the two Gd ions, (Gd_2 and Gd_3 in **figure 2**), there is a strong magnetic frustration. Within a simple mean-field approximation, the associated magnetic energy is

$$E = J_{6,2a} \langle \vec{S}_{\text{Gd}_2} \rangle \cdot \langle \vec{S}_{\text{Mn}_a^{3+}} \rangle + J_{6,2b} \langle \vec{S}_{\text{Gd}_2} \rangle \cdot \langle \vec{S}_{\text{Mn}_b^{3+}} \rangle + J_{6,3a} \langle \vec{S}_{\text{Gd}_3} \rangle \cdot \langle \vec{S}_{\text{Mn}_a^{3+}} \rangle + J_{6,3b} \langle \vec{S}_{\text{Gd}_3} \rangle \cdot \langle \vec{S}_{\text{Mn}_b^{3+}} \rangle$$

In a Pbam group $E = 0$

$$J = J_{6,2a} = J_{6,3a} = J_{6,2b} = J_{6,3b}$$

$$\vec{S} = \langle \vec{S}_{\text{Mn}_a^{3+}} \rangle = -\langle \vec{S}_{\text{Mn}_b^{3+}} \rangle$$

$$\vec{S} = -\langle \vec{S}_{\text{Gd}_2} \rangle = \langle \vec{S}_{\text{Gd}_3} \rangle$$

In order to lift the magnetic frustration one needs both different Gd moments ($\langle \vec{S}_{\text{Gd}_2} \rangle \neq -\langle \vec{S}_{\text{Gd}_3} \rangle$) as found in the magnetic structure (see **figure 1**), and atomic displacements such that the amplitudes of the J_6 interactions coupling the largest AFM Gd_3 – Mn_b interaction lower the magnetic energy. In other words

$$J_a = J_{6,2a} = J_{6,3a} \neq J_b = J_{6,2b} = J_{6,3b} \text{ and } |J_a| < |J_b|$$

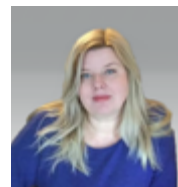
$$\vec{S}_2 = \langle \vec{S}_{\text{Gd}_2} \rangle \neq \vec{S}_3 = -\langle \vec{S}_{\text{Gd}_3} \rangle \text{ and } S_2 < S_3$$

that yield

$$E = (J_a - J_b) (\vec{S}_3 - \vec{S}_2) \cdot \vec{S} < 0$$

As the Mn–Gd magnetic exchanges are mediated by the oxygens, a displacement of the Gd ions will result in an equal modification of $J_{6,2b}$ and $J_{6,3b}$ (similarly $J_{6,2a}$ and $J_{6,3a}$), and thus will not lift the frustration. That means that one must shorten the O1– Mn_b^{3+} bond and lengthen the O1– Mn_a^{3+} bond, as pictured in **figure 2**. These displacements do not interfere with the original exchange striction issued from the release of the J_3 frustration. They result in a further increase in the polarisation along b , which is responsible for the very large value of the GdMn_2O_5 polarisation within the RMn_2O_5 family.

At 12 K the structural data exhibit a crossover between the Gd–O1 and Gd–O2 distances, the Gd–O2 becoming the shortest. In contrast to the O1 oxygen the O2 ions do not mediate any magnetic frustration, and thus at $T > 12$ K the frustration weakens (as observed experimentally), as do the extra polar displacements.



Mariya Gvozdikova. Ukrainian High Magnetic Field Laboratory (LNCMI) and INAC-CEA, Grenoble

'I have a PhD in Theoretical Physics. Today I hold post-doctoral positions at the Grenoble High Magnetic Field Laboratory (LNCMI) and in the INAC, CEA-Grenoble. I worked on

several collaborations with theorists at the ILL, and it was during one of my visits that this study was completed.'

Multipoles versus dipole fans near a quantum critical point

One of the holy grails of modern magnetism is the phases of spins that constitute really exotic states of matter and whose properties are dominated by quantum fluctuations even from macroscopically large samples. The observation of such phases is often claimed, in some cases prematurely, on the basis of evidence that admits an exotic explanation but is really incomplete: the actual structure is seen only indirectly through its relation to the observed properties, and the attribution to one state rather than another depends on theory that relates the observables uniquely to the new phase.

AUTHORS

M. Gvozdikova and T. Ziman (ILL)
M. Zhitomirsky (CEA-INAC, Grenoble)

ARTICLE FROM

Phys. Rev. Lett. (2018) —doi: 10.1103/PhysRevLett.120.067203

REFERENCES

- [1] B. Willenberg *et al.*, Phys. Rev. Lett. 116 (2016) 047202
[2] E. Cemel *et al.*, Phys. Rev. Lett. 120 (2018) 067203

The advantage of neutron experiments is that both statics and dynamics can be seen rather directly and completely, providing for real confrontation between experiment and theory. A recent example of this is provided by the detailed experiments carried out on a frustrated linear magnet, a mineral called linarite $\text{PbCuSO}_4(\text{OH})_2$. This is promising as it is known to be, up to small corrections, almost but not quite described by a model at a quantum critical point, *i.e.* it is close to a state that is known mathematically to have large quantum fluctuations but not the normal order based on some regular pattern of the magnetic dipoles. The slight departures from criticality are thought to make it a candidate for an unusual state, where the order in the magnetic dipoles present on each copper atom is lost to each site to fluctuation but a higher, multipolar order involving entanglement of pairs of magnetic moments on adjacent sites prevails. The question is, which of the many possible ordered, or disordered, states prevails in the real mineral? Elastic and inelastic scattering of neutrons in a magnetic field can resolve the question—with the help of theory.

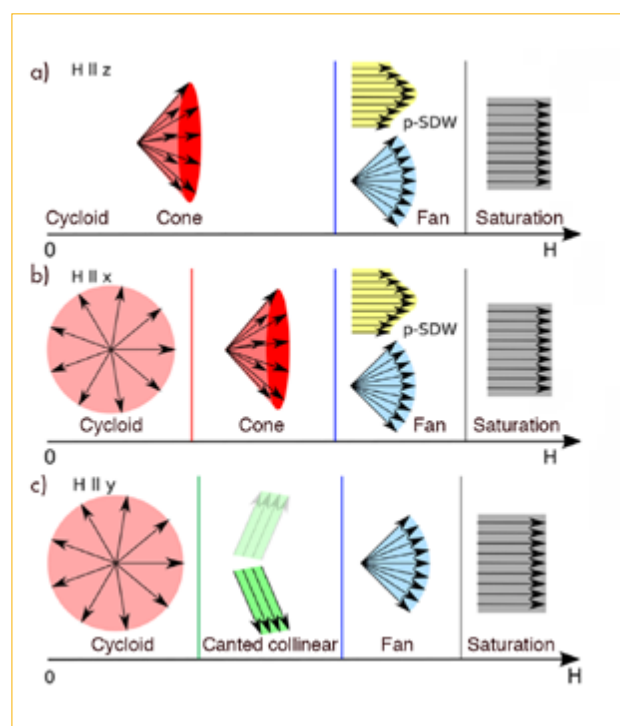


Figure 1
Schematic phase sequence in the vicinity of a quantum critical point.

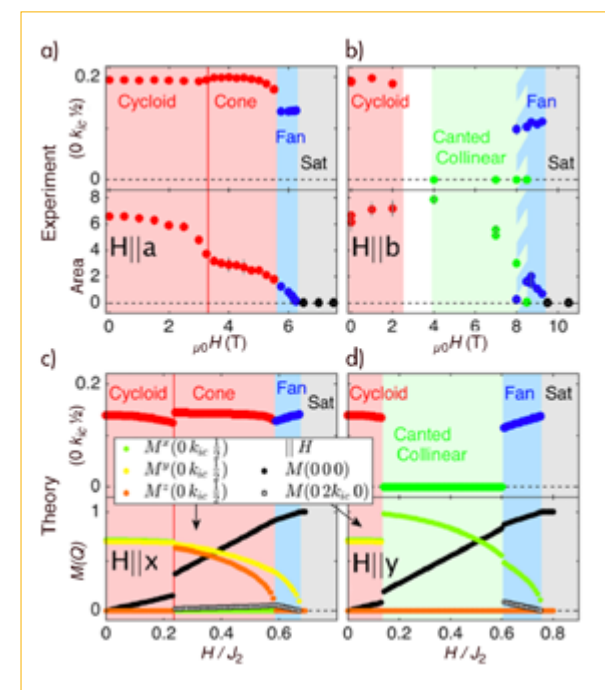


Figure 2
Comparison between ordering wave-vectors for experiment and theory.

The keys to answering this question lie in both the extremely detailed measurements and the theoretical modelling, which allow us to make real comparisons of different hypotheses. Earlier experiments favoured multipolar order [1]. New measurements [2] of both static and dynamical correlations were carried out at low temperatures, in order to isolate quantum from thermal fluctuations, and high magnetic fields, to alter the balance of frustration to order. The theoretical modelling required us to take into account the fact that even order in the dipoles can occur at wave-vectors that are incommensurate with the underlying lattice, so that the magnetic unit cell is in principle infinitely larger than the structural. In practice, this means that we need tools to calculate and compare the stabilities of new unit cells, hundreds, or even, thousand times larger than would suffice for a simple periodic structure. In fact, what allows us to say ultimately that the order is based on dipoles and not multipoles is that the calculated wave-vector

changes as a function of external magnetic field, which is compatible with this interpretation and incompatible with multi-polar order. The different phases are illustrated in **figure 1**. Furthermore, the calculations show that a surprisingly small but biaxial exchange anisotropy is necessary and sufficient to stabilise a sequence of phases: cycloid to cone to fan, in the easy-axis direction (see **figure 2** on the left-hand side), with the correct dependence on external field; and cycloid to canted-collinear to fan in the intermediate direction (right-hand side). The multipolar state does not appear.

In conclusion, while detailed experiments with neutrons provide a wealth of information that can distinguish competing complex, but subtly different, quantum phases, theoretical work is needed to provide the details on which comparisons can be made and to make plausible the relation between the small additional interactions and the consequent stability.

MODERNISATION PROGRAMMES AND TECHNICAL DEVELOPMENTS

- 74 MODERNISATION PROGRAMME AND INSTRUMENT UPGRADES
- 80 TECHNICAL DEVELOPMENTS
- 84 PROJECTS AND TECHNIQUES DIVISION ACTIVITIES

60M€
ENDURANCE
 8 YEARS (2016–2023)

WASP
 RECEIVED ITS FIRST NEUTRONS IN **2018**



- INCREASED FLUX
- REDUCED BACKGROUND
- LARGER DETECTORS
- IMPROVED RESOLUTION
- ENHANCED CAPABILITIES
- RELIABILITY & PERFORMANCE



KEEP UP-TO-DATE:

- facebook.com/ILLGrenoble
- twitter.com/ILLGrenoble
- linkedin.com/company/institut-laue-langevin

ONE of the main ingredients of the ILL's success in maintaining its position as international leader in neutron science is the continuous upgrade of its facilities. This is the secret behind its excellent, modern and highly efficient instruments and infrastructure.

Ever since it was founded, the ILL has invested in innovation programmes as part of a constant effort to enhance the performance of its instruments; this has included incorporating the latest technological advances, whether they be state-of-the-art detectors and neutron guides, improvements to sample environment equipment or innovative tools for data analysis and acquisition.

The Projects and Techniques Division is at the heart of these efforts. Its activities are carried out in a project-oriented manner in close liaison with the Science Division, whose prime responsibility is to define the scientific framework and level of performance to be achieved.

Looking more closely at the ongoing upgrade programmes, 2018 marked the start of the commissioning of the ILL's new wide-angle spin-echo spectrometer, WASP, and its receipt of its first neutrons. WASP was the last instrument to be completed under the Millennium Programme, which has now been succeeded by Endurance. The first phase of this ambitious follow-up programme began in 2016. Depending on the funding available, the complete programme will guarantee even better performance from the ILL's instruments, further enhancing the quality of research our users can produce with our neutrons.

Some of the new instruments included in the Endurance programme are already in operation, such as the new fission-fragment spectrometer FIPPS which saw its first experiment at the end of 2016. Others, such as the new thermal time-of-flight (TOF) spectrometer PANTHER and the ultra-cold neutron source SuperSUN, are due to be commissioned in 2019.

The instrument performance gains expected from Endurance will also call for research and innovation in other technical fields, including simulation techniques such as virtualisation, to improve the design of the instruments and their environment. The Projects and Techniques Division is also currently exploring state-of-the-art computing technology with the aim of developing an alternative, virtual access mode for neutron experiments. This will allow users to connect to any instrument in the ILL's suite via a web portal—an exciting prospect indeed!



Other projects, including the creation of new detectors and guides as well as innovative data acquisition and storage techniques, will ensure that the ILL's instruments continue to set new standards in their respective fields. One of the Division's objectives is to develop new detectors that can be tailored to meet the individual requirements of instruments. Another innovative research programme in the field of polarising neutron optics is also currently underway, aimed at developing advanced tools for neutron instrumentation.

One major challenge facing the Institute is how to cope with the ever-increasing volume of experimental data generated by our instruments. In 2011, a full cycle of 50 days and 40 instruments generated approximately 1TB of data. Today, we are generating 2–3TB of data per day, and we expect this figure to rise to a phenomenal 10TB in the next few years!

Of course, the Projects and Techniques Division also has an important part to play in the day-to-day running of our research facility. This covers everything from maintaining and upgrading the ILL's non-scientific software applications, to the renovation and improvement of our buildings, roads and green spaces.

Finally, the level of expertise and experience available within the Division has naturally led to our involvement in a number of European projects and conferences. This not only allows us to share our knowledge; it also helps us to further enrich our own know-how, whether that be for developing new instruments (detectors, guides, instrumentation, electronics, and so on), new data-sharing systems or a new reactor fuel design—and all this, with the aim of constantly improving our capacity for collaboration and, ultimately, providing our users with the excellent instrumentation and quality of service they have come to expect.

Jérôme Estrade
 Associate Director
 Head of the Projects and Techniques Division

Endurance: ILL Instrument Upgrade Programme

Exciting times are ahead for Endurance, the ILL's current instrument upgrade programme. The first phase, Endurance1, benefitted from an additional contribution from the ILL's Associates of 4.5 M€ / year for the period 2016 to 2018. Among the projects involved, the new fission product prompt gamma-ray spectrometer, **FIPPS**, was the first of the new instruments to begin commissioning and delivering science at the end of 2016. The majority of components for **SuperSUN**, the new source of ultra-cold neutrons (UCN), are in the advanced stages of construction for installation and a first phase of commissioning during 2019. The first UCNs from **SuperSUN** will allow the next-generation, neutron electric dipole moment (EDM) experiments to begin in the PanEDM collaborative experiment. New and upgraded sample environment capabilities have been, and will continue to be, steadily delivered by the **NESSE** project throughout the course of Endurance, while the **BASTILLE** project to deploy the multi-facility Mantid software is making great headway in delivering modernised data treatment software for most ILL instruments.

AUTHORS

C. Dewhurst and J. Estrade (ILL)

The winter shutdown of 2018–2019 has already seen the rather bittersweet dismantling of IN4C to make way for the new, thermal time-of-flight (TOF) spectrometer, **PANTHER**. IN4C began user operation in 1998, benefitting from additional upgrades during the Millennium programme. Its intense neutron flux paved the way for much high-impact science, thought to be impossible elsewhere, and was a cornerstone of thermal neutron spectroscopy at the ILL. **PANTHER** will boast an overall performance increase of 60 times that of IN4C, by exploiting a much larger position-sensitive detector (PSD) and improved optics with large double-focusing monochromators. Enhanced instrument shielding and the roll-out of five background choppers will significantly improve the signal-to-noise ratio, contributing to the anticipated massive improvement in data quality and capabilities of **PANTHER** compared with IN4C. Importantly, the instrument optics and PSD allow for work on single-crystal samples, while the fully non-magnetic instrument will allow polarisation-analysis experiments using the PASTIS3 insert.

The backbone of Endurance1 is the 'Chartreuse' project, involving the renewal of the **H24** thermal neutron guide and the upgrade of the **D10+** single-crystal diffractometer and **IN13+** (CRG) backscattering spectrometer, as well as a new extreme-conditions powder and single-crystal diffractometer, **XtremeD** (CRG). Each instrument will benefit from a dedicated end-of-guide position, allowing for optimised beam-shaping and monochromator optics. As a result of constraints in the functioning of the ILL reactor during 2017, the 'Chartreuse' projects will now be finalised upon completion of the H1-H2 guide renewal, at the end of 2020.

An additional injection of funds for instrumentation upgrade came in 2017 in the form of a CPER* grant of 4.3 M€ from French national and regional funds. This financial stimulus has allowed us to advance and inject additional projects into Endurance1, specifically allowing us to: complete **PANTHER** to its full specification; renew the ageing **H16** cold neutron guide and focusing optics on **IN5**, with estimated gains of x3 in neutron flux for small samples (delivery 2019); undertake a **D3-Liquids** project to provide a PSD detector and improved polarisation and analysis capabilities for work on hydrogenated liquid samples (delivery 2019); provide anti-Compton discrimination detectors for **FIPPS** (delivered 2018); purchase a velocity selector to eliminate higher-order wavelength contamination as part of the **IN20-Upgrade** project (delivery 2020); purchase ^3He for future detector-upgrade projects; and, fund design studies for Endurance2.

* CPER – Contrat Projet Etat Région



Figure 1

The fission product prompt gamma-ray spectrometer **FIPPS** began commissioning and entered the scientific user programme at the end of 2016.

The second phase of Endurance had its provisional scope and budget set during 2017, following a review and recommendations by a dedicated Instrument Subcommittee and endorsement by the Scientific Council. Continued funding for Endurance has been assured by the ILL's Associates for 2019 and is anticipated for the full Endurance2 phase (2019–2023). The level of funding of Endurance2 should be similar to that of Endurance1, with a dedicated contribution from the Associates and the ILL's own budget over the five-year period 2019–2023 reaching a total budget of ~32 M€. As well as the injection of some more advanced projects into Endurance1, two projects are to be accelerated: a second **LADI-B** protein crystallography station will double capacity and improve instrument resolution; while neutron-imaging activities on the current D50 instrument will become full time and accessible to the public from 2021, with corresponding upgrades to instrumentation and access to expertise through collaboration with UGA-Grenoble and HZB-Berlin – **IM2020-NeXT**. Other Endurance2 projects are in the process of being launched—such as, new or additional detectors for the small-angle neutron scattering (SANS) instruments **D11** and **D22++**; upgrades to monochromators and analysers as part of **IN20-Upgrade**; and a wide-angle detector for **D16**—while the sample environment, **NESSE2**, software and **BASTILLE2** projects are continuing.

The lion's share of Endurance2 will see the renewal of the cold neutron guide **H15** and the associated suite of upgraded instruments **D7+**, **D11** and **T3**, as well as the new expected CRG instruments, **GAPS** (cold-TAS spectrometer), **SAM** (SANS) and **RAMSES** (cold TOF spectrometer), each of which will receive its own high-performance and dedicated end-of-guide beam position. The **H15** project is vast in terms of scope as well as both engineering and optical complexity. The conceptual and optical design of the first expanding part of the guide from the in-pile to ILL7 entrance has been validated and moved onto the detailed design phase, with installation anticipated during the H1-H2 shutdown (2020). The guide branches and instrument siting on the new **H15** guide are under conceptual study, with a view to installation during the 18-month period from 2021 and delivery of the instruments in 2023.

Endurance is ambitious and will keep the ILL at the forefront of science that uses neutrons for the coming years. Exciting times are indeed ahead!

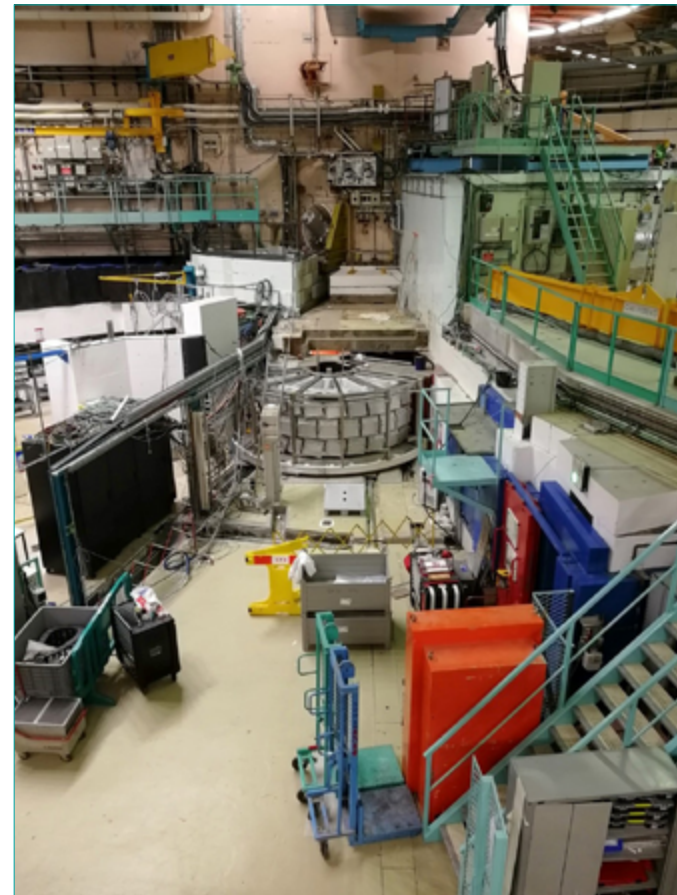
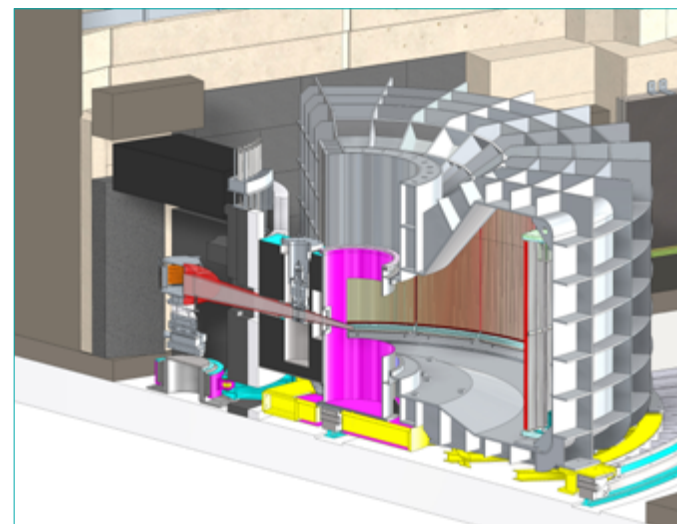


Figure 2
Dismounting IN4 in preparation for the new thermal time-of-flight spectrometer, **PANTHER** which will begin commissioning in early 2019.



3D design model of **PANTHER**.

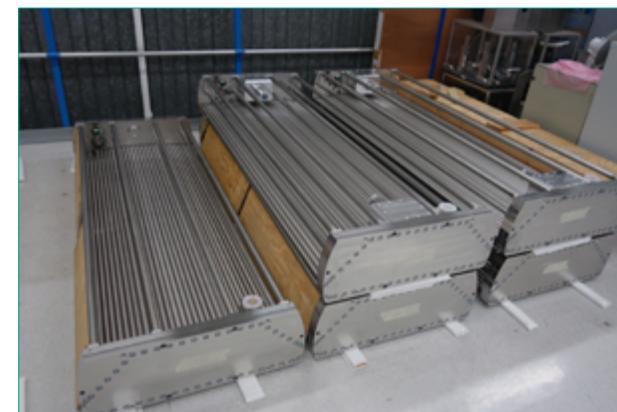


Figure 3
Principal components for **PANTHER** awaiting installation during the winter shutdown 2018–2019. Monochromator shielding, flight chamber, double-focusing monochromator.



First results with BATS on IN16B – inverted neutron time-of-flight spectroscopy

While neutron backscattering spectrometers at reactors attain unequalled energy resolutions below 1 μeV , they are rather limited in their accessible energy-transfer range. With the BATS option commissioned in 2018, the IN16B backscattering spectrometer at the ILL now offers a flexible set-up with an extension in energy transfer exceeding one order of magnitude at the cost of a slightly broadened resolution. Ongoing enhancements of the neutron optics will also make the count rates of the new BATS option highly competitive.

AUTHORS

M. Appel (ILL and FAU Erlangen-Nürnberg, Germany)
B. Frick (ILL)
A. Magerl (FAU Erlangen-Nürnberg, Germany)

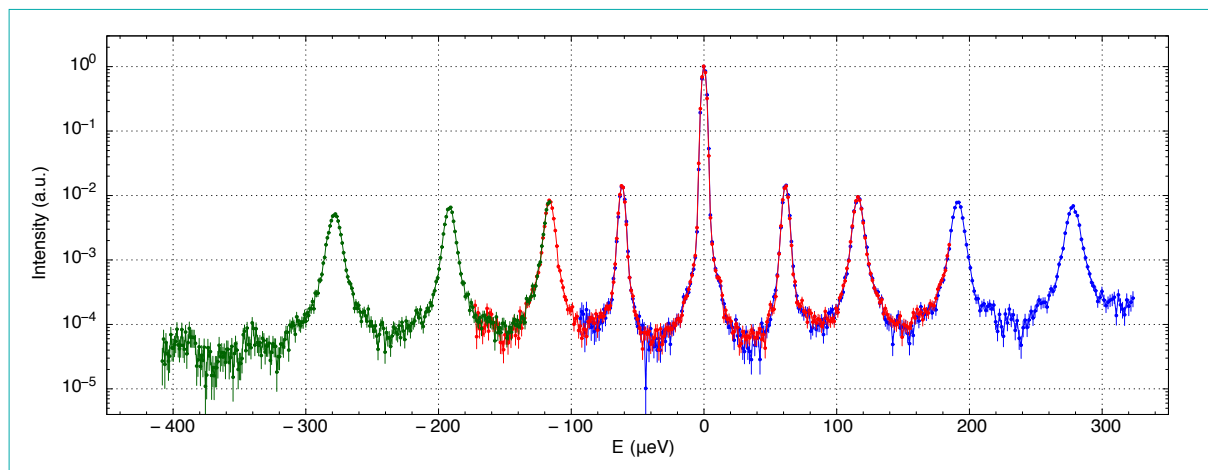
REFERENCES

- [1] B. Spiegelhalter, U. Keller and E. Käppeler, German Patent No. DE 10 2014 004 994 B3 (2015)
- [2] M. Appel, B. Frick and A. Magerl, *Sci. Rep.* 8 (2018) 13580
- [3] M. Appel, B. Frick and A. Magerl, *Physica B* 562, 6-8 (2019), DOI: 10.1016/j.physb.2018.11.062

Many neutron spectroscopy experiments aim to study dynamics on the pico- to nanosecond time scale over distances of Ångstrom to several nanometres, such as the rotational or translational diffusion of molecules, the diffusion of protons or lithium in energy materials or the multi-scale dynamics in biological or glassy materials. Frequently, separate measurements on neutron time-of-flight (ToF) and backscattering machines need to be combined to cover the necessary, broad dynamic range. The recently commissioned Backscattering and ToF Spectrometer (BATS) option on IN16B at the ILL combines the advantages of both techniques in one set-up. In BATS mode, the incident neutron beam is not conditioned using a crystal monochromator; instead, a novel, flexible chopper system installed 34 m upstream of the sample position creates short neutron pulses such that the incident neutron energies in the sample can be reconstructed from a ToF measurement. Neutrons scattered from the sample are analysed by the same, large backscattering crystal analysers (typically Si 111) as in IN16B's conventional mode of operation. The chopper system is the first to use a new generation of oriented carbon fibre-reinforced polymer composite disks [1] of 750 mm diameter, rotating at up to 19 000 rpm. It has been designed for maximum flexibility [2] and features multiple slits of seven different widths on two counter-rotating chopper pairs. While the BATS option was anticipated in the ILL's design of IN16B from the beginning, the design and realisation of the chopper system over the last few years was made possible by grants from the German Ministry of Education and Research (BMBF, grants 05K13WE1 and 05K16WEA).

Figure 1

Neutron scattering spectrum recorded on γ -picoline-N-oxide at $T = 1.8$ K with BATS on IN16B summed over all detectors. Three consecutive measurements (6 h counting time each) with different offsets of the observed energy-transfer window are shown in different colours. The energy resolution FWHM at the elastic peak is 3.8 μeV (from Ref. [3]).



Using Si 111 analysers, the energy resolution for spectroscopy experiments can now be varied between 1.5 μeV and 7.5 μeV in seven steps, with an energy-transfer window with a full width of 360 μeV and the additional possibility of inelastic offsets. In comparison, the standard, conventional backscattering mode of IN16B provides 0.75 μeV resolution within a window of ± 31 μeV . The maximum elastic momentum transfer is identical in both cases, namely 1.8 \AA^{-1} .

First results obtained during the commissioning are now available [3]. **Figure 1** shows the tunnelling spectrum of methyl groups in γ -picoline-N-oxide measured at $T = 1.8$ K with an energy resolution of 3.8 μeV at the elastic line. Consecutive measurements with shifted energy observation windows have been conducted. The result demonstrates a clean, straightforward stitching of spectra with different offsets, as well as an excellent signal-to-noise ratio above 10^4 . **Figure 2** shows a measurement of the broad quasi-elastic scattering on a glycerol sample at $T = 400$ K. For this experiment, the resolution was relaxed to 6.2 μeV in order to benefit from a higher beam intensity. As in the previous example, several measurements with different offsets were performed, demonstrating the feasibility of reaching energy transfers beyond -600 μeV .

In the near future, enhancements of the neutron optics system are to be completed in order to unlock the full potential of BATS. First, beam focusing on the sample will be much improved by an optional exchange of the last neutron guide piece—the expected flux density on small samples necessary for best BATS resolution (4×10 mm²) is expected to increase by one order of magnitude. Secondly, the challenging and innovative project of realising an adaptive, variable, horizontal focusing and defocusing line around the BATS chopper system will eliminate the intensity loss caused by using slits in the chopper disks that are narrower than the existing neutron guide width. The latter system will increase the neutron flux for the best resolution setting by another factor of five. With these future enhancements, the BATS option will be highly competitive and enable excellent experiments from various scientific fields—beamtime proposals are welcome!

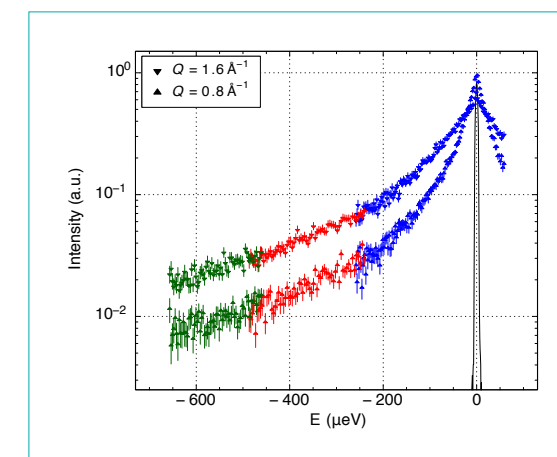
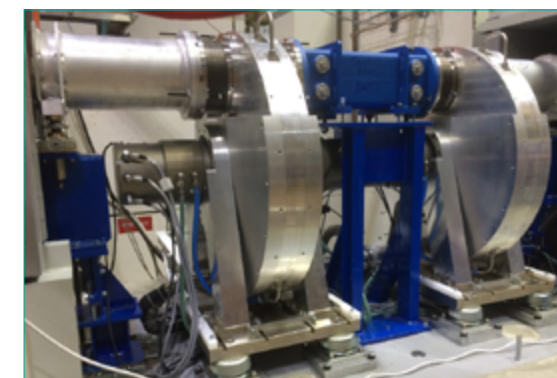


Figure 2

Neutron scattering spectra recorded on glycerol at $T = 400$ K with BATS on IN16B for two different momentum transfers Q . Three consecutive measurements (3 h counting time each) with different offsets of the observed energy-transfer window are shown in different colours. The energy resolution FWHM at the elastic peak obtained with a Vanadium standard (black line) is 6.2 μeV (from [3]).



The new BATS chopper system: each housing contains a counter-rotating pair of disks spinning at up to 19 000 rpm.

Development of a low-roughness, transparent, hydrogen-tight sample container for ultracold and very cold neutron experiments

The loss mechanisms in ultracold neutron converters based on solid deuterium are still poorly understood. To gain more knowledge about them, neutron transmission measurements need to be carried out on deuterium. We have developed a sample container with low-roughness, amorphous silica windows that allows for the precise measurement of the total cross section of cryogenic liquids and solids, while suppressing surface scattering.

AUTHORS

S. Dögé and J. Hingerl (ILL and TU Munich, Germany)
C. Morkel (TU Munich, Germany)
T. Jenke (ILL)

ARTICLE FROM

Sci. Instrum. (2018)—doi: 10.1063/1.4996296

REFERENCES

- [1] F. Atchison *et al.*, Nucl. Instrum. Methods A 611 (2009) 252
- [2] G. Bison, D. Ries *et al.*, Phys. Rev. C 95 (2017) 045503
- [3] S. Dögé and J. Hingerl, Rev. Sci. Instrum. 89 (2018) 033903
- [4] S. Dögé *et al.*, Phys. Rev. B 91 (2015) 214309

For several decades, the ultracold neutron facility PF2 has been providing the highest density of ultracold neutrons (UCNs) worldwide. Nevertheless, most experiments performed at PF2 have been limited by neutron counting statistics, triggering the development of new UCN converters based on solid deuterium (sD₂) across Europe and North America. Initial simulations and test measurements predicted a significant increase in UCN density compared with that achieved by PF2 [1]. This density is the crucial parameter in any UCN storage experiment. However, the actual UCN output of these new converters is lower than expected [2].

This discrepancy might be explained by the scattering of UCNs from rough surfaces and defects inside the sD₂ crystal.

We have conceived, constructed and tested a sample container for cryogenic liquids and solids that addresses the issue of surface scattering [3] (see **figure 1**). Its highly polished, amorphous silica windows, which are its key feature, allow samples to be grown with a smooth



Figure 1

Sample container with highly polished and transparent windows.

surface, thereby suppressing the scattering of UCNs from the sample surface as much as possible. Due to the high rigidity of silica compared with commonly used aluminium windows, the container does not bulge under pressure differentials of 1 to 2 bar. Also, amorphous silica has the advantage of not producing any small-angle scattering. This reduces the influence of the container on the measurement to a minimum. The main challenge in constructing the container was to make it hydrogen-tight at low temperatures. This was achieved by using an indium seal and chamfered clamps. Careful assembly and leak testing at room temperature ensure a reliable performance at cryogenic temperatures.

Any sample condensed into or grown inside this sample container can be verified optically before the neutron measurement is started (see **figure 2**). To this end, a suspended mirror can be lowered into the neutron beam path in the sample preparation phase. The mirror is then held at a 45° angle to the neutron beam path and can be observed through a vacuum-tight viewport perpendicular to the beam path.

We have used this sample container in recent UCN transmission measurements of liquid and solid deuterium. The scattering cross sections of liquid deuterium overlap very well with a model we published in 2015 [4]. From the results for solid deuterium we were able to determine the concentration and size of defects in two sD₂ crystals, as shown in **figure 3**. These findings will help us to gain a realistic understanding of the processes inside sD₂-based UCN sources.

This new type of sample container will help experimenters obtain scattering data of cryogenic liquids and solids using long-wavelength neutrons, without the side effects hitherto commonly encountered with aluminium windows.

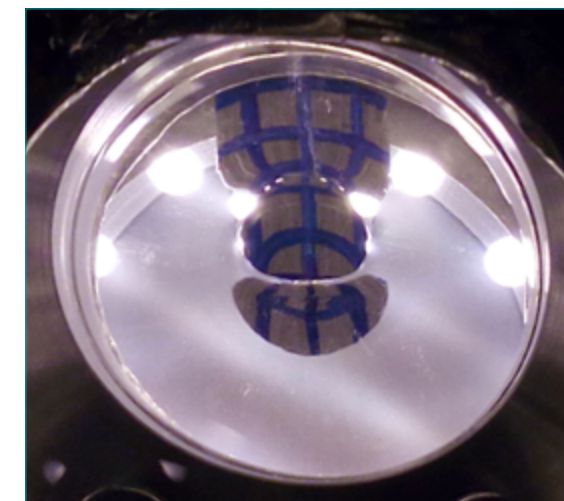


Figure 2

Direct view of a back-lit deuterium crystal at 1.5 K in the sample container described here. The vacuum bubble in the middle of the sample is blinded out by a cadmium absorber.

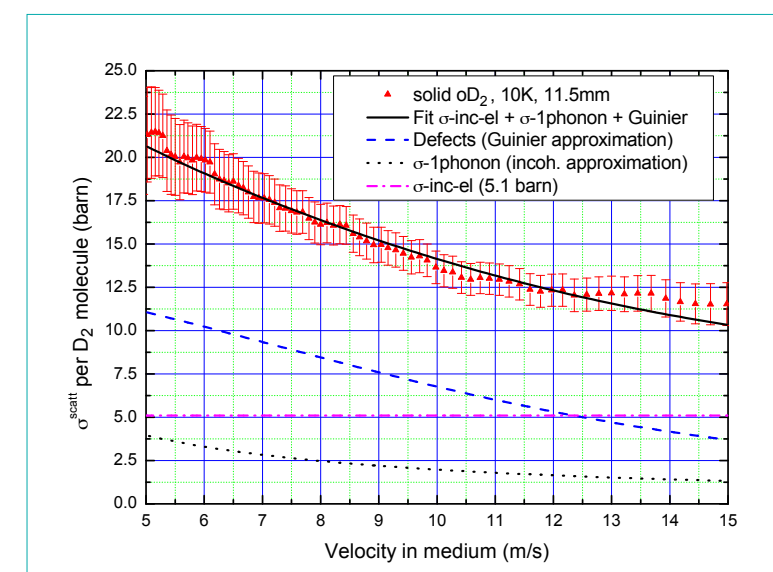


Figure 3

Experimental scattering cross section of solid deuterium (red triangles) and fit to the data with calculated 1-phonon cross section and Guinier two-phase model (preliminary data). The radius of defects as extracted from the Guinier model is $R_d = 88 \text{ \AA}$, the concentration of defects $c_p = 8.2 \times 10^{-11}$.

Fluorinated nanodiamonds as a unique neutron reflector

With the pronounced, worldwide trend of increasing the range of useful neutrons towards smaller energies—driven in particular by large-scale structure diffractometers, reflectometers, time-of-flight and spin-echo techniques as well as by particle physics—progress is limited by the low fluxes of the less energetic part of the cold neutron spectrum. One fundamental reason lies behind this drop in flux: regardless of the choice of materials for neutron reflectors, they are all composed of atoms. Atoms in solids and liquids are separated by distances of a few tenths of nm. If the neutron wavelength is larger than that, neutrons are weakly scattered by atoms/nuclei and the diffraction is limited by the inter-plane distances available; thus, neutrons pass through a reflector with low interaction with its material and are lost.

AUTHORS

V. Nesvizhevsky (ILL)

ARTICLE FROM

Carbon 130 (2018) 799—doi: 10.1016/j.carbon.2018.01.086

REFERENCES

- [1] V.V. Nesvizhevsky, Phys. Atom. Nucl. 65 (2002) 400
- [2] P.J. DeCarli and J.C. Jamieson, Science 133 (1961) 1821
- [3] E.V. Lychagin, A.Yu. Muzychka, V.V. Nesvizhevsky, G. Pignol, K.V. Protasov and A.V. Strelkov, Phys. Lett. B 679 (2009) 186
- [4] V.V. Nesvizhevsky, U. Köster, M. Dubois, N. Batisse, L. Frezet, A.B. Bosak, L. Gines and O. Williams, Carbon 130 (2018) 799

To construct efficient slow-neutron reflectors, currently there is no alternative other than to mimic conventional reflectors by replacing atoms/nuclei with nanoparticles of low-absorbing, highly scattering materials—thereby changing the characteristic length scale and consequently the neutron wavelength corresponding to efficient neutron reflection [1]. Nanodiamonds [2] are an obvious choice for the material of such reflectors, as the cross section of absorption in carbon is exceptionally low, the coherent scattering length is very high and the volume density is higher than that for other carbon materials. The characteristic sizes of available nanodiamonds are found to be in the range of optimum theoretical values. In addition, the reflectivity of available nanodiamonds has been assessed to be much higher than that of any alternative reflector [3]; however, it remains low for neutron velocities above 160 m/s, mainly because of the high content of hydrogen impurities.

We overcome this principal difficulty by using fluorinated nanodiamonds [4]. We performed a detailed analysis of samples of this material using several complementary techniques, as follows. Using X-ray diffraction, we found that the diamond cores (sp^3) of nanoparticles remain unaffected upon fluorination, while the sp^2 carbon disappears almost completely from the nanoparticle shells. A combination of Raman scattering and infrared absorption qualitatively confirms the disappearance of sp^2 carbon, carbon-hydrogen bonds, oxygen-hydrogen and carbonyl-containing functional groups. Analysis of the multinuclear solid-state NMR data essentially confirms the results of vibrational spectroscopy, while being more quantitative. The ultimate mean of hydrogen content is determined by prompt- γ analysis. This shows the hydrogen content in nanodiamonds to be drastically reduced by the fluorination, reaching a level 35–60 times lower than that before fluorination. Neutron activation analysis reveals impurities, which become radioactive in high neutron fluxes, as well as impurities that strongly absorb neutrons. Their content can be reduced by the purification of nanodiamonds in strong acids at high temperature; however, the degree of purification remains to be improved in the future.

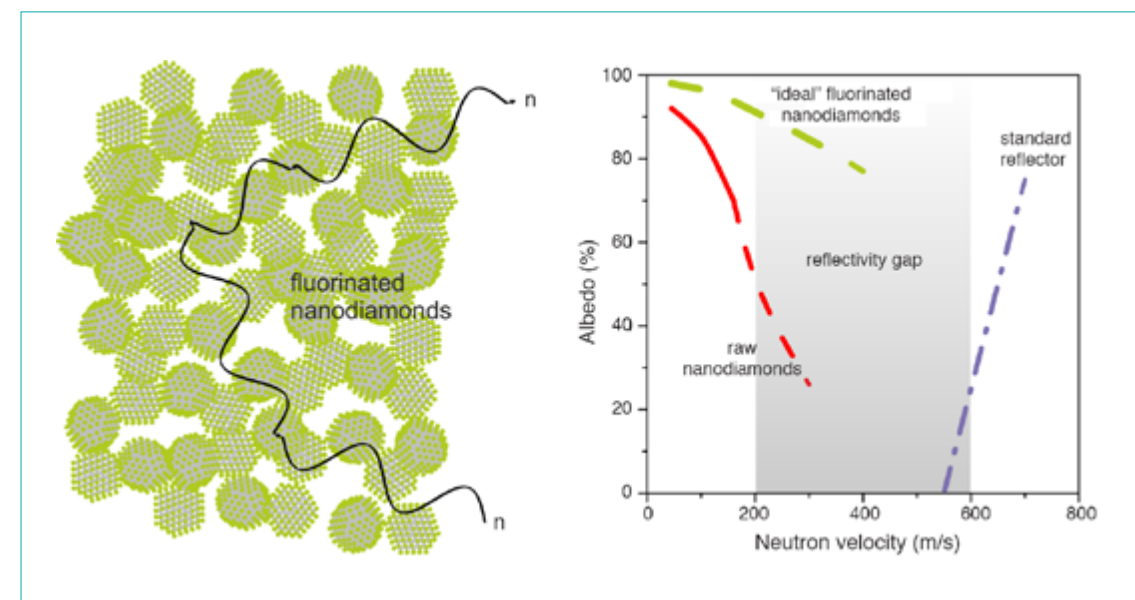


Figure 1

The **left** insert illustrates the diffusion of slow neutrons in the powder of the fluorinated nanodiamonds. On the **right**, the neutron albedo is shown as a function of neutron velocity for: (i) raw nanodiamonds with a thickness of 3 cm (solid red line, data from [3]); (ii) the albedo extrapolated from the same raw-nanodiamond layer (dashed red line); (iii) a simulated albedo from an 'ideal', infinitely thick layer of impurity-free optimal-size diamond nanoparticles (dotted green line)—fluorinated nanodiamonds are expected to provide the albedo between these two lines, approaching the 'ideal' line; (iv) cutoff velocities for graphite (dashed-dotted blue line). The incident neutron flux is assumed to be isotropic. These estimations are preliminary and should be confirmed in the future by direct measurements.

The most important effect of the fluorination of nanodiamonds is the removal of hydrogen and sp^2 carbon, which respectively decreases the absorption of neutrons and increases their scattering. Using this information, we evaluated the albedo of slow neutrons from reflectors consisting of this powder. In **figure 1**, we present the reflectivity of reflectors of various types as a function of neutron velocity, and comment on the quality of this new reflection in the figure caption.

In reference [4] we proposed a new class of reflectors, based on designed fluorinated nanodiamonds, that can provide a continuous reflectivity curve with high albedo, thus minimising the existing 'leak' of neutrons through the so-called reflectivity gap. This high diffusive and quasi-specular reflection will dramatically improve the performance of neutron sources, the efficiency of neutron delivery and thus the fluxes of slow neutrons in neutron instruments. It might also allow a new generation of neutron sources and experiments to be designed.

Neutron detector service

B. Guérard (ILL)

The Neutron Detector Service (SDN) at the ILL has two principal objectives: one, to ensure that the detectors at the Institute function well; and two, to develop new detectors that can be tailored to meet an instrument's individual requirements. The demand for detectors has increased dramatically in recent years, in terms not only of performance but also production capability.

Nine (+ one spare) multi-tube vessels have been constructed for the Endurance phase 1 project PANTHER. They are now at different phases of mounting (**figure 1**) and several modules are already fully operational. The plan is to have all ten modules completed and tested by mid-2019.

The curved ^3He detector of XtremeD, also an Endurance phase 1 project, is now in production. The pressure vessel has already been delivered and tested for gas tightness (**figure 2**). XtremeD itself will be delivered by the end of 2019.

The construction of an aluminium mono-block ^3He multi-tube (MAM) for the Platypus reflectometer at neutron scattering facility ANSTO has been completed. Following a successful test with neutrons in October this year, it will be shipped to Australia at the beginning of 2019.

Another MAM detector is being built for the D3 Endurance phase 2 project. Here, each detection cell consists of four proportional counters positioned at the same angle and electrically connected together. This design allows high efficiency at short wavelengths to be achieved. The detector will be delivered at the beginning of 2019.

New detectors are also being considered for the D16 and D20 Endurance phase 2 projects. Both detectors are based

Figure 1

Multi-tube vessels for the Endurance phase 1 project PANTHER.

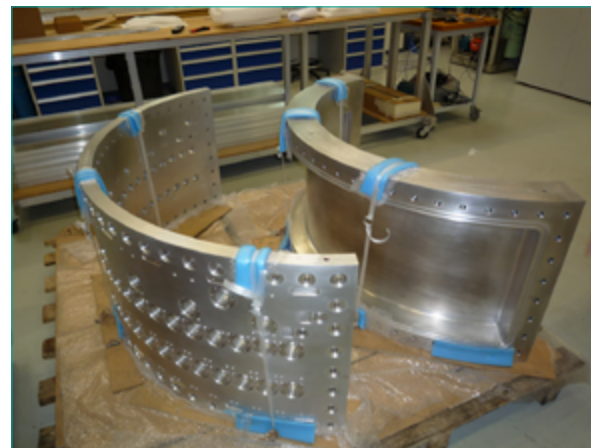


Figure 2

The curved detector of XtremeD, an Endurance phase 1 project.

on the trench-MWPC concept introduced for XtremeD. The design of the D16 detector is under discussion, while a prototype of the D20 detector is under construction.

The ILL's detector service has also been involved in several European collaborations. The BrightnESS project came to an end in 2018. The ILL's task here was to optimise the ^{10}B -multi-grid detector for operating in a vacuum chamber: a gain of 50 % in detection efficiency has been obtained with new grids. We also demonstrated that filling the detector vessel with gas at low pressure, typically 50 mbar, provides many advantages—in particular, the mechanics are simpler, gamma sensitivity is reduced and the counting rate is increased. These results have helped to further reduce the technical gap between ^{10}B -multi-grid detectors and ^3He PSDs, and to secure the development of future neutron instruments in the context of the ^3He shortage.

The SINE2020 project will be completed in 2019. As part of it, a new ^3He micro-strip gas chamber with a new readout scheme has been developed and tested on a neutron beam line: cathodes are read out individually at both ends to measure the neutron impact position along the strips by charge division measurement, while a centre of gravity algorithm is used for the direction perpendicular to the strips. This development represents a new step towards detectors with a 1 MHz counting rate and 1 mm spatial resolution.

Figure 3

The different parts of the multi-tube detector of D3 ready for mounting.



Neutron optics service

P. Courtois (ILL)

The Neutron Optics Service carries out the maintenance, repair and replacement of neutron optics components used on the ILL's Instruments and provides ^3He spin filters for polarised neutron experiments. We also play an active part in the modernisation programmes Millennium and Endurance phase 1, producing new optical components such as crystal monochromators and supermirrors. In addition, an innovative research programme in the field of polarising neutron optics is currently underway with the aim of developing advanced tools for neutron instrumentation.

The year 2018 was a special one for the Neutron Optics Service, seeing as it did the completion of the neutron spin analyser for the instrument WASP. After eight years of intense activity, more than 3 500 double-sided $m = 2.8$ Co/Ti supermirrors have been manufactured by our Multilayer Group using the Pi sputtering-deposition machine. This represents a total active area of 238 m^2 ! The analyser is made up of 91 individual bender cassettes, each containing 37 supermirrors (**figure 1**). Recently mounted onto the instrument for the commissioning phase, the analyser will cover a detection angle of 90° .

Under the framework of one of the Endurance phase 1 projects, several monochromators are under preparation. As a first step, we successfully focused our work on assembling the double-focusing HOPG monochromator for PANTHER (**figure 2**). This consists of an array of 165 crystals mounted in 15 columns and 11 rows, forming an active area of $297 \times 220 \text{ mm}^2$ (width x height). The alignment of the monochromator was performed by neutron diffraction. The crystal plates have been oriented in both directions with an accuracy of 0.1° with respect to each other. The monochromator will be installed on PANTHER in 2019 for the commissioning phase.

A new type of Fe/Si supermirror coated on a sapphire substrate has been developed. This device results in dramatically better polarisation efficiency over a broad angular and wavelength range of the incident neutrons than that achieved using typical Fe/Si supermirrors. A broadband solid-state supermirror polariser is also under construction for the fundamental physics instrument PF1B, in order to deliver cold neutron beams with polarisation up to 99.9 %.

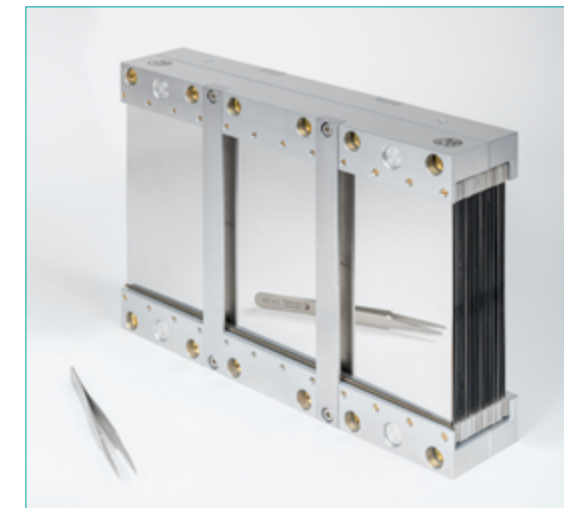


Figure 1

An individual bender cassette of the WASP spin analyser. Each cassette contains 37 Co/Ti polarising supermirrors and covers a detection angle of 1° .

Neutron polarisation analysers that can cover a wide angular range can also enhance the performance of neutron scattering instruments. XYZ polarisation analysis using ^3He spin filters has therefore been further developed, with improvements to the performance of the so-called PASTIS system achieved by increasing the ^3He relaxation time up to 100 hours. The design of the new system, PASTIS3, is now complete and the first prototype is being constructed for the triple-axis spectrometer IN20.

Finally, to cope with the expected rise in demand for ^3He spin filters, we have begun work on upgrading the filling station known as 'Tyrex', in order to increase its production capacity by a factor of two. This project is on track and we expect to complete refurbishment during the long reactor shutdown in 2019–2020.

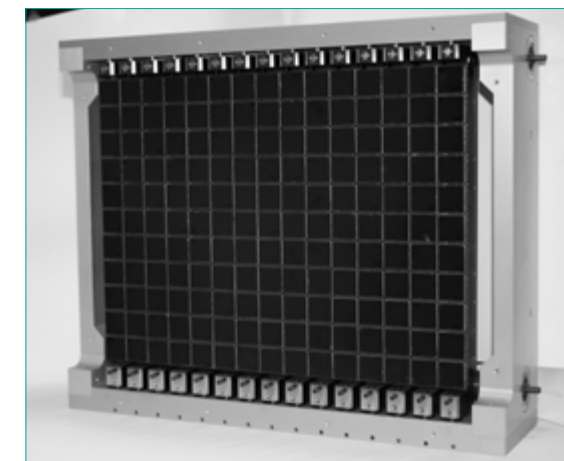


Figure 2

The double-focusing HOPG monochromator for the Endurance phase 1 project PANTHER. The horizontal and vertical curvatures can be varied independently.

Instrument control service

P. Mutti (ILL)

The Instrument Control Service is exploring state-of-the-art computing technology to develop an alternative, virtual access mode for neutron experiments. We propose to merge existing instrument control software, computing and scientific software tools, advanced communication technology and modern 3D animation into a new virtual platform. Through a web portal, users will be able to connect to any instrument in the ILL suite *via* a digitally rendered twin of the instrument and its movements in real time. At the same time, thanks to an application such as vExp [1] (figure 1), users will be able to describe the composition and atomic structure of a sample and explore its diffusion pattern directly in reciprocal space. Once the interesting structures have been identified, it is possible to define the most appropriate trajectory for the instrument for optimising data collection time. The desired settings are then sent directly to the instrument control software for execution.

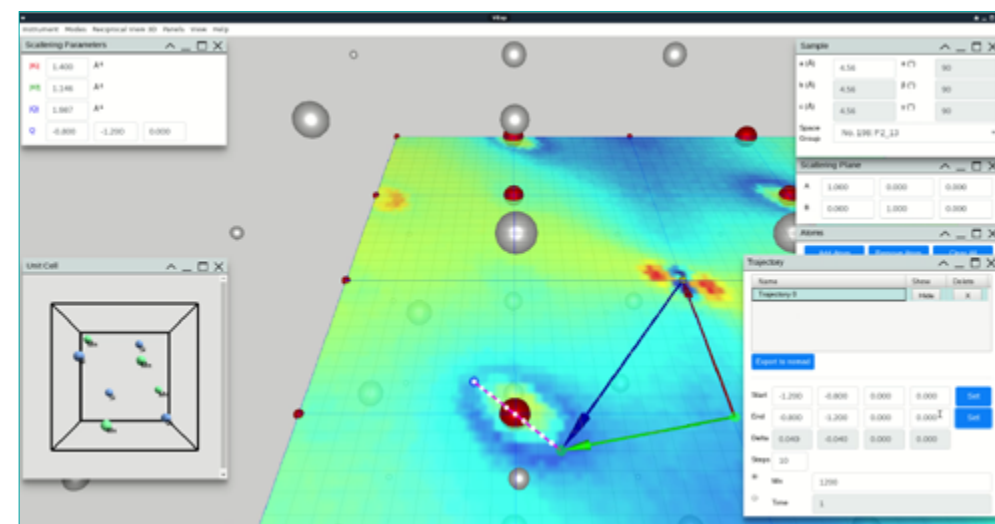


Figure 1

A view of the graphical user interface of vExp.

REFERENCES

- [1] P. Mutti, M. Boehm, Y. Le Goc and T. Weber, (2018) Proc. IEEE Nuclear Science Symposium
- [2] T. Weber, R. Georgii and P. Böni, SoftwareX 5 (2016) 121
- [3] M. Boehm, A. Filhol, Y. Raoul, J. Kulda, W. Schmidt, K. Schmalzl and E. Farhi, Nucl. Instr. Meth. A 697 (2013) 40

Portability is the keyword for this entire system. To achieve this, we have chosen to use modern web technologies. For vEXP, we designed a web and a desktop application, both based on Node.js, HTML 5, CSS, WebGL. The desktop application uses Electron. This combines Node.js for the back end and HTML5 for the front end, the main advantage being the ability to share the maximum of code between the two applications. Only direct communication between the GUI and the functional part of the desktop application is replaced by sockets in the web application. Node.js is a JavaScript engine that uses the open source V8 JavaScript engine developed by Google. One advantage of using Node.js and V8 in the vEXP context is the ability to mix native code written in C++, when high computational performance is required, and JavaScript code. The 2D and 3D interactive rendering is achieved using WebGL API. For complex 3D animations, we have adopted the high-level library Three.JS. In this way, the display can be rendered directly in a browser (hidden in the desktop Electron application) without the kind of effort required for a traditional standalone application or plugin. Moreover, it provides access to a mathematical library in order to make 3D manipulation easier (linear algebra operations).

This platform is meant not to replace existing tools for instrument control, data sorting and data analysis, but to complement them. It provides a generic interface for importing, illustrating and sharing information relevant to the experiments. In parallel with the virtual platform we are exploring the usefulness of augmented reality in the instrument and experimental areas for scientists and technical staff on-site. First concepts of a virtual platform have been successfully tested based on experience of existing single-crystal, inelastic neutron scattering software (TAKIN [2], vTAS [3]). NEVA is open source and platform-independent, and can be used with different instrumental techniques and at **different facilities**.

IT service

J.F. Perrin (ILL)

Since 2012, the ILL has experienced a significant increase in the volume of experimental data generated by our instruments. In 2011, a full cycle of 50 days and 40 instruments generated roughly 1TB of data. Today, we are generating 2–3TB per day (figure 1). This increase is mainly due to improvements to the guides and instruments as a result of the Millennium and Endurance programmes. However, these fantastic results are not without consequence for the IT infrastructure, especially our network, storage and computing facilities.

The IT service has initiated three main activities in an attempt to accommodate this evolution.

1. Network

In August 2018, we refurbished our core network equipment. We are now able to reach a capacity of 100 Gb/s in the core. For now, this is probably not particularly noticeable to end-users but it allows us to further upgrade the network. In 2019, we intend to upgrade the distribution equipment (where the computers are connected) in order to offer 1Gb/s to everyone, while in more specific cases 10 Gb/s will be available for those instruments generating a large volume of data.

2. Storage

After six years of service, Serdon, the ILL's well-known experimental data archive, became unable to cope with the volume of data and performance required. It was therefore refurbished in August 2018, after a year of preparation for the 1PB storage capacity that is now available. This new system was able to handle the pace of the third cycle in 2018, but some optimisation is still ongoing. We are also working closely with our instrument control colleagues to allow users immediate access to the data in the archive.

3. Computing facilities

This is the third pillar in our ability to process data. The expansion in data volume has hit not only the ILL but all other European analytical facilities (neutron scattering centres, Synchrotrons, free electron lasers, etc.). We have agreed to tackle this subject together, with the support of the European Commission, as part of a collaboration project called PaNOSC. An ILL-only pilot began in 2018 on two instruments, while the European collaboration will officially start in January 2019. More detailed and practical information will be communicated during the course of 2019.

We hope that the ILL's users will greatly appreciate these efforts, which will allow them to continue to deliver excellent science despite the 'data deluge' reported by the media.

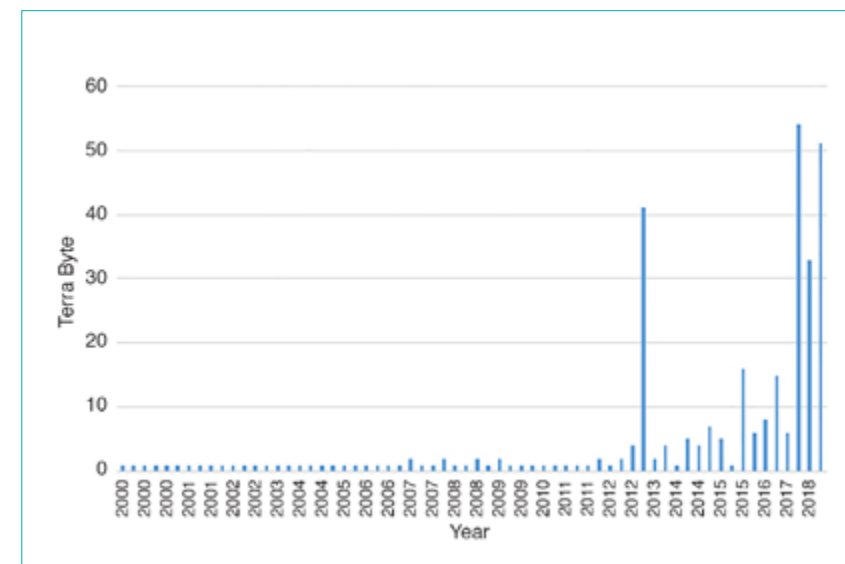


Figure 1

Volume of experimental data/cycle.

Projects and calculations service

Y. Calzavara (ILL)

The Bureau des Projets et Calculs (BPC) supports all the ILL's divisions through its twofold objective: carrying out engineering calculations and managing projects. Thus, as well as offering technical expertise throughout the ILL, the BPC manages instrument projects (within the ILL modernisation programmes) and safety projects for the Reactor division (DRe). Today, our engineers are in charge of several instrument projects, such as WASP, XTremeD, LADI-B, IN20 and NeXT, and have responsibility for several DRe projects.

Overcoming all the challenges of its groundbreaking design, the WASP spin-echo instrument started its final commissioning phase with neutrons on 3 October 2018. From an engineering point of view, WASP (see **figure 1**) is definitively one of the most complex instruments ever made at the ILL. In an amagnetic environment, a huge system of coils was built in order to achieve the very high level of precision required to operate the instrument. Many severe constraints had to be worked around, such as the 16 tonne magnetic pressure and high expectations concerning the planarity of the large coils. Innovative designs were developed to address these challenges, leading to new engineering concepts such as the Flight Box and the He Fan. The commissioning of WASP and its optimisation will without doubt require several cycles; because of their complexity, many components still need to be improved to achieve ultimate precision.

The BPC was also involved to a large extent in some of the STR projects. Running parallel to these, the project to convert highly enriched uranium into low enriched uranium (LEU) as a fuel element is now up and running. LEU configurations are intended to limit performance losses to as low as 10 %, taking into account both cycle length and flux. Partially funded by the EU, two series of comprehension irradiations were carried out in 2018 but with unfortunately limited success so far. A back-up solution is being explored with an alternative LEU fuel technology. However, the road to conversion remains challenging; it will require a whole fuel qualification process, which means several irradiations of test plates and prototypes.

Last but not least, the BPC has been heavily involved in the cleaning up of the D-level contamination. The project was delayed because of difficulties encountered by our subcontractor but was eventually completed before the end of 2018.



Figure 1
The WASP instrument.

Building and site maintenance service

P. Cogo (ILL)

The Building and Site Maintenance Service focused this year mainly on the following projects:

Preventive and remedial maintenance of buildings and equipment: The ILL4 roof has been resealed and the facade of ILL3 refurbished, while the ILL19 sanitary facilities have been completely renewed. The self-service workshop has been equipped with LED lighting, as has all the fencing surrounding the EPN campus. Following problems with the compression refrigeration system, the cold unit installed in the CarlHvar Brändén Building has been replaced.

General improvements to existing installations: The ILL20 second floor lab and the NPP Group labs in ILL1 have been renovated, while the ILL7 building has been completely renewed to L2 norms with the creation of a clean room.

We also prepared the location for the PAN-EDM experiment and ensured that WASP was equipped with fluids and electricity.

The ILL now has its own waste-recycling centre, located beyond the Works Council and PCS3 buildings. This will facilitate waste management, particularly in light of security standards for Basic Nuclear Installations.

New offices have been created on the first floor of ILL22, with 40 cm concrete reinforcement measures. These will accommodate ILL staff currently located in the ILL7 offices, which will now be used for experiment casemates.

Post-Fukushima reinforcement: Work on the truck unloading bay has been completed, as has the water-proof painting of the annular space.

Reinforcement of Physical Protection project (RPP): All the projects for installing the new controlled-access area have been launched. These include the installation of barriers around the area, a new reception building and a liaison building between ILL4 and ILL7.

A network of surveillance cameras has also been installed to improve protective measures on the ILL site.

The Building and Site Maintenance Service was also responsible for converting the old SANE laboratories in ILL26 into new stores. Most of the ILL3 stores were transferred in mid-June. This is also part of the physical protection project; the new stores will be located outside the controlled-access area and will serve as a checkpoint for all in-coming goods.



Figure 1
New ILL stores ILL26.

INDUSTRIAL ACTIVITIES

The ILL provides industrial users with access to state-of-the-art neutron instrumentation and the expertise of its scientific and technical staff.

Contact: industry@ill.fr

<https://www.ill.eu/neutrons-for-society/industry-and-business/>

300K€
BEAMTIME
REVENUE

8 SINE2020
FEASIBILITY STUDIES

14

CUSTOMERS



KEEP UP-TO-DATE:

-  [facebook.com/ILLGrenoble](https://www.facebook.com/ILLGrenoble)
-  twitter.com/ILLGrenoble
-  [linkedin.com/company/institut-laeue-langevin](https://www.linkedin.com/company/institut-laeue-langevin)

THE Industry Liaison Unit (ILU) in the Science Division is the focal point of industrial activities at the ILL. The objective of the Unit is to bridge the gap between the ILL as a facility that is historically oriented to serving the academic research community, and industrial research and development (R&D). This involves significant efforts in terms of outreach to increase awareness of neutron scattering techniques and explore different ways of working with industry, ranging from funded research projects to paid-for services.

Funded projects are a key mechanism for opening up academically developed research techniques to industry R&D in order to drive innovation. Indeed, many European and nationally funded projects now require industry-academia partnerships in order to enhance innovation potential. Thus the European project, SINE2020, includes an industry consultancy (<https://www.sine2020.eu/industry.html>) that publicises neutron capabilities and offers feasibility studies. In 2018, nine such measurements over 13 days were performed at the ILL, distributed as follows—stress measurement: seven (three for additive manufacturing); SANS: one; powder diffraction: one. Since the start of the project in October 2015, 33 companies, most of them new to neutron techniques, have carried out feasibility studies. Another way of collaborating with industry is through training, and in September we submitted a COFUND proposal (InnovaXN) for a PhD programme with the ESRF. If successful, this will provide funding for 40 PhD projects over five years, with the condition that each student must spend at least one month per year with an industrial partner.

The IRT-nanoelec (Research Institute for Technology for Nanoelectronics) is a French funded project that has led to the creation of the Platform for Advanced Characterisation in Grenoble (PAC-G), offering a range of advanced neutron (ILL), X-ray (ESRF) and other analytical techniques to the electronics industry. In 2018, a collaboration agreement was signed with SERMA Technologies (<https://www.serma-technologies.com/>) with the objective of promoting PAC-G's unique services. Nine feasibility studies were performed with SERMA and IRT industry partners in 2018. As the IRT nears the end of its current phase, 2018 also saw the opportunity to discuss the future of the project beyond 2020. If funded, it will focus on the radiation sensitivity of electronics, a field that is assuming great importance with the increasing deployment of autonomous devices and vehicles.

D50 is an instrument that was developed at the ILL within the scope of the IRT. Through a collaboration between the ILL and Grenoble Alpes University, a neutron imaging station was added (D50-tomo – see <https://next-grenoble.fr>) with industry funding, thus providing new possibilities for R&D in many applied domains. In 2018,



SALS team with Fraunhofer IWS Dresden.

D50-tomo reached excellent levels of performance, including 1-second complete tomography measurements and 4-micron spatial resolution, and 85 % of experiments combined its neutron and X-ray capability *in situ*. In the context of phase 2 of the Endurance upgrade programme, it has been decided that D50 will become a dedicated, public, imaging instrument in the Large Scale Structures group from 2020. An international advisory committee will bring together expertise from major neutron facilities to guide the upgrade project and the ILL is currently recruiting an instrument scientist.

Most techniques of interest to industry are high throughput, like imaging, SANS, reflectometry and powder diffraction, where the cost of direct industry use is relatively low since one day of beamtime is often sufficient. Strain scanning is an exception to this rule. With the development of additive layer manufacturing (3D printing), which was the subject of a very successful workshop at the ILL in 2018, the technique is of growing interest to industry. However, measurement times are necessarily long and experiments are therefore relatively expensive. In this context, and over a three-year period, we are exploring the possibility of developing longer-term collaborations with industry, via such organisations as Fraunhofer IWS Dresden and the Additive Manufacturing Centre of Excellence in Manchester. In 2018, 36 % of beamtime on SALS was used for industrial activity, of which 61 % was for collaborative projects.

Finally, energy materials and battery research in particular are presenting new, exciting opportunities for advanced neutron analytical techniques in industry and innovation. Following a workshop at the end of 2017 organised by the ILL, ESRF and CEA, which attracted more than 100 local participants, the three institutions will start a common PhD project in 2019 with UMICORE as industrial partner. In this field, the ILU attended the Graz Battery Days conference in 2018 and we will attend the International Electric Vehicle Symposium in Lyon in 2019.

EXPERIMENTAL AND USER PROGRAMME

93 USER PROGRAMME

94 USER AND BEAMTIME STATISTICS

98 INSTRUMENT LIST

The **User Guide** contains all the practical information required to prepare a visit

<https://www.ill.eu/users/user-guide/>

Detailed information on the experimental programme can be found at <http://www.ill.eu/users>

821

**STANDARD
EXPERIMENTS**

Plus **18 DDT**, **63 EASY** and
79 internal research experiments



158 DAYS OF NEUTRONS
4 548 DAYS FOR SCIENCE



1 597

DISTINCT USERS

2 336

USER VISITS

USER
SATISFACTION
ABOVE

95 %



KEEP **UP-TO-DATE:**

[facebook.com/ILLGrenoble](https://www.facebook.com/ILLGrenoble)

twitter.com/ILLGrenoble

[linkedin.com/company/
institut-laue-langevin](https://www.linkedin.com/company/institut-laue-langevin)

User programme

PROPOSAL SUBMISSION FOR ACADEMIC RESEARCH

Neutrons beams and instrument facilities are free of charge for academic users whose proposals have been accepted. There are various ways of submitting a proposal to the ILL, as summarised in the following table.

Detailed information can be found at <https://www.ill.eu/users/applying-for-beamtime/>.

INDUSTRY-SPONSORED ACADEMIC RESEARCH AND INDUSTRIAL USERS

Neutrons have significant, specific applications for industry. Beamtime can be sold directly for proprietary research, in which case the experimental data is not made publicly available. The Industry Liason Unit (ILU) is the single point of contact for industry looking to use the ILL's facilities (see p.90). However, around 25 % of industry's use of the ILL is done via academia. The data from these experiments is publicly available and the results may be published. The ILL is now measuring the number and nature of industry-via-academia experiments more accurately, with a view to promoting this use of neutrons and potentially enhancing it in the future. In 2018, 32 experiments were sponsored by industry.

Table 1

Mechanisms for submitting a proposal to the ILL. All types of access (except DDT) are reserved for users from ILL member countries or for collaboration between non-member and member teams. The stopwatch symbol indicates quick access. Most types of proposals are submitted via the User Club interface, at <https://userclub.ill.eu/userclub/>.

| TYPE | APPLIES TO | WHEN | WHO FOR | RESPONSE TIME |
|-----------------------------|--------------------------------------------------------------------------------------------------------------------------------------------------------------|-------------------------------------------|----------------------------------------------------------------|------------------------------|
| External peer review | | | | |
| Standard | All experiments, all instruments, all conditions | Deadlines twice a year, spring and autumn | All users from member countries (and non-members via 2/3 rule) | 4 to 8 months after deadline |
| BAGs | College 8 proposals on D22 | Deadlines twice a year, spring and autumn | All users from member countries (and non-members via 2/3 rule) | 4 to 8 months after deadline |
| CRG | All experiments, CRG instruments, all conditions | Depends on CRG policy | All users from CRG collaboration | Depends on CRG policy |
| D-Lab | Access to the ILL sample deuteration lab | All year | All users from member countries | |
| Internal peer review | | | | |
| DDT | Urgent experiments, hot topics, excellent science from non-member countries, all instruments, all conditions | All year | All users | ASAP |
| EASY | A small amount of beamtime, not a full experiment: must be very simple measurements, all instruments, limited number of configurations | All year | All users from member countries | From one to a few weeks |
| LTP | All instruments, for projects over several cycles if it can be demonstrated that they bring extra resources or capabilities that are of benefit to all users | Once a year, autumn round | All users from member countries | 4 to 8 months after deadline |
| No peer review | | | | |
| TEST | Test of sample, equipment, instrument configuration, all instruments | All year | All users from member countries | Usually on same day |
| INDU | Proprietary beamtime | All year | Contact the Industrial Liason Office | ASAP |

USER AND BEAMTIME STATISTICS

FIND US ON:   

NATIONAL AFFILIATION OF ILL USERS IN 2018

The ILL welcomed 1 597 users in 2018, including 442 from France, 233 from Germany and 207 from the UK. Many of our visitors were received more than once (making a total of 2 336 user visits).

Figure 1
National affiliation of ILL users in 2018.

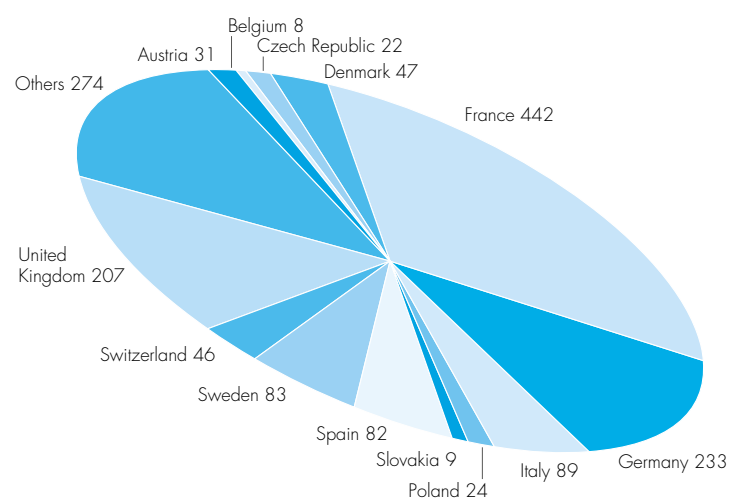
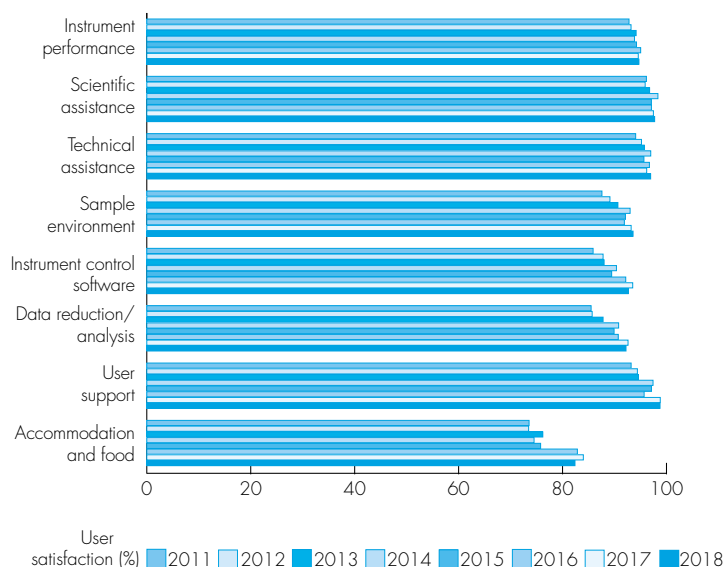


Figure 2
User satisfaction survey results for 2018 compared with those obtained in previous years. The user feedback rate was approximately 60 % in 2018.



During 2018 the reactor operated for three cycles, representing 158 days of neutrons. As the ILL was not able to operate two of its originally planned three cycles in 2017, the November 2017 panel meeting was cancelled and the backlog experiments scheduled for the first two cycles in 2018.

Hence, the allocation of beamtime during the April 2018 panel meetings was restricted to the third cycle of 2018 only.

Overall, the panel meetings examined 537 proposals requesting 3 499 days for scheduling in the third cycle of 2018. Of these, 308 proposals received beamtime, requiring the allocation of 1 697 days of beamtime on the different instruments and corresponding to 338 experiments.

Added to the scheduled backlog experiments, a total of 821 peer-reviewed experiments were scheduled in 2018.

Proposals are divided amongst the various colleges. Figure 3 shows the distribution of accepted proposals amongst the colleges (<https://www.ill.eu/users/colleges/>) and research areas.

Figure 3
April 2018: accepted proposal distribution over colleges.

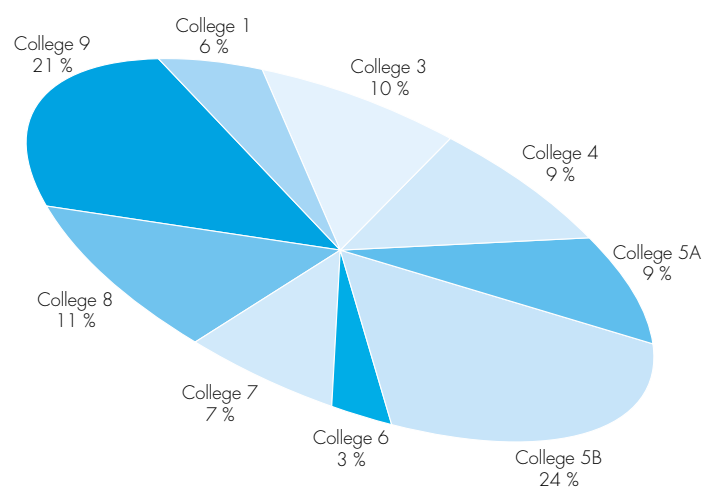


Table 1
Distribution amongst the ILL member countries of beamtime requests and allocation in the April 2018 panel meeting. *Proposals from purely non-member countries do not appear in this table, and therefore the total requests and allocations are different in Table 2.*

| | Request days | Request % | Allocation days | Allocation % | Allocation days | Allocation % |
|------------------------------|-----------------|---------------|-------------------------|---------------|------------------------|---------------|
| Member countries only | | | Before national balance | | After national balance | |
| AT | 79.96 | 2.30 | 49.78 | 2.93 | 51.13 | 3.01 |
| BE | 24.3 | 0.70 | 12.43 | 0.73 | 9.43 | 0.56 |
| CH | 128.51 | 3.69 | 57.71 | 3.39 | 35.14 | 2.07 |
| CZ | 21.91 | 0.63 | 9.29 | 0.55 | 9.43 | 0.56 |
| DE | 837.48 | 24.07 | 395.10 | 23.22 | 394.32 | 23.24 |
| DK | 101.02 | 2.90 | 35.99 | 2.12 | 36.74 | 2.17 |
| ES | 158.62 | 4.56 | 88.55 | 5.20 | 97.45 | 5.74 |
| FR | 844.69 | 24.27 | 447.29 | 26.29 | 448.33 | 26.43 |
| GB | 708.31 | 20.35 | 348.07 | 20.46 | 357.12 | 21.05 |
| IT | 264.21 | 7.59 | 150.05 | 8.82 | 150.09 | 8.85 |
| PL | 95.08 | 2.73 | 39.57 | 2.33 | 39.58 | 2.33 |
| SE | 193.78 | 5.57 | 61.45 | 3.61 | 61.85 | 3.65 |
| SK | 21.94 | 0.63 | 6.22 | 0.37 | 5.87 | 0.35 |
| Total | 3 479.81 | 100.00 | 1 701.50 | 100.00 | 1 696.50 | 100.00 |

In calculating the statistics for beamtime per country shown in Table 1, attribution is based on the location of the proposers, not their individual nationality. For a proposal involving laboratories from more than one member country, the total number of days is divided amongst the collaborating countries and weighted by the number of people from each. Local contacts are not counted as proposers. The beamtime requested by and allocated to scientists from the ILL is allocated to the member countries according to a weighting system based on the fractional membership of the country of the institute concerned. When a proposal involves collaboration with a non-member country, the allocated time is attributed entirely to the collaborating member countries. Proposals in which all proposers are from non-member countries therefore do not appear in this table.

Table 2 gives a summary of instrument performance for 2018. Around 4 250 days were made available to our users in 2018 on ILL and CRG instruments (via either standard request or EASY and DDT routes), representing about 77 % of available beamtime. A total of 297 days were used by ILL scientists to carry out their own scientific research. Approximately 13 % of the total beamtime available on the ILL instruments was allowed for tests, calibrations, scheduling flexibility, recuperation from minor breakdowns and student training. In all, 262 days were lost as a result of various malfunctions, representing less than 5 % of total available beamtime.

Beam days given to science (for users and internal research) in 2018 amounted to 4 548 (82 %) for a total of 821 standard experiments. In addition, 18 DDT, 63 EASY and 79 internal research experiments were performed.

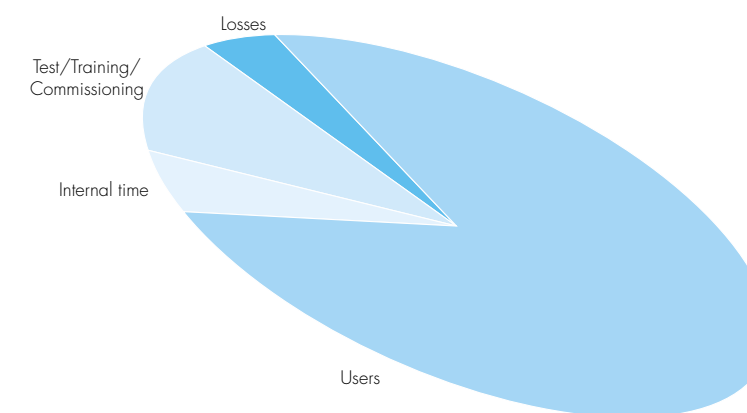


Figure 4
Use of ILL beamtime.

USER AND BEAMTIME STATISTICS

 FIND US ON:   

96-97

Table 2

Beamtime request/allocation (via standard subcommittees and Director Discretion Time (DDT) together) by instrument and instrument performance. CRG instruments are in blue.

* 'days allocated' refers to only those days reviewed by the Subcommittees (i.e. excluding CRG days and DDT)—only one cycle in 2018 (the other two were used to scheduled backlog from 2017)

** 'days available' are the days of reactor operation (the difference between 152 or 151 days relates to the delay in opening the shutters for certain instruments in the last cycle)

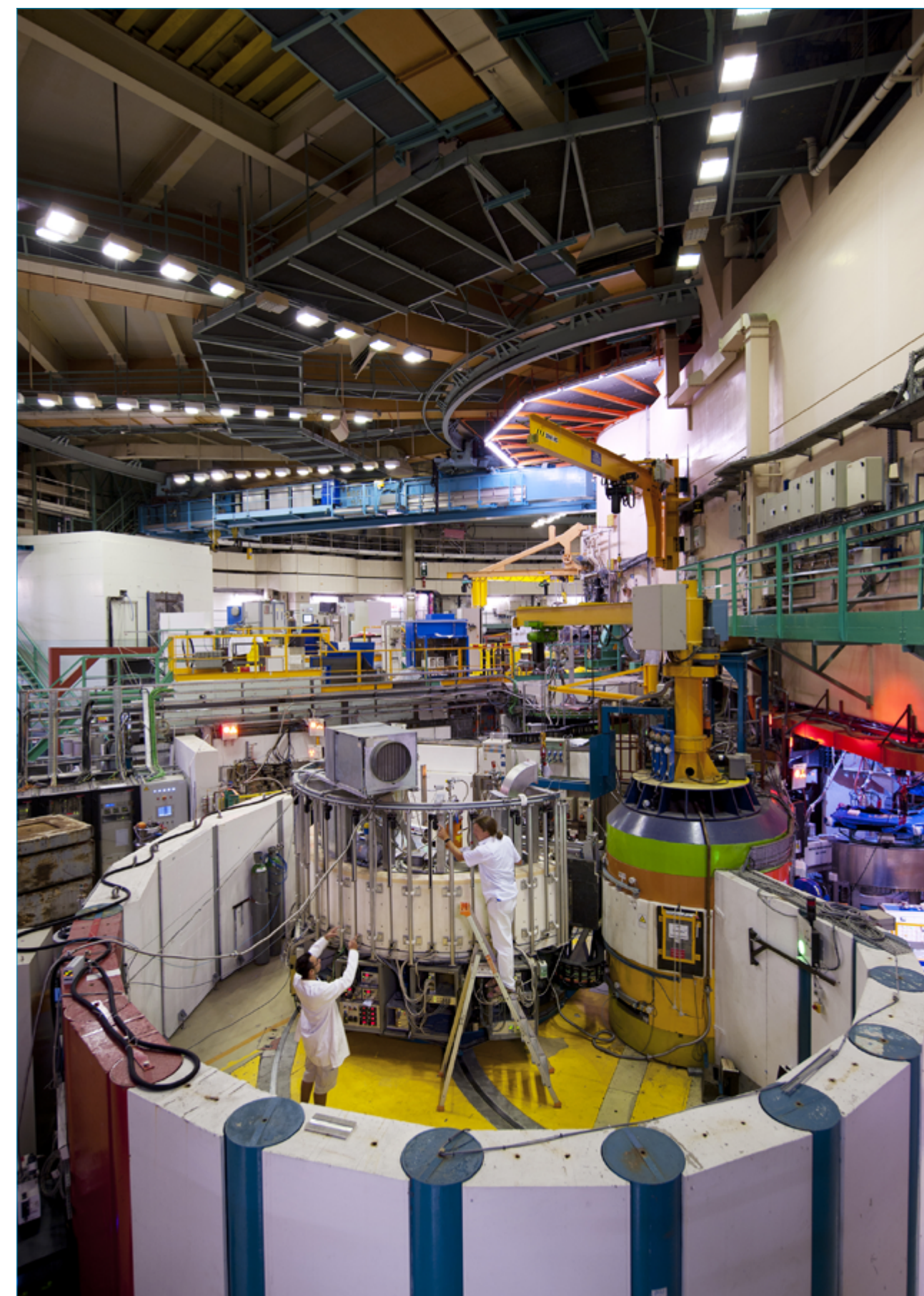
*** 'days used' refers to the total number of days given to users (i.e. including CRG days for CRGs, DDT and EASY)

PF2 consists of different set-ups where several experiments are run simultaneously. The values given are averages for these positions.

D4 and IN1 share the same beam port and cannot be run simultaneously.

IN4 was dismantled in the second part of the year to allow PANTHER to be installed.

| Instrument | Numbers from panels in April 2018 (third cycle in 2018) | | | Numbers from the 3 cycles in 2018 (two of backlog experiments) | | | | | |
|----------------------------------|------------------------------------------------------------|------------------|--------------------------------|-------------------------------------------------------------------|-------------------------|---------------|----------------------------------------|----------------------------|--------------------|
| | Days requested | Days allocated * | Number of accepted experiments | Available days ** | Days used for users *** | Days lost | Days for test/ commissioning /training | Days for internal research | Days for EASY/ DDT |
| D10 | 88 | 56 | 10 | 151 | 143.00 | 0.00 | 4.00 | 2.00 | 2.00 |
| D11 | 123 | 48 | 22 | 152 | 111.00 | 2.25 | 29.50 | 9.00 | 0.25 |
| D16 | 79 | 42 | 9 | 151 | 120.00 | 2.50 | 13.50 | 15.00 | 0.00 |
| D17 | 127 | 45 | 15 | 152 | 122.29 | 2.88 | 13.16 | 11.67 | 2.00 |
| D19 | 118 | 52 | 8 | 151 | 118.67 | 8.33 | 16.00 | 4.00 | 4.00 |
| D1B | 52 | 17 | 8 | 151 | 120.11 | 2.76 | 21.50 | 5.50 | 0.50 |
| D20 | 94 | 50 | 22 | 151 | 123.66 | 6.84 | 6.00 | 11.50 | 3.00 |
| D22 | 113 | 51 | 19 | 151 | 106.00 | 1.50 | 32.50 | 10.00 | 1.00 |
| D23 | 52 | 24 | 5 | 152 | 137.00 | 0.00 | 10.00 | 5.00 | 0.00 |
| D2B | 77 | 44 | 18 | 151 | 119.00 | 3.00 | 15.00 | 10.00 | 4.00 |
| D33 | 87 | 54 | 24 | 152 | 102.00 | 4.25 | 39.75 | 4.00 | 2.00 |
| D3 | 106 | 56 | 8 | 152 | 127.00 | 15.00 | 3.00 | 2.00 | 5.00 |
| D4 | 55 | 16 | 5 | 65 | 50.00 | 2.00 | 7.00 | 0.00 | 6.00 |
| D7 | 96 | 41 | 9 | 151 | 112.50 | 1.50 | 27.00 | 10.00 | 0.00 |
| D9 | 106 | 50 | 7 | 152 | 122.70 | 16.80 | 2.50 | 7.00 | 3.00 |
| FIGARO | 99 | 56 | 20 | 151 | 111.93 | 15.17 | 15.90 | 8.00 | 0.00 |
| FIPPS | 216 | 169 | 9 | 151 | 117.00 | 12.00 | 9.00 | 13.00 | 0.00 |
| IN10 | 100 | 100 | 1 | 100 | 100.00 | 0.00 | 0.00 | 0.00 | 0.00 |
| IN11 | 83 | 43 | 6 | 151 | 101.25 | 4.75 | 31.00 | 14.00 | 0.00 |
| IN12 | 67 | 14 | 2 | 149 | 126.00 | 3.00 | 16.00 | 4.00 | 0.00 |
| IN13 | 53 | 25 | 4 | 152 | 134.00 | 0.00 | 18.00 | 0.00 | 0.00 |
| IN15 | 105 | 21 | 5 | 151 | 95.00 | 2.00 | 45.00 | 7.00 | 2.00 |
| IN16B | 114 | 33 | 9 | 151 | 84.00 | 5.00 | 53.50 | 4.00 | 4.50 |
| IN1 | 54 | 22 | 8 | 87 | 48.00 | 18.45 | 15.55 | 5.00 | 0.00 |
| IN20 | 87 | 49 | 7 | 151 | 112.50 | 11.25 | 20.25 | 7.00 | 0.00 |
| IN22 | 54 | 24 | 4 | 151 | 115.00 | 8.00 | 26.00 | 2.00 | 0.00 |
| IN4 | | | | 151 | 72.00 | 33.00 | 43.00 | 3.00 | 0.00 |
| IN5 | 162 | 47 | 13 | 152 | 92.50 | 2.33 | 44.17 | 11.00 | 2.00 |
| IN6-SHARP | 80 | 22 | 7 | 151 | 129.00 | 6.00 | 10.00 | 6.00 | 0.00 |
| IN8 | 61 | 40 | 7 | 151 | 105.00 | 7.25 | 31.75 | 7.00 | 0.00 |
| LADI | 156 | 58 | 5 | 151 | 132.00 | 4.00 | 12.00 | 3.00 | 0.00 |
| PFIB | 100 | 58 | 4 | 139 | 122.00 | 13.00 | 2.00 | 2.00 | 0.00 |
| PF2 normalised | 101 | 84.5 | 9 | 151 | 99.14 | 1.00 | 23.50 | 27.50 | 0.00 |
| PN1 | 138 | 70 | 6 | 151 | 124.00 | 27.00 | 0.00 | 0.00 | 0.00 |
| S18 | 25 | 25 | 2 | 151 | 139.00 | 5.00 | 0.00 | 7.00 | 0.00 |
| SALSA | 109 | 24 | 7 | 151 | 88.33 | 11.67 | 19.50 | 29.00 | 2.50 |
| SUPERADAM | 64 | 17 | 5 | 151 | 98.00 | 0.00 | 33.00 | 20.00 | 0.00 |
| THALES | 98 | 49 | 9 | 152 | 126.00 | 2.00 | 13.00 | 11.00 | 0.00 |
| Total | 3 499 | 1 696.5 | 338 | 5 532 | 4 206.58 | 261.48 | 722.53 | 297.17 | 43.75 |
| Percentage of the total beamtime | | | | | 76.00% | 4.70% | 13.00% | 5.40% | 0.80% |



INSTRUMENT LIST

INSTRUMENT LIST – JANUARY 2019

| ILL INSTRUMENTS | | |
|-----------------------------|---------------------------------------------------|---------------|
| D2B | powder diffractometer | operational |
| D3 | single crystal diffractometer | operational |
| D4 (50 % with IN1-LAGRANGE) | liquids diffractometer | operational |
| D7 | diffuse-scattering spectrometer | operational |
| D9 | single crystal diffractometer | operational |
| D10 | single crystal diffractometer | operational |
| D11 | small-angle scattering diffractometer | operational |
| D16 | small momentum-transfer diffractometer | operational |
| D17 | reflectometer | operational |
| D19 | single crystal diffractometer | operational |
| D20 | powder diffractometer | operational |
| D22 | small-angle scattering diffractometer | operational |
| D33 | small-angle scattering diffractometer | operational |
| FIGARO | horizontal reflectometer | operational |
| FIPPS | fission product prompt gamma-ray spectrometer | operational |
| IN1-LAGRANGE (50 % with D4) | three-axis spectrometer | operational |
| IN4 | time-of-flight spectrometer | dismantled |
| IN5 | time-of-flight spectrometer | operational |
| IN8 | three-axis spectrometer | operational |
| IN11 | spin-echo spectrometer | operational |
| IN16B | backscattering spectrometer | operational |
| IN20 | three-axis spectrometer | operational |
| PF1 | neutron beam for fundamental physics | operational |
| PF2 | ultra-cold neutron source for fundamental physics | operational |
| PN1 | fission product mass-spectrometer | operational |
| PN3 – GAMS | gamma-ray spectrometer | operational |
| SALSA | strain analyser for engineering application | operational |
| ThALES | three-axis spectrometer | operational |
| WASP | wide-angle spin-echo spectrometer | commissioning |

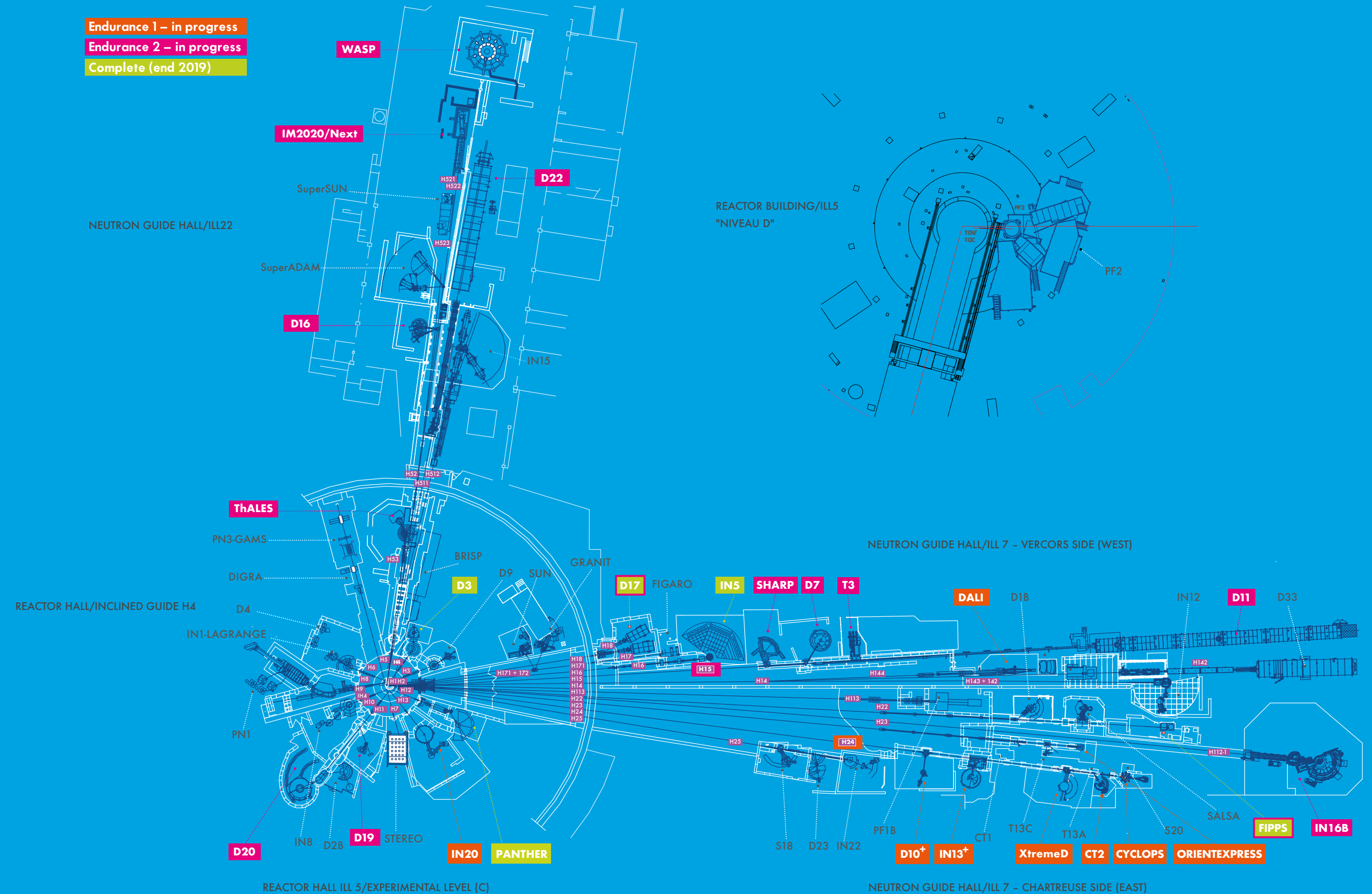
| CRG INSTRUMENTS | | |
|-----------------|-------------------------------|-------------------|
| BRISP | Brillouin spectrometer | CRG-B on hold |
| D1B | powder diffractometer | CRG-A operational |
| D23 | single crystal diffractometer | CRG-B operational |
| GRANIT | gravitation state measurement | CRG operational |
| IN6-SHARP | time-of-flight spectrometer | CRG-A operational |
| IN12 | three-axis spectrometer | CRG-B operational |
| IN13 | backscattering spectrometer | CRG-A operational |
| IN22 | three-axis spectrometer | CRG-B operational |
| SuperADAM | reflectometer | CRG-B operational |
| S18 | interferometer | CRG-B operational |

| JOINTLY FUNDED INSTRUMENTS | | |
|----------------------------|-------------------------------|----------------------------------------------------------------------|
| LADI (50 %) | Laue diffractometer | operated with EMBL |
| IN15 | spin-echo spectrometer | operated with FZ Jülich |
| GRANIT | gravitation state measurement | operated with LPSC (UJF, CNRS) |
| STEREO | search for sterile neutrino | operated with CEA Saclay, LAPP Anecy, LPSC Grenoble, MPIK Heidelberg |

| TEST AND CHARACTERISATION BEAMS | |
|---------------------------------|------------------------------|
| CT1, CT2 | detector test facilities |
| CYCLOPS | Laue diffractometer |
| TOMOGRAPHY | neutrography |
| OrientExpress | Laue diffractometer |
| T3 | neutron optics test facility |
| T13A, C | monochromator test facility |
| T17 | cold neutron test facility |

FIND US ON:   

Endurance 1 – in progress
Endurance 2 – in progress
Complete (end 2019)



Details of the instruments can be found at <http://www.ill.eu/users/instruments/>.

The instrument facilities at the ILL are listed in the table on the left, and shown in the plan on p. 99. Besides the 28 ILL instruments, there are 10 Collaborative Research Group (CRG) instruments.

CRGs can build and manage instruments at the ILL to carry out their own research programmes. The instrument is made available for the ILL's scientific user programme at a level of 50 % (CRG-A) and 30 % (CRG-B). CRG-C external groups have exclusive use of the beam. Details about the framework of operation of CRGs can be found at <https://www.ill.eu/users/instruments/crgs/>.

All current CRGs are either A- or B-type, the only exception being GRANIT which is a CRG-C instrument and therefore not available as a 'user' instrument. IN15 has special status because it is a joint venture of the ILL with FZ Jülich. The instrument STEREO is jointly funded by the ILL and CEA Saclay, LAPP Annecy, LPSC Grenoble and MPIK Heidelberg.

INSTRUMENT LAYOUT

REACTOR OPERATION

102 REACTOR OPERATION IN 2018

THREE CYCLES AND
152
DAYS OF
OPERATION
IN 2018



A THERMAL
POWER OF
58.3 MW
A SINGLE,
HIGHLY ENRICHED
URANIUM
10 KG
FUEL ELEMENT



KEEP UP-TO-DATE:

-  facebook.com/ILLGrenoble
-  twitter.com/ILLGrenoble
-  linkedin.com/company/institut-laue-langevin

THE ILL'S High-Flux Reactor (HFR) produces the most intense neutron flux in the world: 1.5×10^{15} neutrons per second per cm^2 , with a thermal power of 58.3 MW. It normally operates four reactor cycles per year. At the end of each a shutdown period is instigated during which the fuel element is changed and a number of checks are carried out. Occasional longer shutdowns are scheduled to allow for equipment maintenance.

At maximum power, the reactor's fuel element can provide 46 days of operation per cycle. For almost the last ten years, our 'contract' with our scientific users has been to provide 200 days of operation per year (excluding maintenance and upgrade work). At nominal power this allows for 4.5 cycles per year. For obvious, practical reasons, this number of annual cycles is not ideal; for the Reactor Division it involves the same amount of work as having five operating cycles, since the tests and fuel-loading operations to be carried out are the same before every start-up irrespective of the length of cycle. As the performance of the instruments has generally been increased by a factor of 20 thanks to the Millennium Programme, we have recently decided to provide the 200 days of operation over four 50-day cycles, at slightly lower power.

Following the nuclear disaster at Fukushima in 2011, the French nuclear safety authority (ASN) ordered additional safety assessments to be carried out on all French basic nuclear installations (INBs), including the ILL. The ASN has also asked the ILL to reorganise its working methods, in order to make them better and more secure, under a newly created Integrated Management System (IMS).

The post-Fukushima programme has now ended. The safety of the reactor is now guaranteed, even in the event of an extreme earthquake-and-flood combination following a rupture of the dams upstream, well beyond previous dimensioning standards. The IMS implementation, on the other hand, is still running.



Reactor operation

Three reactor cycles were completed in 2018, using three fuel elements and providing a total of 152 days of scientific activity.

| Cycle n° | Start of cycle | End of cycle | Number of days of operation | Number of days scheduled | Power in MW | Number of unscheduled shutdowns |
|--------------|----------------|--------------|-----------------------------|--------------------------|---------------|---------------------------------|
| 182 | 28.02.18 | 26.04.18 | 55.5 | 56 | 40, then 58.3 | 1 |
| 183 | 22.05.18 | 05.07.18 | 44.3 | 51 | 52.6 | 0 |
| 184 | 03.09.18 | 28.10.18 | 52.5 | 52 | 51.6 then 35 | 1 |
| Total | | | 152.3 | 159 | 49.2 | 2 |

The end of the second cycle had to be brought forward due to a defect on one of the cladding failure detection systems; the other systems that make up the protection circuit remained operational. In addition, two unscheduled reactor shutdowns occurred:

1. The first was due to disruptions to the electricity supply.
2. The second was an automatic shutdown. A defect on the pressure-measuring channel of the horizontal cold neutron source led to an emergency shutdown. The reactor was restarted using the second measuring channel.

The winter shutdown was used for a host of important maintenance and other operations:

- Replacement of beam tubes H3 and H8
- Removal of beam tube H6/H7 and its replacement with two sealing plugs
- Work on the emergency core reflow (CRU) and water makeup (CES) systems
- Work on the groundwater circuit (CEN)
- Replacement of beam tube V7
- Replacement of the start-up source and installation of start-up source n° 5
- Commissioning of the instrumentation and control units in the reactor control room and the emergency control room (PCS3) for the emergency cooling circuits (CRU, CES, CEN)
- Wiring of the control unit, located in the PCS3, of the system for manually 'dropping' fuel elements onto the floor of the transfer canal

- Leak testing of the reactor building (an initial test was carried out in March 2018 prior to the installation of the truck entrance airlock, and a second test was performed in November 2018 with the new truck entrance airlock in place)
- Replacement of the pyrotechnic valve VPFN 3AM (on the light water pool side)
- Qualification of handling cask WF2: testing of the fuel element emergency drop system
- Major maintenance work on the second main diesel generator
- Implementation of new hafnium safety rods
- Replacement of beam tubes H4 and H10.

The **post-Fukushima programme** has been completed. The safety of the reactor is now guaranteed even in the event of an extreme earthquake-plus-flood scenario following a breach of the dams upstream of the ILL. Our installations now comply with requirements well above the previous design basis.

At the end of 2018 we submitted the last set of documents for our ten-yearly safety review, which will determine whether any further work is required to ensure that the ILL reactor installations comply with the latest safety standards. Requests for additional work are likely to be limited given the extent of the reinforcement work already carried out under the Reactor Refit programme (2002 to 2007) and the post-Fukushima programme (2012 to 2017). The safety authorities will begin their examination of the safety review report at the very beginning of 2019.

THE KEY REACTOR COMPONENTS (KRC) PROGRAMME

The aim of the KRC programme is to ensure the upgrade and maintenance of the reactor's most important components, thus guaranteeing the future reliability of reactor operations. The main components concerned are the cold neutron sources, the fire protection equipment and the physical protection equipment.

RADIOACTIVE WASTE AND EFFLUENTS

The ILL's activities in 2018 generated waste and effluents respecting the regulatory limits applicable to our installation, as follows:

| Evacuation of radioactive waste | Quantity |
|-------------------------------------------------------------------------|----------|
| Decay bin (60 L)* | 0 |
| 5 m ³ pre-concreted crate (low and intermediate level waste) | 0 |
| 5 m ³ crate (low and intermediate level waste) | 3 |
| HDPE 200 L drums of 'incinerable' waste | 144 |
| HDPE 120 L drums of 'incinerable' waste | 0 |
| HDPE 120 L drums (laboratory waste) | 8 |
| 30 L cylinders (liquid) | 2 |

*The decay bins contain very active waste. They will be transferred to ANDRA's new storage centre CIGEO as soon as it becomes available, after an interim period in special storage.

| Gaseous effluents | Released in 2018 (TBq) |
|-------------------|------------------------|
| Tritium | 8.8 |
| Rare gas | 0.90 |
| Carbon 14 | 0.12 |
| Iodine | 0.0000011 |
| Aerosols | 0.00000033 |

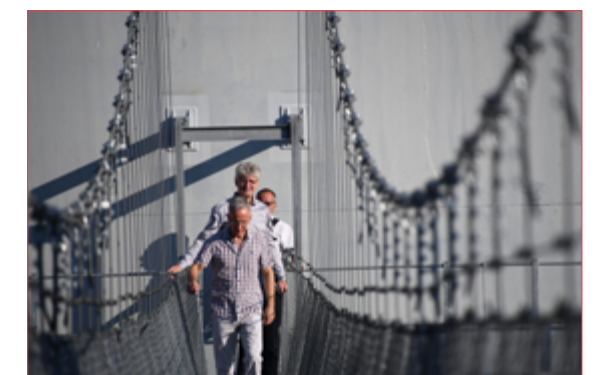
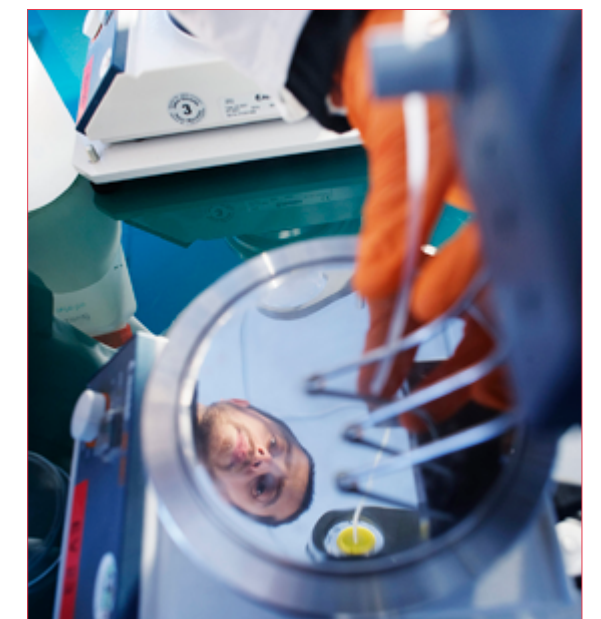
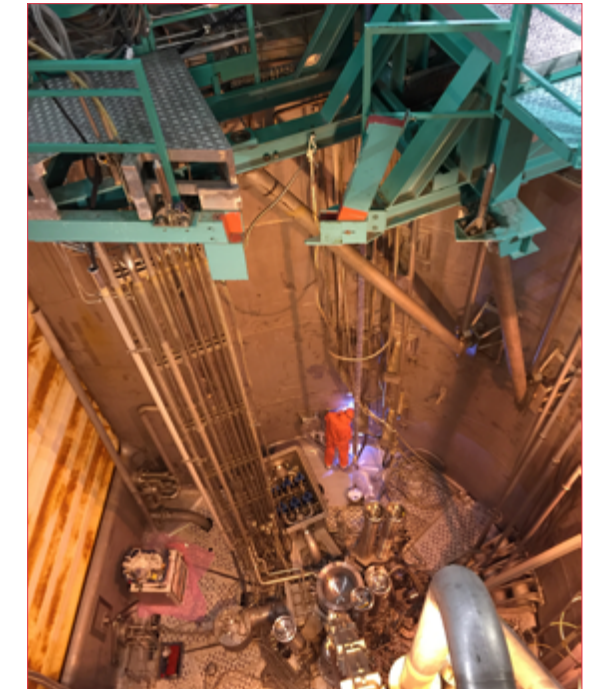
| Liquid effluents | Released in 2018 (TBq) |
|---------------------------|------------------------|
| Tritium | 0.14 |
| Carbon 14 | 0.00021 |
| Iodine | 0.00000054 |
| Other activation products | 0.000024 |

From top:

Work on the emergency core reflow (CRU).

The ILL operates a laboratory for monitoring radioactivity in the environment.

Safety exercise on 20 September: the ILL directors on the walkway connecting the reactor control room with the emergency PSC3 control room.



MORE THAN SIMPLY NEUTRONS

106 SCIENTIFIC SUPPORT LABORATORIES

108 TRAINING AND OUTREACH

110 EUROPEAN PROGRAMMES

ACCESS

TO **13** LABORATORIES
HOSTING **25** MAJOR PIECES
OF EQUIPMENT VIA PSCM



40

PHD STUDENTS

76

TRAINEES



20 PARTICIPANTS
@ILL-ESRF SUMMER SCHOOL

**HERCULES: 82 PARTICIPANTS OF
29 DIFFERENT NATIONALITIES
WORKING IN 21 DIFFERENT COUNTRIES**



KEEP UP-TO-DATE:

- facebook.com/ILLGrenoble
- twitter.com/ILLGrenoble
- linkedin.com/company/institut-laue-langevin

IN ORDER to maintain their ranking on the international scene, European research institutes must optimise their resources and develop synergies at every level.

The ILL is firmly committed not only to building high-performance instruments, but also to offering the best scientific environment to the user community. We have established successful collaborations with neighbouring institutes over the years, and launched many successful scientific and support partnerships.

The history of the ILL is that of European collaboration, and the Institute is today involved in no fewer than eight different projects funded by the European Commission. The benefits are not merely financial, for the ILL also benefits from the networks and resources that improve its integration with other facilities and the user community. The ILL is currently the co-ordinator of two of these projects: the SINE2020 and the FILL2030.

Local collaboration is equally important. The ILL and the ESRF have transformed our joint site into a research campus—the European Photon and Neutron science campus, or EPN Campus for short—with a truly international reputation. The EPN campus provides a unique international science hub for Grenoble, hosting three major European institutes—the EMBL, ESRF and ILL—along with the IBS (<http://www.epn-campus.eu/>).

Last but not least, the ILL is committed to training and outreach, providing this in many different forms. The ILL Graduate School and PhD programme are now training future generations of neutron users. We also run neutron schools and other events for MSc and PhD students, and our open days and regular participation in the local science festival are helping to attract young talent to the disciplines of science and enhance the general public's understanding of the science we perform.



© R. Cubitt

PARTNERSHIP FOR SOFT CONDENSED MATTER

The Partnership for Soft Condensed Matter (PSCM) is a joint initiative established by the ILL and the ESRF in Grenoble, France. The main PSCM mission is to provide enhanced support services to ILL and ESRF users tackling contemporary challenges in soft matter research including nanomaterials, environmental and energy sciences, biotechnology and related fields. Currently the PSCM offers access to 13 laboratories hosting 25 major pieces of equipment as well as sample preparation facilities.

In addition to normal user operations, the PSCM is continually searching for new Collaborative Partners with whom to strengthen the soft matter research community by establishing long-term collaborations devoted to the development of specialised sample environments and instruments. In 2018, the call for Expression of Interests for new Collaborative Partners attracted high-quality proposals from the soft matter user community of the ILL and ESRF. The evaluation of the proposals is ongoing.

The PSCM is located on the 2nd floor of the Science Building, along with the Soft Matter Science and Support group. Users wishing to use the PSCM laboratories and equipment in conjunction with neutron measurements should indicate this when submitting their request for beamtime.

Further details can be found at <http://www.epn-campus.eu/pscm/>.

PARTNERSHIP FOR STRUCTURAL BIOLOGY

The Partnership for Structural Biology (PSB) contains a powerful set of technology platforms, provided and operated by our various partner institutes (ILL, ESRF, EMBL, IBS). These platforms include advanced capabilities that strongly complement the neutron-scattering facilities available to ILL users: synchrotron X-rays, electron microscopy, high-field nuclear magnetic resonance (NMR), high-throughput methods (e.g. soluble expression and crystallisation), and a range of biophysical techniques such as isothermal calorimetry (ITC) and surface plasmon resonance (SPR). The PSB also includes the Deuteration Laboratory (see below), operated as a user platform within the ILL's Life Sciences Group, and the joint SANS/SAXS platform. There is strong connectivity and collaboration between the ILL and ESRF life sciences/structural biology and industry groups.

The ILL, through its partnership with Keele University (UK), is now participating fully in the cryo-electron microscopy initiative being spearheaded by the ESRF. As of June 2019, a Keele University Faculty position, based in the Life Sciences Group in Grenoble, will participate in the operations team of the Titan Krios microscope, with one of the main missions being to stimulate natural synergies with neutron scattering analyses of macromolecular systems.

The aim of the PSB is to enhance the interdisciplinary capabilities of each of the facilities located on the site and to widen the scientific scope of the external user communities. The Carl-Ivar Brändén building (CIBB) acts as home to the PSB and its partner organisations.

Check the website for more information: <http://www.psb-grenoble.eu/>.

DEUTERATION LABORATORY D-LAB

The Deuteration Laboratory (D-Lab) is located and operated within the ILL's Life Sciences Group. Its user programme uses innovative *in vivo* recombinant expression approaches to provide tailor-made deuterated analogues of proteins, nucleic acids and lipids for the study of structure (crystallography, SANS, fibre diffraction, reflection) and dynamics (EINS) using neutron scattering [1]. The platform is therefore of central importance to all the ILL instrument groups engaged in biological activities.

The Life Sciences Group is involved in a wide variety of externally-funded programmes, exploiting the capabilities of the PSB as well as promoting interdisciplinary structural biology. It also interacts strongly with industry. Each year the Group takes a small number of undergraduate placement students for training in many of these techniques. It is also involved in the operation of the cryo-EM capabilities being set up with the installation of Titan Krios at the ESRF, in partnership with the ESRF, IBS and EMBL.

Access to the D-Lab platform is gained through a rapid peer-review proposal system (for more information: <http://www.ill.eu/instruments-support/instruments-groups/groups/lsg/user-platforms>). It is available to all ILL member countries regardless of where the neutron scattering study will be carried out. The facility is also available to users from non-member state countries, although these users are expected to cover the costs involved.

[1] M. Haertlein, M. Moulin, J.M. Devos, V. Laux and O. Dunne, *Methods Enzymol.* 566 (2016) 113–57

CHEMISTRY LABORATORIES

The Soft Matter Science and Support Group (SMSS) manages the ILL chemistry laboratories together with the PSCM laboratories. The main goal is to give ILL users the ability to prepare and characterise their samples during

their neutron experiments, but also to support the in-house research conducted by instrument scientists and PhD students.

The main facilities are located in the Science Building. In addition, three sample preparation labs can be found in the guide halls ILL7 and ILL22.

The laboratories are stocked with the basic equipment, glassware, consumables and chemicals necessary to prepare samples for a variety of different neutron experiments. More specific items of equipment, such as high-temperature furnaces, a glovebox and an enclosure for handling nano-powders, are also available. The PSCM laboratories provide various methods of sample characterisation, such as UV-Vis, FTIR and light scattering.

Further information on the Chemistry Laboratories can be found at <https://www.ill.eu/fr/instruments-support/labs-facilities/chemistry-laboratories/>.

MATERIALS SCIENCE SUPPORT LABORATORY

The joint ILL-ESRF Materials Science Support Laboratory (MSSL) provides a range of support to our users, from advice on experiment proposals to assistance with sample preparation and performing the experiment. We provide equipment for tensile testing, hardness testing and microscopy as well as the fabrication of specialised sample holders. The Laboratory also works with users to optimise their experimental methodology before the start of an experiment. This can involve standardised specimen mounting, digitisation of samples or the definition of measurement macros. It is recommended that users contact us well in advance and arrive at the ILL a day or two prior to the start of an experiment to enable these off-line preparations to be performed.



TRAINING AND OUTREACH

FIND US ON:   



The ILL PhD students during the annual clip session on 7 June.

STUDENT TRAINING

The ILL Graduate School has grown in strength over recent years, through the development of the ILL PhD programme. The Graduate School provides training and financing for the equivalent of 40 full-time, three-year PhD projects from various European countries, as well as welcoming a number of PhD students with external funding. We received a total of 60 applications in response to our last call for PhD proposals; of these, 11 full-time-equivalent projects have been selected, for which PhD students will subsequently be recruited in 2019.

Since the students work in different disciplines, their annual clip session on 7 June gave them the opportunity to exchange ideas and get to know each other better. A series of weekly seminars is also organised throughout the year. The speakers are the PhD students themselves, and the topics alternate annually between presentations on their own research and those on neutron scattering topics.

For the fifth year, the ILL and the ESRF organised an International Summer School for undergraduate students, which ran during September 2018. This programme invites undergraduate students from all member countries to spend a month at the Institute. During their stay, a series of lectures and seminars is organised to introduce them to the fundamentals of X-rays and neutrons and their applications in today's science. Each participant works on an individual scientific project, supervised by the scientists and PhD students of the ILL. This year the ILL hosted ten such projects, that is, for half of the 20 participants on the programme. The participants themselves were selected from more than a hundred applications from universities in Germany, Italy, Great Britain, the Netherlands, Slovenia, Norway, Israel, Russia, Spain, Poland and Switzerland.

The ILL also welcomed a total 76 trainees in 2018 (10 from the ILL-ESRF Summer School, 2 from the STFC), of 18 different nationalities (including 9 German, 34 French, 11 British and 10 from other ILL member countries).

HERCULES SCHOOL

This one-month course, held every year since 1991, provides training for students and young scientists in the field of neutron and synchrotron radiation for condensed matter studies. It includes lectures, hands-on practicals and tutorials in small groups (~35%), visits of partner facilities and a poster session.

The 2018 HERCULES took place from 25 February to 30 March. It welcomed 82 participants of 29 different nationalities working in 21 different countries, most of them from Europe but some from Taiwan, India, New Zealand, Russia and the USA. The students were selected from more than 170 applicants. A special 'Practicals and Tutorials' session was included in this year's programme, hosted in partner institutions: one full day at the ILL and two at the ESRF, two days at the CNRS, CEA and/or IBS, and one week outside Grenoble at SOLEIL and ILB (Paris-Saclay, France), Elettra and FERMI (Trieste, Italy), European XFEL and DESY (Hamburg, Germany) or PSI (Villigen, Switzerland).

More information is available at <http://hercules-school.eu/>.



Participants of the HERCULES 2018 session.

DARK MATTER DAY

This event, instigated on the initiative of the Laboratoire de Physique Subatomique et de Cosmologie (LPSC) and co-organised by the ILL, was held on October 31, 2018, at the Museum of Grenoble. Dark matter is the explanation often given for a number of mysterious phenomena—including the fact that galaxies rotate instead of flying apart—and is thought to account for approximately 85% of the matter in the universe and about 25% of its total energy density. Researchers presume that dark matter exerts a strong influence on the structure and evolution of the universe.

The ILL has been studying dark matter, one of the biggest enigmas in science, for quite some time. Its neighbour on the Presqu'île, the LPSC, is a leader in the field. As the two institutes often collaborate, they decided to organise 'Dark Matter Day', an event designed to help families learn more about dark matter and how it is being studied. Attendees of all ages got to ask researchers all sorts of questions, and were then led on a virtual reality-driven Cosmic Tour.

SCIENCE FESTIVAL

The ILL was present at Grenoble's version of France's national Science Festival on Saturday 13 October, sharing a stand with the three other EPN Campus institutes. This is our main occasion, every year, to meet the public. We were happy to meet around 1 600 enthusiastic visitors that day. This year, there was a special focus on two recent studies carried out on the SALSA strain machine: one about new welding techniques in the car industry, and another on a mediaeval sword study.



Unravelling the secrets of dark matter during 'Dark Matter Day'.



Explaining the magic of diffraction (©: C.Argoud).

European collaborations

EUROPEAN PROJECTS

SINE2020—Science and Innovation with Neutrons in Europe in 2020—was launched in October 2015. It is a four-year, 12 M€, infrastructure development project under the Horizon2020 Framework Programme, bringing together 18 facilities and academic partners. Its main objective is twofold: prepare the European community for the first neutrons at ESS in 2020, and explore the potential for innovation of neutron facilities and their scientific partners.

SINE2020 is largely user-oriented. Its Joint Research Activities (JRAs) focus on key techniques for present and future neutron experiments. This covers sample preparation techniques, more sophisticated sample environment facilities and software development. For example, the project is actively involved in the Mantid data reduction project (<http://www.mantidproject.org>), a framework for high-performance computing and the visualisation of materials science data across specialised European facilities.

Given the promising but under-exploited potential of research collaboration with industry, SINE2020 is engaged in strengthening direct links with industrial users, demonstrating the potential of neutron techniques and the value of access to the network's neutron facilities. Thanks to SINE2020, industrial users can now easily perform feasibility studies in eight different European neutron centres, in areas such as failure analysis or materials and component development. SINE2020 also has a special focus on the education of users new to neutrons. To this end, the virtual e-learning platform has been developed further and support is being provided for introductory and specialised neutron schools all over Europe. The opportunities now encompass a wider range of audiences, applications and levels of learning, and as a consequence demand is rising.

SINE2020 illustrates the ever-growing commitment of the European neutron community to exploiting the potential of neutron science. It is expanding the capacity of the neutron user community to provide tailor-made solutions, thus boosting innovation and addressing the challenges society is facing. More information is available at: <http://sine2020.eu>.

Unlike most of the other projects funded by the European Commission, **FILL2030** is a mono-beneficiary project entirely dedicated to ensuring the long-term sustainability of the ILL business model. FILL2030 is part of the EU's Horizon 2020 research and innovation programme and has been granted 3.98 M€ to achieve its mission. This budget will finance the development of new service packages for academia and industry, innovative improvements to the ILL's funding model, tools to identify emerging user groups and show cases illustrating the socio-economic impact of ILL research.

FILL2030's overall objective is to achieve an increase of 5 M€ in the ILL's annual budget (~5 % of its current budget). Initial efforts will concentrate on securing continuous income from the existing Associate and Scientific Member countries. Relations are being strengthened in this respect, focusing on the needs and expectations of each partner country. The ILL is now actively communicating on the impact of the neutrons it produces and the return on investment received by its funders, country by country.

Simultaneously, FILL2030's outreach activities (tours of the installations, roadshows, workshops and media communications) will extend the pool of potential new partners, in Europe and beyond.

The ILL's strategy of engaging with new users and attracting sources of additional funding is based on obtaining a much clearer picture of the European neutron scattering landscape. The aim is to identify new international partners, attract new scientific communities and ensure that users are fully exploiting the European potential.

FILL2030 is therefore developing a set of bibliometric tools capable of analysing the activity of European and other neutron scattering communities. This will help unravel the existing complex, transnational networks of collaboration and identify potential areas of growth. By arranging relationships with new member states, FILL2030 will almost certainly be changing the framework conditions. Existing paradigms will be adapted and extended, with the introduction of new mechanisms for access and funding corresponding more closely to the new communities' needs. Last but not least, as part of FILL2030's 'Transnational Access' scheme, beamtime is granted to users from new communities, either in existing Associate and member states or in non-member countries. Priority will be given to new users from non-member countries. For more information, go to: <http://www.fill2030.eu/>.

The project **ATTRACT** is a pioneering initiative bringing together Europe's fundamental research and industrial communities to lead the next generation of detection and imaging technologies.

ATTRACT is currently selecting breakthrough technology concepts across the above-mentioned domain. In total 17 M€ will be awarded as seed funding for 170 disruptive projects.

Discover the project at: <https://attract-eu.com/>.

The project **PaNOSC**—Photon and Neutron Open Science Cloud—is one of five cluster projects funded under the European Horizon2020 programme. The project, which will run until December 2022, brings together six strategic European research infrastructures (the ESRF, CERIC-ERIC, ELI-DL, ESS, XFEL and ILL) and the e-infrastructures EGI and GEANT. Together, they will contribute to the construction and development of the EOSC, an ecosystem allowing universal and cross-disciplinary open access to data through a single access point for researchers in all scientific fields.

Large-scale research infrastructures produce a huge amount of scientific data on a daily basis. For their storage and future (re)use, data need to be managed according to FAIR principles, *i.e.* be Findable, Accessible, Interoperable and Re-usable. Via PaNOSC, the partner facilities will collaborate to develop common policies, strategies and solutions in the area of FAIR data policy, data management and data services. More information is available at: <https://panosc-eu.github.io/>.

THE LEAGUE OF ADVANCED EUROPEAN NEUTRON SOURCES (LENS)

LENS is a new strategic consortium of European neutron sources that hopes to guide and advocate for the European neutron user community by highlighting neutron science as fundamental to addressing society's grand challenges.

LENS brings together the transnational European neutron source facilities, the group's aim, according to its charter, being to 'facilitate any form of discussion and decision-making process that has the potential to strengthen European neutron science via enhanced collaboration among the facilities'.

Prospective partners in the consortium include nearly a dozen facilities in the Czech Republic, France, Germany, Hungary, Norway, Sweden, Switzerland and the United Kingdom.

Find out about this initiative at www.lens-initiative.org.

NB: the www.lens-initiative.org website is not yet operating but will be soon!



Maria Dolores Ruiz Martin, Andrea Lassenberger, Nebil Ayape Katcho, Felix Kandzia and Andrea Tummino are the 5 post-docs recruited within the framework of FILL2030. © Monfront/ILL.



On 15 January 2019, the PaNOSC meeting took place on the EPN campus. © Chantal Argoud/ESRF.



WORKSHOPS AND EVENTS

113 CHRONICLE

114 SCIENTIFIC EVENTS

 **25** **44**
SCIENTIFIC EVENTS GENERAL
 (WORKSHOPS, SCHOOLS AND SEMINARS
 AND CONFERENCES) AND **7**
 COLLOQUIA

OVER **500** PARTICIPANTS
 TO THE FIRST JOINT ILL AND
 ESS EUROPEAN USER MEETING



KEEP UP-TO-DATE:

-  [facebook.com/ILLGrenoble](https://www.facebook.com/ILLGrenoble)
-  twitter.com/ILLGrenoble
-  [linkedin.com/company/institut-laue-langevin](https://www.linkedin.com/company/institut-laue-langevin)

ILL Chronicle 2018

30 JANUARY

Visit of Prof. Eng. Krzysztof Kurek – Director of the National Centre for Nuclear Research, Warsaw

13 MARCH

Visit of German consul, Mr Maldacker, accompanied by the general consuls of Spain, Portugal, Italy, Switzerland, Poland and Romania.

27 MARCH

Visit of a delegation from the Russian Federation led by Vladislav Panchenko (Full Member of the Russian Academy of Sciences) and Mikhail Kovalchuk (President of the NRC-KI)

10-13 APRIL

Meetings of the ILL's Scientific Council and its Subcommittees

18 APRIL

Visit by Dr Volkmar Dietz – BMBF – Ministry of research and infrastructure

17 MAY

Meeting of the Subcommittee on Administrative Questions (SAQ)

18 MAY

Visit by Mona Nemer – Chief Science Advisor for Canada

28-29 JUNE

Meeting of the Steering Committee

4 SEPTEMBER

Visit by Harriet Kung – US Department of Energy (DOE)

16-17 OCTOBER

Meeting of the Subcommittee on Administrative Questions (SAQ)

7 NOVEMBER

Visit by Fernando Carderera Soler – Ambassador of Spain in France

27 NOVEMBER

Visit by Laurence Piketty – General Administrator of CEA

13-16 NOVEMBER

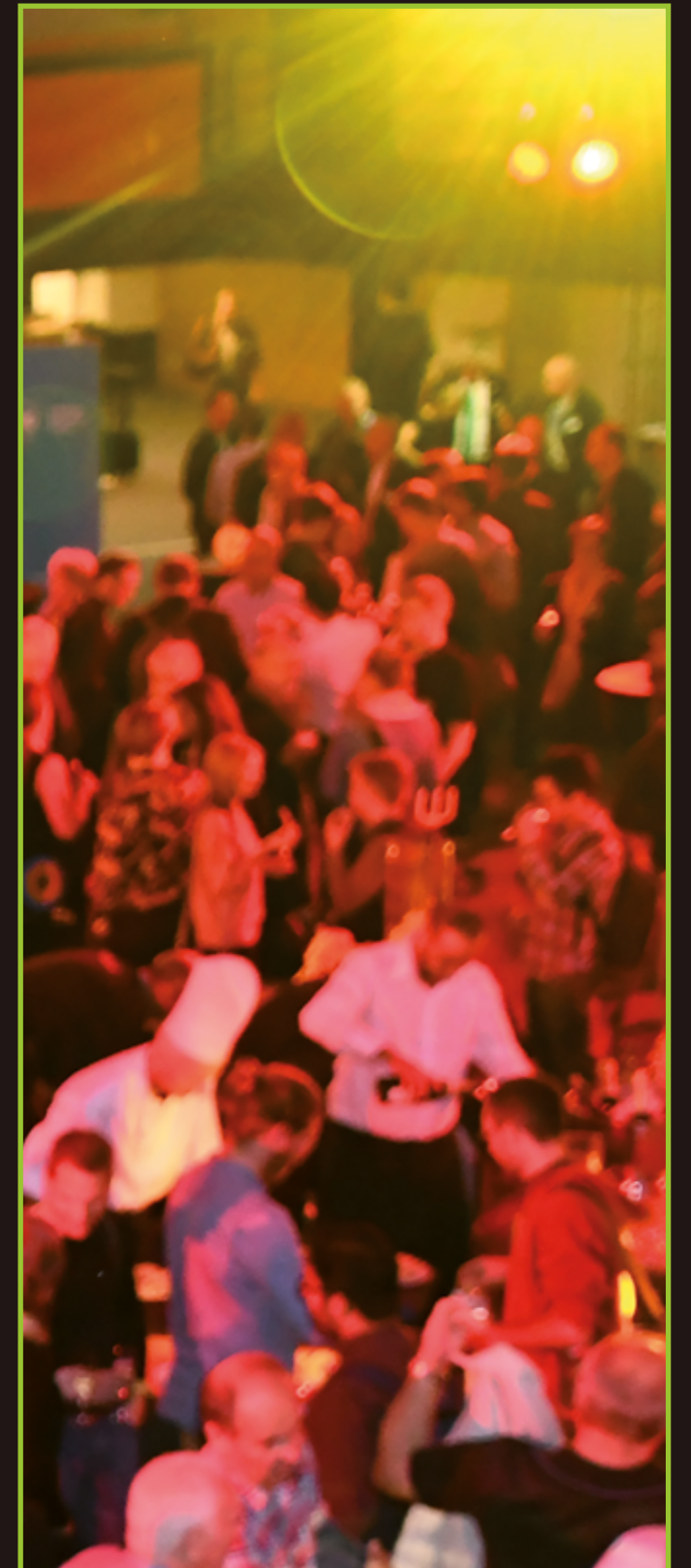
Meetings of the ILL's Scientific Council and its Subcommittees

28-30 NOVEMBER

Meeting of the Steering Committee with the celebration of the 31st anniversary of Spanish scientific membership at the ILL

14 DECEMBER

Visit by Antoine Petit – PDG of CNRS



Scientific events

In 2018, the ILL organised (or co-organised) 25 scientific events (workshops, conferences and schools). A total of 44 general seminars were organised at the ILL in 2018, in addition to 7 colloquia.

30 JANUARY

Xtreme D-Science at extreme conditions done with neutrons workshop, ILL

9 APRIL

AM 2018 – Additive manufacturing and characterisation at large installations workshop, ILL

12 MAY

EMBO practical course, Grenoble

14 MAY

JDN2018: French Neutron Scattering Association Meeting, Roquebrunes sur Argens

24 SEPTEMBER

MDANSE 2018 – Simulation of Inelastic Neutron Scattering using McStas and material dynamics models, Tenerife

24 MAY

PPNS 2018 – International Workshop on Particle Physics at Neutron Sources, Grenoble

26 MAY

Neutrons and biology day, ILL

28-29 JUNE

SLON 2018: Nanodiamond reflectors for slow neutrons workshop

19 JUNE

Bombannes 2018 – School on scattering methods for soft condensed matter, Bombannes

26-26 JUNE

NDS2018 – Neutron delivery systems workshop, ILL

15 JULY

GENS/WINS 2018 – Quasi elastic and inelastic neutron scattering workshop, Hong Kong

3-6 JULY

PNCFI 2018 – Polarised Neutrons for Condensed-Matter Investigations, Abingdon

24 JULY

International school on fundamental forces governing softmatter systems



21 AUGUST

Workshop on neutron macromolecular crystallography at the European Crystallographic Meeting 2018, Oviedo

27 AUGUST

JMC 2018 – Journées de la Matière Condensée, Grenoble

3 SEPTEMBER

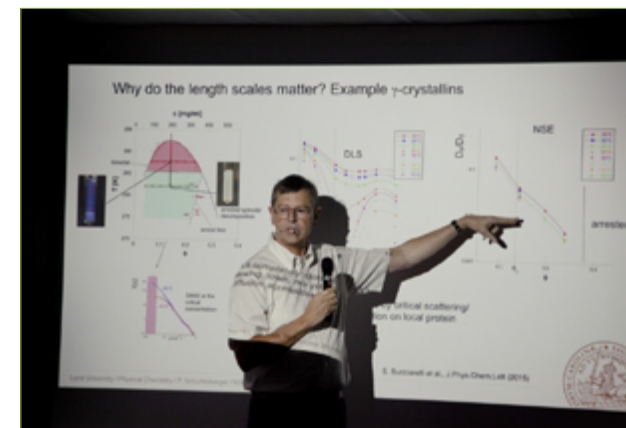
POLYSOLVAT 12 – 12th International IUPAC Conference on Polymer-Solvent Complexes and Intercalates, ILL

14 SEPTEMBER

SISN – Italian Neutron Scattering Association school, ILL

10-12 OCTOBER

ILL and ESS European User Meeting & its satellite workshops (Workshop Interfaces, Molecular Spectroscopy, Magnetism Matters, Neutron Spin-Echo 2018, Energy and Diffraction), Grenoble



The joint ILL and ESS user meeting – held last 10 to 12 October in Grenoble – was a fantastic display of scientific fireworks. Of the 500 participants, about 160 scientists were able to speak, either in the plenary sessions or at satellite meetings, giving presentations on the status of their research.

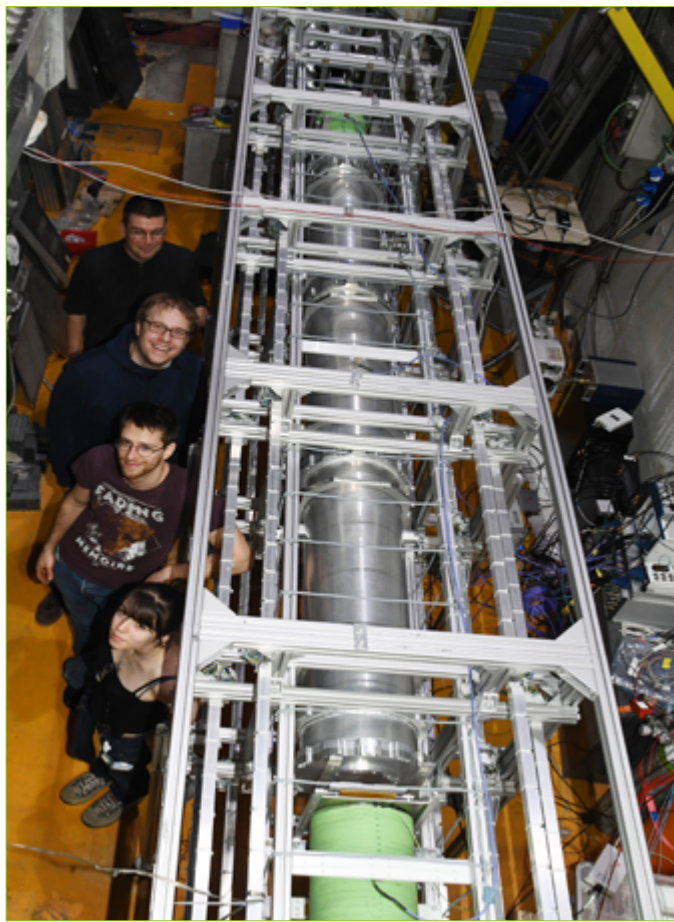
HAPPY USERS @ILL

FIND US ON:   

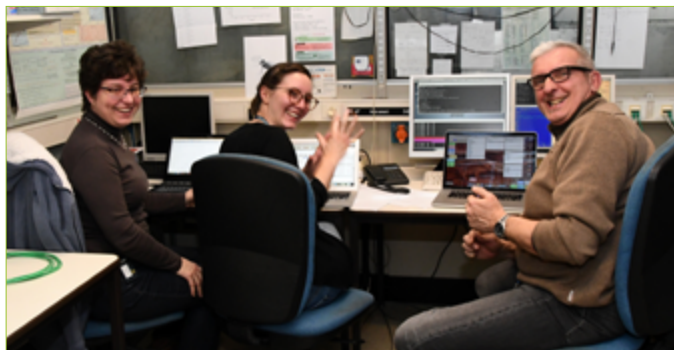
116-117



1.



2.



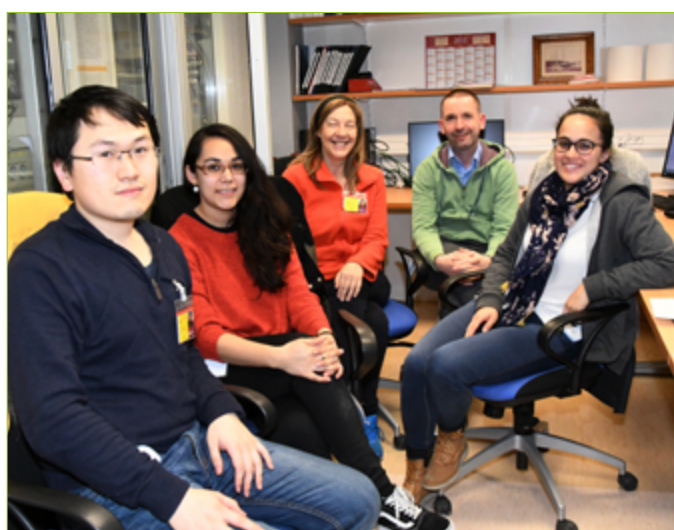
3.



4.



5.



6.



1. From left: Daeyeon Lee, Emily Lin, Neha Manohar and Tomoko Akiyama (University of Pennsylvania) with Philipp Gutfreund (ILL, second from the left) visiting the ILL for an experiment on D17.
2. From front to back: Estelle Chanel, Marc Solar, Florian Piegsa (Laboratory for High Energy Physics, University of Bern) and Torsten Soldner (ILL) during the preparation of a measurement of the neutron electric dipole moment on PF1B.
3. From left: Natalija van Well (Bayreuth University), Ketty Beauvois (ILL) and Eric Ressouche (CEA Grenoble) during an experiment on a low dimension magnetic system on D23.
4. A group of extremely cool and unfrustrated scientists looking at extremely cool (< 50mK) frustrated magnets. From left: Ross Stewart (ISIS), Andrew Wildes (ILL) and Philip Welch (ISIS and Oxford University).
5. From left to right: Joachim Bosina, Carina Killian, Vito F. Pecile and Elisabeth Kreuzgruber (TU Wien) with Hartmut Lemmel, during a qBounce experiment on PF2.
6. Richard Campbell (Manchester University) and his colleagues during their experiment on FIGARO.

FACTS AND FIGURES

119 FACTS AND FIGURES

121 PUBLICATIONS

123 ORGANISATION CHART

570

ILL PUBLICATIONS
RECORDED IN 2018

1 597 VISITORS FROM
42 COUNTRIES IN 2018



821

STANDARD
EXPERIMENTS
PERFORMED*



515

MEMBERS OF
STAFF



KEEP UP-TO-DATE:

- facebook.com/ILLGrenoble
- twitter.com/ILLGrenoble
- linkedin.com/company/institut-laue-langevin

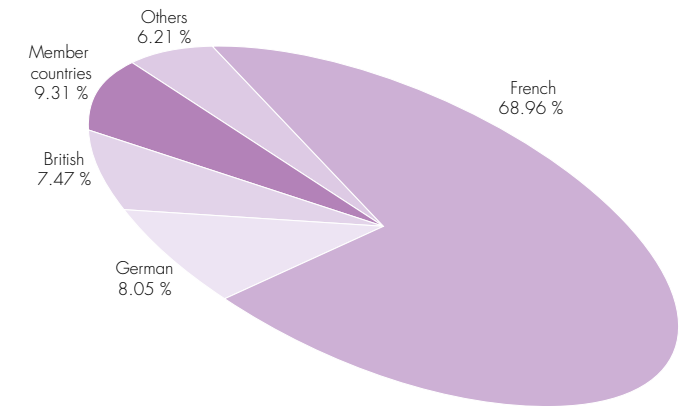
*selected by a scientific review committee

STAFF ON 31/12/2018

515.5 people, including 69 experimentalists in the scientific sector and 38 thesis students.

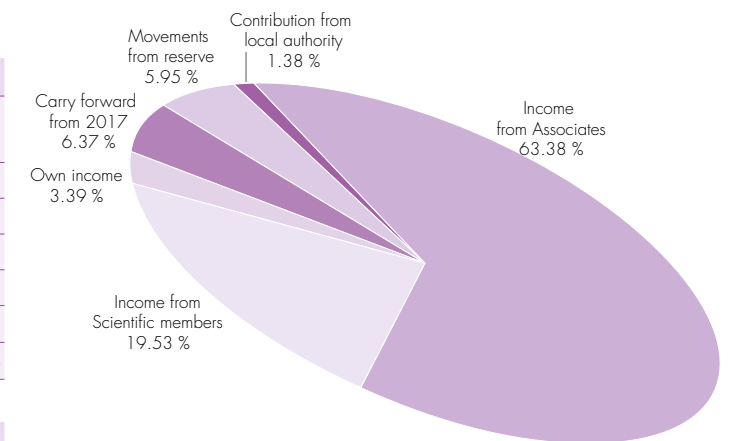
355.5 French; 41.5 German; 38.5 British; 48 scientific participating countries; and 32 others.

| Nationality | | % |
|------------------|--------------|--------------|
| French | 355.5 | 68.96 % |
| German | 41.5 | 8.05 % |
| British | 38.5 | 7.47 % |
| Member countries | 48.0 | 9.31 % |
| Others | 32.0 | 6.21 % |
| Total | 515.5 | 100 % |

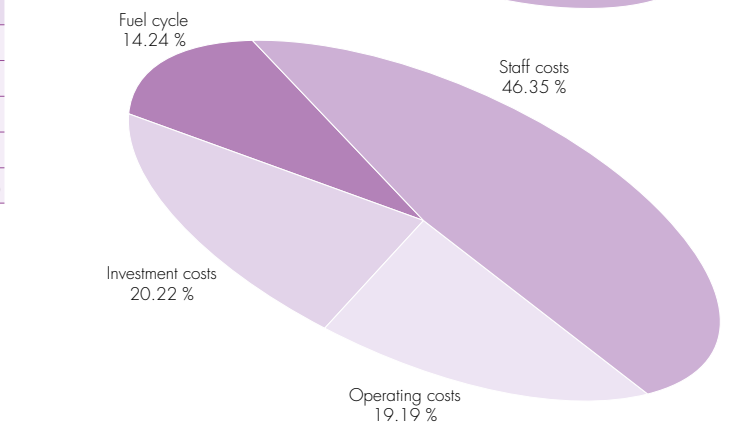


REVISED BUDGET 2018: 102.908 M€ (excluding taxes)

| Income | M€ | % |
|------------------------------------------------------------------------------------|---------------|-----------------|
| Income from Associates (incl. Fukushima & Millennium Programme & add. nuclear tax) | 65.22 | 63.38 % |
| Income from Scientific members | 20.10 | 19.53 % |
| Own income | 3.49 | 3.39 % |
| Carry forward from 2017 | 6.56 | 6.37 % |
| Movements from reserve | 6.12 | 5.95 % |
| Contribution from local authority | 1.42 | 1.38 % |
| Total | 102.91 | 100.00 % |

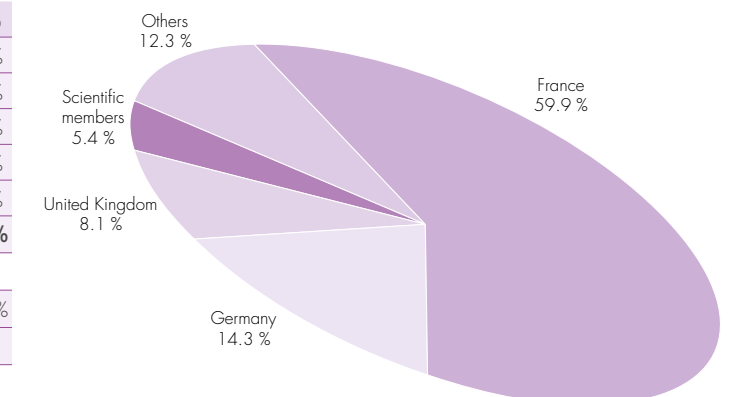


| Expenditure | M€ | % |
|------------------|---------------|-----------------|
| Staff costs | 47.70 | 46.35 % |
| Operating costs | 19.75 | 19.19 % |
| Investment costs | 20.81 | 20.22 % |
| Fuel cycle | 14.65 | 14.24 % |
| Total | 102.91 | 100.00 % |



PURCHASING STATISTICS 2018

| | M€ | % |
|--------------------|--------------|-----------------|
| France | 16.29 | 59.9 % |
| Germany | 3.89 | 14.3 % |
| United Kingdom | 2.21 | 8.1 % |
| Scientific Members | 1.46 | 5.4 % |
| Others | 3.36 | 12.3 % |
| Total | 27.21 | 100.00 % |



| | | |
|----------------------------------|--------------|----------|
| France captive market | 10.62 | 28.1 % |
| Total captive/non captive | 37.83 | 0 |

FACTS AND FIGURES

FIND US ON:   

120-121

NAME

Institut Max von Laue-Paul Langevin (ILL)

FOUNDED

19 January 1967

Intergovernmental Convention between France, Germany and United Kingdom (19/07/1974)

ASSOCIATES

France

Commissariat à l'Énergie Atomique et aux Énergies Alternatives (CEA)

Centre National de la Recherche Scientifique (CNRS)

Germany

Forschungszentrum Jülich (FZJ)

United Kingdom

United Kingdom Research & Innovation (UKRI)

COUNTRIES WITH SCIENTIFIC MEMBERSHIP

Spain

MCIU Ministerio de Ciencia, Innovación y Universidades

Switzerland

Staatssekretariat für Bildung, Forschung und Innovation (SBFI)

Italy

Consiglio Nazionale delle Ricerche (CNR)

CENI (Central European Neutron Initiative)

Consortium composed of:

Austria: Österreichische Akademie der Wissenschaften

Czech Republic: Charles University, Prague

Slovakia: Comenius University, Bratislava

TRANSNI

(Belgian-Danish-Swedish Transnational Neutron Initiative Consortium)

Belgium: Belgian Federal Science Policy Office (BELSPO)

Sweden: Swedish Research Council (VR)

Denmark: Danish Agency for Science and Higher Education

Poland: (NDPN) Consortium of Polish Scientific and Research Institutions

SUPERVISORY AND ADVISORY BODIES

Steering Committee, which meets twice a year

Subcommittee on Administrative Questions, which meets twice a year

Audit Commission, which meets once a year, and statutory auditor

Scientific Council with 9 Subcommittees, which meets twice a year

REACTOR

Operating 3 cycles in 2018

152 days in total, average power (p. 102)

EXPERIMENTAL PROGRAMME

821 experiments accepted by the Subcommittees on 28 ILL funded and 10 CRG instruments

1 597 visitors from 41 countries

Publications in 2018

In 2018, the ILL received notice of 570 publications by ILL staff and users.

They are listed on the ILL website:

<https://www.ill.eu/about-ill/documentation/scientific-publications/scientific-publication-list/>.

THE DISTRIBUTION BY SUBJECT IS AS FOLLOWS

| | |
|---------------------------------------------------|----|
| Applied Physics, Instrumentation and Techniques | 27 |
| Biology | 53 |
| Crystallography and Chemistry | 58 |
| Liquids and Glasses | 19 |
| Magnetic Excitations | 42 |
| Magnetic Structures | 99 |
| Materials Science and Engineering | 50 |
| Medicine | 4 |
| Nuclear and Particle Physics | 79 |
| Soft Matter | 93 |
| Spectroscopy in Solid State Physics and Chemistry | 28 |
| Theory | 15 |
| Other | 3 |

ILL PHD STUDENTSHIPS

| | |
|----------------------------------|----|
| PhD students at the ILL in 2018* | 45 |
| PhD theses completed in 2018* | 15 |
| PhD theses completed in 2018** | 5 |

* Receiving a grant from the ILL.

** Receiving an external grant.

REVIEW PANELS



Key
Chair/focus group Chair
 ILL college secretary/focus group secretary
 ILL specialist

REVIEW PANELS

APPLIED METALLURGY, INSTRUMENTATION AND TECHNIQUES

G. Bruno (BAM, Berlin, Germany)
 S. Cabeza
 T. Pirling/A. Wildes/ L. Porcar

NUCLEAR AND PARTICLE PHYSICS

M. Van der Grinten (STFC, UK)
 S. Degenkolb
 M. Jentschel

MAGNETIC EXCITATIONS

A. Boothroyd (Oxford University, UK)
 L. Mangin-Thro
 B. Fák

CRYSTALLOGRAPHY

H. Ehrenberg (Karlsruher Institut für Technologie, Germany)
 O.R. Fabelo Rosa
 C. Ritter

MAGNETIC STRUCTURES

O. Zaharko (PSI, Villigen, Switzerland)/
M. Laver (Birmingham University, UK)
 N. Qureshi/D. Honecker
 T. Fernandez-Diaz

STRUCTURE AND DYNAMICS OF LIQUIDS AND GLASSES

L. Bove (Pierre and Marie Curie University, Paris, France)
 M.M. Koza
 T. Seydel

SPECTROSCOPY IN SOLID STATE PHYSICS AND CHEMISTRY

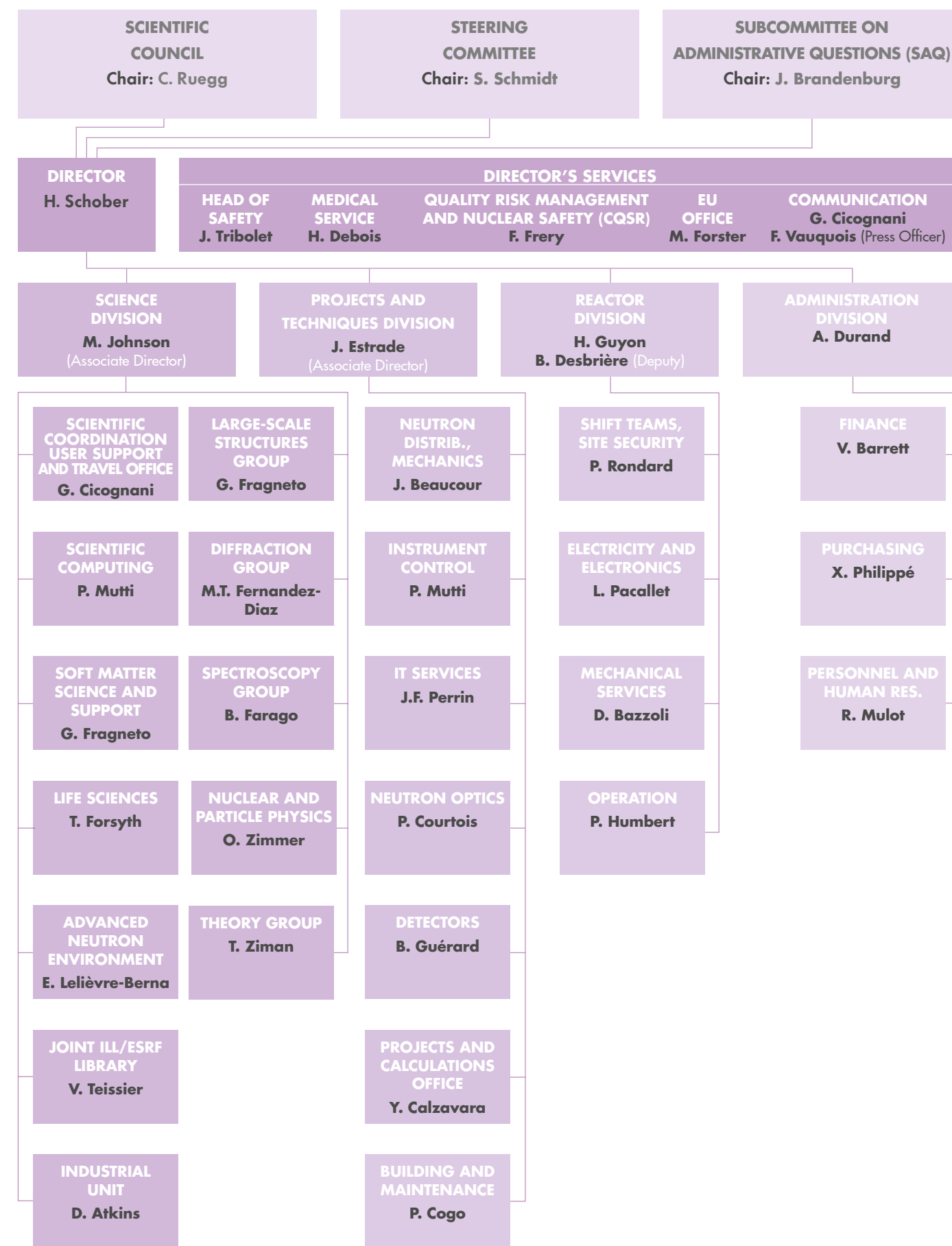
M. de Boissieu (Simap, Grenoble, France)
 T. Weber
 M. Zbiri

STRUCTURE AND DYNAMICS OF BIOLOGICAL SYSTEMS

R. Biehl (JCNS and ICS-1 Jülich, Germany)
 N. Coquelle
 M. Blakeley/J. Peters

STRUCTURE AND DYNAMICS OF SOFT CONDENSED MATTER

R. Jacobs (Oxford University, UK)/
A. Zarbakhsh (University of London, UK)
 I. Hoffman/P. Gutfreund
 O. Czakkel/I. Grillo



71, avenue des Martyrs
38000 Grenoble
France

www.ill.eu



This report has been printed using FSC certified paper www.fsc.org